K. Ganesh Babu
H. Sudarsana Rao
Y. Amarnath   *Editors*

Emerging Trends in Civil Engineering

Select Proceedings of ICETCE 2018

Springer

Lecture Notes in Civil Engineering

Volume 61

Lecture Notes in Civil Engineering (LNCE) publishes the latest developments in Civil Engineering - quickly, informally and in top quality. Though original research reported in proceedings and post-proceedings represents the core of LNCE, edited volumes of exceptionally high quality and interest may also be considered for publication. Volumes published in LNCE embrace all aspects and subfields of, as well as new challenges in, Civil Engineering. Topics in the series include:

- Construction and Structural Mechanics
- Building Materials
- Concrete, Steel and Timber Structures
- Geotechnical Engineering
- Earthquake Engineering
- Coastal Engineering
- Ocean and Offshore Engineering; Ships and Floating Structures
- Hydraulics, Hydrology and Water Resources Engineering
- Environmental Engineering and Sustainability
- Structural Health and Monitoring
- Surveying and Geographical Information Systems
- Indoor Environments
- Transportation and Traffic
- Risk Analysis
- Safety and Security

To submit a proposal or request further information, please contact the appropriate Springer Editor:

- Mr. Pierpaolo Riva at pierpaolo.riva@springer.com (Europe and Americas);
- Ms. Swati Meherishi at swati.meherishi@springer.com (Asia - except China - and Australia/NZ);
- Ms. Li Shen at li.shen@springer.com (China).

Indexed by Scopus

More information about this series at http://www.springer.com/series/15087

K. Ganesh Babu · H. Sudarsana Rao ·
Y. Amarnath
Editors

Emerging Trends in Civil Engineering

Select Proceedings of ICETCE 2018

Springer

Editors
K. Ganesh Babu
Indian Institute of Technology Madras
Chennai, Tamil Nadu, India

H. Sudarsana Rao
JNTUA College of Engineering
Anantapur, Andhra Pradesh, India

Y. Amarnath
Srinivasa Ramanujan Institute of
Technology
Anantapur, Andhra Pradesh, India

Contents

About the Editors

Dr. K. Ganesh Babu   is a retired professor of the Ocean Engineering Department at IIT Madras. His areas of specialization are offshore structures, rehabilitation of structures, corrosion and high performance composites. He has published more than 200 research articles in international journals and conferences of repute, and also authored a book on high performance self-consolidating cementitious composites. Dr. Babu is actively involved in the rehabilitation of many of the centuries-old temples and also other world heritage sites in the country. He has received several awards including the Alexander von Humboldt Foundation Fellowship. He is a former Director of the Central Building Research Institute, Roorkee - a constituent national laboratory of the Council of Scientific and Industrial Research. He has organized several national and international workshops at IIT Madras, and is an expert committee member of various scientific committees.

Dr. H. Sudarsana Rao   is a professor at the Civil Engineering Department at JNTUA Anantapuram. His areas of specialization are rehabilitation of structures, finite element analysis, and high performance cementitious composites. He has published more than 150 research articles in international journals and conferences of repute. Dr. Rao is also actively involved in various administrative capacities in JNTUA like Vice-Chancellor I/C, Rector, Director (ICS), Director of Evaluation and Vice-Principal. He has received several awards such as the International Engineer of the Year 2008, from Cambridge Press. He has organized several national and international workshops at JNTUA Anantapuram.

Dr. Y. Amarnath   is a professor at the Civil Engineering Department at SRIT Anantapuram. His areas of specialization are development of light weight composites, sustainable materials and high performance composites. He has published several research articles in international journals and conferences proceedings. He is a structural design consultant and involved in design of RCC and steel structures.

He has received CTU fellowship from University of Dundee, UK for his PhD and worked on WRAP, UK sponsored project for his doctoral degree. Dr. Amarnath is a reviewer of several scientific journals and is an expert committee member of various scientific committees.

Shear Strength of Rock Quarry Dust and Sand Mix

Natasha Kakati and Malaya Chetia

Abstract Soil shear strength is an important parameter to study for civil engineering applications. The soil beneath any geotechnical structure describes the safe shear strength of it. The investigation of strength parameter of rock quarry residues will help in alleviating issues identified with the gathering of undesirable material and in the meantime to boost asset use and productivity. It is found that if other replacement of river sand is not found, then entire manufacturing industry will be hampered. Hence, shear parameters of rock dust have been measured as it is the maximum capacity that a soil can mobilize in order to withstand, without failure, any applied stress along a plane. It is important because we need to understand failure and design structures for safe and satisfactory performance. Hence shear parameters of rock quarry dust and sand mix are found out at different dry unit weight of the sample by direct shear test. The quarry dust and sand mix were taken with different dry unit weights like 12.17 kN/m^3, 16.71 kN/m^3, and 19.62 kN/m^3 at different strain rates of 0.25 mm/min, 0.625 mm/min, and 1.25 mm/min, respectively. The internal friction angles were found to increase as the strain rate increases. Again the notice has been made on the increase of internal friction angle as the dry unit weight of the sample increases.

Keywords Rock quarry dust · Sand · Shear strength · Strain rate · Angle of internal friction · Dry unit weight

1 Introduction

Last few decades show a drastic growth of infrastructure mostly in developing countries hereby massive amount of river sand is being used to cater to the constructional demand. With this, it is found that river sand has become highly priced conjointly

N. Kakati (✉)
Department of Civil Engineering, National Institute of Technology Meghalaya, Shilong, India
e-mail: natashakakaty12@gmail.com

M. Chetia
Department of Civil Engineering, Assam Engineering College, Guwahati, India

a scarce material. Studies show that the natural river sand has abruptly decreased during recent times which motivates study of identifying alternate material to sand for subsequent utilization as fine aggregates. In such a scenario, the rock quarry dust or quarry dust can be an associate degree in order to replace partially or fully river sand. Quarry dust is formed as a waste material which is non-voluble, residue tailing fine particles having size less than 4.75 mm. These are produced during process of processing and extraction of course aggregates. Further rock quarry dust is found abundantly amounting to approx 200 million tons per annum resulting in landfill disposal problems causing health and environmental threat. Hence utilization of these unwanted hazards creating wastes can lead to minimizing accumulations of waste piles creating utility in recoverable and efficient way. Hence the strength parameters were checked so as to suggest for replacement of fine aggregate.

2 Motivation and Objective of the Study

The probability of scarcity of fine aggregates as in sand in recent times which is due to surplus utilization of river sand in various constructional and geotechnical purposes has lead researchers to stress upon a substitute material bearing similar properties as like fine aggregates (sand). The idea of consumption of quarry dust came into account as it has similar mineral composition like sand and is regarded as a waste product formed during crushing process that enhanced the utilization possibilities. Many research works have been conceded out on the effective utilization of quarry dust single-handedly or with other additives having principles as to treat and stabilize various types of soil but no comparison have been made for resultant properties with sand added to quarry dust. Hence there is the need for this study. Again no studies were made on the effect of shearing rate on the shear strength parameters of quarry dust and quarry dust sand mix. There is also a need to study the variation of shear strength of the samples with respect to variable dry unit weight of the sample. Different drainage conditions were checked in all the samples.

3 A Brief History of Previous Works

A considerable amount of works related to the strength of quarry dust has been studied in replacement of fine aggregates. Various properties were studied in comparison to fine aggregates.

Sridharan et al. [1] stated in his study that addition of certain amount of quarry dust in clayey soil shows significant increase in shear strength properties. of any amount of quarry dust to clayey soil showed considerable increase in shear strength. The study concluded that when 60% dust is added to clayey soil 100% increase in shearing resistance was observed.

Bshara et al. [2] determined the effect of quarry dust on geotechnical properties of poor soil and concluded that California Bearing Ratio (CBR) and Maximum Dry Density (MDD) of these poor soil can be enhanced by utilizing and mixing quarry dust. Further, they determined liquid limit, plastic limit, plasticity index, and optimum moisture content and found that it decreased with addition of stone dust. Thus concluding quarry dust as useful utilization as highway grade materials.

Yamamuro and Lade [3] determined the effect of strain rate in terms of stability of coarse soil performed under high pressure. A study showed that the strain rate didn't affect the location of instability line and the amount of particles crushing was related to amount of sample sheared. They concluded that at higher strain rates the soil was found to be less compressive and gave more strength as much time was not received for particles crushing and rearrangement.

Mamo and Dey [4] studied the effect of strain rate on shear strength parameters resulting from direct shear tests on dry cohesionless soil. Direct shear test was performed at three different strain rates. From the study, it was found that the angle of internal friction increased with the strain rate. The peak shear strength also varied with strain rate for specific normal stress.

Bolton [5] did extensive study on 17 sand samples in axisymmetric or plane strain conditions and checked on the strength and dilatancy at different densities and confining pressures. They concluded mineralogy effects on angle of shearing resistance and found 33° for quartz and 40° for feldspar.

4 Materials and Methodology

4.1 Materials

The rock dust sample used for the study was taken from the Gorchuk quarry and the sand sample was taken from Kulsi river. The sample had been air-dried, pulverized, and sieved through IS 4.75 sieve. The soil sample was identified as SP soil as per the Indian Standard Soil Classification System (ISSCS). The specific gravity was found to be 2.65 for quarry dust and 2.6 for sand.

4.2 Methodology

In order to have a thorough study on shear parameter of quarry dust and sand sample, few characteristics have been studied. With respect to geological test, petrological tests were done and the engineering tests done were specific gravity, sieve analysis and direct shear taking various dry unit weights of the sample. The direct shear parameter is checked for quarry dust and sand-quarry dust mix samples, which is

done at various dry unit weights of the sample and at different shearing rate. Diverse drainage conditions and its outcome on shear strength were observed.

5 Test Results and Interpretations

As mentioned above, the samples prepared having dry unit weight as 12.17, 16.71, and 19.62 kN/m^3 have been subjected to direct shear test. The samples were tested in different strain rates as 0.25, 0.625, and 1.25 mm/min and maintaining various ratios of Q:S (quarry dust: sand) 100:0 and 70:30.

5.1 Petrological Test

Petrography test is the test that focuses on exhaustive descriptions of rocks and thereby it comes under geology branch. The mineral content with the textural interaction can be described with the rock.

The classification of rocks is based on the information acquired during the petrographic analysis. As per IS 2386 (PART VIII)-1963 (reaffirmed 1997), the test was performed (Tables 1 and 2).

Table 1 Shape and mineral characterization of rock quarry dust

Minerals	Amount (%)	Shape
Quartz	70–73	Angular to subangular
Feldspar	10–15	Elongated
Biotite	10–12	Elongated, flaky
Muscovite	5–6	Elongated, flaky
Others	7–8	Subangular, elongated

Table 2 Shape and mineral characterization of sand

Minerals	Amount (%)	Shape
Quartz	75–80	Rounded, subrounded
Biotite	10–12	Elongated, flaky
Feldspar	3–5	Elongated
Rock Fragments	5–6	Irregular
Muscovite	3–4	Elongated, flaky
Others	2–4	Subangular, elongated

Fig. 1 Variation of dry unit
weight with height
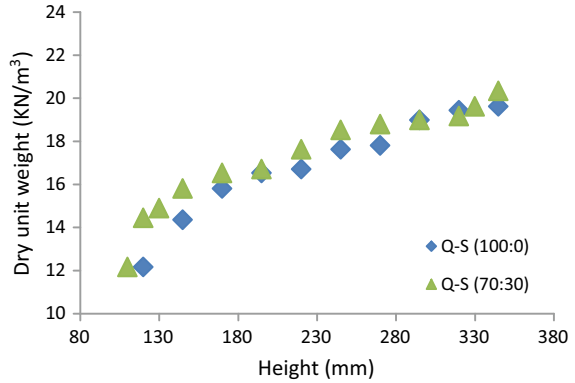
5.2 Determination of Dry Unit Weight

Determination of three dry unit weights of quarry dust aggregates is done by pouring the sample from different heights. And hence three dry unit weights were chosen (Fig. 1).

5.3 Angle of Internal Friction at Dry Unit Weight 12.17 kN/m³ for Quarry Dust

At dry unit weight 12.17 kN/m^3, considering different shearing rates of 0.25, 0.625, and 1.25 mm/min, the direct shear test was performed. It was done considering different drainage conditions. The conditions taken were at dry and drained state (Fig. 2).

Fig. 2 Angle of internal
friction versus shearing rate
at dry unit weight
12.17 kN/m^3 for quarry dust
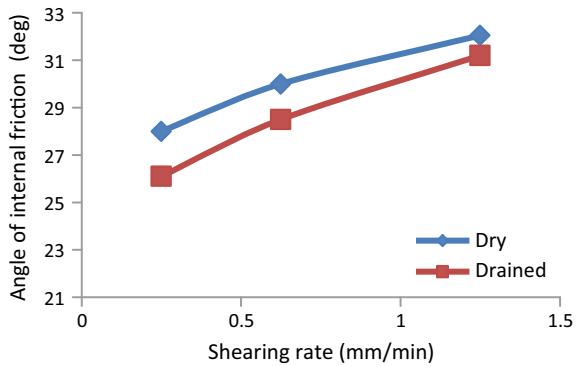
Fig. 3 Angle of internal friction versus shearing rate at dry unit weight 16.71 kN/m^3 for quarry dust
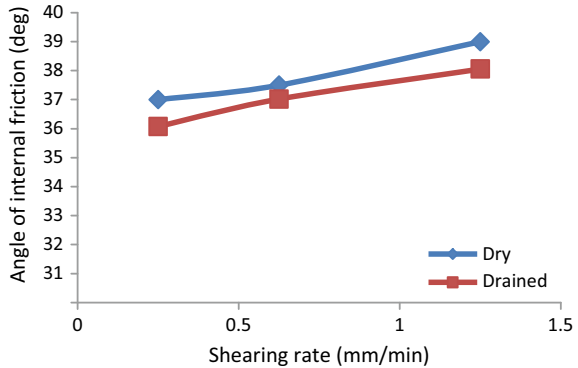
5.4 Angle of Internal Friction at Dry Unit Weight 16.71 kN/m^3 for Quarry Dust

At dry unit weight 16.71 kN/m^3 considering different shearing rates of 0.25, 0.625, and 1.25 mm/min, the direct shear test was performed. It was done considering different drainage conditions. The conditions taken were at dry and drained state (Fig. 3).

5.5 Angle of Internal Friction at Dry Unit Weight 19.62 kN/m^3 for Quarry Dust

At dry unit weight 19.62 kN/m^3 considering different shearing rates of 0.25, 0.625, and 1.25 mm/min the direct shear test was performed. It was done considering different drainage conditions. The conditions taken were at dry and drained state (Fig. 4).

5.6 Angle of Internal Friction at Shearing Rate 0.25 mm/min for Quarry Dust

At shearing rate 0.25 mm/min considering different dry unit weights, the direct shear test was performed. It was done considering different drainage conditions. The conditions taken were at dry and drained state at 12.17, 16.71, and 19.62 kN/m^3 dry unit weight (Fig. 5).

Fig. 4 Angle of internal friction versus shearing rate at dry unit weight 19.62 kN/m^3 for quarry dust
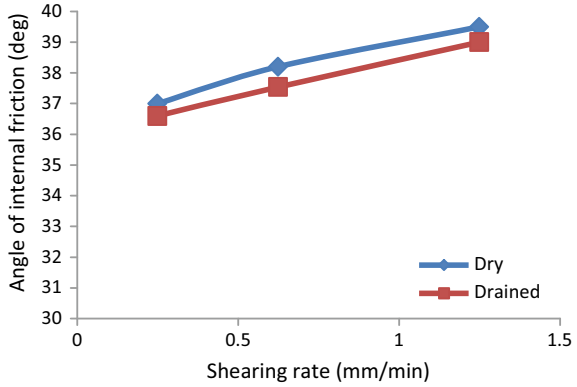
Fig. 5 Dry unit weight versus angle of internal friction at shearing rate 0.25 mm/min for quarry dust
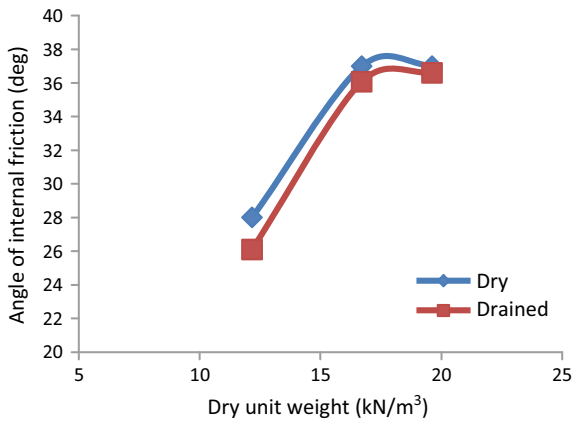
5.7 Angle of Internal Friction at Shearing Rate 0.625 mm/min for Quarry Dust

At shearing rate 0.625 mm/min considering different dry unit weights, the direct shear test was performed. It was done considering different drainage conditions. The conditions taken were at dry and drained state at 12.17, 16.71, and 19.62 kN/m^3 dry unit weight (Fig. 6).

5.8 Angle of Internal Friction at Shearing Rate 1.25 mm/min for Quarry Dust

At shearing rate 1.25 mm/min considering different dry unit weights, the direct shear test was performed. It was done considering different drainage conditions. The

Fig. 6 Dry unit weight versus angle of internal friction at shearing rate 0.625 mm/min for quarry dust
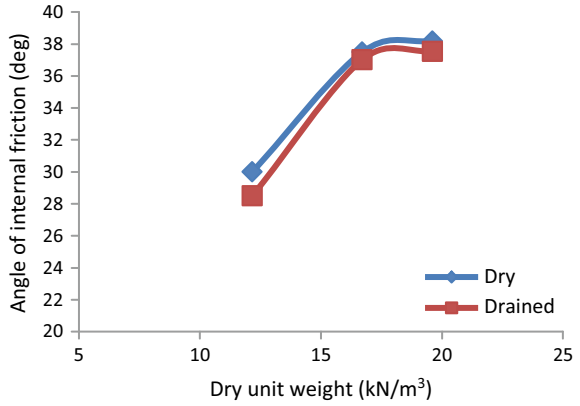
Fig. 7 Dry unit weight versus angle of internal friction at shearing rate 1.25 mm/min for quarry dust
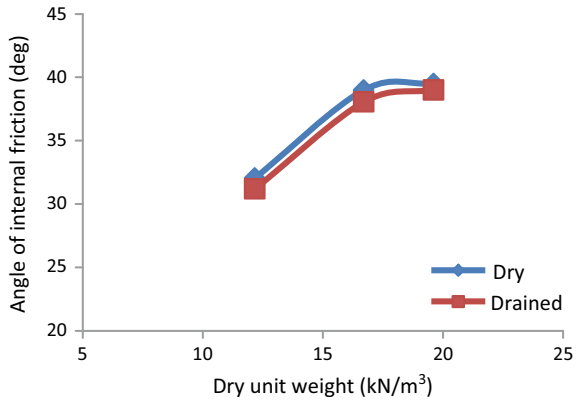
conditions taken were at dry and drained state at 12.17, 16.71, and 19.62 kN/m^3 dry unit weight (Fig. 7).

5.9 Angle of Internal Friction at Dry Unit Weight 12.17 kN/m^3 for Quarry Dust and Sand Mix (70:30)

At dry unit weight 12.17 kN/m^3 considering different shearing rates of 0.25, 0.625, and 1.25 mm/min, the direct shear test was performed. It was done considering different drainage conditions. The conditions taken were at dry and drained state (Fig. 8).

Fig. 8 Angle of internal friction versus shearing rate at dry unit weight 12.17 kN/m^3 for quarry dust and sand mix (70:30)
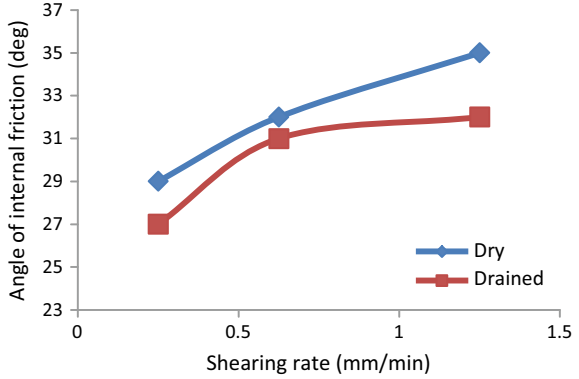
Fig. 9 Angle of internal friction versus shearing rate at dry unit weight 16.71 kN/m^3 for quarry dust and sand mix (70:30)
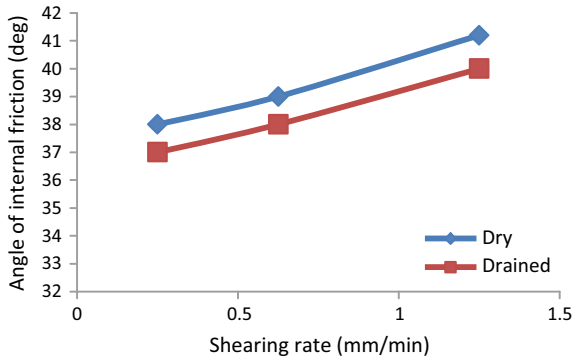
5.10 Angle of Internal Friction at Dry Unit Weight 16.71 kN/m^3 for Quarry Dust and Sand Mix (70:30)

At dry unit weight 16.71 kN/m^3 considering different shearing rates of 0.25, 0.625, and 1.25 mm/min the direct shear test was performed. It was done considering different drainage conditions. The conditions taken were at dry and drained state (Fig. 9).

5.11 Angle of Internal Friction at Dry Unit Weight 19.62 kN/m^3 for Quarry Dust and Sand Mix (70:30)

At dry unit weight 19.62 kN/m^3 considering different shearing rates of 0.25, 0.625, and 1.25 mm/min the direct shear test was performed. It was done considering different drainage conditions. The conditions taken were at dry and drained state (Fig. 10).

Fig. 10 Angle of internal friction versus shearing rate at dry unit weight 19.62 kN/m^3 for quarry dust and sand mix (70:30)
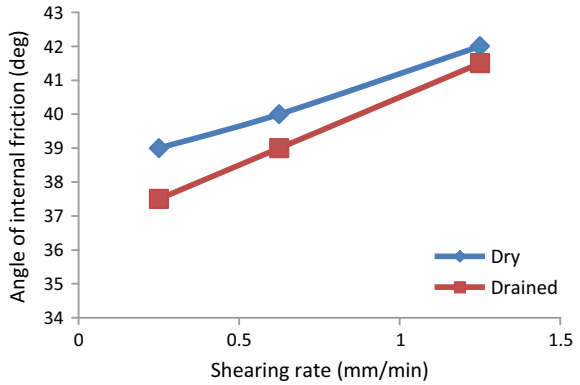
Fig. 11 Dry unit weight versus angle of internal friction at shearing rate 0.25 mm/min for quarry dust and sand mix (70:30)
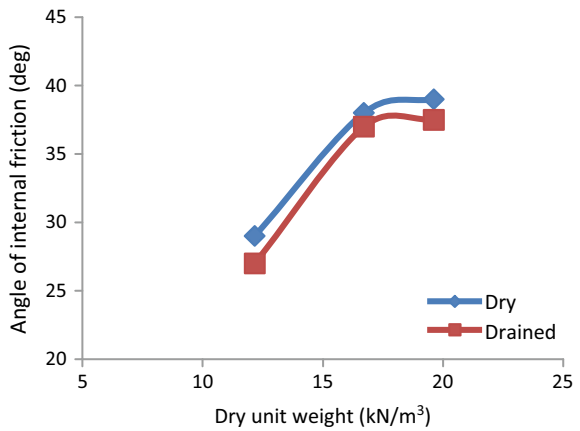
5.12   Angle of Internal Friction at Shearing Rate 0.25 mm/min for Quarry Dust and Sand Mix (70:30)

At shearing rate 0.25 mm/min considering different dry unit weights, the direct shear test was performed. It was done considering different drainage conditions. The conditions taken were at dry and drained state at 12.17, 16.71, and 19.62 kN/m^3 dry unit weight (Fig. 11).

5.13   Angle of Internal Friction at Shearing Rate 0.625 mm/min for Quarry Dust and Sand Mix (70:30)

At shearing rate 0.625 mm/min considering different dry unit weights, the direct shear test was performed. It was done considering different drainage conditions. The

Fig. 12 Dry unit weight versus angle of internal friction at shearing rate 0.625 mm/min for quarry dust and sand mix (70:30)
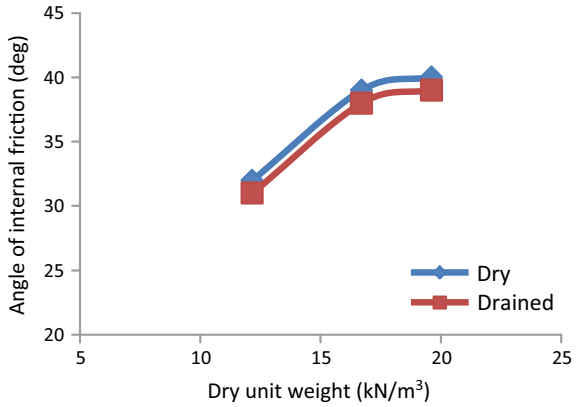
conditions taken were at dry and drained state at 12.17, 16.71, and 19.62 kN/m³ dry unit weight (Fig. 12).

5.14   Angle of Internal Friction at Shearing Rate 1.25 mm/min for Quarry Dust and Sand Mix (70:30)

At shearing rate 1.25 mm/min considering different dry unit weights, the direct shear test was performed. It was done considering different drainage conditions. The conditions taken were at dry and drained state at 12.17, 16.71, and 19.62 kN/m³ dry unit weight (Fig. 13).

Fig. 13 Dry unit weight versus angle of internal friction at shearing rate 1.25 mm/min for quarry dust and sand mix (70:30)
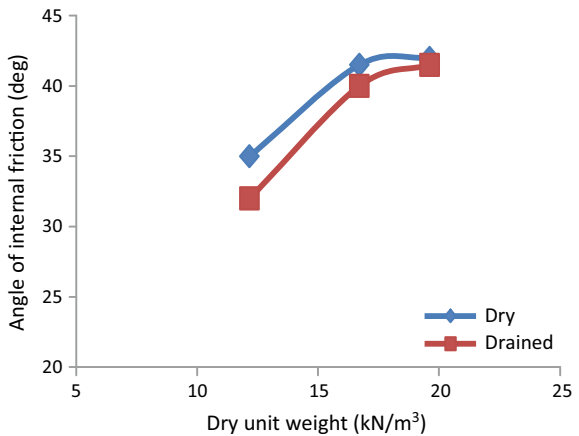
6   Conclusions

Shear strength has been a topic of utmost importance in the field of soil mechanics. The angle of internal friction of a structure is related to this property of soil. Hence understanding the phenomenon of shearing and its behavior with respect to dry unit weight and shearing rate becomes a matter of great concern for engineers. From the above-mentioned study, the subsequent conclusions can be made for the quarry dust and sand sample mix taken for laboratory investigations.

1. It was found that the angle of internal friction increases with an increase in dry unit weight of the sample.
2. It was found that the angle of internal friction increases with the increase in shearing rate of the sample.
3. The specific gravity of quarry dust was determined as 2.65, which is almost similar in value with river sand hence it can be used in partial replacement of river sand.
4. The angle of internal friction of quarry dust ranged from 26° to 39°, which is sufficient for fractional replacement of sand.
5. The values of internal friction for dry state were found to be higher than that of drained state.
6. It was found that as sand was added to quarry dust, the value of internal friction angle increases to 27–42.

It can be concluded that the quarry dust can be utilized for fractional replacement of river sand in field of construction. This will not only be cost-effective but also helpful from environmental point of view as utilization of this waste will reduce its deposition in the nearby areas of quarries. Quarry dust has given promising results to reach the endeavor of going "green". And the mixed samples gave much better results. However, further studies in a greater scale are required for a conclusive statement to be made in this regard.

References

1. Sridharan, A., Soosan, T. G., Jose, B. T., & Abraham, B. M. (2006). Shear strength studies on soil-quarry dust mixture. *Geotechnical Geological Engineering, 24,* 1163–1179.
2. Bshara, A. S., Bind, Y. K., & Sinha, P. K. (2014). Effect of stone dust on geotechnical properties of poor soil. *International Journal of Civil Engineering and Technology, 5*(4), 37–47.
3. Ymamuro, J. A., & Lade, P. V. (1993). Effects of shearing rate on instability of granular soils. *Geotechnical Testing Journal, 16*(3), 304–313.
4. Mamo, G. B., & Dey, A. (2014). Critical overview of the effect of shearing rate on direct shear test results, North east student's geo-congress on advances in geotechnical engineering-2014.
5. Bolton, M. D. (1986). The strength and dilatancy of sands. *Geotechnique, 36*(1), 65–78.
6. IS 27200: (Part III/Section 2:1980) Indian Standard Method of test of soil, Determination of specific gravity, fine, medium and coarse grained soils, Bureau of India Standards, New Delhi.
7. IS 2720: (Part IV:1985) Indian Standard Methods of test for soils, Grain size analysis.

8. IS 2720: (Part XIII:1986) (Reaffirmed 1997) India standard method of test of soils, part XIII Direct shear test, Bureau of India standards, New Delhi.
9. IS: 2720 (Part XXXIX:1977) Indian standard method of tests of soils: Direct shear test, Bureau of Indian Standards, New Delhi.

Design of Prototype Model of Robot for Cleaning

Tarun Verma and Abhishek Mishra

Abstract Open space cleaning is one of the important routine works in any place. In this work, a prototype model of robot for cleaning is developed for open spaces. The frame, body, and parts of prototype model of robot are created and assembled using CAD software. The specifications of the parts required to construct the real-life model are mentioned in various sections and subsections of this work. It is designed fully automated and able to sense the waste and remove it with the help of its cleaning mechanism. The basic advantage of this prototype model of robot is that it will be cost-effective with no human enrollment.

Keywords Open space cleaning · Robot · Prototype model · Automation

1   Introduction

Open space cleaning machines have become more popular in recent years, these machines operate semi-autonomously to clean parks, streets, roads, etc. Different types of cleaning machines are available such as road sweeper machine, vacuum-based mechanical sweepers, municipal/contractor machine, etc. These machines are driving by driver so the accuracy in cleaning depends upon human capabilities. The limitations of these machines are manual controlling, wet cleaning, vacuum is needed to take trash from the path, etc. The need of prototype of robot for cleaning was originating from limitations of cleaning machines. Some of observations in literature are that it constructed a robot that was used in inspection of pipe. The static stress analysis of the pipe inspection robot was done in ANSYS 13 [1]. The cleaning of surface by using setup of RGB-D camera and robot arms without force control was presented. Cleaning of surface of table was task of robot which was performed by arm of robot using rag [2]. A mobile robot for floor cleaning was used. Floor cleaning performance of various domestic mobile robots was measured, analyzed and then finally modeled [3]. The semi-automatic floor-cleaning machine was fabricated. The

T. Verma · A. Mishra (✉)
Department of Mechanical Engineering, National Institute of Technology, Delhi 110040, India
e-mail: abhishekmishra@nitdelhi.ac.in

solar panel was used to charge the batteries of robot within four hours. The principle of working of this manufactured robot was nearly same as wiping mechanism in car [4]. The robot for cleaning of power plants was fabricated. This robot was used to handle radioactive load [5].

2   Design Considerations

The first step of design of the prototype is defined constrains based on demonstration model and initially assumed specifications. Then calculation of torque was done based on the specifications, i.e., speed, weight (includes assumed frame weight, battery weight, motor weight and some extra weight for accessories, and other parts), acceleration, radius of wheel, inclination angle. Based on calculated torque select the motor which was produced torque more than calculated torque. Select the battery, number of battery, and weight by using cross-section of frame, length, specifications of components was calculated or defined. Based on maximum load-carrying capacity thickness of frame and select leaf spring suspension or Mac Pearson suspension system was designed.

The components of the prototype are given below:

1. Frame
2. Primary container lifting mechanism
3. Rear suspension assembly
4. Front suspension assembly
5. Secondary Container
6. Scrubber
7. Power unit
8. Control system and sensing systems.

2.1   Frame

Cross-section of frame is hollow rectangular having dimensions 50.8 mm width and 76.2 mm height. The cross-section was initially assumed using a reference to vehicle of same load-carrying capacity. Thickness of section of frame is 3 mm. The thickness of frame was reduced further, depends upon the outcomes of results of ANSYS, thickness was decided. Material of frame was initially assumed structured steel. The arc welding was preferred to join the cross-section. The image of frame is shown in Fig. 1.
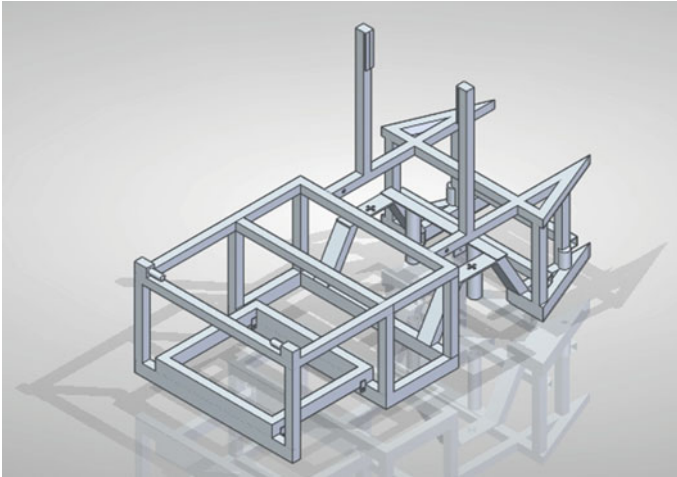
Fig. 1 Isometric view of frame of prototype

2.2 Primary Container Lifting Mechanism

It consists of two lead screws which act as guide ways of primary container the container is lifted by nut on lead screws. The pitch of the lead screw is 2 mm which was one of parameter which controlled upward motion of primary container. The formula of velocity is rotational speed multiplied to pitch of lead screw. Lead screw was simply supported to both ends. At end of lifting of primary container, rotational motion to primary container with 30° of angle to horizontal axis was given. The 30° of angle helped in giving outward flow motion to trash. When primary container was completely empty, then flapper was closed and primary container was lifting down. The selected lead screw (Precision Industrial Components, Acme lead screws, ARS1X082 M -1.8) and the specification of selected motor (Techtonics, Planetary DC Geared Motor With Encoder 600 RPM 24 V) The assembly of primary container lifting mechanism is shown in Fig. 2 and primary container is shown in Fig. 3.

2.3 Rear Suspension Assembly

It consists of leaf springs, motors, shafts, wheel, and tire assembly, outer casing of shafts, hub, bearings and mounting units, etc. The selected leaf springs (i.e., Trojan, Multi-Leaf slipper sprigs- Double-eye galvanized and part number 261056) the selected motors (i.e. Oriental motor, Hollow shaft flat gearhead, BLV640N-F). Geometry of rear suspension assembly is shown in Fig. 4.

Fig. 2 Isometric view of primary container lifting mechanism assembly of prototype
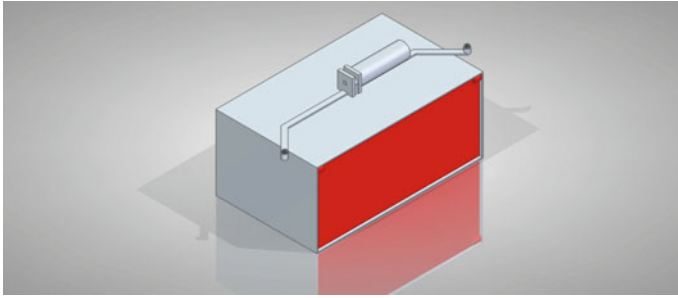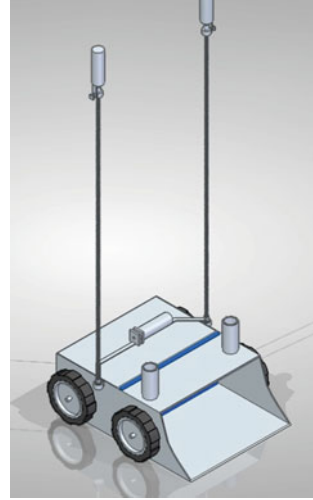
Fig. 3 Isometric view of primary container assembly

Fig. 4 Isometric view of rear suspension assembly
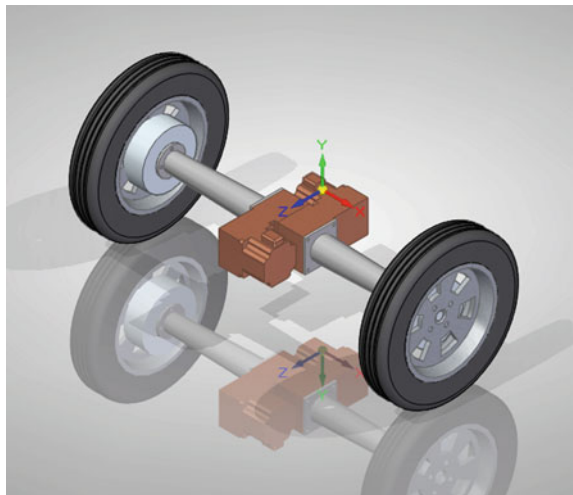
Fig. 5 Isometric view of the
front suspension

Fig. 6 Isometric view of
tire-wheel assembly

2.4 Front Suspension Assembly

Front suspension assembly consists of Mac-Pearson suspension, hub, steering rod
and wheel-tire assembly, etc. The selection of suspensions is based on direction of
forces acting and magnitude of force. The hydraulic damper was used to damp the
oscillations magnitude. The image of front suspension assembly is shown in Fig. 5
and wheel with hub assembly is shown in Fig. 6.

2.5 Secondary Container

Initially, the trash was primary/temporary stored in primary container then if the pri-
mary container was full then sensor commands to motor to start rotation of lead screw
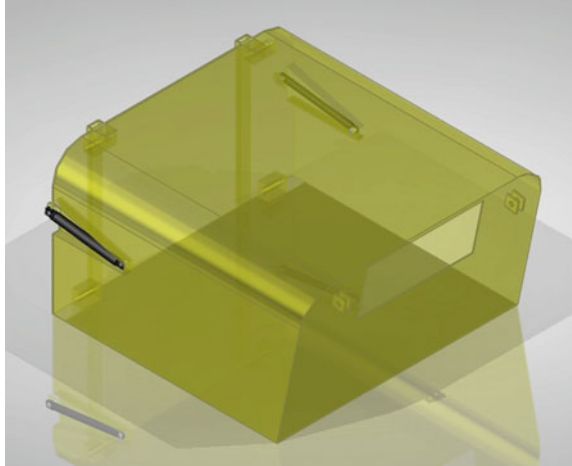
and primary container was lift-off. The trash was dropped down in secondary container. The capacity of secondary container is 400 L. The material of secondary container is low carbon steel. The pneumatic jack was used to lift upward and downward to container. Image of secondary containers is shown in Fig. 7.

2.6 Scrubber

The scrubber was designed for maximum dimension of trash intake. Size of trash is an important parameter for the design of scrubber. The prototype was designed to collect the trash from 6 to 215 mm of height and 465 mm of width. According to response of collected trash on path of prototype and if small modifications were required then it could be done. Position of trash is displaced by using brush which was guided the trash from path to inner cover area of scrubber. It consists of brush, arm, and motor. The motor which is used to rotate the brush is revolving by using arm. Arm is linearly feed using pneumatic actuator. Maximum working area is cover using this assembly. Trash that is placed below to the tire and in between tire and outer casing of primary storage was moved to area of scrubber with the help of brushes. The arm is rotated and comes back undercover area at the end of whole operation. The arm is cantilever beam type support. The image of scrubber and brush is shown in Figs. 8 and 9, respectively.

Fig. 8 Isometric view of
scrubber
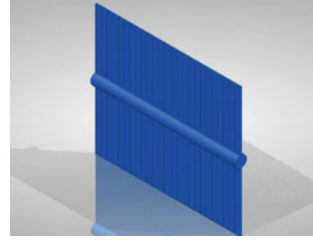
Fig. 9 Isometric view of
brush

2.7 Power Unit

The six batteries were used to run the function of components of prototype. Four
batteries were used in the driving of prototype from one place to another place.
Two batteries were used in lifting the primary container, scrubber, brush rotation
controller, etc. The voltage requirement for rear driving unit motor was 48 V. The
selected battery is Exide, Exide E-Ride Plus, ERFLPLUS120L.

2.8 Control System and Sensing System

The Raspberry Pi 3 Model B is the third generation Raspberry Pi. The size of this
computer is approximately a credit card. This popular board format the Raspberry
Pi 3 Model B is a more powerful processor and ten times faster than first-generation
Raspberry Pi. Moreover, it adds Bluetooth connectivity and wireless LAN, HDMI
connections, Ethernet socket, etc. TSOP and LiDAR sensors were used as sens-
ing systems. TSOP sensor was used for short-range or nearest object detection and
LiDAR sensor is used for detection of far objects. The main components of TSOP
sensor are epoxy package, pin diode, amplifier, and band pass filter. In TSOP sensor,
there are three pins namely ground, voltage, and output pin. Output pin was connected
to the Raspberry Pi which inputs the signal. The programming was done in Python
language. Reflected light is first transferred through epoxy package, then signal is
transmitted to pin diode, then signal is amplified, and then filter out signal through

bandpass filter; after that signal goes to Raspberry Pi. The sunlight and ambient light are not passed through the bandpass filter, whereas, the wavelength of IR ranging from 700 nm to 1 mm are passed. It acts as transmitter of system which transmits the infra-red wave signal in IR module. The type of IR signal is square wave.

3   Sequence of Process in Working of Prototype

The assembly of prototype consists of eight main components and assemblies like frame, front suspension assembly, rear suspension assembly, scrubbing mechanism, power unit, primary container lifting mechanism, secondary container, and direction control brush assembly. The brief descriptions of these components and assemblies are discussed in above section. Overall dimensions of frame of prototype are 2192 mm, 1054 mm, and 1430 mm length, width, and height, respectively. The procedure of working of prototype was divided into steps. The number of steps, is ten, which are used in completion of single cycle are reset, open doors of collector, moving forward, detect trash, collect trash, close doors of collector, lifting of primary container, drop trash in secondary container, close door of primary container, lifting down of primary container, and finally moving forward. The side view of assembly of prototype with components name is shown in Fig. 10.

The brief description of sequence of process in working of prototype is shown below:

1. **Reset**:
   Scrubber
   Right and left brushes.

1. Container
2. Battery
3. Frame
4. Pneumatic jack
5. Lead screw
6. Front suspension
7. Brush motor
8. Brush
9. Scrubber
10. Collector
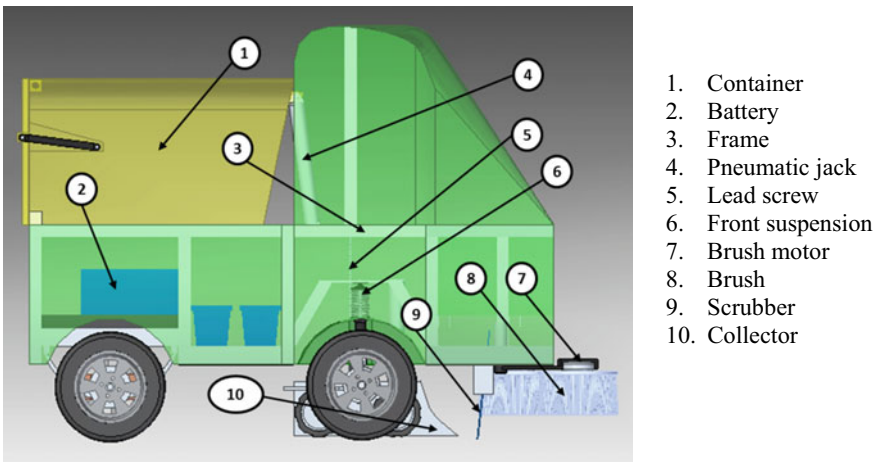
Fig. 10 Side view of the prototype with description

2. **Open doors of collector**:
   Front door of outer casing of primary container and collector are open.
3. **Moving forward**:
   Prototype moving forward
   Collector moving forward
   Both left and right brush starts rotating.
4. **Detect trash**:
   When trash size is large or small, trash is collected using scrubber and then forced to collector.
   During process of collection prototype is stop moving forward and sends message "trash detected".
   TSOP sensor is present at 215 mm of height to ground which senses and inputs the signal to prototype.
5. **Collect trash**:
   Using scrubber the trash is collected in primary container through collector.
   Scrubber starts rotating at 180º rotation when the trash detecting sensor input signal to scrubber.
6. **Close doors of collector**:
   When primary container is full, then the front door of collector and primary container is closed.
7. **Lifting of primary container**:
   Through lead screws, the primary container is lifted upward and stops lifting when upper part of nut touches to bracket of motors.
8. **Drop trash to secondary container**:
   When primary container attains height then the rear door of primary container is open. After opening the door, the trash is dropped in the secondary container.
9. **Close door of primary container**:
   When all trash is dropped in secondary container then rear gate of primary container is closed.
10. **Lifting down of primary container**:
    After trash is dropped and closing of door then the primary container is returned back to its space. Then open the doors of primary container and collector and same process from step 3 is followed until prototype is command for program stop.

4 Conclusions

The design of the prototype of robot for cleaning was done in CAD software. The simulation results give good visualization GUI to understand the motion of mechanisms. The mechanism used in collecting trash from open space is simple, effective, and less power-consuming as compared to different sweeping trucks. This prototype is ecofriendly because batteries are used in working of prototype of robot.

There are two sensors that are proposed—first is TSOP sensor and second is LiDAR senor. LiDAR sensor is most predominantly used to measure the far object distance measurement applications. The lasers do not completely cover the nearest area of prototype. Mechanism for working of prototype function is good in simulation by using software. Vacuum-based cleaning machines are good but wastage of power is there when there are no trashes on road.

References

1. Gargade, A., Tambuskar, D., & Thokal, G. (2013). Modelling and analysis of pipe inspection robot. *International Journal of Emerging Technology and Advanced Engineering, 3,* 120–126.
2. Martínez, D., Alenyà, G., & Torras, C. (2015). Planning robot manipulation to clean planar surfaces. *Engineering Applications of Artificial Intelligence, 39,* 23–32.
3. Palleja, T., Tresanchez, M., Teixido, M., & Palacin, J. (2010). Modeling floor-cleaning coverage performances of some domestic mobile robots in a reduced scenario. *Robotics and Autonomous Systems, 58,* 37–45.
4. Ladage, V., Jawanjal, S., Kamat, D., Majgaonkar, R., & Kadam, B. (2016). Semi-automatic floor cleaning machine. *International Journal of Design and Manufacturing Technology, 8,* 1–7.
5. Shukla, P., & Shimi, S. L. (2014). Design of inspection and cleaning robot. *International Journal of Scientific Research Engineering & Technology, 3,* 970–975.

Identifying and Analysing Key Factors Associated with Risks in Construction Projects

Saurav Dixit, Kaaraayaarthi Sharma and Subhav Singh

Abstract The construction industry has a fragmented nature associated with it. It is necessary to identify the impact of the key factors associated with risk on construction projects so that the timely alternatives or solutions could be taken to avoid them. The objective of the paper is to identify and analyse the various risks factors globally associated with construction projects. In this, the risks factors in the international construction sector were compared to the Indian industry of construction, in order to find out the similar risks globally. The methodology adopted for the study is to review the previous year's research papers for the international industry of construction and Interview of a construction company in India and after analyzing the data the common risks in both the industry were found. It is concluded that the retention good quality of labourers has the highest impact globally in the construction sector. The categories of risks related to clients, subcontractors, finance, contractors and government were found common. The appropriate management plan for risks in construction should be implemented right from the beginning of the project in order to minimize its impact and proper solution or alternatives could be taken accordingly at each and every stage of the project. One of the solutions to transfer risk in this sector is by taking appropriate insurance policy for the project.

S. Dixit (✉)
RICS School of Built Environment, Amity University Noida, Noida, India
e-mail: sdixit@ricssbe.edu.in

K. Sharma
M/s the Open Survey World, Jammu, India

S. Singh
K R Mangalam University Gurgaon, Haryana, India

1 Introduction

In India, the construction industry is one of the oldest industries with ample amount of employment opportunities for the rural and urban population. The size of this industry varies from single ownership to a large industry providing employment to thousands of people. Before independence, the construction work was confined to the individual and community level. Under the rule of Lord Dalhousie, Public Welfare Department was established for the construction of roads, canals, etc., in the years 1875 AD. But after independence as well Indian construction industry continued the evolution with the projects like Bhakra Dam, which was a breakthrough project for India [1, 2].

Previous studies have revealed that the construction industry does not have a good record track in performing a risk assessment as compared to other industries. Construction activities are hazardous in nature due to which there are frequent accidents, which are sometimes severe as well. Also, construction activities need a large amount of investment majorly on public projects. All these factors also increase the risk of the project. Construction projects require many people with disparate skills, knowledge and interests, as well as the coordination of a variety of different, yet related activities. There is no such project which will not have a risk in it, so a project can be successful only when the risks are identified at the initial stage and proper mitigating measures are taken at every step to minimize the impact of that risk [1, 3–5].

1.1 What Is Risk?

According to BS 6079-3:2000: "An uncertainty inherent in plans and the possibility of something happening that can affect the prospect of business or project goals ("BS 6079-3:2000 Project management. Guide to the management of business related project risk," 2000)".

According to the Association of Project Management: "It is defined as the combination of a probability or frequency of occurrence of a defined threat or opportunity and the magnitude of the consequences of the occurrence."

According to PMBOK Guide 5th edition: "Project risk is "an uncertain event or condition that if it occurs as a positive or negative effect on one or more project objectives such as scope, schedule, cost or objectives (A Guide to the Project Management Body of Knowledge (PMBOK® Guide) – Fifth Edition, 2013)"

According to ISO-31000 "Risk is defined as the effect of uncertainty on objectives ("ISO-31000-2000(E)," 2009)".

2 Review of Literature

Baccarini and Archer in the year 2001 presented a methodology, which ranks project based on risk. This was taken up by the department of contract and management services in Western Australia. Hillson in 2002 proposed a methodology for the assessment of threat along with the opportunity concurrently within the P-I models quantitatively as well as qualitatively. Ward and Chapman in 2003 proposed a six steps path for estimation of uncertainty which is "minimalist" path. Jannadi along with Almishari in the year 2003 gave a software for the generation of risk scores, the variables for the software were fed on the basis of a model of risk as probability, the harshness of impact and vulnerability to all hazards of activity [2, 6–8]. For the purpose of quantification of risk which was allocated to each element of the project Cagno et al. in 2007 identified the sources of uncertainty, affected activities and risk owners by using the P-I model. They tried to improve the model of risk by giving the controllability concept which is the ratio of expected risk impacts before and after mitigation actions have been applied. Zhang in 2007 introduced project susceptibility by giving the argument that once the event of risk will occur, a projection system will have interactions with these events, which would determine the risk consequences that are ultimately experienced. Han et al. in 2008 gave a three-dimensional model of risk, i.e. Significance of risk -Probability of risk -Impact of risk. In the year 2009, Cioffi along with Khamooshi suggested a method that leads to the relevant budget for contingency by combining the impact of risks and at a given confidence level evaluating its overall impact. In international construction projects. Hastak and Shakes in 2000 used AHP, with a model of risk modelled as Probability and its impact. DSS was given by Dey in 2001so that the risk can be easily managed right from the beginning stage of the construction project. To find out and identify which is the best strategy for the management of risk EMV of each risk response strategy is used in the construction project [9–14]. For assessment of risk as well opportunity in international projects. Dikmen and Birgonul in 2006 used AHP along with a framework for multi-criteria decision making. For joint ventures related construction works, Hsueh et al. in 2007 used utility as well as AHP theory to develop multi-criteria for the purpose of assessment of risk. However, the author does not give any risk assessment tool in this paper. AHP was used by Zayed et al. in 2008 to allocate weight to risks before project risk levels are been calculated. Tah and Carr in 2000 developed a qualitative risk assessment model and in the year 2001 tried to overcome the limitation of FST [15–20]. Baloi and Price in 2003 after comparing many theories found FST as a vital means of solving the problem for estimating the nature of construction uncertainty. DSS was developed by Shang et al. in the year 2005 for facilitation of evaluation of risk at the design and conceptual stages. Zeng et al. in 2007 attempted to mix the strengths of FST and AHP [21–24].

3 Research Methodology

The methodology used for the research was a thorough literature review, a postal questionnaire to practitioners in China and a statistical result analysis of the questionnaire and the risks identified from those results. In addition to this, in the Australian industry of construction, a comparative study was also performed [25–27]. The two sections of the questionnaire included the general informal of the respondents and the 85 risks associated with the construction projects. Respondents were asked to indicate what was the likelihood of happening or occurrence of the mentioned risks as "highly likely, likely or less likely" and the magnitude of consequences on the various objectives related to project that would result as "high, medium or low". 85 risks factors identified were categorized into 7 groups: 8 risks related to clients, 8 related to designers, 39 related to contractors, 4 related to sub-contractors/suppliers, 5 related to government bodies, 5 related to superintendents, 16 related to external issues. After the analysis of the questionnaire survey, it is found that out of 85 risks many were repetitive and the count was cut down to 25 after the filtration. On the basis of the analysis of the survey following risks were found in China construction industry (Figs. 1 and 2).

The risks from a previous year's research paper in the sector of construction have been identified in the international construction market and compared to that
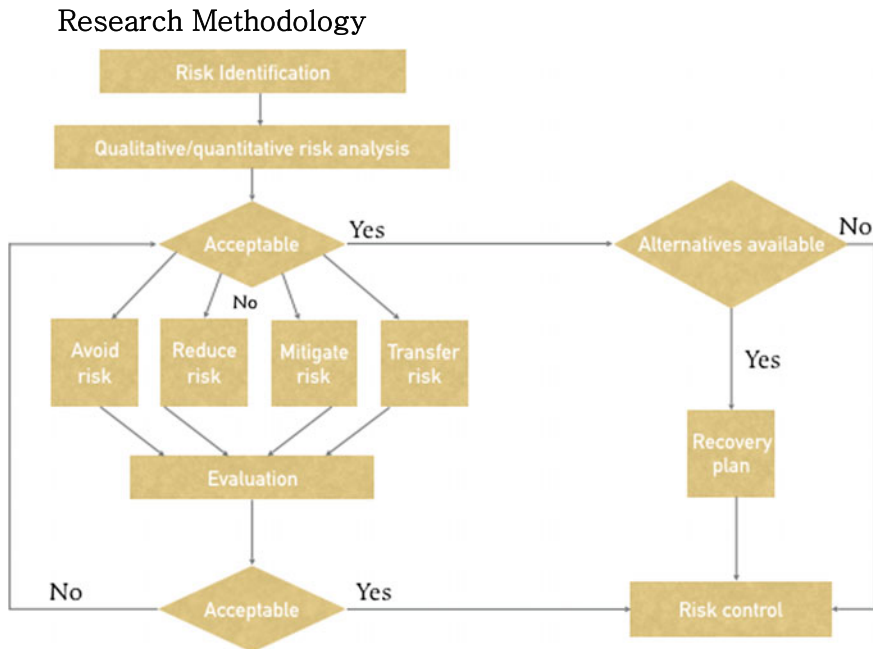
Fig. 1 Project risk management process

Fig. 2 Risk management
flow chart

of the Indian industry of construction which was found through an interview. It was
observed that the labourers have the maximum impact on the construction projects
globally. Their quality of workmanship, their capabilities and availability have a vital
role to play in minimising the risk impact globally. After which project feasibilities
related risks have an effect on the project if not performed with accuracy [28–31].

4   Results and Discussion

Risks related to plant and machinery, funds of the project, quality and competency of
contractors and government policies were the global risk factors. And various other
risks associated with client, contractors, sub-contractors, suppliers and government
had an effect on the construction projects globally. The project should have a man-
agement plan for risks right from the beginning in order that the identified risks could
be evaluated properly so that the proper plan for risk response could be made and
implemented at the right time (Fig. 3).

By using a risk management assessment techniques like PERT, Monte-Carlo Sim-
ulation, etc. appropriate strategy could be adapted to identify whether the risks could
be avoided or not, is reducible or not, transferable or not and can be mitigated or
not. If these strategies do not work, then again the analysis of risk is performed. The
proper plan should be made and implemented in the project right from the feasibility

Fig. 3 Representation of new risks factors

stage to the construction phase so that the risks related to client, contractors and other stakeholders could be reduced.

In order to make the construction project safe appropriate policy of insurance could be taken so it can act as a risk transfer tool in case of any mishappening or the failure of the project.

4.1   Limitations of the Study

Since the construction industry is very vast and is fragmented in nature so many new risks can arise during the project depending on multiple factors such as force majeure, unknown risks, risks related to political issues, government policies, etc., so with every new different risk different solution or mitigation strategies are to be proposed. And the risk is a vast field in itself and there are no appropriate risk assessment techniques which can identify all the risks integrated into the project [32–34].

Ethical approval: "*For this type of study formal consent is not required.*" In the present research there is no direct involvement of human/respondents. All the data were collected using structured questionnaire survey and there is no test/procedure/observation is conducted with the respondents while collecting the data.

Informed consent: "*Informed consent was obtained from all individual participants included in the study.*" A statement of formal consent was added in the introductory part of the questionnaire while sharing with the respondents.

References

1. Factor, R., PROJECT MANGEMENT PLAN EXAMPLES Prepare Project Support Plans and Documentation—Project Risk Assessment Examples, pp. 3–5.
2. Alkaf, N., Karim, A., Rahman, I. A., Memmon, A. H., & Jamil, N. (2012). Significant risk factors in construction projects: Contractor's perception. *IEEE Colloquium on Humanities, Science and Engineering*, 351–354.
3. Zou, P. X. W., Zhang, G., & Wang, J. (2007). Understanding the key risks in construction projects in China. *International Project Management, 25*(6), 601–614.
4. Renault, B. Y., & Agumba, J. N. (2016). Risk management in the construction industry: A new literature review. *MATEC Web Conferences* (Vol. 66, p. 00008).
5. Rezakhani, P. (2012). Classifying key risk factors in construction projects. *Bulletin of the Polytechnic Institute of Jassy, Construction Architecture Section, 62* (2), 27–38.
6. Jayasudha, K., & Vidivelli, B. (2016). Analysis of major risks in construction projects. *ARPN Journal of Engineering and Applied Sciences, 11*(11), 6943–6950.
7. ISO 31000. (2009). ISO 31000:2009 Risk management—Principles and guidelines. *Risk Management, 31000,* 24.
8. Pawar, A., & Pagey, P. S. (2017). Survey and analysis of risk management in building construction work. *International Journal of Research in Engineering and Technology, 4*(4), 2297–2299.
9. Goji Tipili, L., & Ibrahim Yakubu, P. (2016). Identification and assessment of key risk factors affecting public construction projects in Nigeria: Stakeholders perspectives. *International Journal of Engineering and Advanced Technology, 4* (2), 20–32.
10. Zou, P. X. W., Zhang, G., & Wang, J. (2012). *Identifying key risks in construction projects: Life cycle and stakeholder perspectives* (pp. 1–14). Sydney: University of New South Wales.
11. Ashly Babu, M., & Kanchana, S. (2014). Role of insurance in construction and infrastructure projects. *Proceedings of the International Conference on Emerging Trends in Engineering and Management*, pp. 30–31.
12. Built, T., & Review, H. E. (2011). Construction risk modelling and assessment: Insights from a literature review. *The Built and Human Environment Review, 4*(1), 87–97.
13. Renuka, S. M., Umarani, C., & Kamal, S. (2014). A review on critical risk factors in the life cycle of construction projects. *Journal of Civil Engineering Research, 4*(2A), 31–36.
14. Mishra, S., Mishra, B., & Professor, A. (2016). A study on risk factors involved in the construction projects. *International Journal of Innovative Research in Science, Engineering and Technology* (*Monthly Peer Reviewed Journal*), 5 (2), 1190–1196.
15. ASSOCIAÇÃO DE GERENTES DE SEGUROS E RISCOS (AIRMIC). (2002). A Risk Management Standard AIRMIC. *Airmic, 57*(2), 1–6.
16. Akintoye, A. S., & MacLeod, M. J. (1997). Risk analysis and management in construction. *International Journal of Project Management, 15*(1), 31–38.
17. Sathishkumar, V., Ragunath, P. N., & Sugana, K. (2015). Critical factors influencing financial risk in construction projects. *The International Journal of Applied Engineering Research, 10* (3), 7033–7047.
18. BSI. (2012). ISO 21500:2012—Guidance on project management. *BSI Standard Publications.*
19. Sohrabinejad, A., & Rahimi, M. (2015). Risk determination, prioritization, and classifying in construction project case study: Gharb Tehran commercial-administrative complex. *Journal of Construction Engineering, 2015,* 1–10.

20. G. E. T. T. Book, *The Owner's Role in Project Risk Management*. 2005.
21. Desai, A., & Kashiyani, B. Role of Insurance As a Risk Management Tool, pp. 1–8.
22. Banaitiene Nerija, B. A. (2012). Risk management in construction projects. *Risk Management - Curr. Issues Challenges*, 429–448.
23. BS 6079, Project Management. *Br. Stand.*, no. September, 2000.
24. Humphreys, E. (2010). *Information Security Risk Management Handbook for ISO/IEC 27001*.
25. Dixit, S., Singh, S., Singh, S., Varghese, R. G., Pandey, A. K., & Varshney, D. (2018). Role of Solar energy and issues in its implementation in the Indian context. In *MATEC Web of Conferences* (Vol. 172).
26. Singh, S., Dixit, S., Sahai, S., Sao, A., Kalonia, Y., & Subramanya Kumar, R. (2018). Key benefits of adopting lean manufacturing principles in Indian Construction Industry. In *MATEC Web of Conferences* (Vol. 172).
27. Singh, A., Agarwal, P., Dixit, S., Singh, S., & Sahai, S. (2018). The transition towards sustainable supply chain management: An empirical study. In *MATEC Web of Conferences* (Vol. 172).
28. Dixit, S., Mandal, S. N., Thanikal, J. V., & Saurabh, K. (2018, July). Construction productivity and construction project performance in Indian Construction Projects, pp. 379–386.
29. Singh, S., Bala, A., Dixit, S., & Varshney, D. (2018). Critical analysis of causes of delay in residential construction projects in India. *International Journal of Civil Engineering and Technology, 9* (1), 330–345.
30. Sao, A., Singh, S., Dixit, S., Pandey, A. K., & Singh, S. (2017). Quality, productivity and customer satisfaction in service operations: An empirical study. *International Journal of Mechanical Engineering and Technology, 8* (10), 579–596.
31. Singh, S., Dixit, S., & Varshney, D. (2018). Sustainable construction management in education sector, *7*(2), 300–304.
32. Dixit, S. (2018, November). Analysing enabling factors affecting the on-site productivity in indian construction industry. *Periodica Polytechnica Architecture, 49*(2), 185–193.
33. Dixit, S., & Saurabh, K. (2019, April). Impact of construction productivity attributes over construction project performance in Indian construction projects. *Periodica Polytechnica Architecture, 50,* 89–96.
34. Dixit, S., Mandal, S. N., Thanikal, J. V., & Saurabh, K. (2019). Evolution of studies in construction productivity: A systematic literature review (2006–2017). *Ain Shams Engineering Journal, 10*(3), 555–564.

Building Information Model: A Graphical User Interface to Generate a Three-Dimensional Building

Trishala Daka and Venkata Dilip Kumar Pasupuleti

Abstract From the past few decades, Building Information Modeling (BIM) has been evolving to become one of the robust domains connecting different dimensions from Architecture, Engineering and Constructions. Even though it started to take over a large part of the globe in understanding various components of structure, it is yet to reach a common person for generating a 3D building for a given area. In this study, a three-dimensional graphical user interface is developed to generate a 3D building from given parameters such as height of each floor, number of bays in each direction, dimensions of major structural elements and information related to windows and doors. The future work of this tool is to give different three-dimensional structures for any given plan including its analysis, design and material quantities at any location of the globe considering local structural types with inclusion of structural standard codes.

Keywords Building Information Model (BIM) · 2D plans · 3D building modeling · MATLAB · Graphical user interface

1 Introduction

Earlier contractors and designers used to face a lot of complications during the construction or after the completion of the project like failure or tilting of the structure even though they were designed very well and perfectly executed according to the plan. These occur due to the misinterpretations during the design period of the structure. So, from the past few years to overcome such incidents many companies in Architecture, Engineering, and Construction industry have realized major IT-based change processes in their operations [1]. These technologies, commonly referred to as Building Information Modeling (BIM), are emerging with IT-based information

T. Daka (✉) · V. D. K. Pasupuleti
Mahindra École Centrale, College of Engineering, Hyderabad, Telangana, India
e-mail: trishaladaka@gmail.com

V. D. K. Pasupuleti
e-mail: venkata.pasupuleti@mechyd.ac.in

systems which promote collaborative and integrated design, assembly, and operation of buildings. BIM can be best termed as a platform of IT tools engaged to design virtual models working to present all physical and functional characteristics of a building [2]. After the development of BIM which has complete details of the building, researchers have started to focus more on detailing or information towards a structure or building. For example, regular computer-aided design software imitates traditional hand drafting, in which drawings are almost in 2D, with lines and arcs signify objects in floor plans, elevations, framing plans and details [3]. In late 1980s, a completely different kind of design software was developed. Instead of imitating hand drafting, it uses 3D models to represent the real-world structures that makeup buildings, such as the walls, floors, windows, and doors. In fact, a true BIM model consists of the virtual and essential equivalents of the actual building segments that are used to complete a building. The digital 3D model not only contains architectural data but also has information regarding physical and functional characteristics of the traditional building elements such as walls, columns, doors, staircase, etc. If there are any modifications in any of these structural elements, each section view, elevation, floor plan will be automatically updated with the new change in the model. This allows the engineers to understand and simulate the structures even before the construction initiates. Junang and team had developed software to reconstruct 3D buildings from 2D vector floor plan [4, 5]. But till now there has not been enough research on building a BIM tool for a common person who can see complete three-dimensional building from a simple input of area and location of the built area. This research mainly focuses to develop a graphical user interface where a common person can enter the details of the plot area and its location irrespective of the geographical boundaries, and the developed tool will be able to suggest a user with wide varieties of the building types based on the location. And when the building type is selected the user would be able to see the complete three-dimensional building, with the analysis and design results. This should be able to give quantity estimation with approximation pricing of the selected structure. In this paper a very fundamental graphical user interface developed is presented which can develop a complete three-dimensional building with certain input parameters from the user. The study will be carried out further in the future to build a complete tool that can be used by any common person for building their dream houses.

2   Background

Currently, in most of the developed tools architectural drawings are either scanned or imported to develop a three-dimensional plan. Dosch presented a system for the analysis of architectural drawings by dividing the whole area into tiles, and each of them being processed and analyzed independently [5]. Ahmed and their team converted the raster image into vector image except [6] which proposed directly on the raster image or proposed a highly automated approach to generate 3D plans from a 2D floor plan assuming polylines to a wall [7]. Kishen devised a 3-Phased recognition

approach to generate a 3D building from a 2D floor plan assuming closed boxes as walls [8]. Park suggested a method to identify main walls based on extension line [9]. Zhu had provided a detailed review on techniques that were used to convert floor plans to buildings. In their paper, they have discussed a new reconstruction method for a 3D building from 2D vector plans [10]. From 2D drawings it is difficult to visualize the space management and for this difficulty, BIM helps to select the appropriate designs. According to a report from McGraw Hill Construction regarding the extension of BIM in the infrastructure in recent years, about 31% are using BIM on 75% or more of their projects in the year 2013 and in 2009 it was 7%. The percentage that is not using BIM on 25% or less of their projects was rapidly decreased from 73% in 2009 to 21% in 2013 [11]. Implementing the BIM does not simply create the production of construction but also operates as a support to the results from design and structural analysis to contribute to keep the data at one location. With the current technology it would be possible to add an additional segment to BIM where a user can just enter the details of area and location to visualize the structure, which is developed based on the local conditions (for instance, if the specific location is earthquake-prone) and this study focuses towards that.

3   Components of BIM

There are majorly four components of BIM, Planning, Designing, Analysis, and Implementation. Even though the current section is in generic with BIM tool but it is background for development of this tool. And the details of four components have been detailed.

3.1   Planning, Design, Analysis and Implementation

The developed tool should be able to plan the structure depending on the availability of local materials and geographical location.

- Quantify: To express the cost of members or elements used BIM collects and counts the amount of members.
- Qualify: The status of any member can be identified by using BIM. This means that it provides information about the behavior of the member and if it is fabricated.

The design is governed by the vision of the user and it is a process which may change due to constraints.

- Specify: The designer has to identify the needs and select members according to the requirement. Similarly, BIM generator determines if there is a need for a specific element.
- Arrange: BIM places the selected element in a pre-determined location. So BIM produces results according to the user's requirement.

- Scale: BIM determines the size and magnitude of the element which is specified.

The viability of a member is determined by analysis. BIM examines and evaluates the results obtained. There are different types of analysis like energy analysis, structural analysis, lighting analysis, mechanical analysis.

- Coordinate: The members designed have to be effective and should work in conjunction with one another. This relationship is ensured by BIM. This helps achieve the design purpose of various elements during design, co-ordination, fabrication, and installation.
- Simulate: BIM predicts the future performance of members and elements used. This helps the user in understanding how the structure works in longrun.
- Check: BIM validates information of members. This also includes checking information for accuracy and assures that it is rational and reasonable.

The information obtained from BIM is used to construct members accordingly. It is this ability that eventually leads to the increased efficiency of construction

- Fabricate: Using the information obtained, the user has to manufacture members. BIM can generate models to fabricate replacement parts that can be used in future.
- Assemble: The different members manufactured are to be brought together and assembled. The inaccuracies thus occurring will be minimal as it eliminates manual errors.

4 Flowchart

Figure 1 explains the flow chart of the methodology carried for this study.

Requirements and inputs are taken from the user and are given a shape through 2D drawings. Second, these drawings are developed to 3D digital models using image processing. The user is given a choice depending on the feasibility of construction of the structure in that particular area. The challenges in each case are discussed to identify why it is worth analyzing. The disadvantages of each scenario have to be identified and addressed along with the main problem. This process will reveal the innovation of the project. The third part of the study will adopt a strategy to overcome these challenges. Conclusions are made and final detailed drawings are submitted to the end user. With the known land area and user requirements, 2D drawings are obtained and 3D digital model is generated with variations in the structural elements (like roof with slope or flat, height of individual areas, etc.). This is followed by analysis using stiffness matrix method and design details. To make the study simple and understanding, the flow chart is divided into three parts.

Fig. 1 Work flow of the project
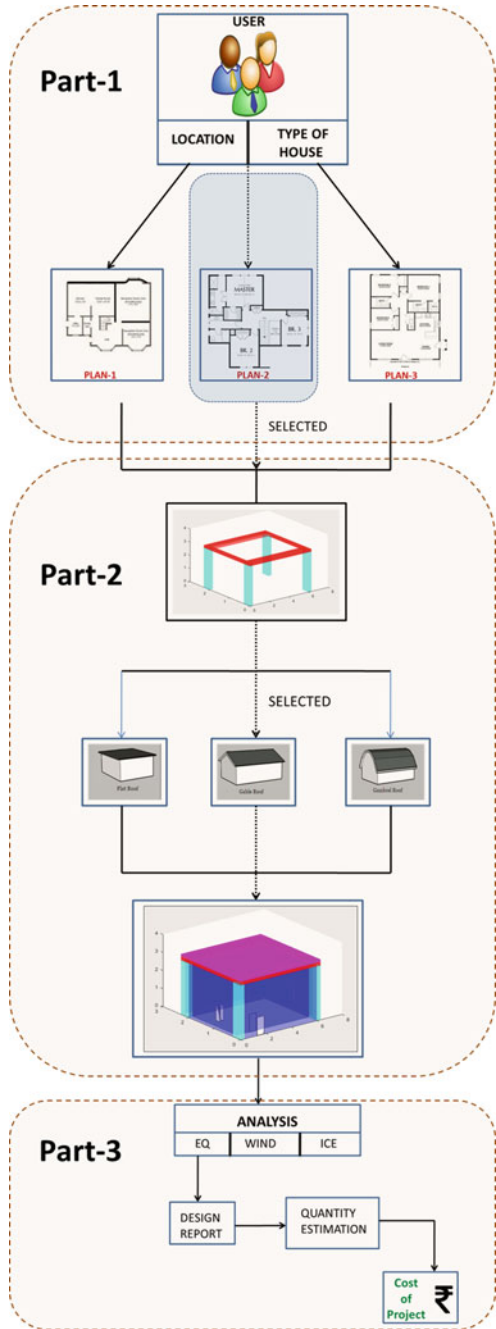
4.1 User

As per the prerequisites of the user such as location, type of house and aesthetic appeal, a different 2D plan is provided in order to congregate these requirements. Depending on plot area and constraints most appropriate plan is selected.

4.2 Generation of Three Dimensional Building

From the scanned image of the plan using image processing technique, basic 3D structure is developed. Based on the preferences of the user, the roof of the building is selected and all the structural elements are added to the building. At this stage, final 3D structure is obtained with all the specifications.

4.3 Analysis, Design, and Estimation

This 3D model is further analyzed where the structure is subjected to different loads such as earthquake, wind and snow and their combinations depending upon the geographical conditions. Modifications are made to the final structure as per the analysis report. Design details of the structure are provided followed by quantity estimation of the building to know the capital required for total construction. Final designs and estimations are put forth to the user.

5 Modeling

This paper presents preliminary results obtained from a developed code for a single bay structure with the inputs such as height of the structure, column and beam dimensions, etc. For this purpose, MATLAB GUI platform was utilized for its ease. Generally structures are modeled with three basic geometries point, line and areas. By connecting these areas, a closed structure in 3D is formed. For any point, 3 coordinated are defined in three-dimensional space. Assuming the first point to be a (x, y, z) and connecting this point with another point b (x_1, y_1, z_1), a line is formed. Connecting four such lines, a surface (rectangle) is generated and grouping these surfaces gives a 3D model. Structural bay is the span from one vertical element to the immediate adjacent vertical element. A bay consists of four columns, four beams, slab, walls, door, and window.
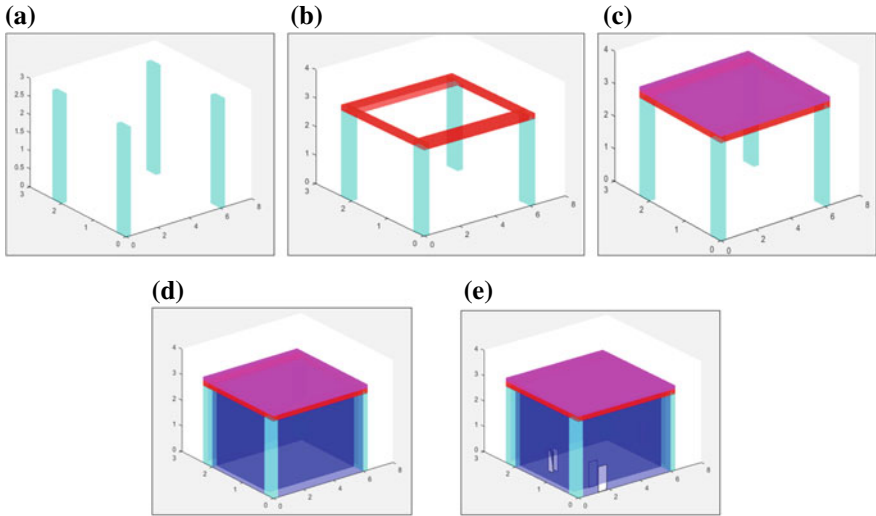
Fig. 2 **a** Generation of column elements, **b** Generation of beams over columns, **c** with beams and columns, **d** Walls with slab, beams and columns and **e** Door and Windows with walls, slab, beams and columns

5.1 Columns

With reference to Fig. 2a, first column is at the origin. The coordinates of the second column are obtained by shifting the coordinated of the first column in y-direction. Similarly, the third and fourth columns are obtained by shifting the first column in x and y direction respectively.

5.2 Beams

Beams are situated on the tops of the columns. Each beam is supported at either ends by two columns. With the co-ordinates of the top surface of the columns known, by connecting the required points, the bottom surface of the beam is formed. These coordinates are then shifted in the z direction to obtain the beam. Similarly, the remaining three beams are obtained as seen in Fig. 2b.

5.3 Slabs

Slab is located on the top of four beams. By connecting the corners of the four beams, the outline of the bottom surface of the slab is obtained. The slab is completed by shifting the coordinates in z direction and generated slab is shown in Fig. 2c.

5.4 Walls

Walls are situated in between the columns. To get the wall, the points are connected such that the surfaces formed will cover the empty space between the columns as shown in Fig. 2d.

5.5 Doors and Windows

Doors and windows will be on the walls or practically in between the wall, so the coordinated of the four points forming the wall should be identified to form a small surface. These coordinates are then reduced in respective directions to form doors or windows based on the requirement from the user. And single-bay developed three-dimensional model can be seen in Fig. 2e.

6 GUI Developed and Case Study

This paper presents a three-dimensional developed Graphical User Interface and this section shows the arrangement of edit boxes and push-buttons. In the Panel 'Geometry of BAY', details such as length, breadth, and height of bay of the structure are taken as input from the user, where as in 'Geometry of column', dimensions of the column are specified. Then within the 'Geometry of Beam', height of the beam is given in the direction of gravity. And as slab is an area, which has been created on beams, only the thickness of the area is provided, which is shown in different colors of the GUI presented. Representation of Door and Window requires distance between column and the door or window, height and breadth, so the same has been defined in the GUI. And the additional requirement for window is the distance from the bottom of the column. All the requirements can be seen clearly in Fig. 3. It represents the basic and preliminary results obtained.
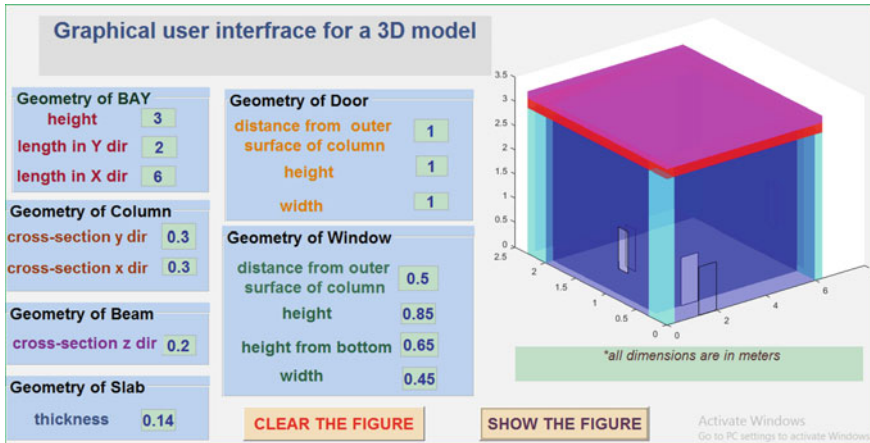
Fig. 3 Developed GUI tool in MATLAB

7   Conclusions and Future Work

Conclusions of the current study are, with the currently available computer programs and hard work, it is not a very difficult challenge to develop a tool which can generate the complete three-dimensional structures with all the details. And the future work of this study will be (i) taking input as area from the user and providing the user with different plans or directly taking the scanned image of the plan is the user already has one, (ii) generating the three dimensional building which has already been developed and showcased in this paper, (iii) doing complete analysis and design based on geographical location, (iv) developed tool will be able to generate 2D and 3D diagrams of complete designs which can be understood by any common person or user. All the above work has its own challenges, which will be discussed in the extension of this paper.

References

1. Gal, U., & Jensen, T. (2008). Organizational identity and the appropriation of information systems. *ICIS 2008 Proceedings*, pp. 305–308.
2. National Institute of Building Sciences. (2007). Washington, DC: United States National Building Information Modeling Standard-Final Report.
3. Ralph, G. (2010). *CAD and BIM-Is there a free pass*. A Report on Graphis of ArchiCAD's DWG workflow.
4. Zhu, J., Zhang, H., & Wen, Y. (2014). A new reconstruction method for 3D buildings from 2D vector floor plan. *Computer-Aided Design and Applications, 11*(6), 704–714.
5. Dosch, P., & Masini, G. (2005). Reconstruction of the 3D structure of a building from the 2D drawings of its floors. *Proceedings of the Fifth International Conference on Document Analysis and Recognition*, pp. 487–490.

6. Ahmed, S., Liwicki, M., Weber, M., & Dengel, A. (2011). Improved automatic analysis of architectural floor plans. *International Conference on Document Analysis and Recognition (ICDAR)*, pp. 864–869.

7. Or, S., Wong, K. H., Yu, Y., Chang, M. M., & Kong, H. (2005). Highly automatic approach to architectural floor plan image understanding and model generation. *Proceedings of the Vision, Modeling, and Visualization Conference*, pp. 723–734. IOS Press.

8. Moloo, R. K., Sheik Dawood, M. J., & SalmaanAuleear, A. (2011). 3-phase recognition approach to pseudo 3D building generation from 2D floor plan. *International Journal of Computer Graphics & Animation, 1*, 13–27.

9. Park, J., & Kwon, Y. B. (2004). Main wall recognition of architectural drawings using dimension extension line. In J. Lladós & Y. B. Kwon (Eds.), *Graphics Recognition, Recent Advances and Perspectives*. GREC 2003. Lecture Notes in Computer Science, Vol. 3088. Springer, Berlin, Heidelberg.

10. Zhu, J., Zhang, H., & Wen, Y. (2013). *A new reconstruction method for 3D buildings from 2D vector floor plan. Computer-aided design and applications*. Lombardy, Italy.

11. Hunt, C. A. (2013). *The benefits of using building information modeling in structural engineering*. Utah: Utah State University.

Lateral Response Reduction of Tall Buildings Using Portal Frame as TMD

Raaga Varshita Chilakalapallii, Priyanka Palvai, Eshwar kuncham and Venkata Dilip Kumar Pasupuleti

Abstract Majority of construction industries are aiming to go for taller and lighter buildings which may result in flexible and slender structures. Hence serviceability and safety become a critical issue during the occurrence of heavy winds and high magnitude earthquakes. Therefore, considerable techniques are adopted to minimize the vibrations caused by these natural responses of the structures. One of the techniques used prominently for tall structures is Tuned Mass Damper (TMD). TMD's have been very effective in controlling structural vibrations. This study proposes a detailed analysis of a 2D frame structure with a TMD system placed at different levels of the structure in order to evaluate the behaviour of structure for given earthquake ground motions. The results obtained indicate installation of simple frames can decrease the response of the structure during an earthquake and location of TMD is also discussed in detail.

Keywords TMD- tuned mass damper · Damping · And vibration control

1 Introduction

A growing population and advancement in technology have led to the evolution of new construction techniques which focuses on alternatives to reduce the damage caused to the structure due to heavy winds and seismic loads. Size and density of the cities influence the height of the building hence taller structures are majorly adopted

R. V. Chilakalapallii · P. Palvai · V. D. K. Pasupuleti
Mahindra Ecole Centrale, College of Engineering, Hyderabad, Telangana, India
e-mail: varshita14231@mechyd.ac.in

P. Palvai
e-mail: priyanka14134@mechyd.ac.in

V. D. K. Pasupuleti
e-mail: venkata.pasupuleti@mechyd.ac.in

E. kuncham (✉)
Indian Institute of Technology Patna, Patna, India
e-mail: eshwar.research@gmail.com

by many of the construction industries. However, taller structures are sensitive to wind and seismic excitations. These excitations can cause large displacements in the structures such that they fail to satisfy the serviceability criteria. Therefore, to reduce these structural responses in tall structures different types of damping systems are used. Dampers act as shock absorbers. Base isolation is ideal for short structures which tend to undergo shear failures during an earthquake. The most commonly used base isolation units used in the construction are laminated rubber bearing. These bearings are made of alternative layers of vulcanized rubber and steel [1]. But this phenomenon doesn't give effective results for high rise buildings. The concept of tuned mass damper (TMD) was evolved and first suggested by Frahm in 1909 to enervate unenviable vibrations in ships. The device predominantly consists of a mass (m), spring (k) and damping devices (c). The device is mounted on the structure to avert the failure of building [2]. The working principle of TMD is when building begins to oscillate, it sets the TMD into motion by means of spring, when building sways to the right side, and consequently the TMD sways to left side in order to narrow down the excitation of structure.

A TMD is naturally tuned to the first natural frequency of the structure. The energy dissipation effectiveness of a TMD depends on (a) The accuracy of its tuning, (b) Mass of damper compared to modal mass of its target mode and (c) Extent of internal damping built-in TMD [3]. The main advantage of incorporating TMD in tall structures is they don't need any external power sources for their operation, unlike other dampers. TMD's are easy to maintain and also respond small excitations. Few other dampers used in structures for the controlling of the wind and seismic excitations are Tuned Liquid Column Dampers (TLCD), Pendulum modelled TMD, Viscous dampers, etc.[4]. TLCD was proposed by sakai [5] to test the vibrations induced by wind and seismic excitations in the structure. The efficiency of TLCD depends on tuning the frequency of TLCD with respect to the frequency of structures.

The viscous damper for structures is similar to the shock absorber on an automobile but operates at a much higher force level [6]. It is constructed of stainless steel. Pendulum Tuned Mass Dampers (PTMDs) are substituted with a translational spring and damper system with a pendulum, it comprises of a mass sustained by a cable which pivots about a point. They are often designed as a simple pendulum [7]. Even slight angular oscillations make the PTMD act similar to a translational. It is preferred over the translational TMD system because of the absence of any type of bearings. PTMDs are economical, adaptable and easy to maintain. PTMD is implemented in Taipei 101 tower in Taipei and Crystal Tower in Osaka [8].

2 Existing TMD's

2.1 One Wall Center, Sheraton Vancouver, Canada

One Wall Centre is a skyscraper hotel opened in Vancouver's downtown. The building is of 157.8 m height above the ground level and extends up to 4 floors below the ground level [9]. As the building is tall and slender wind tunnel tests signified that storm winds approaching in the vicinal of the building would sway the structure. Therefore, a conventional technique is followed to minimize the displacements without changing the mass and stiffness of the structures; the structure is connected to a damper which functions as a shock absorber.

Two water tanks each with 16 m long × 4.5 m wide × 8 m tall and each tank designed with a capacity of 50,000-imperial-gallon are installed as a pendulum modelled Tuned Water Damper in the building. The frequency of the splash of the water in the tanks counteracts the frequency of the swaying of the building. Therefore, when the building proceeds to sway under wind loading, the water moves to and fro transmits its momentum to the structure and restrains the effects of wind vibration.

2.2 Taipei 101 Tower, Taipei

The Taipei 101 is an iconic super-tall structure. The structure used high-performance steel and concrete in its construction. Besides five basement levels, It also comprises of 101 floors above ground. Outrigger trusses were installed at eight-floor intervals, which joins the columns in the building's core to those on the exterior. These components made Taipei 101 one of the most stable buildings. It is located just above 201.16 m from a major fault line, as a result, it is viable to earthquakes, and even stormy winds are common in this area of the Asia-Pacific. Therefore, to attain stability and lessen the impact of violent motion engineers had to design a gigantic TMD that could withstand gale winds up to 216 km/h and the strongest earthquakes.

It's basically an enormous weighted ball of 728 tons steel pendulum that serves as a TMD, which is placed on hydraulic cylinders and counteracts the building's movement. The TMD system is suspended from the 92nd to 87th floor with the design of the simple pendulum. And this pendulum oscillates to counterbalance movements triggered in the building by strong gale. The dimensions of the sphere are 5.48 m in diameter, comprising 41 circular steel plates of varying diameters, each 0.125 m thick, welded together to form a 5.5 m diameter sphere. Two additional TMD's, each weighing 6 tones, are installed at the tip of the spire which halts the damage to structure due to strong wind loads [10].

2.3 Chiba Port Tower, Japan

Chiba Port Tower (125 m high) is a high-rise steel structure incorporated with steel-framed reinforced concrete construction. A two-mass model TMD is installed at the top of the tower to reduce the wind vibrations on the structure. The damper system consists of a mass of 15 tones, two frames overlapped at right angles, these frames can slide in X and Y direction with the help of roller bearings. These frames consist of coil springs and damping devices. The damping devices have a rotator in high viscosity liquid and produce a damping force by shearing the liquid.

The TMD is designed by setting the damper weight to 100th of the first mode of effective weight [11]. Thereby the TMD reduces the earthquake vibrations by 30% and wind vibrations by 10% effectively.

2.4 Chiba Port Tower, Japan

The Shanghai Center Tower (SHC) is a high-rise building with an elevation of 631.85 m. The design company stated that a building of this tall could be malleable to more than 1.524 m of sway during the typhoon conditions. In order to counterbalance its vibrations during wind storms, a new eddy-current TMD was stationed on the 125th floor.

Special protective appliances were blended to prevent excessively large amplitude motion of the TMD under extreme wind or earthquake scenarios. The damper is a 1000-ton weight is suspended with the aid of steel cables. TMD is incorporated with two systems (hydraulic rams, and a 'tuneable' self-generated magnetic field) which prevent the weight from moving too fast. The iron weight hangs above 10 m × 10 m copper plate, which is studded with 125 powerful magnets. As the iron swings over the magnets, it initiates electrical current in the copper plate, which is enough to limit the motion of the mass. The merit is in its simplicity, there's no necessity of power source, and is a completely a self-regulating system [12].

3 Numerical Formulation

The present paper is centred on an MDOF structural system interconnected with single TMD on top, an overture has been evolved to detect the optimum parameters of TMD placed in a multi-storied building for minimum top deflection caused by lateral excitation. Over the last few decades, considerable numbers of buildings were incorporated with TMD's all over the world.

3.1 Dynamic Analysis

The first step for performing a dynamic analysis is to set up the equations of motions and most basic is Newton's second law of motion which states that "the rate of change of momentum of a mass equals the force acting on it" [13] . Figure 1 shows steps involved in derivation of dynamic equation of motion with and without damper.

$$\frac{d}{dt} m (du/dt) = F(t) \tag{1}$$

If one affixes a spring and a damper to the mass, by postulating that the spring complies with Hooke's law and the damping is of viscous type (the damping force is proportional to the velocity of the mass), the equilibrium is formulated by summing up the terms of spring and damping-induced forces.

$$M\ddot{u}(t) + C\dot{u}(t) + Ku(t) = P(t) \tag{2}$$

where the dot over the symbol represents differentiation with respect to time t. M, C, K represents the mass, damping, and stiffness of the structure respectively.

Undamped Free vibration: During the initial excitation, when $P(t)$ and damping are zero the response is termed as free vibration.

From Eq. (1),

$$m\ddot{u}(t) + ku(t) = 0 \tag{3}$$

Linear, homogeneous second-order differential equation

$$\ddot{u} + \frac{k}{m} u = 0 \tag{4}$$

For notational convenience, let's assume
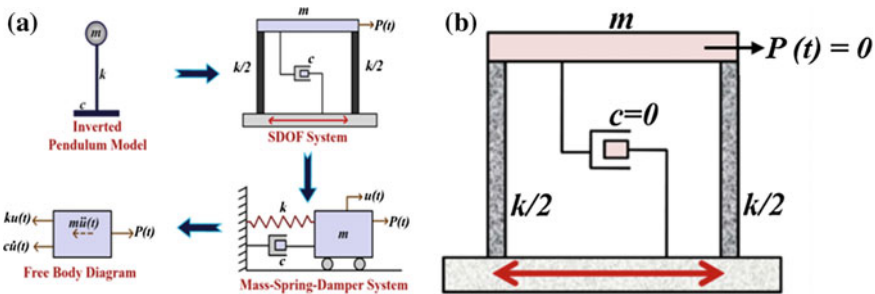
Fig. 1 **a** Equation of single degree of freedom system, **b** Undamped free vibration system

$$\frac{k}{m} = \omega^2 \text{ (Hence } \omega^2 \text{ is positive number).} \tag{5}$$

$$\frac{\mathrm{d}^2 u}{\mathrm{d}t^2} = -\omega^2 u \tag{6}$$

This is the differential equation for SHM. The sinusoidal solution for displacement of spring can be given by

$$x = A * \cos(\omega t) \tag{7}$$

where A is the amplitude of the motion and ω is the angular frequency.

$$\omega^2 = \frac{k}{m} => \omega = \sqrt{\frac{k}{m}} \tag{8}$$

3.2 Optimization Theory for TMD

Many studies have been carried out in the past to understand and determine the optimal parameters for a TMD under different kinds of excitations, to predict the vibrational behaviour of the main structures and assess the efficiency of the TMD contributions in terms of attenuating vibrations in the main structure. Outcome of few studies has clearly mentioned that usage of elastic body can be supplanted by an equivalent SDOF system for reduction of amplitudes during natural disasters. Provided that the frequencies of the elastic body are well distinguished and the damper response is majorly contributed by the fundamental mode.

In the damping of the main system, it is recommended that constrained damping of the main system has a very small effect on the TMD's optimal parameters. In real systems with light damping, if this frequency condition is satisfied, it is plausible to apply the optimal parameters of the TMD for the undamped equivalent system to lessen the dynamic response of the system.

Single Degree of Freedom System.
The equations of motion for an undamped SDOF system with TMD

$$M\_m\ddot{u} + K\_mu + c\_a\dot{u} + k\_au - c\_a\dot{u}\_a - k\_au\_a = p(t) \tag{9}$$

$$m_a\ddot{u}_a + c_a\dot{u}_a + k_au_a - c_a\dot{u} - k_au = 0 \tag{10}$$

where M, K, U represents mass, stiffness, and displacement, respectively, whereas m and a refers to the parameters of structure and TMD, respectively.

If harmonic forces act on the system, then $p(t) = pe^{i\omega t}$. Therefore, the displacement of the main system can be reduced if the vibration of system is with its natural

Fig. 2 Schematic diagram of SDOF with TMD
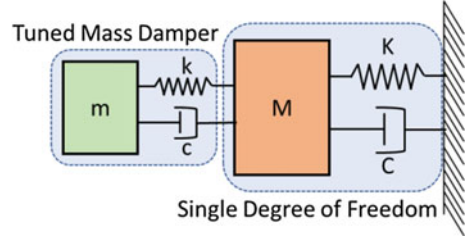
frequency, schematic diagram of SDOF with tuned mass damper is shown in Fig. 2.

$$u = \frac{(k_a - m_a\omega^2 + i\omega c_a)pe^{i\omega t}}{(K_m + k_a - M_m\omega^2 + i\omega c_a)(k_a - m_a\omega^2 + i\omega c_a) - (k_a + i\omega c_a)^2} \tag{11}$$

Velocity of the system is

$$\dot{u} = \frac{(k_a - m_a\omega^2 + i\omega c_a)i\omega pe^{i\omega t}}{(K_m + k_a - M_m\omega^2 + i\omega c_a)(k_a - m_a\omega^2 + i\omega c_a) - (k_a + i\omega c_a)^2} \tag{12}$$

Acceleration of the system is

$$\ddot{u} = \frac{-\omega^2(k_a - m_a\omega^2 + i\omega c_a)pe^{i\omega t}}{(K_m + k_a - M_m\omega^2 + i\omega c_a)(k_a - m_a\omega^2 + i\omega c_a) - (k_a + i\omega c_a)^2} \tag{13}$$

Mass ratio:

$$\mu = m_a/M_m \tag{14}$$

Tuning ratio:

$$f = \omega_a/\omega_m \tag{15}$$

$$\omega_a^2 = \frac{k_a}{m_a} \tag{16}$$

$$\omega_m^2 = K_m/M_m \tag{17}$$

Forced frequency ratio:

$$r = \omega_a/\omega_m \tag{18}$$

Absorber damping ratio:

$$\gamma_a = c_a/2m_a\omega_a \tag{19}$$

$P(t) = $ Force vector

$$m_a Z_{jr} \ddot{u}_a + c_a Z_{jr} \dot{u}_a + k_a Z_{jr} u_a - c_a Z_{jr} \dot{U}_j - k_a Z_{jr} U_j = 0 \qquad (20)$$

Z is the matrix of orthogonal characteristics modes of the system and Z_r is the vector of the rth
Mode,

$$Z_r = \left(Z_{1r}, Z_{2r}, \ldots, Z_{jr}, \ldots, Z_{nr} \right)^T \qquad (21)$$

4   Numerical Modelling

Initially, a two-Dimensional 15 storey structure is modelled using ETABS as shown in Fig. 4. Respective dimensions for the structure are assigned based on Table 1. Modal analysis has been carried out. The time period of the structure is found to be 1.141 cycles/sec. Using trial and error basis, a single portal frame is analysed to get same frequency of the structure. This portal frame is mounted on the top of 15th storey and time history analysis is carried out. Same procedure is followed with TMD on different floors of the structure. For the next trial, the dimensions of the portal frame are changed to 5 m (beam) × 2 m (column) and made sure that its frequency matches with 15 storey structure. Portal frame is mounted on various floors of the structure and checked for the minimum response. Similarly, same procedure is carried (for both the portal frames) by placing the portal frame in inverted position.

Table 1 Geometry and material property of 2D framed structure

Property	Dimension
Structure Column dimension	450 mm × 300 mm
Structure Beam dimensions	300 mm × 300 mm
Column dimensions of TMD	161 mm × 161 mm
Beam dimensions of TMD	1324 mm × 1324 mm
Grade of Concrete	M 25
Rebar's	HYSD 415
Height of storey	3 m

5 Case Study

5.1 System Model

The 15 storey structure consisting of rigid floors and beams which are supported by deformable columns is modeled with uniform bay with 3 m. All the numerical models presented in this study are developed using commercially available ETABS software. And natural period of 15 storey structure 1.141 s.

The joints at the base of the structure are restrained to rotation and translation in both x and y directions. The designed TMD is tuned to the same natural frequency of the building and installed on the building.

Case 1. Erected TMD system of height 2 m installed on top of slab. In this study, a TMD of column and beam length of 2 m specified in Table 1 is placed at 15th, 14th and 13th storey of building as shown in the Fig. 3a.

Case 2. Inverted TMD system of height 2 m: In this case the TMD is placed in an inverted position and analysis is carried. The same TMD dimensions mentioned in the Table 1 are considered.

Case 3. Erected TMD system of height 5 m installed on top of slab: In this case, the column length of the TMD is increased to 5 m and the dimensions of the column and beam of TMD remain same as mentioned in Table 1.

Case 4. Inverted TMD system of height 5 m: In this case, we have placed the TMD inverted at 13th, 14th and 15th storey as shown in fig i, ii and iii, respectively. The dimensions of TMD are unchanged.
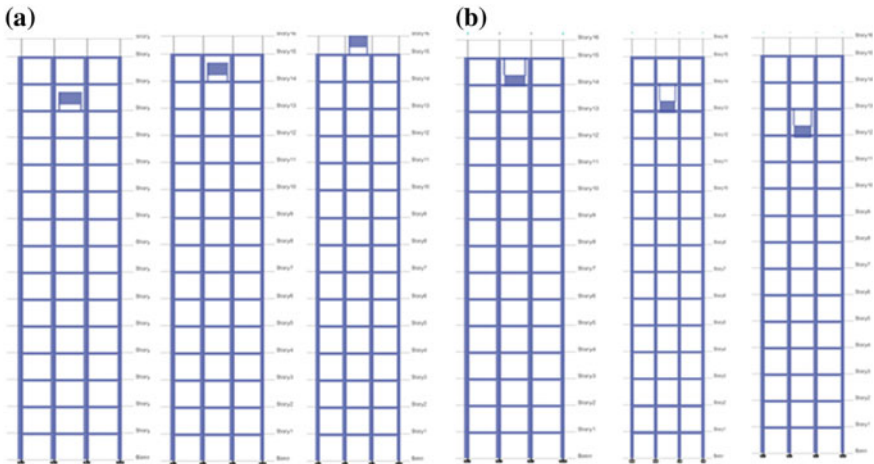
Fig. 3 **a** Installation of TMD on 13 th, 14th, 15th floor, **b** Installation of inverted TMD on 15th, 14th, 13th floor

6 Results

A parametric study for installation of TMD at three different heights is carried to understand the response of the structure.

6.1 Model Analysis

Structural displacement response is compared with and without TMD and for the same plots have been plotted in Fig. 4. It is observed that the response of the structure having the TMD decays faster than that of without TMD. It is observed that when the TMD is placed over the 14th storey, the structural response to the applied ground motion is less when compared to the responses of the building with TMD installed at 12th or 13th storey of the structure.

6.2 Dynamic Analysis

To analyse the 2D frame EL CENTRO (Centro 1940 North–South Component, Peknold Version) earthquake ground motion with a scale factor of 10 with equal time interval of 0.02 s. Figure 5 shows the comparisional time history for various scenarios. Maximum seismic response reduction is found when TMD of height 5 m is erected of 14th storey of the structure. Comparably from the analysis and results obtained, erected portal frame TMD is more effective than inverted portal frame TMD model.

7 Conclusion

This study indicates using a portal frame as TMD can be very effective in controlling vibrations of structure due to seismic or high wind loads and few major observations of this research work are give as follows:

i.   Portal frame in the structure is more effective TMD than on the top.
ii. Inverted TMD's are observed to be more efficient in reducing the lateral vibration.
iii. Location of the TMD has greatly affected the vibration behavior of the structure.
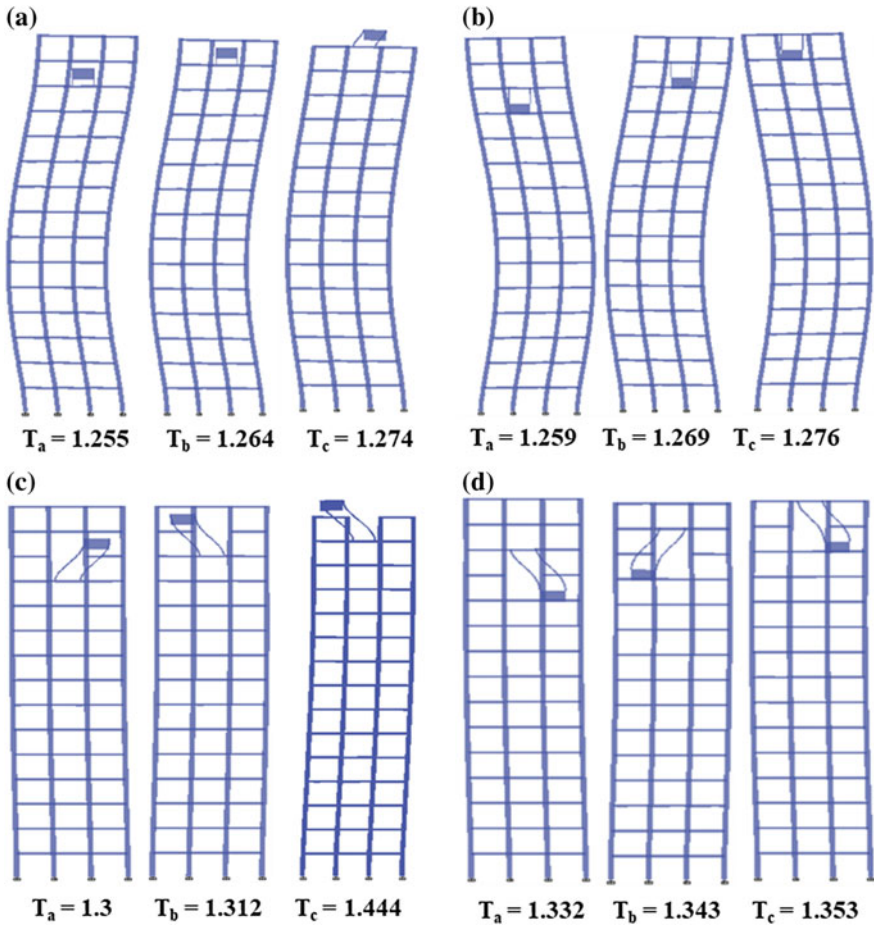
Fig. 4 Mode shapes of the structure with TMD of **a** column length 2 m placed at 13th, 14th, 15th, **b** column length 2 m placed inverted at 13th, 14th, 15th, **c** column length 5 m placed at 12th, 13th, 14th and **d** column length 5 m placed inverted at 15th, 14th, 13th

References

1. Tsai, H.-C. (1994). The effect of tuned-mass dampers on the seismic response of base-isolated structures. *International Journal of Solids and Structures, 32*(8–9), 1195–1210.
2. Tuan Alex, Y., & Shang, G. Q. (2014). Vibration control in a 101-storey building using a Tuned Mass Damper. *Applied Science and Engineering, 17*(2), 141–156.
3. Tuned Mass Dampers, http://www.deicon.com/air-suspended-tuned-mass-damper/. Accessed 9 Sepetember 2018.
4. Tuned Mass Dampers, https://www.slideshare.net/subhajitbiswas102/tuned-mass-damper.
5. Tuned Liquid Column Dampers, Natural Hazards, University of Notre Dame.
6. Samuele, I., Jamieson, R., & Rob, S. (2008). Viscous dampers in high rise buildings. *14th World Conference on Earthquake Engineering*.
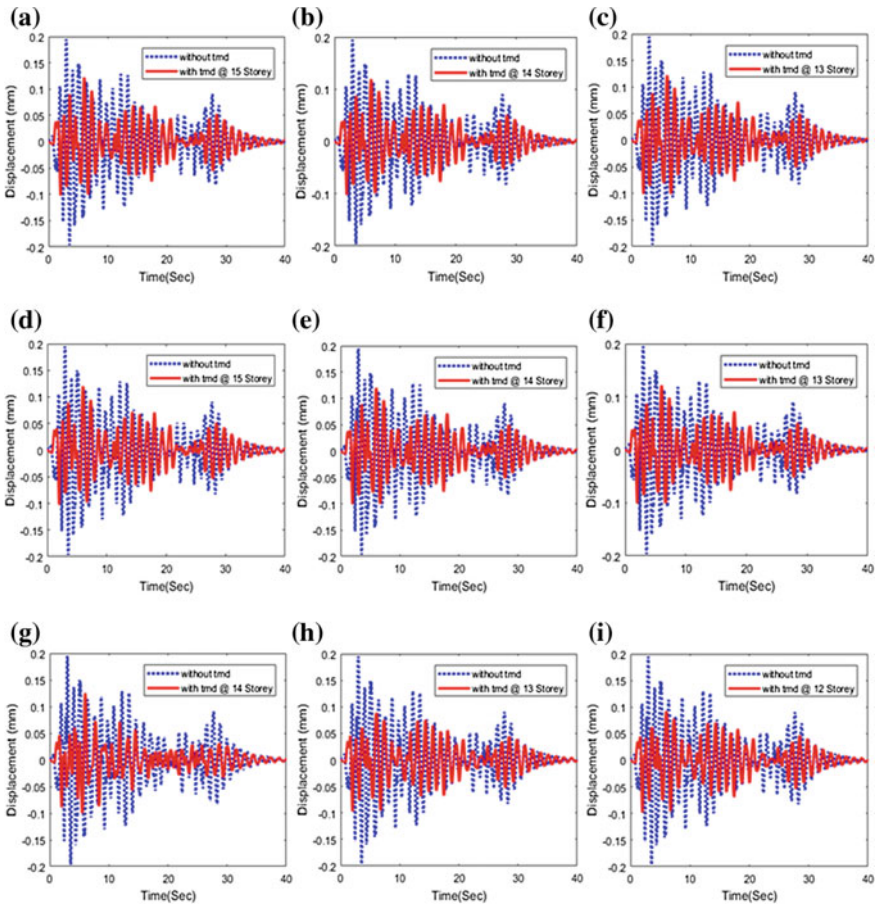
Fig. 5 Displacement of structure with **a** 2 m TMD at 15th storey, **b** 2 m TMD at 14th storey, **c** 2 m TMD at 13th storey, **d** 2 m inverted TMD at 15th storey, **e** 2 m inverted TMD at 14th storey, **f** 2 m inverted TMD at 13th storey, **g** 5 m TMD at 14th storey, **h** 5 m TMD at 13th storey, **i** 5 m TMD at 12th storey, **j** 5 m inverted TMD at 14th storey, **k** 5 m inverted TMD at 15th storey and **l** 5 m inverted TMD at 13th storey
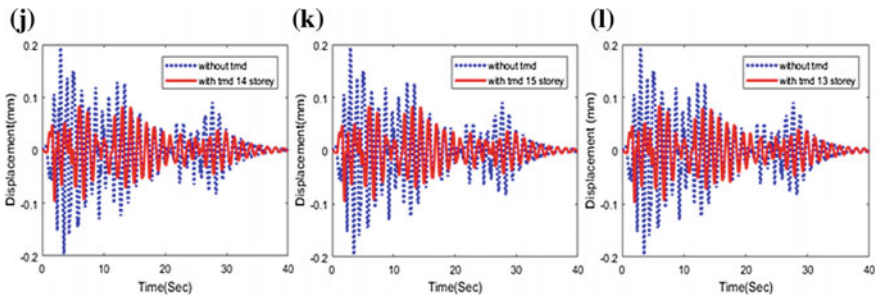
Fig. 5 (continued)

7. Richard, L. (2011). *Design, construction and testing of an adaptive pendulum tuned mass damper*. University of Waterloo.
8. https://en.wikipedia.org/wiki/Tuned_mass_damper.
9. Robert, S. (2001). One Wall Centre, Vancouver. Canadian Consulting Engineer magazine.
10. Eric, L. (2015). Taipei 101's mass damper. Popular mechanics.
11. Harruyuki, K., & Takafumi, F. (1988). Design and analysis of a tower structure with a Tuned Mass Damper. *Ninth World Conference on Earthquake Engineering*.
12. Chris, M. (2015). How a 121 storey building uses a giant magnet to prevent swaying, Gizmodo.
13. Chopra, A. K. (2017). *Dynamics of structures: Theory and applications to earthquake engineering* (5th ed.). Englewood Cliffs, NJ: Prentice Hall.

Structural Health Monitoring from Human-Induced Vibrations Using Accelerometer Sensors

Lokesh Udatha ⓘ **, Venkata Dilip Kumar Pasupuleti** ⓘ
and Bharghava Rajaram ⓘ

Abstract Most of the structures are subjected to dynamic loads during their life period such as wind, floods, earthquakes, impact, and blast loads, which affects the structural health. Structural Health Monitoring (SHM) can mitigate high repair costs by detecting and measuring the damage phenomena. In this study, Winkler's concept-based prototype model has been prepared. Winkler's model represents the soil medium as a system of identical but linearly elastic, mutually independent, discrete, closely spaced springs. An accelerometer is used to measure the actual vibration, by measuring acceleration in the x, y, z directions, which is converted to displacement, and finally translated into stiffness of the soil. This research study focused on the calculation of acceleration of the system for single and multiple human disturbances. All the results obtained indicated the presence of continuous noise vibrations.

Keywords Structural health monitoring · Static and dynamic loads · Winkler's foundation model · Accelerometer · Stiffness

1 Introduction

Structures are subjected to natural and man-made hazards as shown in Fig. 1a. Depending upon the intensity, structures may undergo minor to major damages and these damages can be measured with current technology such as a seismometer for Structural health monitoring (SHM).

SHM is the process of executing a characterization plan and damage detection for the engineering structures as shown in Fig. 1b. It consists of operational evaluation,

L. Udatha (✉) · V. D. K. Pasupuleti · B. Rajaram
Mahindra École Centrale, College of Engineering, Hyderabad, Telangana, India
e-mail: lokesh9.udatha@gmail.com; lokesh.udatha@hotmail.com

V. D. K. Pasupuleti
e-mail: venkata.pasupuleti@mechyd.ac.in

B. Rajaram
e-mail: bharghava.rajaram@mechyd.ac.in
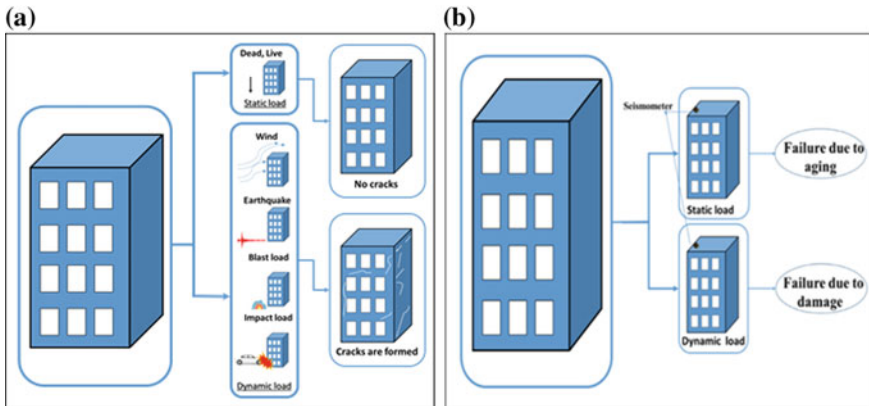
Fig. 1 **a** Natural and man-made loads acting on a building **b** Damage detection using sensors

data feature extraction, data compression, and the development of statistical models. SHM aids in the improvement of the safety and functionality of structures. It also helps to gather information on the realistic performance of the engineering structures, which in turn will help to design better structures for future.

For data feature extraction, speed/position sensors are used. A sensor is a device that converts some physical quantity into electrical signals [1]. A position/speed sensor translates physical movement and its derivatives into electrical signals. These signals are represented in the form of a seismograph, which is the fundamental measure used for SHM. Thus, a seismograph generally consists of a seismometer that captures the ground motion (using a sensor) and a data logging mechanism called as seismic recording system. Measuring damage directly with sensors is not possible. Statistical classification and feature extraction are required to convert the acquired sensor data into damage information.

Winkler's model represents the soil medium as a system of identical but linearly elastic, mutually independent, discrete, closely spaced springs as shown in Fig. 2. According to this idealization, deformation of foundation due to applied load is confined to loaded regions only. Figure 2 shows the physical representation of the Winkler foundation. Winkler assumed the foundation model to consist of linear-closely spaced independent springs. If such a foundation is subjected to a partially distributed surface loading, beyond the loaded region the springs will not be affected [2].

The principle behind the accelerometers is a mechanical sensing element which consists of a mass attached to a mechanical suspension system with respect to a reference frame. Inertial force due to moment of the earth causes mass to deflect. The acceleration is measured electrically with the physical changes in mass displacement with respect to the reference frame.

Fig. 2 Equivalent foundation resting on Winkler spring bed
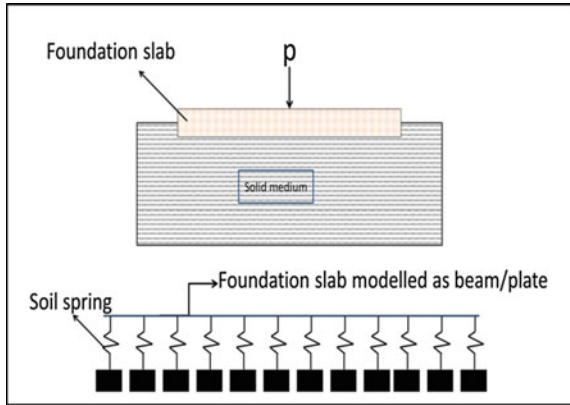
Fig. 3 Mass-spring-damper system
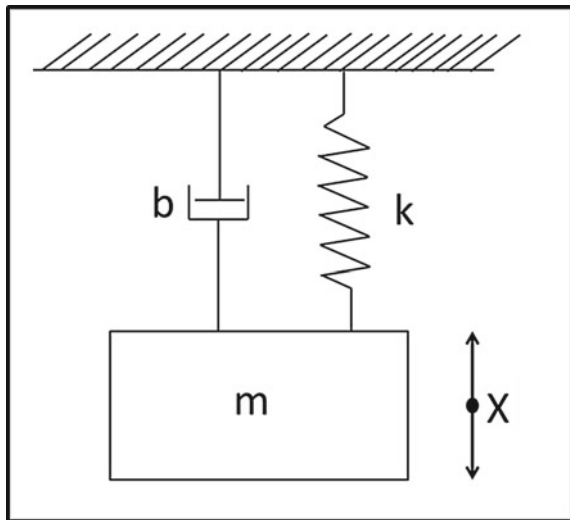
2 Methodology

Consider the model of the fixed mass-spring-damper system as shown in Fig. 3.

2.1 Basic Formulation

$$F_{\text{spring}} = -Kx; \; F_{\text{friction}} = (-D\dot{x}); \; F_{\text{gravity}} = -m\ddot{x}$$

K Spring Coefficient
b Friction Coefficient
m Mass of seismometer

From D'Alembert's Law

$$F_{\text{spring}} + F_{\text{friction}} + F_{\text{gravity}} = 0.$$

From 1

$$-Kx + (-b\dot{x}) + (-m\ddot{x}) = 0$$

Rearranging the above equation

$$m\ddot{x} = -Kx - b\dot{x}$$

$$\ddot{x} = \frac{-K}{m}x - \frac{b}{m}\dot{x}$$

Assuming $w_0^2 = \frac{K}{m}, r = \frac{b}{2m}$

$$\ddot{x} + 2r\dot{x} + w_0^2 x = 0. \tag{2}$$

The general solution of above equation is
$x = H(t)e^{Pt}$ $H(t)$ is the step function.
Substituting x in 2

$$P^2 + 2rP + w_0^2 = 0$$

$$P = -r \pm \sqrt{r^2 - w_0^2}$$

Substituting P in x

$$x(t) = H(t)e^{-rt \pm t\sqrt{r^2 - w_0^2}}$$

Under Dumped: $w_0^2 > r^2$
General Solution: $x(t) = c_1 e^{-rt + iw_1} + c_2 e^{-rt - iw_1 t}$

$$w_1 = \sqrt{w_0^2 - r^2}$$
$$= c_1 e^{-rt}(\cos w_1 t + i \sin w_1 t) + c_2 e^{-rt}(\cos w_1 t - i \sin w_1 t)$$
$$= c_1 e^{-rt} \cos w_1 t + i c_1 e^{-rt} \sin w_1 t + c_2 e^{-rt} \cos w_1 t - i c_2 e^{-rt} \sin w_1 t$$

$$x(t) = c_3 e^{-rt} \cos w_1 t + i c_4 e^{-rt} \sin w_1 t \tag{3}$$

Differentiating 3 with respect to *t*

$$v(t) = c_3\left(-\gamma.e^{-\gamma t}(\cos w_1 t) - w_1.\sin w_1 t.\left(e^{-\gamma t}\right)\right) \\ + \left(ic_4\left(\left(-\gamma.e^{-\gamma t}(\sin w_1 t) + w_1 \cos w_1 t\left(e^{-\gamma t}\right)\right)\right)\right) \quad (4)$$

Differentiating 4 with respect to *t*

$$a(t) = c_3\left(\left(-\gamma^2.e^{-\gamma t}(\cos w_1 t) + w_1.\sin w_1 t.\left(\gamma e^{-\gamma t}\right)\right) - \left(w_1^2 \cos w_1 t\left(e^{-\gamma t}\right)\right. \\ \left.-\gamma e^{-\gamma t}(w_1.\sin w_1 t)\right)\right) + ic_4\left(\left(\gamma^2.e^{-\gamma t}(\sin w_1 t) - w_1 \cos w_1 t\left(\gamma.e^{-\gamma t}\right)\right)\right. \\ \left. - \left(w_1^2 \sin w_1 t\left(e^{-\gamma t}\right) + \gamma e^{-\gamma t}(w_1 \cos w_1 t)\right)\right) \quad (5)$$

As seen from the Eq. (5), the graph obtained between time and acceleration will be combination of sine wave, cosine wave, and exponential function.

3 Experimental Setup

Mechanical suspension system of two plywood boards, plywood-1 of $300 \times 300 \times 12$ mm and plywood-2 of $200 \times 150 \times 8$ mm, four steel springs (specifications as shown in Table 1), eight M8 bolts, washers, nuts are used as shown in the Fig. 4.

The proposed seismometer consists of a microcontroller (ATmega8), and an accelerometer (ADXL335). The accelerometric data received by the microcontroller is logged on a PC which is then plotted offline. The specifications of these devices are elucidated in the following sections [3].

3.1 ADXL 335 Accelerometer

ADXL 335 accelerometer as shown in Fig. 5a is a 3-axis movement sensor, which outputs a signal conditioned voltage depending on the acceleration in the x, y, z

Table 1 Springs specifications

Specification	Value
Spring constant(K)	2.154 N/mm
True maximum load	75.580 N
Diameter of spring	1.40 mm
Inner diameter	9.00 mm
Free length	116 mm
Active coils	15
Coil pitch	7.453
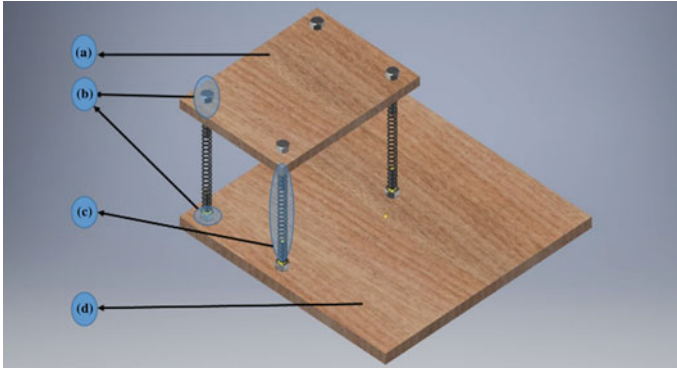
Fig. 4 Mechanical suspension system **a** Plywood-1, **b** M8 Bolt, nut and washer, **c** Spring as specifications shown in Table 1, **d** Plywood-2
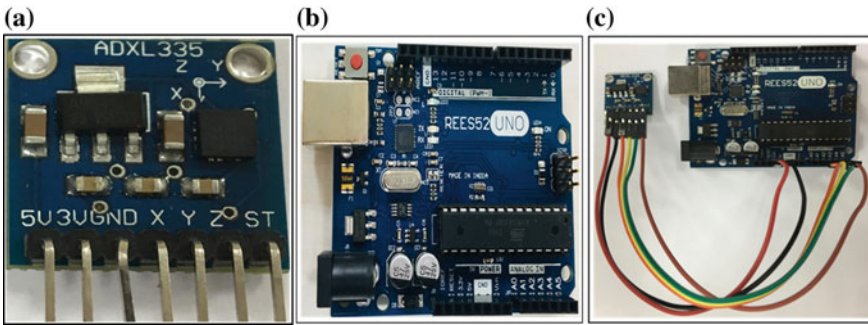
Fig. 5 **a** ADXL 335 accelerometer used in this study **b** Arduino Uno R3 microcontroller board used in this study **c** Interfacing ADXL 335 with Microcontrollers

directions. It measures the dynamic acceleration resulting from shock, motion, or vibration. It measures acceleration within the range of -3 g to $+3$ g, where g is the acceleration due to gravity in m/s^2 [4].

3.2 ATmega328p Microcontroller

For the data acquisition, an Arduino Uno R3 is used, which is an off-the-shelf microcontroller board based on the ATmega328 microcontroller. This is shown in Fig. 5b. The Arduino can receive input in the form of digital, analog or serial data. The inbuilt Analog to Digital Converter (ADC) makes it easier to interface the ADXL335, as the accelerometer generates analog voltage values. This accelerometric data is acquired roughly every 15 ms. The ADC resolution of the Arduino is 10bits which is sufficient

for our study. Using jumpers, accelerometer and Arduino are connected as shown in Fig. 5c [5].

3.3 Flow-Chart

Figure 6 shows the flow chart which is used to acquire real-time data, which in turn helps in understanding stabilization of vibration for all the three dimensions. At any point of time for this study a single direction is considered.

3.4 Experimental Free Vibration Recording

In Fig. 4, plywood 1 is assumed to be the foundation slab (in Fig. 1b) in Winkler's foundation model. For this case study, plywood 1 is displaced by 30 mm.

From Fig. 7 the graph between acceleration verses time clearly indicates the presence of damping which makes the vibration decay. From the decay, the damping of the developed system can be calculated. Apart from damping, stiffness of the system can also be calculated.
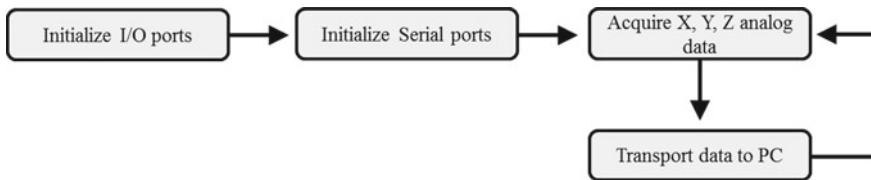
Fig. 6 Flow chart representing the collection of data
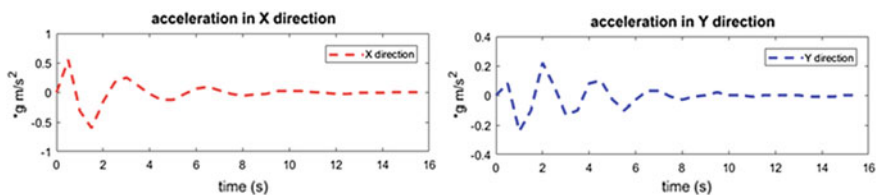
Fig. 7 Acceleration versus time for case study1

4   Case Study

4.1   Case Study 1

Accelerometer is connected to a deck of 24 ft that connects two buildings in our college. Excitation is given to the deck by jumping of a person.

4.2   Case Study 2

Accelerometer is connected to a deck that connects two buildings in our college, four persons jumping on the deck as shown in the Fig. 8b, for which the readings have been taken.

5   Analysis and Results

5.1   Case Study 1

From the Fig. 9a, the graph between acceleration versus time indicates the constant gravitational force with slight noise. When compared with experimental readings, the vibrations are very small, so noise is clearly seen and the only peak observed at 9th second is indication of jumping load.
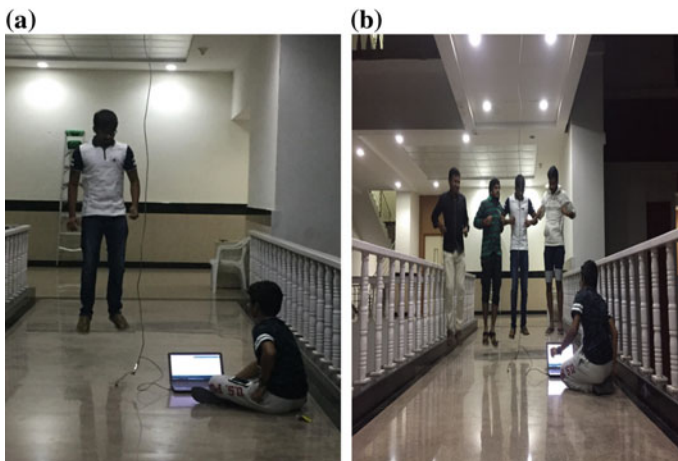
Fig. 8   a Representing the case study 1 **b** Representing the case study 2
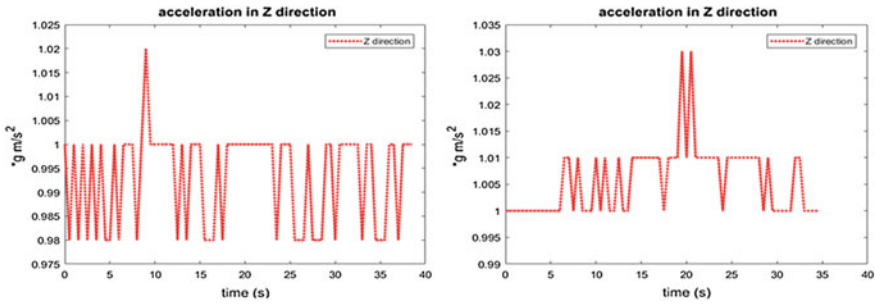
Fig. 9 Acceleration versus time for **a** case study 1 **b** case study 2

5.2 Case Study 2

From the Fig. 9b, the graph between acceleration versus time clearly indicates the constant gravitational force with slight noise. When compared with case-1, the graph shows two peaks indicating the delay in jumping b four persons.

5.3 Calculation of Stiffness of the System

The period of oscillation is defined as the time between two peaks, as shown in Fig. 10. If the signal is (supposedly) periodic, it is often best to write T as

$$T = \frac{t_n - t_0}{n} \qquad (6)$$

where t_n is the time period at which the nth peak occurs,

$$T = \frac{3 - 0.4}{1} = 2.6 \text{ sec}$$

Fig. 10 Displacement versus time for general case [6]
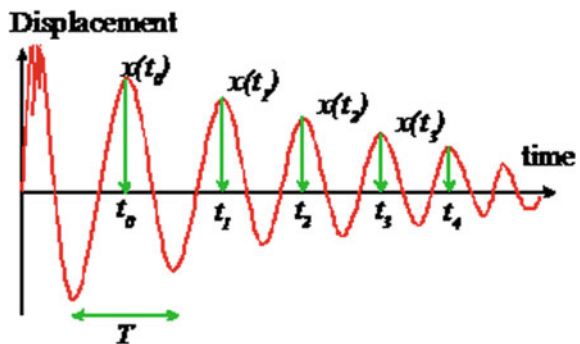
The Logarithmic Decrement is defined as,

$$\delta = \ln \frac{x(t_n)}{x(t_{n+1})} \tag{2}$$

where $x(t_n)$ is the displacement at the nth peak,

$$\delta = \ln\left(\frac{5}{2.5}\right) = 0.693147$$

The damping factor is defined as,

$$C = \frac{\delta}{\sqrt{4\pi^2 + \delta^2}}$$
$$= 0.10965251 \tag{7}$$

The Natural Frequency is defined as,

$$\omega_n = \frac{\sqrt{4\pi^2 + \delta^2}}{T}$$
$$= 2.4312\,\text{rad/sec} \tag{8}$$

The Stiffness is defined as,

$$k = m\omega^2$$

mass of the plywood-1, $m = 972$ g
   therefore, $k = 5.79638$ N/m

6   Conclusions

The accelerometer ADXL 335 is a potential device sensing the earthquake on Winkler's foundation model as well as human-induced vibrations. Both the case studies done on the deck shows acceleration due to noise is continuously varying in the range of 0.01–0.02 g m/s^2, in the longer run this would affect the health of the structure as minute stress change is continuous. Damping factor and stiffness of the system are 0.10965251 and 5.79638 N/m respectively. In future work, the research will be carried with multiple sensors on the real structures to calculate their health using structural dynamics formulation. And multi-degree of freedom (MDOF) scaled model will be placed on the current developed Winkler's foundation device and will be compared with analytical results.

References

1. Patel, V. K., & Patel, M. N. (2017). Development of smart sensing unit for vibration measurement by embedding accelerometer with the arduino microcontroller. *International Journal of Instrumentation Science*, *6,* 1–7.
2. Harden, C. W., & Hutchinson, T. C. (2009). Beam-on-nonlinear-winkler-foundation modeling of shallow. *Rocking-Dominated Footings. Earthquake Spectra, 25*(2), 277–300. https://doi.org/10.1193/1.3110482.
3. Daka, T., Udatha, L. Pasupuleti, V. D. K., Kalapatapu, P., & Rajaram, B. (2018). Ancient sandbox technique: An experimental study using piezoelectric sensors. In M. Ioannides, E. Fink, R. Brumana, P. Patias, A Doulamis, J. Martins, M. Wallace (Eds.), *Digital Heritage. Progress in cultural heritage: Documentation, preservation, and protection*. EuroMed 2018. Lecture Notes in Computer Science (Vol. 11197). Cham: Springer.
4. Manjiyani, Z. A. A., Jacob, R. T., Keerthan Kumar, R., Varghese, B. (2014). Development of MEMS based 3-axis accelerometer for hand movement monitoring. *International Journal of Scientific and Research Publications, 4*(2), 1.
5. Adabara, I. (2018). Patient medication reminder circuit using ATMEGA328/P microcontroller: Design and implementation. *Mediterranean Journal of Basic and Applied Sciences* (MJBAS)*, 2*(1), 40–51.
6. *Introduction to dynamics and vibrations*, School of Engineering Brown University. https://www.brown.edu/Departments/Engineering/Courses/En4/Notes/vibrations_free_damped/vibrations_free_damped.html.

Comparison of Different Types of Pylon Shapes on Seismic Behaviour of Cable-Stayed Bridges

Govardhan Polepally, Venkata Dilip Kumar Pasupuleti and Archanaa Dongre

Abstract Cable-stayed bridges are the most flexible bridges and getting popularity because of its economy for longer spans and aesthetics. This study focuses on the effect of the shape of the pylon on the seismic response of cable-stayed bridge. For this study, complete geometry, material properties, loads and boundary conditions of the Quincy Bayview Bridge are considered from the past published literature. The bridge span dimension and other parameters are kept constant, and the only shape of the pylon is varied viz. A type, H type, inverted Y shapes. The height of the pylon is kept constant for all the numerical models for comparison purposes. The 3D bridge model is modeled using SAP 2000 software and analyzed for three earthquake ground motions Bhuj 2001, Loma Prieta 1989 and El Centro earthquake 1940. The seismic response of bridge at various locations are considered and compared. The study shows that the shape of the pylon has got great influence on the seismic behavior of cable-stayed bridge.

Keywords Quincy Bay view bridge · Cable-stayed bridge · Pylon shape · Time history analysis

1 Introduction

Cable-stayed bridges have gained a lot of popularity in the last few decades, especially in developed countries, though this practice has raised, there are few parameters like wind loads, seismic loads, impact loads and other natural dynamic loads are

G. Polepally (✉)
Vidya Jyothi Institute of Technology, Hyderabad, Telangana, India
e-mail: polepallygovardhan@gmail.com

V. D. K. Pasupuleti
College of Engineering, Mahindra Ecole Centrale, Hyderabad, Telangana, India
e-mail: venkata.pasupuleti@mechyd.ac.in

A. Dongre
Northcap University, Gurgaon, Haryana, India
e-mail: archanaadongre@ncuindia.edu

still a concern to structural designers, maintenance and construction community. A few of the primary reasons for the increase of cable-stayed bridges all over the world are their structural efficiency, aesthetic appeal, enhanced stiffness compared to suspension bridges, ease of construction, large spans and small size of substructures. Primarily it would be of highest advantage were a large cantilever is needed for a span of the bridge and that point suspension bridge would be uneconomical. There are different types of cable-stayed bridges built based on variations like side-spar cable-stayed bridge, cantilever spar cable-stayed bridge, multi-span cable-stayed bridge, extra dosed bridge and cable-stayed cradle-system bridge apart from four classes of rigging on cable-stayed bridges harp, mono, star and fan. The structural components of a cable-stayed system behave in the following manner: The stiffening girder transmits the load to the tower through cables, which are always in the tension. The stiffening girder is subjected to bending and axial loading. The tower transmits the load to the cable-stayed bridges; their form and configuration depend on the way individual wires are assembled. A strand is generally composed of seven-wires, helically formed around a center wire and its diameter ranges from 3–7 mm. As cables are the most important elements in cable-stayed bridges; they carry the load from the super structure to the tower and to the backstay cable anchorages. In addition to high tensile strength, they must also have high fatigue resistance and corrosion protection. This study mainly focuses on the dynamic analysis of different types of pylon shapes of cable-stayed bridge to understand the effect of span length.

2   Literature

The concept of cable-stayed bridges was first proposed in the seventeenth century [1], however, the modern cable-stayed bridge began with the Stralsund Bridge, which was completed in 1956 in Sweden with a main span length of 183 m [2]. Cable-stayed bridges, due to their large dimensions and flexibility, usually experience long fundamental periods, aspect that makes the difference with respect to other structures, and of course, that affects their dynamic behavior. However, their flexibility and dynamic characteristics depend on several parameters such as the main span length, stay system and their layout, support conditions and many other things [3]. And modal analysis results on cable-stayed bridges are discussed in many papers, with emphasis on the seismic behavior. First vibration modes show a very long period, in the order of several seconds, and they are fundamentally deck modes. They are followed by cable vibration modes, coupled with the deck. The tower modes are usually of higher-order, which can be coupled with the deck depending on the support conditions. Undoubtedly, the modes are very difficult to separate when they are sufficiently coupled [4]. An exact analysis of natural frequencies and modal shapes on cable-stayed bridges is very important, not only for the study of the seismic response but also for wind action and traffic loads [5]. Shah et al., studied the seismic response of bridge considering different shapes of pylon and soil structure interaction [6]. Sarhang thesis mainly concentrated on comparison of three different types of

cable stayed bridges using structural optimization and found to be very useful in optimization of complete structure [7]. Similarly, linear and non-linear dynamic analysis of cable stayed bridges were also carried out to understand the dynamic behavior and for possible failure locations [8, 9].

3   Modeling and Analysis

Cable-stayed bridge can be divided into three primary categories, cables, pylons and bridge deck. The Quincy Bay view bridge consists of 56 cables in two planes along the bridge deck, twenty-eight of them are in main span and the rest of the cables are in the side spans. The total length of the bridge is 541.8 m, the main span is 285.8 m and the two side spans are 128.1 m respectively as shown in Fig. 1a. The bridge deck is made up of concrete with thickness of 0.230 m and the bridge deck consists of two steel composite girders with the total height of 3 m. Two H type pylons support the bridge deck and the cables. The height of the pylons from the piers is 79 m and pylon also consists of two struts, the upper strut and lower strut. The lower strut supports the bridge deck. The cable connections at the pylons are starting at top of the pylons
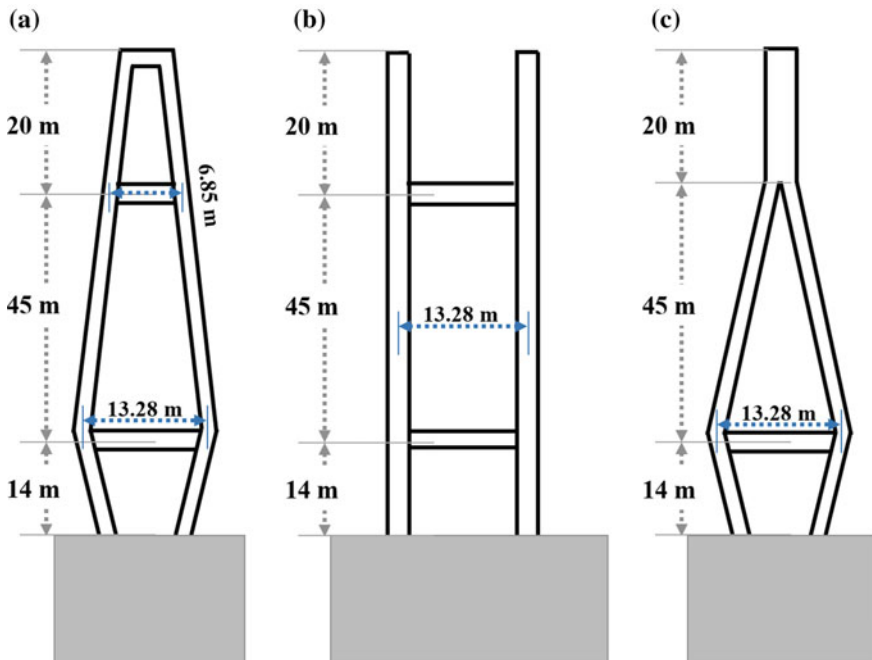
Fig. 1 Schematic diagram of 3 different types of pylon shapes of cable-stayed bridge **a** 'A' shape. **b** 'H' shape. **c** Inverted 'Y' shape

Table 1 Material properties considered for this study and same for all three scenarios

Bridge Parameter	Definition	Value
A_d	The cross-section area of the deck	2.806 m^2
E_{ds}	The modulus of elasticity of the deck	3.8e08 kN/m^2
E_{cs}	The modulus of elasticity of the cables	2.100e8 kN/m^2
F_{ue}	The effective tensile stress of the cables	4.9e5 kN/m^2
W_{cs}	The weight per unit length of the cables	76.9729 kN/m^2
E_c	The modulus elasticity of the concrete	3.8e7 kN/m^2
D	Diameter of the cable	0.146

and each cable is a parted by 2.5 m from the first cable. The lower ends of the cables support the bridge deck and the upper end of the cables connects at the top of pylon with fan type and diameter of the cable is 0.146 m. Rest of models are same as Quincy Bay view bridge but only difference is pylon shape, reaming all are constant including material and geometrical properties. Complete schematic diagram of the mentioned cable-stayed bridges are shown in Fig. 1 with dimensions. As for the modeling and analysis of the bridges, a finite element based software SAP2000 [10] is used. Most of the studies have similar software for effective and faster computations. Material properties assigned for different components explained above are given in Table 1. The bridge is assumed to be a composite structure consisting steel and concrete as prescribed in the past literature. Detailed sections modeled in SAP2000 for pylon and deck are mention in the Fig. 1. Boundary conditions at the bottom of the pylons are considered to be fixed and two edges of the bridge deck are considered to be simply supported. For modeling of cables, this study directly uses the cable element and their attachments to the pylon and deck are considered to be rigidly connected.

3.1 Case Studies

As discussed earlier, in this study three distinct cases have been considered with varying pylon shapes without changing other parameters.

4 Modal Analysis

Dynamics of any structure is governed by a simple equation of motion mention in the (Eq. 1), assuming the damping coefficient to be zero.

$$MU + KU = F(t) = 0 \tag{1}$$

Above basic equation would give mode shapes based on the degree of freedom. Modal analysis is also very important in understanding the boundary conditions and modeling accuracy by seeing the frequencies obtained. Modal analysis is carried for three scenarios to calculate the frequencies and time periods. The obtained mode shapes for A shape, H shape and inverted Y shape pylons are shown in the Figs. 2, 3 and 4 respectively. And comparative modal analysis results for three cases are given in Table 2, where, column 1 represents mode shape number, column 2, column 3 and column 4 represents time period in seconds of A shape, H shape and inverted Y shape pylons respectively. Figure 5 shows developed three dimensional models with different pylon shapes.

Mode=1
T=2.161
F=0.462

Mode=2
T=1.397
F=0.715

Mode=3
T=1.390
F=0.719

Mode=4
T=1.072
F=0.932

Mode=5
T=0.937
F=1.066

Mode=6
T=0.921
F=1.085
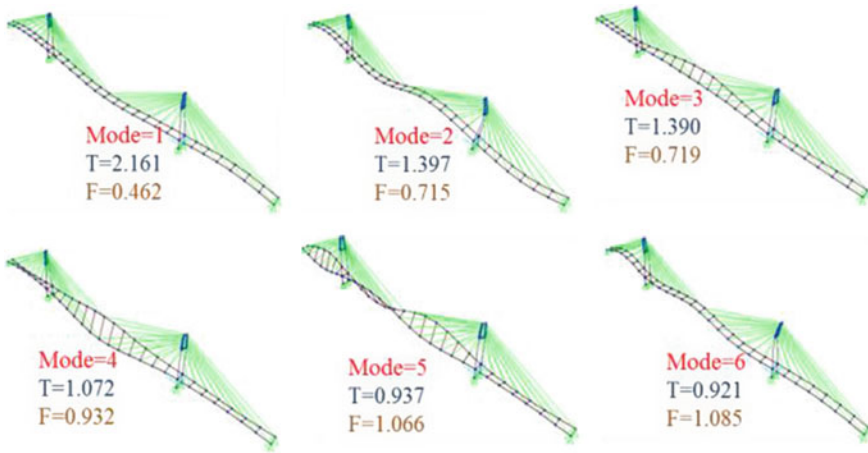
Fig. 2 First six mode shapes of A shape pylon cable-stayed bridge

Mode=1
T=3.225
F=0..10

Mode=2
T=1.964
F=0.509

Mode=3
T=1.680
F=0.595

Mode=4
T=1.250
F=0.799

Mode=5
T=1.214
F=0.823

Mode=6
T=0.988
F=1.011
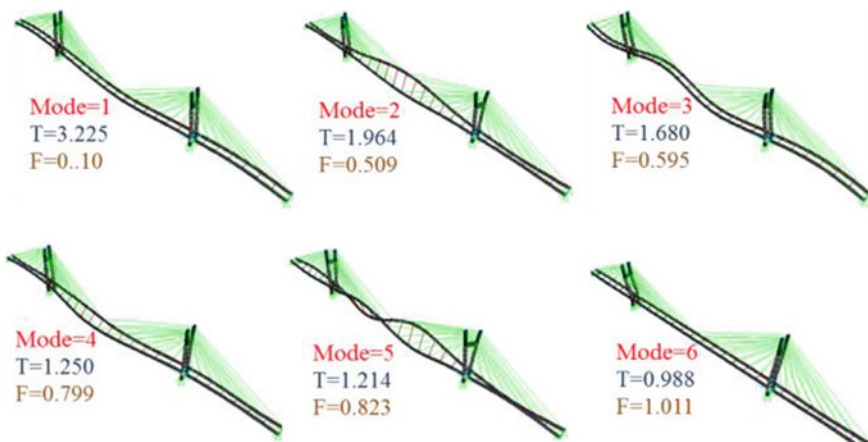
Fig. 3 First six mode shapes of H shape pylon cable-stayed bridge
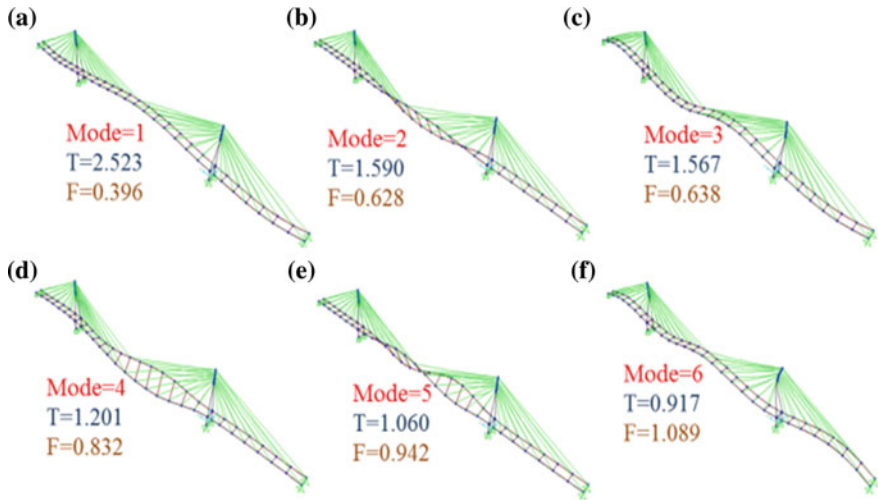
Fig.4 First six mode shapes of inverted Y shape pylon cable-stayed bridge

Table 2 Comparative time periods of different modes of three scenarios

Mode Shape No.	A Shape	H Shape	Inverted Y Shape
	Time Period (s)	Time Period (s)	Time Period (s)
1	2.16015	3.22565	2.5239
2	1.39768	1.96470	1.59021
3	1.39019	1.68051	1.56731
4	1.0729	1.25017	1.20145
5	0.93735	1.21440	1.06089
6	0.92124	0.98868	0.91754
7	0.86907	0.98807	0.85717
8	0.76588	0.93314	0.69984
9	0.75987	0.8324	0.67937
10	0.75891	0.79381	0.66509
11	0.67264	0.76301	0.64585
12	0.63634	0.65200	0.62510

Modal analysis play a vital role in understanding the possible behavior of any structure and its frequency or time period directly gives an ideal idea about the exactness of numerical model and its boundary conditions. In fact parametric studies are most needed for robust conclusions.
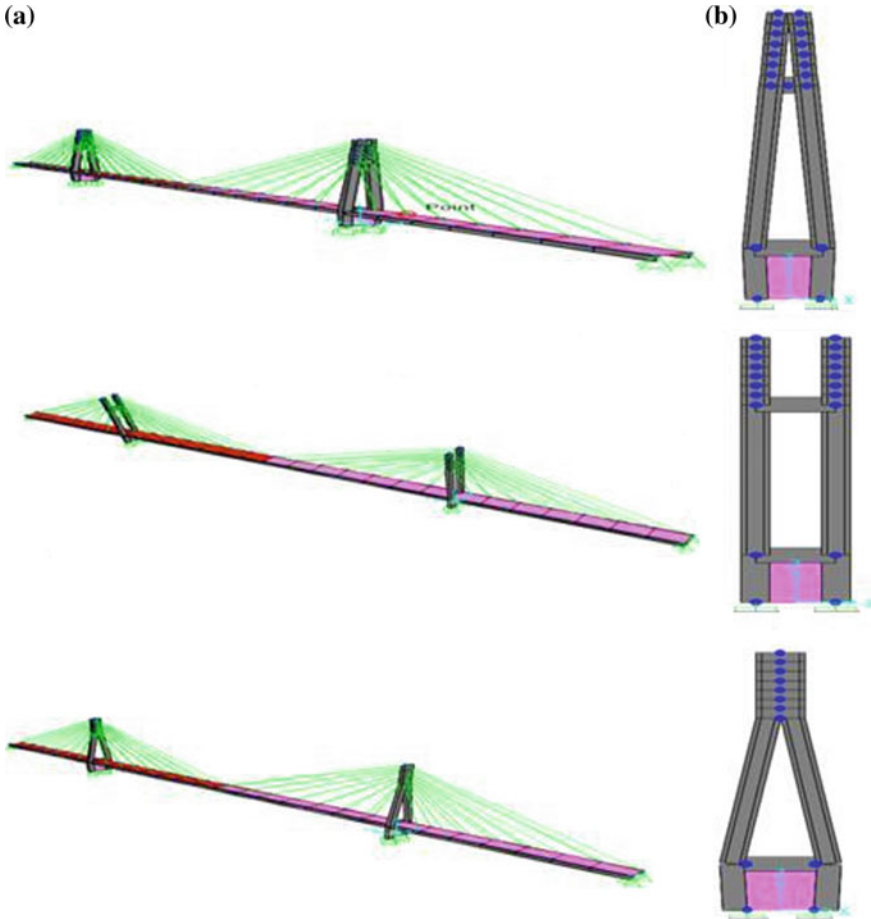
Fig. 5 Different views of developed 3D model of **a** 'A' shape. **b** 'H' shape. **c** Inverted 'Y' shape of cable-stayed bridge in SAP2000

5 Dynamic Linear Analysis

To understand the dynamic behavior of the bridge, three major earthquake ground motions of Loma Prieta, Bhuj earthquake and Elcentro earthquake ground motions have been considered, which are different in their nature of predominant frequencies. Dynamic linear analysis will give the basic idea in understanding the behavior of cable-stayed bridge under the action of wind or earthquake ground motions. This study mainly concentrated on understanding characteristic behavior using modal analysis and linear behavior is calculated using earthquake ground motions. Consideration of seismic effects in the design of any bridge is almost a mandatory step for long life of the structure. As long as all the components of the bridge are lower

than the yield values, linear analysis is the most suitable analysis. Once the effects grow larger, geometric non-linear inclusion needs to be considered for large deformations and material non-linear to be considered for individual member failures. In this study P-Delta effect has been considered as the bridge can undergo very large deformations.

The following analysis results for three cases have been presented to discuss the effect of each earthquake ground motion on the three scenarios. Obtained results have showed different behavior than what is expected logically. This study has also limited itself to the discussion based only on the maximum displacements. For example, obtained plots are divided into 'a' and 'b'. (a) Shows the time history response on top of the pylon in the 'x' and 'y' direction, whereas figure (b) shows the time history response at the mid of the deck in both the directions.

5.1 Behavior Due to Loma Prieta Earthquake Ground Motion

Loma Prieta earthquake has occurred on the San Andreas Fault system and has generated peak acceleration of 0.65 g at the epicenter. This ground motion was applied to all the three case studies and obtained responses at the mid of the deck and top of the pylon are shown in the Fig. 6a, b, respectively and respective peak values at both mid of the deck and top of the pylon for three cases are presented in Table 3, where third, fourth column represent maximum responses at mid and fifth, sixth column represents at the top of pylon.
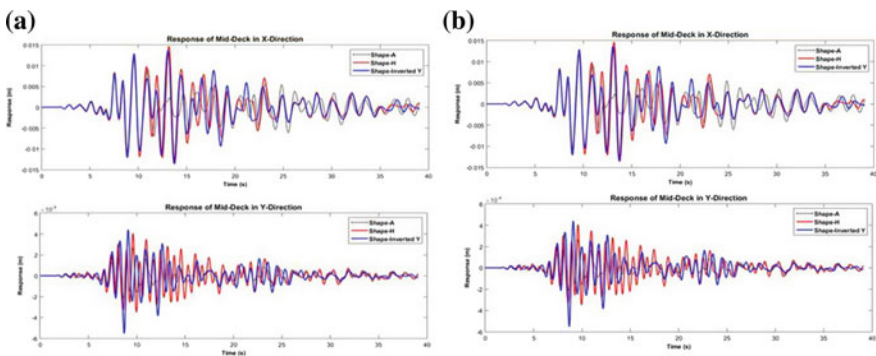
Fig. 6 Response of the bridges suspected to Loma Prieta earthquake ground motion **a** at the mid of the bridge deck. **b** at the top of pylon

Table 3 Maximum responses for Loma Prieta earthquake ground motion of the cable-stayed bridges at the mid of the deck and at the top of the pylon for three scenarios

Case	Loma U_x	Loma U_y	Loma U_x	Loma U_y
	(m)	(m)	(m)	(m)
A Shape	0.012	0.01048	0.01048	0.00269
H Shape	0.01466	0.01298	0.01298	0.00293
Inverted Y shape	0.01365	0.0062	0.0062	0.00335

5.2 Behavior Due to Bhuj Earthquake Ground Motion

One of the most powerful earthquakes occurred on 26 January 2001 of magnitude 7.9 in India and resulted in lot of research thereafter. This earthquake has not only damaged the traditional mud and masonry structures but also new reinforced concrete structures that were constructed questioning the durability of ongoing construction practices. Figure 7 shows the responses of three different pylon shape bridges subjected to Bhuj earthquake ground motion and in Table 4, column 2, column 3 represents the peak values obtained at the mid of the deck and column 4, column 5 represents peak values obtained at the top of the deck.
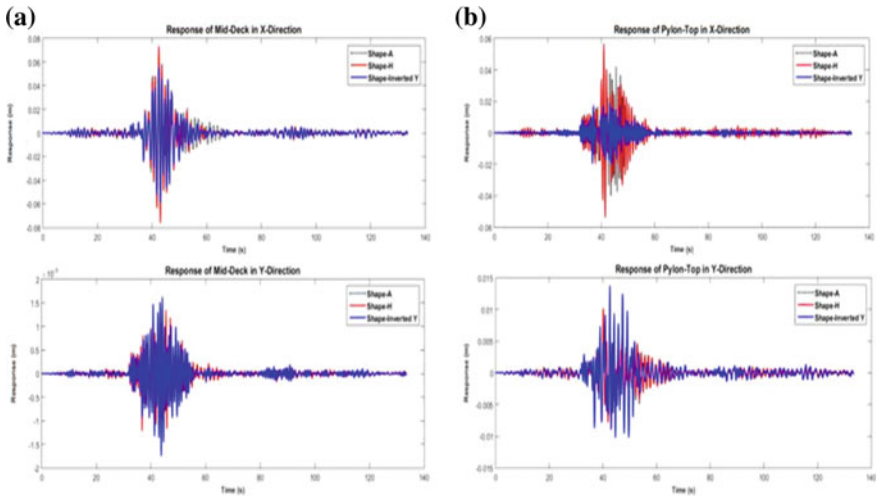
Fig. 7 Response of the bridges suspected to Bhuj earthquake ground motion **a** at the mid of the bridge deck. **b** at the top of pylon

5.3   Behavior Due to El Centro Earthquake Ground Motion

El Centro earthquake was one of the devastating earthquakes in 1940 and affected the USA and Mexico. The north–south component ground motion is considered and applied to all the three scenarios, obtained responses at the mid of the are shown in Fig. 8a and responses obtained at the top of the pylon are shown in Fig. 8b. Table 5 shows the peak responses obtained at the top of the pylon and Table 6 shows the peak values obtained at the mid of the deck.

Table 4 Maximum responses for Bhuj earthquake ground motion of the cable-stayed bridges at the mid of the deck for three scenarios

Case no.	Bhuj U_x(m)	Bhuj U_y(m)	Bhuj U_x(m)	Bhuj U_y(m)
A Shape	0.04796	0.00111	0.04222	0.01108
H Shape	0.07346	0.00135	0.05673	0.01164
Inverted Y shape	0.0556	0.00163	0.01881	0.01383
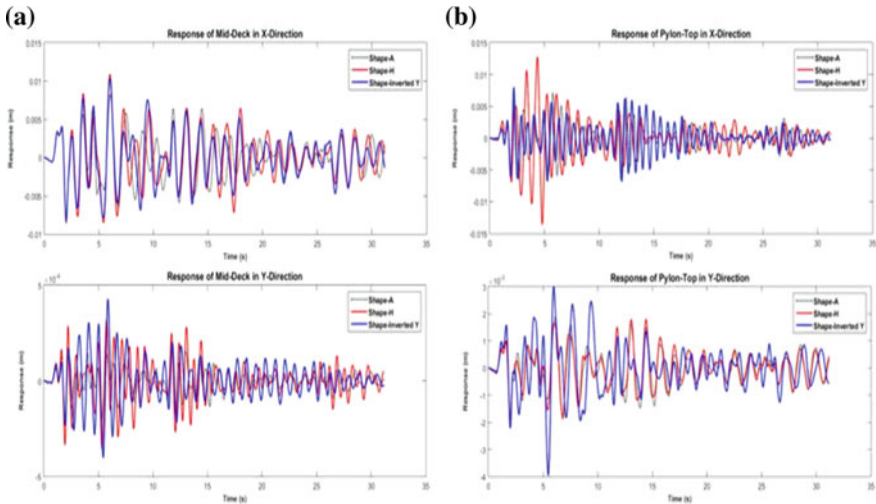
Fig. 8 Response of the bridges suspected to El Centro earthquake ground motion **a** at the mid of the bridge deck. **b** at the top of pylon

Table 5 Maximum responses for El Centro earthquake ground motion of the cable-stayed bridges at the top of the pylon for three scenarios

Case	El Centro U_x(m)	El Centro U_y(m)
A Shape	0.00825	0.000207
H Shape	0.0109	0.000322
Inverted Y shape	0.01033	0.000428

Table 6 Maximum responses for El Centro earthquake ground motion of the cable-stayed bridges at the mid of the deck for three scenarios

Case	El Centro U_x(m)	El Centro U_y(m)
A Shape	0.00825	0.000207
H Shape	0.0109	0.000322
Inverted Y shape	0.01033	0.000428

6 Conclusions

Civil engineering projects always have a shortcoming of understanding through actual scaled experimental models either due to their scale, cost or time taking process. So, largely numerical models play a vital role due to their ease in modeling, computations and faster parametric studies. In this study, the most important key design considerations for cable-stayed bridges under gravity loads and earthquake loads are discussed. The numerical model of a cable-stayed bridge is formulated for single plane of cables with global coordinates for bridges having three different pylon shapes. Different parameters are considered to get the influence of the principal characteristics which are layout of the stays, the inertia of deck and pylons.

Few key observations from this study are time period of the bridge with A-shaped pylon is less when compared to other two pylon shapes, and inverted-Y shaped pylon have a larger time period. And as the numbers of cables are increased, the time period has also increased, but the difference in time period between 6 cables and 7 cables is very high compared to increase in time period between 7 cables and 8 cables bridge for all kinds of pylon shapes. And from time history analysis, the maximum responses obtained for all the bridges are dependent on the type of ground motion they are subjected to. It is observed that the Inverted-Y shape pylon bridge has less response for Loma and Bhuj ground motion, whereas A-shape pylon bridge has less response for Elcentro earthquake when compared other pylon-shaped bridges.

References

1. Leonhardt, F., & Zellner, W. (1991). Past, present and future of cable-stayed bridges. In M. Ito, Y. Fujino, T. Myiata, & N. Narita (Eds.), *Cable-stayed bridge: Recent development and their future* (pp. 1–33). New York: Elsevier.
2. Hongwei, C., & Amjad, J. A. (2014).Three-dimensional geometric nonlinear analysis of composite cable-stayed bridges using a refined double-beam model. *Journal of Bridge Engineering*, *19*(6), 04014017.
3. Walther, R. (1999). *Cable-stayed bridges* (2nd ed.). London, UK: Thomas Telford.
4. Morgenthal, G. (1991). *Cable-stayed bridges—Earthquake response and passive control* (MSc dissertation). Civil Engineering Department, Imperial College of Science, Technology and Medicine, London, UK.
5. Valdebenito, G. E., Aparicio, A. C., & Alvarez. J. J. (2012). Seismic response of cable-stayed bridges for different layout conditions: A comparative analysis. In *Proceedings of 15th world conference on earthquake engineering*. Lisboa, Portugal.

6. Shah, S. G., Desai, J. A., & Solanki, C. H. (2010). Effect of pylon shape on seismic response of cable stayed bridge with soil structure interaction. *International Journal of Civil & Structural Engineering*, *1*(3), 667–682.

7. SarhangZadeh, O. (2012). *Comparison between three types of cable stayed bridges using structural optimization* (Electronic Thesis and Dissertation Repository. Paper 897).

8. Egeseli E. A. (1975). *The nonlinear dynamic response of a cable stayed girder bridge to various loadings* (Ph.D. Dissertation), Department of civil engineering, university of Pittsburgh.

9. Fleming, J. F., & Egeseli, E. A. (1980). Dynamic behavior of a cable stayed bridge. *Journal of Earthquake Engineering and Structural Dynamics*, *8*(1), 1–16.

10. Computers and Structures. (2007). *SAP2000 V. 18.0—Integrated software for structural analysis & design*. Berkeley, CA.

Investigation of Crack Properties Using Image Processing: An User Interface

Sravya Nedunuri, Nihitha Thota, Venkata Dilip Kumar Pasupuleti and Prafulla Kalapatapu

Abstract This research work focuses on processing the images of concrete walls to identify cracks with the help of a Graphic User Interface (GUI) created using MATLAB Guide. The developed GUI gives the length, width and type of the crack as outputs to an input image of a concrete wall. It uses image processing techniques to arrive at the output. The scope of this paper is limited to cracks that do not have any branches. This is being developed primarily to minimize the human error in identifying cracks in various buildings. The images are processed by first converting them into grayscale images and then into binary images. The images used in our case study are taken from Mahindra Ecole Centrale college campus buildings. The results obtained are verified with the manual inspection of the cracks. The accuracy of length is 92.947% and the accuracy of width is 78.09%.

Keywords Cracks · Image processing · Length and width of the crack · Crack detection GUI · Cracks on concrete walls

1 Introduction

Cracks occur on all types of concrete buildings irrespective of the age of the building. They are the earliest indications of failure in a concrete structure. Generally, engineers use manual methods to analyze cracks, which involve, measuring and sketching the crack. The drawbacks of these methods are that they totally depend on the knowledge

---

S. Nedunuri · N. Thota · V. D. K. Pasupuleti (✉) · P. Kalapatapu
College of Engineering, Mahindra École Centrale, Hyderabad, Telangana, India
e-mail: venkata.pasupuleti@mechyd.ac.in

S. Nedunuri
e-mail: sravya14223@mechyd.ac.in

N. Thota
e-mail: nihitha14188@mechyd.ac.in

P. Kalapatapu
e-mail: prafulla.kalapatapu@mechyd.ac.in

of the engineer and are prone to human errors. Today, with the advancement in technology, high-rise buildings, huge dams, etc. are being built. The cracks formed on these structures cannot be manually analyzed. To overcome this problem, we are proposing a technique which can give length and width of the crack when an image of the crack is given as input.

Cracks occur in various shapes and sizes. They can be straight, toothed, non-uniform width and so on. They can also differ in their orientation, some cracks can be vertical, some horizontal and some diagonal. There are many causes for the occurrence of the cracks, but, the Indian Standards code book (SP25) specifies three main causes, which are: size, damage caused and cause of occurrence (Fig. 1).

Based on the size, SP25 classifies the cracks as follows: If the width of the crack is less than 1 mm, then it is a thin crack. If the width is between 1 and 2 mm then it is a medium crack. If the width is greater than 2 mm then it is a wide crack. Based on damage caused, the cracks are classified as Structural and Non-Structural Cracks. Structural cracks are formed due to faults in design or faults in construction practices. These are harmful to the health of the structure. These cracks should be addressed as soon as possible. Non-structural cracks are formed due to internally induced stresses in the materials used. These cracks are not harmful to the structure but may become harmful if not treated on time. They can also allow water seepage into the interior of the building and that in turn can cause corrosion of steel.

Fig. 1 Classification of cracks
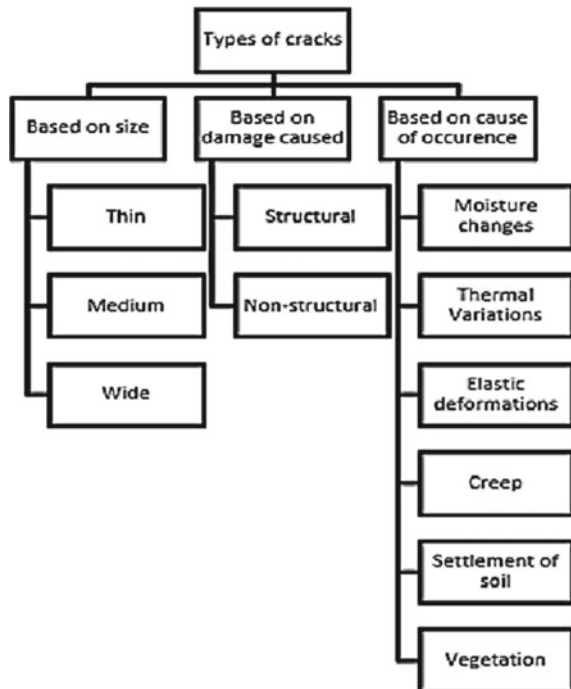
The causes for the formation of cracks as prescribed by the Indian Standard SP25 are: moisture changes, thermal variations, elastic deformations, creep, and movement due to chemical reactions, foundation movement, and settlement of soil and vegetation growth in the concrete walls/foundation [1]. Cracks formed due to moisture changes are called shrinkage cracks while the cracks formed due to thermal variations are called shear cracks (Fig. 2). In this study, we have worked on thin, medium and wide cracks which are the cracks based on size. In our future study, we will be working on cracks based on damage and cause of occurrence by improving our current processing method.

The primary reasons for the study of cracks are:

i.   Safety: Cracks are indicative of structural stability. They are the preliminary signs of a forthcoming failure of an important structural component. Observing them in their early stages is necessary to prevent casualties.
ii. Investment Protection: When a structure is built, it is expected to remain intact as long as it is intended. Therefore, to ensure that happens, monitoring the health of the structures using cracks as an indication serves as a measure to protect the investment.
iii. Minimize repair costs: When non-structural cracks are taken care of at an early stage, the reinforcement is not corroded and other chemical reactions which are

Fig. 2 Shear crack in our campus building

harmful to the health of the structure are prevented. This results in the reduction
of the repair/maintenance costs of the building.

iv. Assess urgency of the repair: By studying the extent of the crack and its type,
     the severity of the damage to the building can be predicted. This can help the
     engineers in assessing the urgency of repair.

The scope of this paper is limited to cracks that have no branches. The platform
being used is MATLAB. A GUI has been developed to make it easier for the user
to give inputs. The input given is an image of a concrete wall. The GUI processes it
and calculates the length, width and type of the crack as outputs. The dimensions of
the image (in pixels) are measured and the dimensions of the concrete wall captured
in the image are also measured beforehand.

2 Background

Moon et al. [2] used a neural network to develop an automatic crack detection system.
Their work analyzed the concrete surface and recognized the cracks. The authors
aimed to develop an algorithm that allows anyone to tune the parameters easily
without the need for a systems engineer. In the first step, to distinguish between
the cracks and the background image, morphological operations were performed.
The existence of crack was determined in the second step. To automate the image
classification, they used back-propagation neural network. The efficiency with which
the crack is being recognized is 92% for non-crack images and 90% for images with
a crack [2].

Doihara [3], in their paper, used hierarchical image processing technique to detect
cracks and length, width and distribution of crack to assess the deterioration of a
concrete structure. The algorithm that measures the cracks uses images of different
resolutions to derive the shape and width of the crack. The recognition rate is 66%
for cracks of width more than 0.1 mm with 0.08 mm Root Mean Square [3].

Yang et al. [4], introduced an image analysis method to minimize the requirements
for pen marking to capture thin cracks in reinforced concrete structures. Their study
included two procedure types: experimental procedure and image analysis. Author's
proposed method is most suitable for laboratory tests but it can be used in the actual
sites as well. The limitation to use it on-site is that it needs good lighting conditions
when the images are being taken [4].

Yamaguchi et al. [5] in their paper introduced a fast crack detection method
for large-size concrete surface images using percolation-based image processing
which is efficient and of high-speed even for the digital image (of 10 megapixels
size) while preserving the accuracy of crack detection. To reduce computational
time, they proposed termination and skip-added procedures. The authors in their
work efficiently reduced the computational cost and the accuracy of crack detection
performance is considered comparable to the original percolation process [5].

Huang et al. [6] presented a novel approach for crack detection of concrete structures in images. Their method is composed of three steps. In the first step, the image is converted into a grayscale image using an edge of the image. An image filter is developed using Sobel's filter for detecting cracks. In the second step, a suitable threshold is used in a binary image and all pixels are classified into two categories: background and foreground. In the third step, after elimination of residual noise using Sobel's filtering, the major cracks are detected using Otsu method. Author's method had clear and accurate crack detection in images. Their results demonstrated that the proposed method is relatively improved than the other widely used techniques [6].

Fujita et al., have developed a method for crack detection. The method follows two pre-processing techniques and one processing technique for noise reduction in an image. After that subtraction pre-processing for irregular illumination is carried out. In the pre-processing for noise reduction, a Hessian matrix is used to distinguish crack line from background. Otsu's technique is used for thresholding [7].

Chen et al. have used a semi-automatic technique to detect and analyze cracks. The algorithm requires the selection of node points, then noise removal and thinning processes are carried out. The crack route is traced using a reference line obtained by joining the initially selected node points. The crack width is calculated using DOG function. Multi-temporal image processing is done to improve efficiency [8].

Ito et al. find the area of the crack for analysis. They are performing shadow correction operations to improve accuracy in low light images. The image first undergoes preliminary thresholding where it is converted into a binary image. It then undergoes further thresholding and thinning processes. The crack is tracked between two edge points and the direction and area of the crack are calculated. Branches of a crack are analyzed as separate cracks [9].

Prasanna et al. use canny edge detection algorithm to classify images. Support Vector Machines (SVM) algorithm with linear kernel function was then used. Curve-fitting was done for pixels whose intensity was below a fixed percentage of the average block intensity. To identify feature vectors, histogram plots are used along the detected curves. The paper mainly focuses on cracks in bridges [10].

Lee et al. are using technique based on image processing to measure cracks. The technique is composed of two steps. In the first step, cracks are detected using binarization and shape analysis. In the second step, crack analysis is done by preprocessing, which includes boundary, thinning, and labeling processes. Within limited testing, the accuracy of the detection and crack analysis is better with the proposed method than with conventional method [11].

Nishikawa et al. have used genetic programming which combines several simple image filters into a tree structure to detect cracks on concrete. They used techniques to address issues of brightness. The crack's width and length are estimated along with the orientation of the crack [12].

3   Methodology

The GUI is being developed using Graphical User Interface Development Environment (GUIDE) in MATLAB software. To visualize the cracks, the image is compressed to dimensions 500×500 pixels. This is taken as the input image to GUI. This input image is converted into a grayscale image. The grayscale image is again converted into a binary image. This image will have only 1 and 0 as values in the pixel matrix. 1 implies white color and 0 is black color. Fig. 3 shows the flow diagram for the procedure followed.

The program traces the 0s to arrive at the length and width of the crack. It works by looking for 0s in each row. The assumption we made is that the size of each pixel is 1×1 mm square. It checks for all neighbors of an element if a zero is found. If the next zero is in the next row, in the vertically opposite direction, it adds $+1$ to the length. If it is found in the diagonally opposite in the next row (both left and right), $\sqrt{}$ is added to the length. If the next zero is in the same row, then it checks all neighbors of the next element in the same manner. All the above values are summed and multiplied with a length factor.

$$\text{Length of wall (in picture)}/500 = \text{Length Factor} \tag{1}$$

where 500 is the number of pixels in the image in the vertical direction. The length of the crack is calculated from both sides to reduce the percentage of error. The maximum of the two values is displayed as output. To calculate the width of the crack, the algorithm looks for the number of consecutive zeros and sums these values over all the rows. The width of the crack is calculated in each row and then the summation of these values is divided by the number of rows. This value is then multiplied with the width factor which is same as the above.

$$\text{Width of wall (in picture)}/500 = \text{Width Factor} \tag{2}$$

Depending on the width values, the type of the crack is determined using the guidelines given in SP25. If the width of the crack is less than 1 mm then it is a thin crack. If it is between 1 and 2 mm, it is a medium crack and above 2 mm is a wide crack.
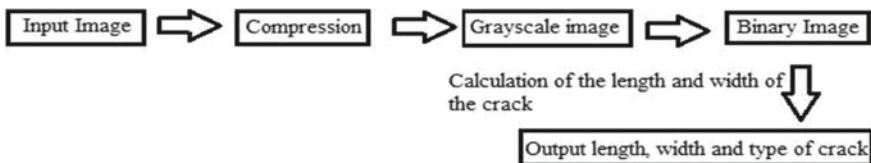
Fig. 3 Procedural flow diagram

4 Case Studies

Case 1: Mahindra Ecole Centrale building is shown in Fig. 4a. A crack was observed on the outer surface of the side wall building. The crack is shown closely in Fig. 4a. By manually measuring, we got the length as 19.1 mm, width as 1 mm and type of the crack is thin.

Case 2: Cafeteria building in Mahindra Ecole Centrale campus is shown in Fig. 4b, a crack was observed on the wall on front side. A close-up of the crack is also shown. By manually measuring, we got the length as 27.3 mm, width as 4.6 mm and type of the crack is wide.

Case 3: Cafeteria building in Mahindra Ecole Centrale campus (Fig. 4c). A crack was observed on the outer surface of the wall. The crack is also shown closely in Fig. 4c. By manually measuring, we got the length as 33.1 mm, width as 1.5 mm and type of the crack is medium.
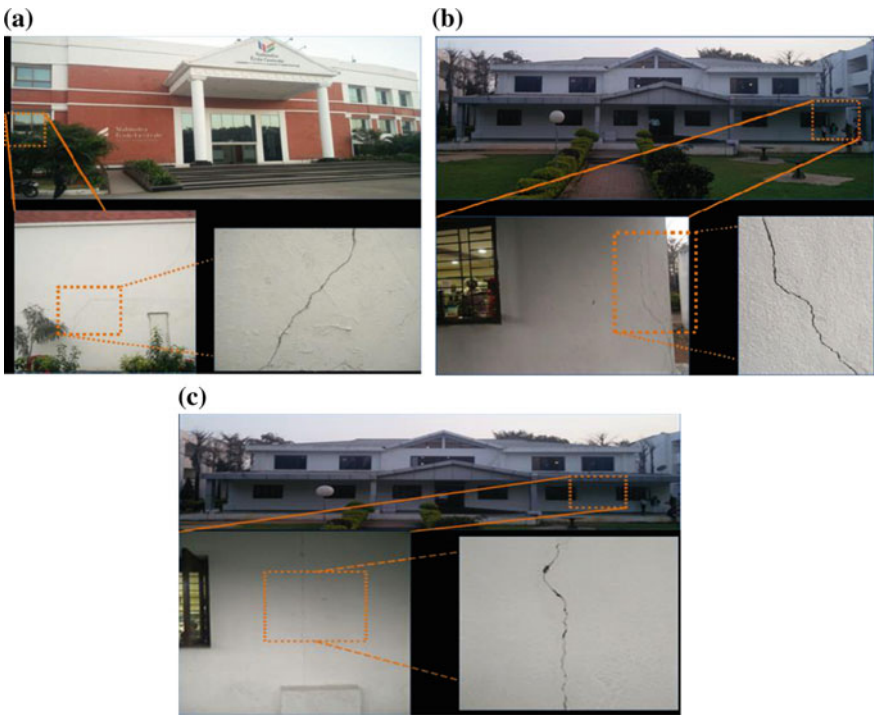
Fig. 4 The location of the crack is shown for better understanding: **a** Crack one. **b** Crack two. **c** Crack three
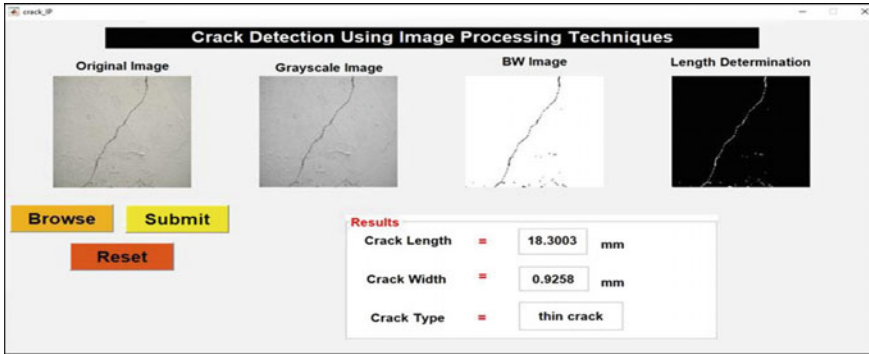
Fig. 5 Image processing for crack one
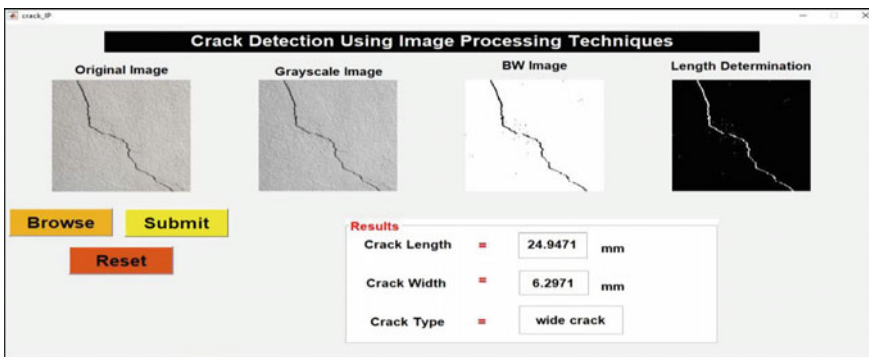
Fig. 6 Image processing for crack two

5 Results

The case study images shown in Fig. 4a-c were given as input to the GUI for processing cracks. The outputs obtained in the GUI are shown in Figs. 5, 6 and 7.

6 Analysis

Table 1 gives the obtained values for each case study image while Table 2 gives the actual values of each case study image obtained through manual inspection along with the error values. The lengths of the cracks obtained as outputs were almost close to the original length of the crack with an error of 7.053% on average. The lengths obtained for all images were lesser than the original values while the width was not
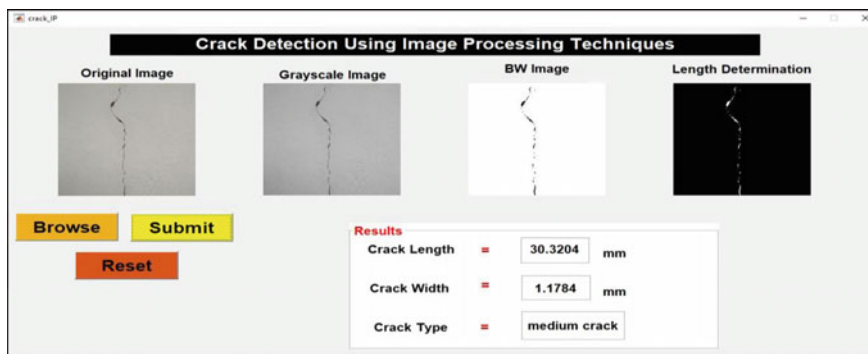
Fig. 7 Image processing for crack three

Table 1 Results obtained in GUI

Case (crack)	Length of crack (mm) obtained	Width of crack (mm)	Type of crack
One	18.3003	0.9258	thin
Two	24.9471	6.2971	wide
Three	30.3264	1.1784	medium

Table 2 Actual values

Case (crack)	Actual length of crack (mm)	Actual Error	Actual Width of crack (mm)	Actual Error
One	19.1	0.0418	1	0.0742
Two	27.3	0.0861	4.6	−0.3689
Three	33.1	0.0837	1.5	0.2144

that accurate. The maximum error while calculating width was obtained in case two images shown in Fig. 6 which is detected to have a width of 6.29 mm while the actual width is only 4.6 mm. The error in width calculation is −21.91% on an average. The accuracy in calculating the length is 92.947% and the accuracy in calculating the width is 78.09%.

7 Conclusion

Our main aim is to make a user-friendly GUI that can detect a crack on the concrete wall and give its length, width, and type as outputs. We converted the original image

into a binary image after compressing it. The procedure we are implementing calculates the length and width of the crack from the binary image. It also gives the type of crack along with length and width as outputs. The error in calculating length is 7.053%. The error in calculating width is 21.91%. In almost all images, the lengths are a little lesser than the original values. The widths obtained are also lesser than the actual values with an exception of crack two.

The errors can be minimized by implementing more sophisticated procedures. Our current attempts at noise reduction were converting into grayscale and compressing the image into 500×500 pixels. This has reduced the noise but it is not fully efficient. To overcome the above shortcomings and to improve the accuracy of our algorithm that uses Deviation of Gaussian (DOG) to calculate the width of the crack and to calculate the length, the work of Liang-Chienchen et al. [8] is being considered.

References

1. BIS. (1984). SP25: Handbook on causes and prevention of cracks in building, Bureau of Indian Standards, New Delhi.
2. Moon, H., & Kim, J. (2011). Intelligent crack detecting algorithm on the concrete crack image using neural network. *Proceedings of the 28th ISARC*, pp. 1461–1467.
3. Doihara, T. (1993). Crack Measuring System Based on Hierarchical Image Processing Technique. *International Archives of Photogrammetry and Remote Sensing, 29*, 155–155.
4. Yang, Y. S., Yang, C. M., & Huang, C. W. (2015). Thin crack observation in a reinforced concrete bridge pier test using image processing and analysis. *Advances in Engineering Software*, *83*, 99–108.
5. Yamaguchi, T., & Hashimoto, S. (2010). Fast crack detection method for large-size concrete surface images using percolation-based image processing. *Machine Vision and Applications*, *21*(5), 797–809.
6. Talab, A. M. A., Huang, Z., Xi, F., & HaiMing, L. (2016). Detection crack in image using Otsu method and multiple filtering in image processing techniques. *Optik-International Journal for Light and Electron Optics*, *127*(3), 1030–1033.
7. Fujita, Y., Mitani, Y., & Hamamoto, Y. (2006, August). A method for crack detection on a concrete structure. In *18th International conference on pattern recognition (ICPR'06)* (Vol. 3, pp. 901–904). IEEE.
8. Chen, L. C., Shao, Y. C., Jan, H. H., Huang, C. W., & Tien, Y. M. (2006). Measuring system for cracks in concrete using multitemporal images. *Journal of Surveying Engineering*, *132*(2), 77–82.
9. Ito, A., Aoki, Y., & Hashimoto, S. (2002, November). Accurate extraction and measurement of fine cracks from concrete block surface image. In *IEEE 2002 28th Annual Conference of the Industrial Electronics Society. IECON 02* (Vol. 3, pp. 2202–2207). IEEE.
10. Prasanna, P., Dana, K., Gucunski, N., & Basily, B. (2012, April). Computer-vision based crack detection and analysis. In *Sensors and smart structures technologies for civil, mechanical, and aerospace systems 2012* (Vol. 8345, p. 834542). International Society for Optics and Photonics.
11. Lee, B. Y., Kim, J. K., Kim, Y. Y., & Yi, S. T. (2007, August). A technique based on image processing for measuring cracks in the surface of concrete structures. In *Proceedings of the 19th International Conference on Structural Mechanics in Reactor Technology (smirt-19)*.
12. Nishikawa, T., Yoshida, J., Sugiyama, T., & Fujino, Y. (2012). Concrete crack detection by multiple sequential image filtering. *Computer-Aided Civil and Infrastructure Engineering*, *27*(1), 29–47.

Axial Strength Estimation of Cold Formed Steel Wall Panels Through Numerical Modeling

Abhinav Dewangan, Govardhan Bhatt and Chanchal Sonkar

Abstract The Cold Formed Steel (CFS) Wall Panels are generally utilized as the structural components in low- and mid-rise CFS structures (residential & industrial buildings). This study presents the Nonlinear Finite Element Analyses (NFEA) using ANSYS of CFS wall panels with 10 different configurations. The non-linearity in the numerical model presented consists of materialistic nonlinearity, geometric imperfections and connection nonlinearity. In this paper, CFS wall panels' response is obtained based on the nonlinear behavior of the structural components. The numerical simulations of geometric imperfection in the models are considered are based on the 1st and 2nd eigenvalue buckling modes. The effect of screw spacing and sheathing has been studied. The analyses results of numerical modelling using ANSYS for axial strength are compared with American Iron and Steel Institute (AISI) specifications.

Keywords Wall · Systems · Nonlinear · Imperfections

1 Introduction

The Cold-Formed Steel (CFS) Wall Panels are generally utilized as the structural components in low- and mid-rise CFS structures (residential and industrial building). Currently, many theoretical and numerical studies have been conducted to investigate the influence of various parameters, including the screw spacing, stud section and spacing, type of sheathing, hole of stud web, and height of wall stud, on the axial load capacity and the failure modes of such wall systems. In some circumstances,

A. Dewangan (✉) · G. Bhatt
National Institute of Technology, Raipur, CG, India
e-mail: abhinav.se19@gmail.com

G. Bhatt
e-mail: gov.ce@nitrr.ac.in

C. Sonkar
CSIR-Central Building Research Institute,
Roorkee, UK, India
e-mail: chanchalsonkar@cbri.res.in

the failure mode and axial strength of the wall studs were not accurately estimated by the design codes, especially for the wall studs with a slender web and sheathing on one side [1]. The increase of the compressive strength on application of sheathing or denser screw connection in the vicinity which is required to be studied along with the variation of load prediction by AISI method and FEA procedure.

2   Numerical Modelling of CFS Stud

The numerical modelling of CFS studies done using ANSYS to evaluate the axial strength of the CFS single Stud wall panel considered with varying the screw spacing. The effect of sheathing has also been studied by varying the parameters. The nonlinearity is considered comprises of material nonlinearity, geometric nonlinearity and connection nonlinearity (Fig. 1).

2.1   Initial Imperfection

In ANSYS, the initial imperfection of a CFS wall stud can be simulated by the correction of the coordinates of the stud. The amplitude of the initial imperfection applied to the wall stud is the sum of the amplitudes of imperfection distribution (1st eigenvalue buckling mode; local and second imperfection distribution; tiny half-wave local deformation). If d is the amplitude of the initial imperfection, and t denotes the thickness of the CFS wall stud, the amplitude of imperfection distribution [1, 6] is given by the equation as follows (Fig. 2):

$$d = 6. \, t^{-2.t} \tag{1}$$

(a) Without sheathing   (b) One side sheathed   (c) Both side sheathed
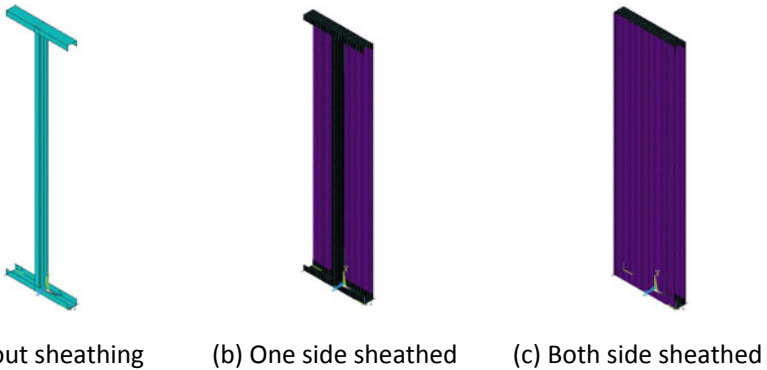
Fig. 1 Stud and track assembly **a** Without sheathing **b** One side sheathed **c** Both side sheathed

1st mode of buckling

2nd mode of buckling
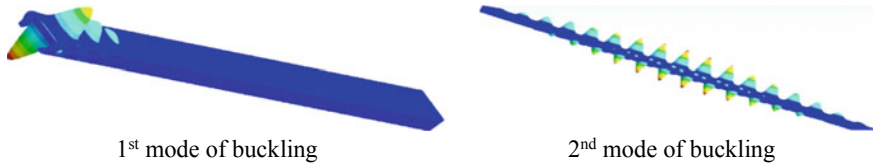
Fig. 2 Modes of buckling considered to impart initial imperfection to stud

Table 1 Mesh convergence for single stud

Mesh size	20 mm	15 mm	10 mm	5 mm	2 mm
ULC (Ultimate Axial Load Capacity of stud) (kN)	28.325	27.665	26.380	25.778	25.570
%difference w.r.t. finest mesh(2 lac nodes)	10.77	8.19	3.16	0.81	0

2.2 Boundary Conditions

The boundary conditions provided in the model are one end is clamped and another end of the wall panel is so restrained that it could move only in vertical that is Y-direction. Another type of boundary condition that is employed in the present numerical model is the nonlinear multipoint constraint which is utilized for simulating screw connections at the desired locations which has only one degree of freedom.

2.3 Mesh Convergence Study

Mesh convergence study has been performed on the single stud and single stud wall panel, found that best mesh size for stud is 5 mm, for tracks 10 mm and for the sheathing it found to be 20 mm. Variations of ultimate load capacity (ULC) of single stud are as follows (Table 1 and Fig. 3):

2.4 Stress-Strain Model (Steel)

The stress–strain model [3] for NFEA considered in the present study is as follows:

$$\varepsilon_T = \frac{f_T}{E_T} + \beta \left(\frac{f_{y,T}}{E_T} \right) \left(\frac{f_T}{f_{y,T}} \right)^n \tag{2}$$

where ε_T, f_T, E_T, β, $f_{y,T}$, n are strain at temperature T, stress at temperature T, elasticity modulus at temperature T, is a temperature coefficient whose value is taken
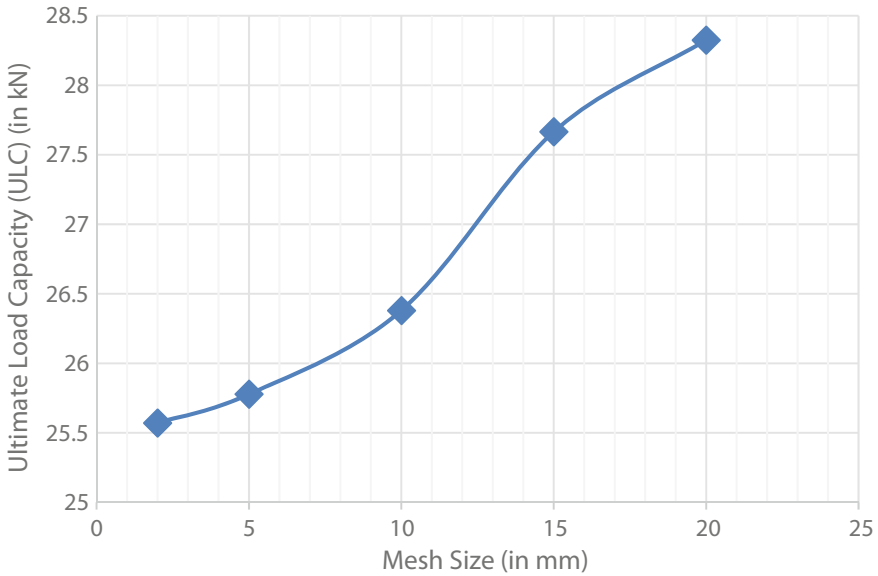
Fig. 3 Mesh convergence curve

as 3.5 (for 20–3000C), yield stress at temperature T and slope deciding parameter whose value is taken as 15, respectively.

3 Direct Strength Method [2]

The Direct Strength Method is essentially an extension of the use of column curves for global buckling, but with application to local and distortional buckling instabilities and appropriate application of interaction and post-buckling reserve in these modes. In order to analyze serviceability, deflections are normally determined at the service stress level of interest [3]. Direct Strength Method utilizes gross cross-section properties but needs a precise calculation of member elastic buckling behavior. Numerical methods like the finite strip method or generalized beam theory, are utilized for the stability calculations. Based on this direct strength method through CUFSM [7], the calculations for the wall panel axial strength by following the AISI [2] procedure, has been calculated.

4 Model Configuration

The general model configuration for the axial strength used in ANSYS software and CUFSM module for direct strength method comprises of stud, track assembly along with arrangement of sheathing with several models. The element type considered in ANSYS to model the stud, sheath and track is four noded shell element (Shell 181)as shown in Fig. 4. The height and width of assembled frame are 2400 mm and 600 mm, respectively. The material used in stud and track is steel whose general and nonlinear properties are defined through its grade (Q345), density (7850 kg/m^3), elastic modulus (200,270.882 MPa) [4], Poisson's ratio (0.3) and multi-linear kinematic hardening total stress-strain curve.

The sheathing properties of MGO board are assigned; density (975 kg/m^3), elastic modulus (4400 MPa), Poisson's ratio (0.2) and thickness (10 mm) are the properties of board assigned. The height and width of the specimen will be as per the assembled configuration covering the full area on one side or two sides, whatever may be the arrangement required.

The screw connections are used for connecting the members of the model together by connecting the stud to track, sheathing to stud, and sheathing to track. The type of element considered for this process is the Nonlinear MPC-184 constraint and selecting the type of joint as screw and giving the input parameters of Screw number 8 having length 25 mm, pitch 1.25 and stops an d locks tolerance as ± 1 mm. The mesh size for the whole assembly is as per mesh convergence results (Fig. 4 and Table 2).

Fig. 4 Cross-section of the stud and track (unit: mm) **a** Single C-channel section of the stud **b** U-channel section of the track
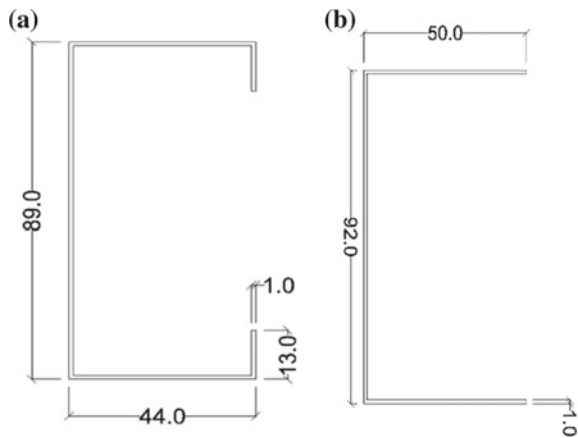
Table 2 Model configurations

Specimen	Sheathing	Section	Screw spacing (mm)		CUFSM		
					Parameters: Spring stiffness		
			1st side	2nd side	Side	dir	Value (kip/in/in)
S1	-na-		-na-	-na-	-na-		
S2	1 side		150	-na-	150 mm spacing side only	X	0.14848
						Z	0.00019
						θ	0.11064
S3	1 side		300	-na-	300 mm spacing side only	X	0.07627
						Z	0.00019
						θ	0.11064
S4	1 side		400	-na-	400 mm spacing side only	X	0.05759
						Z	0.00019
						θ	0.11064
S5	Both sides		300	300	Both sides	X	0.07627
						Z	0.00019
						θ	0.11064
S6	1 side		200	-na-	200 mm spacing side only	X	0.11285
						Z	0.00019
						θ	0.11064
S7	Both sides		200	200	Both sides	X	0.11285
						Z	0.00019
						θ	0.11064
S8	Both sides		300	150	150 mm spacing side	X	0.14095
						Z	0.00009
						θ	0.11064
					300 mm spacing side	X	0.07627
						Z	0.00019
						θ	0.11064
S9	Both sides		150	150	Both sides	X	0.14848
						Z	0.00019
						θ	0.11064
S10	Both sides		400	400	Both sides	X	0.05789
						Z	0.00254
						θ	0.11064

Note 'dir' refers to direction; Conversion factor used for stiffness is 1kip/in/in = 6.895 N/mm/mm

Table 3 Percentage variation of Axial load capacity

Specimen	% increase with respect to single stud capacity	% change with respect to AISI prediction
S1	0	−9.19
S2	34.96	−0.05
S3	25.69	−6.86
S4	24.42	−7.79
S5	74.27	17.14
S6	24.36	−7.88
S7	74.70	16.40
S8	74.33	17.39
S9	77.08	17.38
S10	73.70	18.60

5 Results and Discussion

Comparison between the axial strength of the single wall stud with varying the screw spacing and the specimens with one- or two-side sheathing has been done. The comparison of the results of the AISI prediction and numerical model result has been depicted in the following table and the table of results.

5.1 Comparison Between Axial Strength of Single Stud

See (Table 3).

5.2 Comparison Between Numerical Model and Analytical Design Load

See (Table 4 and Fig. 5).

Table 4 Numerical model: (NM) & Analytical (AISI) method (AM) results comparison

Specimen	CUFSM				NM (kN)
	Buckling type	Load factors	Load	AM (kN)	
S1	L	0.3672	28.400	28.400	25.788
	D	0.850	49.081		
	G	0.690	38.151		
S2	L	0.3737	34.821	34.821	34.803
	D	1.035	53.204		
	G	1.3731	51.590		
S3	L	0.3737	34.804	34.804	32.414
	D	1.0344	53.192		
	G	1.3698	55.144		
S4	L	0.3739	36.369	34.797	32.086
	D	1.0956	54.397		
	G	1.7571	51.535		
S5	L	0.3676	38.365	38.365	44.942
	D	1.3041	58.286		
	G	2.6209	59.871		
S6	L	0.37377	34.814	34.814	32.690
	D	1.0347	53.198		
	G	1.3718	51.575		
S7	L	0.3676	38.694	38.694	45.042
	D	1.3041	58.318		
	G	2.6209	60.665		
S8	L	0.36762	38.294	38.294	44.957
	D	1.3041	58.032		
	G	2.6209	60.256		
S9	L	0.37395	38.902	38.902	45.666
	D	1.3266	58.350		
	G	3.1121	61.170		
S10	L	0.3676	37.766	37.766	44.794
	D	1.3031	57.987		
	G	2.4482	58.979		

Source where L: local buckling; D: distortional buckling; G: global buckling
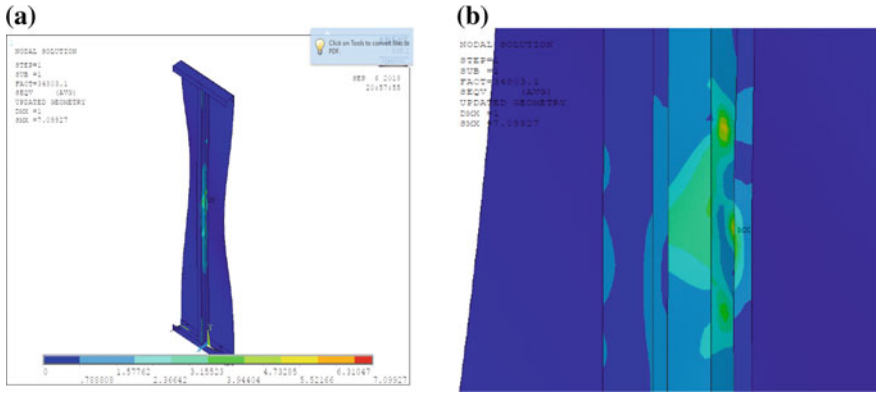
Fig. 5 Post-processing images for numerical model S2: Nodal vonmises stress (Failure pattern: screw pull-through and local buckling of the stud)

6 Conclusion

The Nonlinear Finite Element Analysis (NFEA) is performed over 10 different models. The following conclusions are drawn.

- It is being observed that with the placement of sheathing on both sides of the wall panel and dense screw connection the strength of panel drastically as observed in S9 model
- The S2 model is showing less variation with AISI prediction in comparison to all other models.

References

1. Ye, J., Feng, R., Chen, W., & Liu, W. (2016). Behavior of cold-formed steel wall stud with sheathing subjected to compression. *Journal of Constructional Steel Research, 116,* 79–91.
2. AISI (American Iron and Steel Institute). (2012). North American specification for the design of cold-formed steel structural members. AISI S100–12 .
3. Schafer, B. W. (2008). The direct strength method of cold-formed steel member design. *Journal of Constructional Steel Research, 64*(7–8), 766–778.
4. Lee, J. H., Mahendran, M., & Makelainen, P. (2003). Prediction of mechanical properties of light gauge steels at elevated temperatures. *Journal of Constructional Steel Research, 59*(12), 1517–1532.
5. Schafer, B. W., & Pekoz, T. (1998). Direct strength prediction of cold-formed steel members using numerical elastic buckling solutions.

6. DeSalvo, G. J., & Swanson, J. A. (1985). ANSYS engineering analysis system user's manual. Houston, PA: Swanson Analysis Systems.
7. Schafer, B. W. (2012). CUFSM 4.05–Finite strip buckling analysis of thin-walled members. Baltimore, USA: Department of Civil Engineering, Johns Hopkins University.

Estimation of Local Site Effect on Earthquake Ground Motions for Sites in the State of Haryana, India

Nitish Puri and Ashwani Jain

Abstract One-dimensional nonlinear site response analysis has been carried out to determine site-specific parameters for earthquake resistant design for the state of Haryana. The geotechnical data have been collected from various government and private organizations to have assessment of the soil properties and depth of ground water table in the study area. Shear modulus (G_{max}) value has been calculated for each soil layer at different sites using blow count values from standard penetration test (SPT) data. An extensive literature review has been carried out for the selection of appropriate correlation between G_{max} and SPT N-value. The sites have been classified on the basis of average SPT N-value for the soil profile above bedrock as per the recommendations of National Earthquake Hazards Reduction Program (NEHRP). Site response has been formulated in terms of amplification factor for peak ground acceleration (PGA). The results show that the soils in Haryana are capable of amplifying earthquake ground motions. Therefore, a site-specific design approach should be adopted for important structures.

Keywords Seismic hazard · Site characterization · Local site effect · Amplification · Haryana

1 Introduction

Geographical statistics of India indicate that nearly 60% of the terrain area is susceptible to earthquakes and it calls for an immediate need for site-specific seismic hazard analysis. The damage to life and property caused by 1993 Latur earthquake and 2001 Bhuj earthquake, have been a wakeup call for government to take appropriate mitigation measures. The Indian Seismic Code has classified the country into

N. Puri (✉) · A. Jain
Department of Civil Engineering, National Institute of Technology,
136119 Kurukshetra, Haryana, India
e-mail: nitishpuri.ce.89@gmail.com

A. Jain
e-mail: ashwani.jain@nitkkr.ac.in

four zones; seismic zone II, III, IV, and V with specified peak ground acceleration (PGA) values of 0.10, 0.16, 0.24, and 0.36 g, respectively [1]. The seismic hazard is considered to have significant spatial variability and hence, such broad zoning is undesirable. Therefore, it is necessary to develop regional seismic hazard maps in line with local tectonic setup in line with the latest seismic design provisions used in other countries.

Local site conditions have profound influence on all the important characteristics of ground motions, i.e. amplitude, frequency content, and duration. Characteristics of seismic waves get modified as they travel through different soil layers. This phenomenon is referred to as 'local site effects'. The extent of influence depends upon the thickness and properties of the soil layers, site topography, and on the characteristics of the input motion itself [2]. Therefore, identification of soil layers causing amplification of ground motions is an important task for accurate assessment of seismic hazard in earthquake-prone areas. In a recent study on seismic hazard assessment of Haryana [3], carried out for rock site conditions using ground motion model proposed by NDMA [4], it has been concluded that the state can experience earthquake ground motions with high PGA values. Therefore, estimation of the effect of local soil conditions is essential in order to have a realistic assessment of ground motions required for the design of earthquake-resistant structures in the state.

Site response analysis is often carried out for the determination of site-specific design response spectra, peak accelerations, resonant frequencies, dynamic stresses and strains, and for the evaluation of liquefaction susceptibility. The analysis can be carried out by various numerical approaches, e.g. linear, equivalent linear and nonlinear modeling. The nonlinear site response analysis gives more accurate characterization of the true nonlinear behavior of the soil. Moreover, for the state of Haryana, where high PGA leading to high strain condition is expected during earthquakes, a nonlinear approach is likely to provide reasonable results [5]. One-dimensional approach is believed to provide conservative parameters, but it has been adopted since most of the projects designed using this methodology have survived earthquakes [6]. Several site response studies have been carried out for different places in India using this approach, e.g. for Bhuj [7], Chennai [8], Bangalore [9], Kolkata city [10], Kanpur [11], Delhi [12], Mumbai [13], Mumbai city [14], Kolkata City [15], Uttarakhand [16] and Chandigarh [17].

In the present study, nonlinear site response analysis has been carried for the state of Haryana using DEEPSOIL program [18]. The one-dimensional nonlinear site response analysis model in DEEPSOIL, DS-NL2, has been used to have assessments from vertical propagation of horizontal shear waves in deep soil deposits. Site response has been formulated in terms of amplification factor for PGA. The results show that the soils in Haryana are capable of amplifying earth-quake ground motions. Therefore, a site-specific design approach should be adopted for important structures.

2 Geotechnical Site Characterization

Geotechnical data have been obtained from various organizations to assess soil properties and ground water conditions. The database contains geotechnical information for 1053 distinct locations in Haryana covering various districts. The data from boreholes drilled up to refusal have been considered for site response analysis. The sites have been categorized as Class A, B, C, D, E and F based on National Earthquake Hazards Reduction Program (NEHRP) provisions using average SPT N-value for 30 m depth (N_{30}) for the soil profile [19]. The average N-value (N_{30}) for the soil profile can be calculated using the following Eq. (1).

$$N_{30} = \frac{\sum_{i=1}^{n} d_i}{\sum_{i=1}^{n} \frac{d_i}{N_i}} \qquad (1)$$

where N_i = SPT N-value of a layer and d_i = Thickness of a layer. It has been observed that for 77 sites drilled up to refusal, 73 sites represent site Class D (medium dense soils), 3 sites represent site Class C (dense soils), whereas only one site falls into site Class E (soft soils) category. It has been observed that the average N value for the profiles varies from 13 to 54 with maximum and minimum values observed at sites in Sector 20, Panchkula and Basant Vihar, Jhajjar respectively.

3 Estimation of Local Site Effects

Due to variation in local soil conditions, the surface level PGA and spectral acceleration (S_a) at soil sites can be different from that for rock sites. Local site effects are generally evaluated using 1D site response model, which assumes that seismic waves propagate in the vertical direction through the horizontal layers of the soil profile. All the sites are assumed to have horizontal layers which extend infinitely. The soil layers are modeled as a series of lumped masses connected by spring and dashpots making it multiple degrees of freedom system. Nonlinear analysis requires single relationship between shear stress and shear strain under cyclic loading with the appropriate generation of hysteretic damping. The procedure consists of the following steps [20]: (1) data collection, (2) modeling the data for computer programs, (3) execution of computer program, and (4) interpretation of results. Several input data are required in the site response analysis, which are classified into the following four categories:

1. Geotechnical or geophysical information up to refusal or at least up to 30 m depth below ground level. This can be acquired from the soil profile details obtained from the results of standard penetration test (SPT), cone penetration (CPT) tests or multi-channel analysis of surface waves (MASW) tests.

2. Dynamic soil properties at each layer, e.g., shear modulus G_{max}, modulus degradation vs. shear strain (G/G_{max}-γ) curves and damping ratio vs. shear strain (D-γ) curves.
3. Acceleration time histories of representative earthquakes recorded at rock site.
4. Parameters to control the flow of the computer program or method of analysis.

The pressure-dependent hyperbolic model (MKZ) relates shear modulus (G) and damping ratio (D) of the soil layers to shear strains developed during earthquakes. This demands a value of reference strain (γ_r), stress-strain plot parameter (β), stress-strain plot parameter (s), pressure-controlled parameter (b), reference stress (σ_{ref}) and pressure-controlled parameter (d) for each layer of the soil column. For defining the modulus reduction curve of sandy soils, effective vertical stress is required. However, in the case of clayey soils, information for plasticity index (PI) of soil is also required. The cyclic shear stresses induced by cyclic shear strains or vice versa, are governed by Masing and extended Masing criteria. Curve fitting is then carried in order to obtain the above parameters that provide the best fit for both modulus reduction and damping ratio for each layer using MRDF-UIUC method. The thickness of the soil layers is set in a way that the maximum frequency of the seismic wave that a layer can propagate is always above 25 Hz. The bedrock is taken at refusal, i.e. for SPTN-value > 50 for 15 cm penetration or SPTN-value > 100 for 30 cm penetration of the split-spoon sampler. The engineering bedrock is in general taken as the uppermost layer in the soil profile having shear wave velocity (V_s) greater 760 m/s as per the NEHRP provisions [21]. In general, the V_s value of the bedrock is greater than that of the overlying soil layers. The damping ratio of the bedrock has no effect on the site response in time domain analysis and has a negligible effect on the results in frequency domain analysis [18]. For present study, bedrock has been assumed as an elastic half-space with value of damping taken as 2%, density as 2.5 g/cc and shear wave velocity (V_s) as 760 m/s.

Low strain shear modulus plays a significant role in the estimation of site response parameters. The stiffness of an element of soil is characterized considering the low strain shear modulus (G_{max}) and in the manner its ratio (G/G_{max}) degrades with cyclic strain amplitude (γ) and other parameters. Shear wave velocities are generally used to compute G_{max} by the following relation:

$$G_{max} = \rho V_s^2 \qquad (2)$$

where V_s = shear wave velocity and ρ = unit weight of soil layer. For the present study, in situ measured values of shear wave velocity (V_s) were not available and therefore, several correlations between low strain shear modulus (G_{max}) and SPT N-value for different type of soils have been reviewed [22–30]. These correlations can be selected on the basis of soil type and value of coefficient of correlation (R). For the present study, as per the recommendations of Anbazhagan et al. [31, 32], the correlations given in Table 1 have been used.

In the absence of site-specific shear modulus degradation (G/G_{max}-γ) and damping ratio (D-γ) curves, standard curves have been used for clays and sands. For clays

Table 1 Correlations between shear modulus (G) and SPT N-value

Soil type	Correlation	Investigator
Clays	$G = 1220\ N^{0.62}$	Ohba and Toriumi [23]
Sands/silts/sand-silt mixtures	$G = 650\ N^{0.94}$	Ohsaki and Iwasaki [25]
Clay-sand mixtures	$G = 1182\ N^{0.76}$	Ohsaki and Iwasaki [25]
Gravels	$G = 82.5\ N^{0.767}$	Imai and Tonouchi [27]

and plastic silts, based on PI values, G/G_{max}-γ and D-γ curves developed by Vucetic and Dobry [33] have been selected. For sandy and silty soils, G/G_{max}-γ and D-γ curves developed by Seed and Idriss [34] have been used, as proposed in the study carried out on sandy and silty soils of Delhi and nearby areas, by Hanumantharao and Ramana [35]. For gravelly soils, G/G_{max}-γ and D-γ curves developed by Seed et al. [36] have been used. The same curves have been used by many other investigators for analysis [10, 13, 15].

The final step in site response analysis involves using the available or generating the artificial acceleration time history, which is compatible with the maximum dynamic loading expected at the site of interest. An input acceleration time history can be selected based on PGA value, magnitude of controlling earthquake, source to site distance and the site class. In the present study, the acceleration time histories recorded at rock sites have been considered for the analysis. The PGA values for the rock sites obtained from deterministic seismic hazard analysis of Haryana [3] have been used for the selection of input motions for each site. The rock PGA values for selected 77 sites vary from 0.073 to 0.396 g. Several recorded acceleration time histories of major earthquakes that have occurred in Himalayan Thrust System have been obtained from USGS earthquake data repository. Suitable recorded acceleration time histories of 6.6 M_w 1999 Chamoli earthquake, 6.9 M_w 2011 Sikkim earthquake and 7.0 M_s 1991 Uttarkashi earthquake recorded at rock sites have been selected for carrying out site response analysis. The PGAs of selected acceleration time histories range from 0.117 to 0.36 g. The recorded acceleration time histories of Himalayan Thrust System have been shown in Fig. 1. Acceleration time histories close to rock PGA of a site have been used as an input motion in the analysis.

Non-linear site response analyses have been carried out for 77 sites in the state of Haryana using DEEPSOIL software. It has been observed that amplification factors for PGA range from 0.531 to 1.881. It has been observed that for an input motion having PGA between 0.1 and 0.2 g, the average amplification factor is 1.37, for PGA between 0.2 and 0.3 g it is 1.48, while for PGA greater than 0.3 g, the average amplification factor is 1.05. The observed surface PGA values range from 0.12 to 0.51 g, with minimum and maximum values observed at sites at Bhattu Mandi, Fatehabad and Super Seals, Faridabad respectively. The results of site response analysis show that the soil sites in the state of Haryana are capable of amplifying earthquake ground

Fig. 1 Recorded time histories used in the study
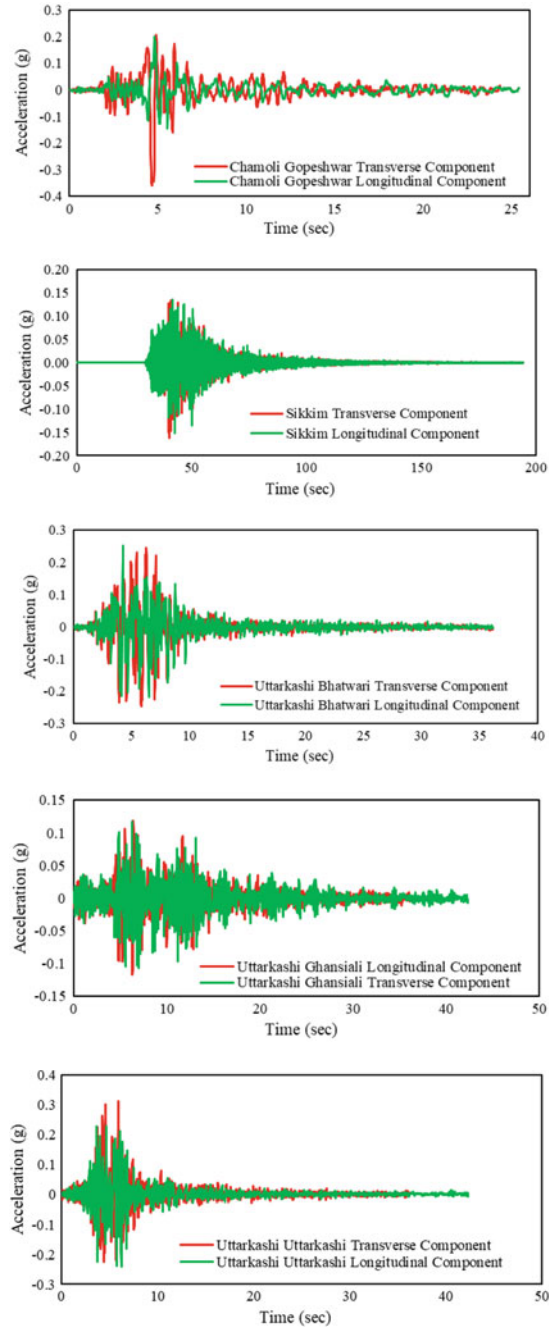
motions and the same must be accounted for in the earthquake resistant design of important structures in the state. The distribution of amplification factor for PGA in the state of Haryana has been plotted using nearest-neighbor interpolation as shown in Fig. 2.

Maximum displacement at surface ranges from 0.003 to 0.175 m. Maximum strain (%) ranges from 0.06 to 5.88% for depth ranging from 2.5 to 30.5 m. It has been observed that earthquakes in Haryana can generate large strains in deeper soil layers also, which indicates vulnerability of the structures due to earthquake-induced liquefaction or settlement. This necessitates a detailed liquefaction hazard assessment of the state.

It has been observed that maximum amplification occurred at sites where rock PGA is on the lower side while lowest amplification factors have been observed at sites with higher rock PGA. It can be attributed to the fact that when a site is analyzed
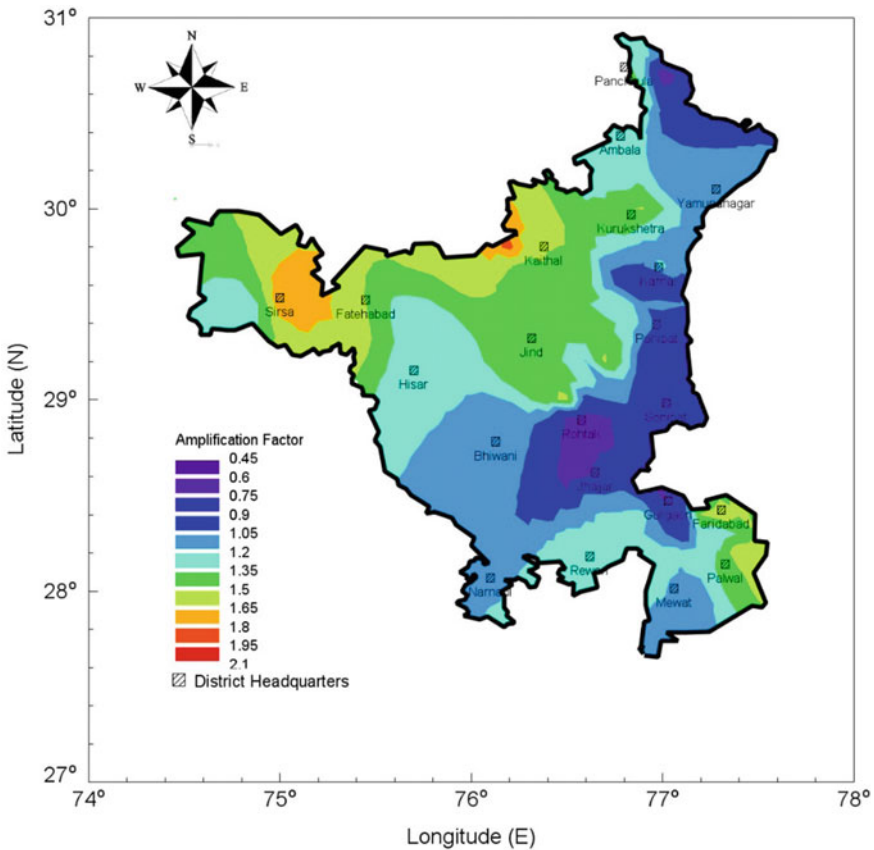
Fig. 2 Amplification factors for PGA based on nonlinear site response analysis

with an acceleration time history having high PGA, most of the energy of the ground motion is dissipated in deforming the soft soil layers.

4 Conclusion

Nonlinear site response analysis has been carried out for some sites in the state of Haryana. Geotechnical site characterization has been done using NEHRP provisions. It has been observed that most of the sites fall into site Class D (medium dense soils) category. The acceleration time histories of earthquakes that have occurred in Himalayan region, Uttarkashi earthquake (1991), Chamoli earthquake (1999), and Sikkim earthquake (2011), have been selected as input motions. It has been observed that amplification factor for peak ground acceleration ranges from 0.531 to 1.881. It shows that soils in the state are capable of amplifying earthquake ground motions. This behavior must be accounted for in the design of earthquake-resistant structures. Using the amplification factors calculated for 77 sites, a PGA amplification map has been plotted for the state using nearest-neighbor interpolation. It has been observed that large strains can occur in deeper soil layers also during earthquakes in the state and, therefore, there are chances of liquefaction of soils.

References

1. IS-1893: Part 1. (2016). Indian standard criteria for earthquake resistant design of structures. Bureau of Indian Standard, New Delhi.
2. Kramer, S. L. (2013). *Geotechnical earthquake engineering*. South Asia: Pearson.
3. Puri, N., & Jain, A. (2016). Deterministic seismic hazard analysis for the state of Haryana, India. *Indian Geotechnical Journal, 46*(2), 164–174. https://doi.org/10.1007/s40098-015-0167-1.
4. NDMA. (2011). *Development of probabilistic seismic hazard map of India*. Government of India: National Disaster Management Authority.
5. Stewart, J. P., & Kwok, A. O. L. (2008). Nonlinear seismic ground response analysis: Code usage protocols and verification against vertical array data. *Geotechnical Earthquake Engineering and Soil Dynamics Congress IV.*
6. Govindaraju, L., Ramana, G. V., Hanumantharao, C., & Sitharam, T. G. (2004). Site specific ground response analysis. *Current Science, 87*(10), 1354–1362. https://www.jstor.org/stable/24109475.
7. Sitharam, T. G., & Govindaraju, L. (2004). Geotechnical aspects and ground response studies in Bhuj earthquake, India. *Geotechnical and Geological Engineering, 22,* 439–455.
8. Boominathan, A., Dodagoudar, G. R., Suganthi, A., & Maheswari, U. R. (2008). Seismic hazard assessment of Chennai city considering local site effects. *Journal of Earth System Science, 117*(2), 853–863.
9. Anbazhagan, P., & Sitharam, T. G. (2009). Estimation of ground response parameters and comparison with field measurements. *Indian Geotechnical Journal, 39*(3), 245–270.
10. Govindaraju, L., & Bhattacharya, S. (2012). Site-specific earthquake response study for hazard assessment in Kolkata city, India. *Natural Hazards, 61,* 943–965.
11. Jishnu, R. B., Naik, S. P., Patra, N. R., & Malik, J. N. (2013). Ground response analysis of Kanpur soil along Indo-Gangetic plains. *Soil Dynamics and Earthquake Engineering, 51,* 47–57.

12. Mandal, H. S., Khan, P. K., & Shukla, A. K. (2014). Soil responses near Delhi ridge and adjacent regions in greater Delhi during incidence of a local earthquake. *Natural Hazards, 70,* 93–118.
13. Desai, S. S., & Choudhury, D. (2015). Site-specific seismic ground response study for nuclear power plants and ports in Mumbai. *Natural Hazards Review, 16*(4), 1–13.
14. Choudhury, D., Phanikanth, V. S., Mhaske, S. Y., Phule, R. R., & Chatterjee, K. (2015). Seismic liquefaction hazard and site response for design of piles in Mumbai city. *Indian Geotechnical Journal, 45*(1), 62–78. https://doi.org/10.1007/s40098-014-0108-4.
15. Chatterjee, K., & Choudhury, D. (2016). Influence of local soil conditions for ground response in Kolkata city during earthquakes. *Proceedings of the National Academy of Sciences, India-Section A, 88*, 1–14. https://doi.org/10.1007/s40010-016-0265-1.
16. Pandey, B., Jakka, R. S., & Kumar, A. (2016). Influence of local site conditions on strong ground motion characteristics at Tarai region of Uttarakhand. *Natural Hazards, 81*(2), 1073–1089.
17. Puri, N., & Jain, A. (2018). Possible seismic hazards in Chandigarh city of north-western India due to its proximity to Himalayan frontal thrust. *The Journal of Indian Geophysical Union, 22*(5), 485–506.
18. Hashash, Y. M. A., Musgrove, M. I., Harmon, J. A., Groholski, D. R., Phillips, C. A., & Park, D. (2016). *DEEPSOIL 6.1: User Manual*. Urbana, IL: University of Illinois at Urbana-Campaign.
19. BSSC. (2000). *National earthquake hazard reduction program (NEHRP) recommended provisions for seismic regulations for new buildings and other structures, part 1: Provisions (FEMA 368)*. Washington, DC: Building Seismic Safety Council.
20. Yoshida, N. (2014). Seismic ground response analysis. *Geotechnical, Geological and Earthquake Engineering Series*. https://doi.org/10.1007/978-94-017-9460-2.
21. Nath, S. K., & Thingbaijam, K. K. S. (2011). Assessment of seismic site conditions: A case study from Guwahati city, northeast India. *Pure and Applied Geophysics, 168,* 1645–1668.
22. Imai, T., & Yoshimura, Y. (1970). Elastic wave velocity and soil properties in soft soil. *Tsuchito-Kiso, 18*(1), 17–22.
23. Ohba, S., & Toriumi, I. (1970). Research on vibration characteristics of soil deposits in Osaka, part 2, on velocities of wave propagation and predominant periods of soil deposits. *Technical Meeting of Architectural Institute of Japan*.
24. Ohta, T., Hara, A., Niwa, M., & Saklano, T. (1972). Elastic moduli of soil deposits estimated by N-values. In *7th Annual Conference* (pp. 265–268). The Japanese Society of Soil Mechanics and Foundation Engineering.
25. Ohsaki, Y., & Iwasaki, R. (1973). Dynamic shear moduli and Poisson's ratio of soil deposits. *Soils and Foundations, 13*(4), 61–73. https://doi.org/10.3208/sandf1972.13.4_61.
26. Hara, A., Ohta, T., Niwa, M., Tanaka, S., & Banno, T. (1974). Shear modulus and shear strength of cohesive soils. *Soils and Foundations, 14,* 1–12. https://doi.org/10.3208/sandf1972.14.3_1.
27. Imai, T., & Tonouchi, K. (1982). Correlation of N-value with S-wave velocity and shear modulus. In *2nd European Symposium on Penetration Testing* (pp. 57–72). Amsterdam: A. A. Balkema Publishers.
28. Seed, H. B., Idriss, I. M., & Arango, I. (1983). Evaluation of liquefaction potential using field performance data. *Journal of Geotechnical Engineering, 109*(3), 458–482.
29. Anbazhagan, P., & Sitharam, T. G. (2010). Relationship between low strain shear modulus and standard penetration test 'N' values. *ASTM Geotechnical Testing Journal, 33*(2), 150–164.
30. Anbazhagan, P., Aditya, P., & Rashmi, H. N. (2012). Review of correlations between SPT N and shear modulus: A new correlation applicable to any region. *Soil Dynamics and Earthquake Engineering, 36,* 52–69. https://doi.org/10.1016/j.soildyn.2012.01.005.
31. Anbazhagan, P., Manohar, D. R., Moustafa, S. S. R., & Nassir, S. A. (2015). Effect of shear modulus correlation on site response study. *Disaster Advances, 8*(2), 16–30.
32. Anbazhagan, P., Manohar, D. R., Sayed, S. R. M., & Nassir, S. N. A. (2016). Selection of shear modulus correlation for SPT N-values based on site response studies. *Journal of Engineering Research, 4*(3), 18–42.
33. Vucetic, M., & Dobry, R. (1991). Effect of soil plasticity on cyclic response. *Journal of Geotechnical Engineering, 117*(1), 89–107.

34. Seed, H. B., & Idriss, I. M. (1970). *Soil moduli and damping factors for dynamic response analyses*. Berkeley, CA: University of California. Earthquake Engineering Research Center. Report EERC-70/10.
35. Hanumantharao, C., & Ramana, G. V. (2008). Dynamic soil properties for microzonation of Delhi, India. *Journal of Earth System Science, 117*(2), 719–730. https://doi.org/10.1007/s12040-008-0066-2.
36. Seed, H. B., Wong, R., Idriss, I. M., & Tokimatsu, K. (1986). Moduli and damping factors for dynamic analyses of cohesionless soils. *Journal of Geotechnical Engineering, 112*(11), 1016–1032. https://doi.org/10.1061/(ASCE)0733-9410(1986)112:11(1016).

Stability Analysis of Tied-Arch Bridges Under IRC Loading Condition Using Finite Element Method

K. S. Yogesh and Anubhav Singh

Abstract Tied-arch bridges are structured so as to guide outward horizontal forces of the arches to the chord tying both arch rib ends and further to the support through deck-connected tie-rods. Finite element is most often used method to analyze real bridges; we have various number of FE software available; Midas is one of its kind used to accurately simulate the real bridge. A very less effort has been done till now to analyze the tied-arch bridges for IRC loading conditions; this paper investigates the stability of 200 m span bridge under IRC loading cases. Efforts are made to find out the influence of straight, inclined, and network hanger arrangements on the structural behavior of bridge and also to justify the results; thickness of deck slab is varied for the above hanger arrangements. Objective of the work was to determine the most optimal arrangement of hangers along the deck slab for a road bridge, consisting of two steel arches using finite element analysis method. Nonlinear static analytical method was used for the analysis by using an FEM software Midas Civil. Validation of software for AASTO LRFD vehicle was done. 3D models of single span 200 m slab tied-arch bridges for different hanger arrangements have been done to determine maximum displacement, bending moment, and reactions. Deck slab was also varied for the different types of hanger arrangements that determine minimum displacement, minimum bending moment, and maximum support reaction to find the best combination of deck slab thickness and hanger arrangement.

Keywords Tied-arch bridges · Hangers · Arch rib · Nonlinear static analytical method · Midas civil

K. S. Yogesh
New Horizon College of Engineering, Banglore, Karnataka, India
e-mail: yogeshkadur@gmail.com

A. Singh (✉)
JSS Academy of Technical Education, Noida, Uttar Pradesh, India
e-mail: anubhavsngh7@gmail.com

1 Introduction

Bridge engineering began with the use of stone and wood for structures as early as from the Neolithic age. Thev oldest arch bridge is the Mycenanean Arkadiko Bridge in Greece which still exists which was built about 1300 BCv". The arches constructed for the bridge were half-circularv, but beginning with the flat arches. Design of arches had further improved by Perrronet at the end of the eighteenth century; his designs were structurally strong to accommodate the upcoming railroad loads. Further, the first theoretical design concepts were introduced by Lahire in the early 1770s using pressure line concept [1].

Tied-arch bridges are structured so as to guide outward horizontal forces of the arches to the chord tying both arch rib ends and further to the support through deck-connected tie-rods. Thrusts acting downwards on a tied-arch bridge's deck are translated to the vertical ties between the deck and the arch through tension force. Same as arch bridge, this tension force tends to flatten the arch and thereby to pushing its tips outward into the abutments. However, in a tied-arch or bowstring bridge, these movements are restrained by the strengthened chord, not by the abutments. This chord ties the tips of abutments together. If we take this thrust as a tension force, the mechanism remains same as our ancient bow with string that is being flattened. Therefore, the design is also called a bowstring-arch or bowstring-girder bridge [2]. The elimination of horizontal forces at the abutments allows tied-arch bridges to be constructed with less robust foundations; thus, they can be constructed atop elevated piers or even on unstable soil. Since their construction does not depend on horizontal compression forces for their integrity, tied-arch bridges can be prefabricated offsite and subsequently floated, hauled, or lifted into place [7].

2 Tied-Arch Structural Behavior

Overall structural arch behavior is demonstrated in Fig. 1, a two-hinged arch. The arch is acted upon by intermediate, transverse, downward point loads. Under this loading, the arch deflects, shortening along the longitudinal axis to create axial thrust which is, in turn, resisted by inclined reactions, R1 and R2. Those reactions have the vertical and horizontal components; therefore, to resist the vertical and horizontal components, we require sizeable foundations or abutments, depending on the subsurface foundation material. The final criterion for the arch requires the arch member to be shaped to avoid bending moments in the rib for downward loads, where in tied-arch brides the pin connections shown for the two-hinged arch are also easily envisioned by the supports affixed to the pier. A typical tied-arch bridge and its components are shown in Fig. 2. The uniform load acts on the concrete roadway deck that is ultimately transferred to the arch hangers. The loading places, the hangers in tension, and displaces the arch rib downward. The arch rib is restrained at each end as for the two-hinged arch, produces an axial shortening, and develops a compressive

Fig. 1 Typical tied arch bridges showing all its major components
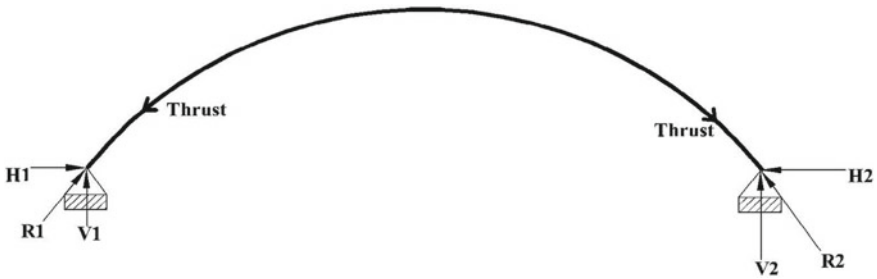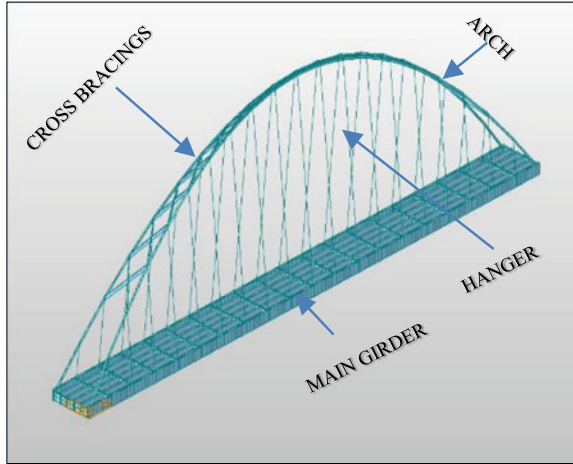
Fig. 2 Typical 2 hinged arch

thrust in the arch rib. Finally, as the arch rib exerts an outward thrust on the supports, the arch tie pulls the supports into equilibrium by loading the ties in tension. From the standpoint of external statics, the single span tied arch behaves in a determinant manner and reacts on the supporting substructure as if it were a simply supported beam [3].

3 Finite Element Analysis of Tied-Arch Bridges

Finite element (FE) is the most suitable method for the static analysis of real bridges [4]. Midas Civil is one of the FE software for designing bridges and civil structures. It has a characteristically user-friendly interface, and the most important is it has an optimal design solution functions. Its highly developed modeling and analysis functions to creating high-quality designs, by overcoming common challenges

and inefficiencies of other FE analysis software. As most of the structural components are predefined, user has to just pick the suitable and give the dimensions and other structural specifications. It is also enabled with FE updated procedure, which made able to assign most sensitive variables to the problems and able to solve as gradient-based methods, response surface methods, and nature-inspired algorithm optimization problems [5].

In this analysis, four-nodedv shell elements were used for concrete slabs deck, solid two-node 3D beam elements were used for transverse cross-beams of the deck, bracing members and ties were modeled as beam elements and hangers, respectively, and solid elements were used for arch ribs. Two lateral box stringers are directly assigned from the material library [6].

4 Methodology

This paper signifies to perform stability analysis of tied-arch bridges under IRC loading cases, as very less effort has been taken till now to analyze the tied-arch bridges for IRC loading conditionsv; this investigation is to determine the stability of 200 m span bridge under IRC loading cases and influence of different hanger arrangements. Efforts are also done to find the deflection, bending moment, and reaction for the varying thickness of deck slab for straightv, inclined, and network type of hanger arrangementsv. Objective of the vwork was to determine the most optimal arrangement of hangers along with range of thickness of deck slab for a road bridge. To publish an approachable design methodology to analyzev and design tied-arch bridges under IRC loading conditions.

4.1 Parametric Study: 1

In this study, different types of hanger arrangements like straight, inclined, and network have been modeled and static nonlinear analysis was carried out to identify the variation in deflection, support reactions, and bending moment for the following specification standards and design parameters (Tables 1 and 2).

Table 1 Model specification standards as per T.J.M Smit [6]

1.	For economical design a single span of the tied-arch bridge should be	200 to 300 m only
2.	Height of the arch	1/5 to 1/7 of span
3.	For a bridge of span greater than 255 m, the number of hangers on each side should be	Between 42 and 52
4.	Profile of arch rib	H profile with 10° inclination from vertical

Table 2 Design parameters for modeling

1.	Span of bridge	200 m
2.	Height of arch	40 m
3.	Width of deck	15 m
4.	Dead load	Self-weight of bridge
5.	Live load	IRC loading conditions as per IRC 6 2000
6.	Lane	2 lane—2 way traffic
7.	Density of concrete	25 kN/m^3
8.	Density of wearing coat	22 kN/m^3
9.	Modulus of elasticity	2.05e + 08 kN/m^2
10.	Poisson's ratio	0.3
11.	Thermal coefficient	1.2e − 05 1/C
12.	Density of steel	76.98 kN/m^3

Figure 3 shows 3D model of bowstring with x-bracing and straight hangers; distance between two hanger rods is 10 m; H profile with varying thickness and distance between each arch rib is provided. Figs. 4, 5, and 6 show its displacement contours, reaction, and bending moment variation, respectively, of the tied-arch bridge modeled using Midas Civil 2018 (v 2.1).

Similarly inclined and network hanger arrangements were modeled to determine maximum displacement, reaction, and bending moment. Fig. 7 shows inclined or V hanger arrangement, and Fig. 8 shows network or Neilsen arch with x-bracing arrangement.

Table 4 shows comparison of maximum values of reaction, bending moment, and deflection, for above hanger arrangements.
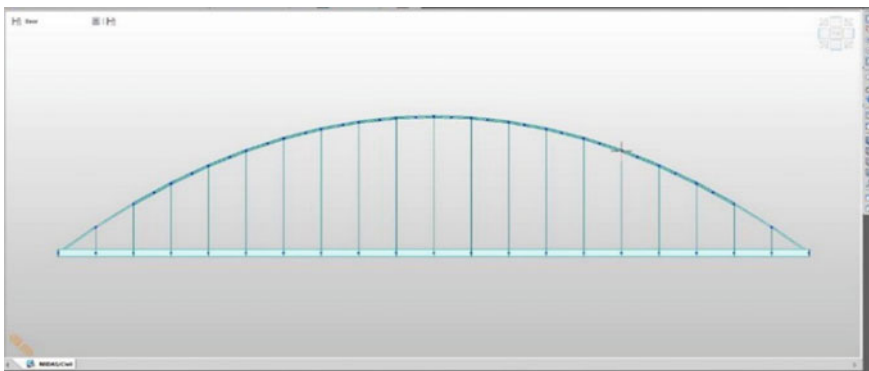
Fig. 3 Bowstring with x- bracing and straight hangers
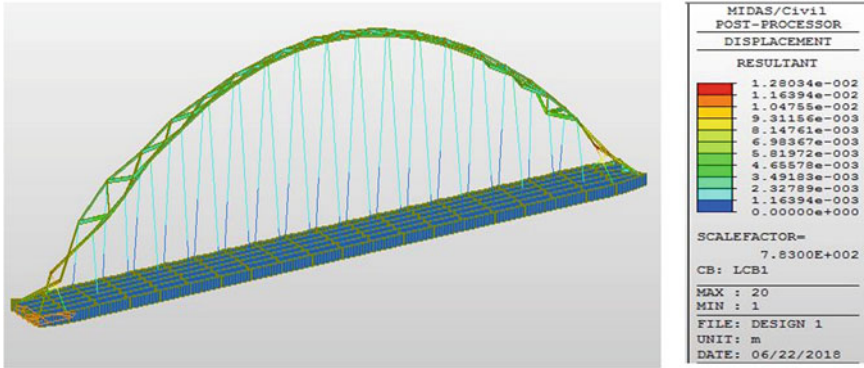
Fig. 4 Displacement contour of bowstring with x-bracing and straight hangers
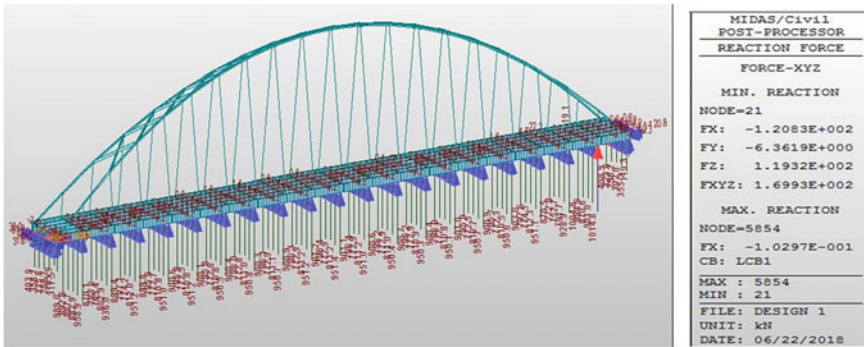
Fig. 5 Reactions of bowstring with x- bracing and straight hangers
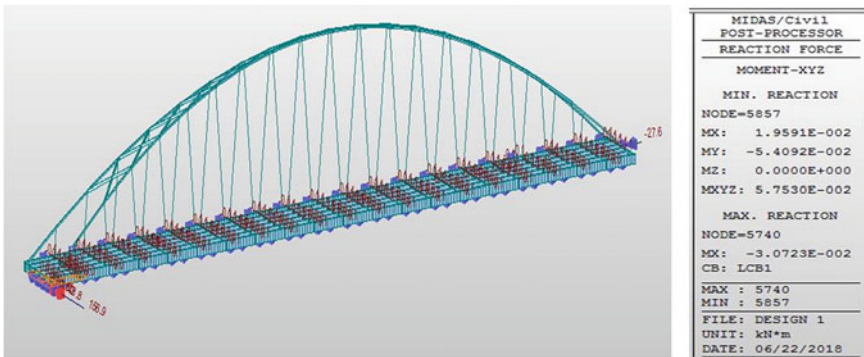
Fig. 6 Bending moment of bowstring with x- bracing and straight hangers
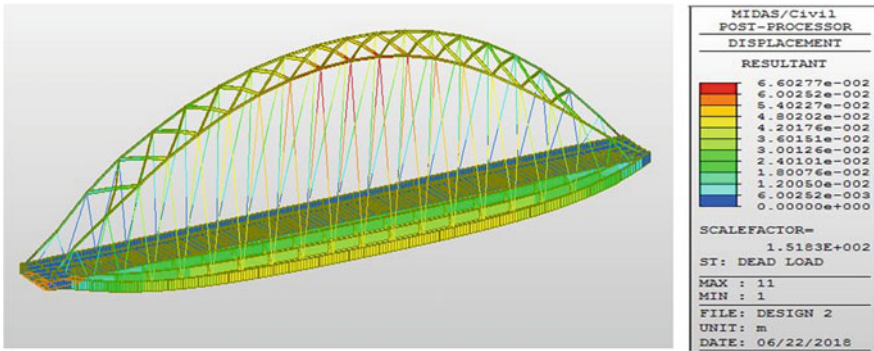
Fig. 7 Displacement contour of x-bracing with inclined or V hanger arrangement
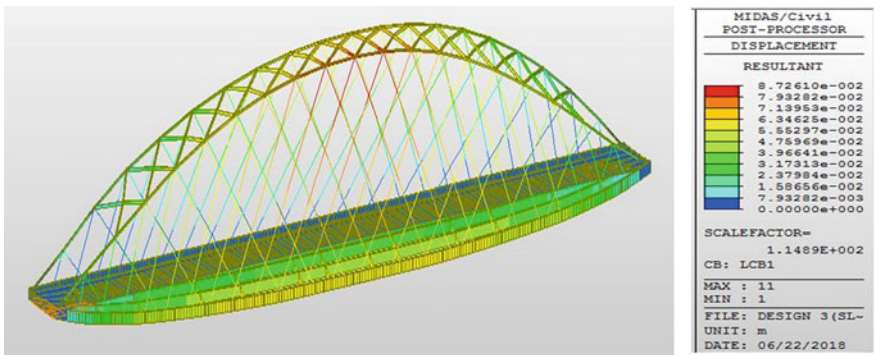
Fig. 8 Displacement contour of x-bracing with network or Neilsen arch

4.2 Parametric Study: 2

Further deck slab thickness is varied as 250, 350, and 450 mm to identify the optimum hanger arrangement with the varying thickness, and the results are given in Table 4.

5 Conclusion

In this paper, static nonlinear analysis of tied-arch bridges is carried out for IRC loading cases using FE methodology using Midas Civil software. The software contains user-friendly interface consuming less time to providing accurate results. As the structural behavior of arch rib is same as two-hinged arch, arch member should be so shaped that there is very less bending moment generated, transfer of reaction should be maximum to the deck support, and maximum deflection should not exceed 1/800 of the span. As per Table 3 for 250 mm-thick slab, we can conclude that network hanger

Table 3 Comparison table

	Straight hanger	Inclined hanger	Network hanger
Maximum support reaction (kN)	5740	5489	5849
Maximum bending moment (kN-m)	151.8	257.8	144.9
Maximum deflection at center (mm)	20	16.6	13.8

Table 4 Comparison table of varying thickness

	Straight hanger			Inclined hanger			Network hanger		
Thickness (mm)	250	350	450	250	350	450	250	350	450
Max. support reaction(kN)	5740	6059	6527	5489	5919	6325	5849	5925	6283
Max. bending moment (kN-m)	151.8	187.5	135.9	257.8	239.4	224.8	144.9	159.6	148.1
Max. deflection at center (mm)	20	17.6	14.3	16.6	13.7	11	13.8	11.2	7.4

arrangement has most optimistic results than straight and inclined arrangements. It transfer around 2% more reactions to the support compared to straight and 6.5% more to the inclined hanger arrangement. Bending moment generated 5% less than straight and 78% less than inclined, similarly straight hanger undergoes 45%, and inclined undergoes 20% more deflection in comparison with network hanger arrangement. Supporting the above statement, Table 4 provides more evidence with the varying thicknesses. Finally, we can conclude that even though straight hanger arrangement transfers comparatively more support reaction and less bending moment to the support but it undergoes more deflection than inclined hanger, whereas the network hanger comparatively transfers maximum reaction minimum bending moment to the support and under goes very less deflection than other two types of arrangements.

References

1. Wikipedia: https://simple.wikipedia.org/wiki/Arch_bridge.
2. Wikipedia: https://en.wikipedia.org/wiki/Tied-arch_bridge.
3. Finke, J. E. (2016). Static and dynamic characterization of tied arch bridges. Missouri University of Science and Technology.
4. Briseghella, B., Gallino, N., Gentile, C., & Zordan, T. (2007). Finite element modelling of a tied arch bridge from operational modal analysis. In *Proc. 5th International Conference on Arch Bridges*.
5. Midas user manual. https://en.midasuser.com/product/civil_overview.asp.
6. Smit, T. J. M. (2013). Design and construction of a railway arch bridge with a network hanger arrangement. *Journal of Civil Engineering Research 2013, Delft University of technology, pg 1 214*.

7. Namin, A. A. (2012). *Structural evaluation of tied-arch and truss bridges subjected to wind and traffic loading* (Doctoral dissertation, Eastern Mediterranean University (EMU)).

8. Rane, Ketan, et al. (March 2018). Structural evaluation of bow string and network arch bridge with different design parameters and bracings. *IJCIET, 9,* 671–689.

9. Koshi, K., & Laju, K. (2016, September). Performance comparison of through arch bridge at different arch position. *IJSER*, *7* (9).

10. Vlad, Mihai, Kollo, Gavril, & Marusceac, Vladimir. (2015). A modern approach to tied-arch bridge analysis and design. *Acta Technica Corviniensis-Bulletin of Engineering, 8*(4), 33.

11. Wang, Y., & Dejin T. (2016). Seismic response analysis of tied arch bridge. *2016 International Conference on Civil, Structure and Environmental Engineering*. Atlantis Press.

12. Krishnan, A. R., Leslie R., & Unnikrishnan S. (2015). Damage detection in bowstring girder bridge using dynamic characteristics. *International Journal of Engineering Research & Technology (IJERT)*, 168–171.

13. Qiu, W. L., Kao, C. S., Kou, C. H., Tsai, J. L., & Yang, G. (2010). Stability analysis of special-shape arch bridge. *淡江理工學刊*, *13* (4). 365–373.

14. Belevicius, Rimantas, Juozapaitis, Algirdas, & Rusakevičius, Dainius. (2018). Parameter study on weight minimization of network arch bridges. *Periodica Polytechnica Civil Engineering, 62*(1), 48–55.

15. Specifications, S. (1999). Code of practice for road bridges. *Section–II, Loads and Stresses-Fourth Revision, IRC*, 6–2000.

16. IRC 24. (1967). *Standard specifications and code of practice for road bridges*.

17. Standard, B. I. (2007). General construction in steel-code of practice. *3rd revision, Bureau of Indian Standard, New Delhi, India, IS*, 800–2007.

An Empirical Study of Major Factors Affecting Productivity of Construction Projects

Saurav Dixit and **Kaaraayaarthi Sharma**

Abstract Productivity analysis in construction is a hot research topic among various research scholars and academicians throughout the globe; because of the increasing globalization in the business, the organization needs to be competent enough to grow. The cost of low productivity in big construction and infrastructure project is too high, and to deal with this, various researches have been done to sort out the factors affecting construction productivity. In this research work, there are four identified areas which are to be assessed in terms of their effect on construction productivity which are "(1) management, (2) technological, (3) labor, and (4) external"; further, these four areas are further subclassified into various parameters which drive these four major areas. A structured set of questionnaires is made and floated among the industry people and academicians. The methodology adopted for the study is to collect the data using a structured questionnaire survey. The collected data have been analyzed, and a few statistical tests were performed on the data. The findings of the study conclude that the top three attributes affecting construction productivity are planning and scheduling, availability of material, and storage areas for materials having a relative importance index of 0.69, 0.68, and 0.67, respectively.

Keywords Construction productivity · Project management · Construction project · Built environment

1 Introduction

The construction sector is the second biggest contributor to India's GDP. It involves high volumes of monetary value as well as among the second highest provider of employment among all the sectors of the Indian economy. The sector was esteemed over $126 billion for the year 2016, and it proceeds on an enduring way to develop

S. Dixit (✉)
RICS School of Built Environment, Amity University Noida, Noida, India
e-mail: sauravarambol@gmail.com

K. Sharma
M/S the Open Survey World, Jammu, India

121

in upcoming years. It is predicted that the estimation of the land and development market will employ 80 million workers by 2020 and expand 7 times by 2028. While the majority of this appears to be empowering, there are many challenges that have been constraining the development prospects of the construction sector in India.

Productivity can be defined as the measure for the rate of performance of work. "It is the set ratio of the produced output to the required inputs to produce it which is measured as the total output produced per unit of the total input given." In the industry of construction, outputs are usually weight, volume, area, and length and the inputs are labor required, material required, and machinery requirement. Productivity in construction is now one of the most talked and researched topics and growing as a hot topic to be discussed at various national and international conferences, seminars, and research publications. The cost of the inputs in construction sector majorly comprises of labor charges which float somewhat around 25–35% of the total construction cost across the developing economies in the world and hence, therefore, it is to be given utmost importance for the success of the project. Seeing this organization followed more focused approach while dealing with the construction productivity because if they reduce this cost by supposing 10%, it will result in good cost savings and a better cash flow and hence the good financial health of the project [1–6].

The cost of increasing the labor productivity can only be the small one-time cost of providing adequate training to the workers, labor, and supervisor of those work since the labor productivity is mainly dependent on the efforts of the human beings and consistent performance by them in their work. Throughout the globe in the discussion of the problems faced by the construction industry, low labor productivity is given the utmost importance. Apart from all the leading technologies available from construction, sufficient amount of construction materials abundantly available, various tools to help the workers, various financial institutions to finance the project, contractors, and subcontractors, one certain thing is noticed that several projects are been delayed and hence surpassing their budgets [7–12].

2 Literature Review

The word "Productivity was first used in 1766 when it was first specified in an article by Quesnay". "In 1950, the Association for European Monetary Participation (OEEC) presented a formal meaning of the Productivity as a remainder acquired by separating yield by one of the creation factors" [13, 14]. Therefore, "it ended up conceivable to talk about the Productivity of investment, or crude materials as per whether the Output is being considered in connection to wealth, speculation, or basic materials." Contingent upon the valuation destinations and the accessibility of information, a few profitability definitions remain experienced.

The "United States Bureau of Trade characterizes Productivity as dollars of yield per individual hour of work input" [15–17]. Peles (1987) "deciphered profitability as the execution achieved by agents," though characterized productivity as "the

proportion of yields of merchandise and additionally administrations to contributions of fundamental assets, e.g., work, capital, innovation, materials and vitality." Finke (1998) characterized "productivity as the quantity of work delivered per man-hour, hardware hour, or team hour." The "American Relationship of Cost Designers, besides, characterizes profitability as a relative measure of work effectiveness, either great or terrible, when contrasted with a setup base or standard" [18]. While [19, 20] "alluded to efficiency as the proportion between add up to yields communicated in Dollars and aggregate information sources communicated in Dollars too" [21, 22] communicated "Productivity as what quantity is delivered per unit input." In view of the first survey, clearly, the accord among the different predictors is to characterize productivity as the proportion of profit to include. So, "the Construction Productivity can be viewed as a measure of yields that are obtained by a mix of data sources."

There are also disadvantages attached in calculation of the productivity some of which are—"(1) It is rigorous task to determine all the resources or input utilized to produce the output; (2) it is very difficult for various research scholars to demonstrate and analyze the effects of various resources utilized in production of the output quantity," whereas at the same time it has also various advantages like if one wants to focus on an aspect of the PFP, e.g., labor, capital, etc., the process of the measurement becomes much simpler and results obtained is "reliable and accurate data can be obtained for study" [23–26] (Table 1).

Table 1 Attributes identified from the literature

Attributes/variables	References
Land-use regulation	[27–29]
Equipment, drawing, tools, weather condition, availability of material, weather condition	[30–32]
Absenteeism, rework, and lack of material	[33–38]
Shop drawings, equipments, motivation and support, scheduling, material	[39–42]
Revision in drawings, delays in inspection, competency of supervisor, martial availability	[25], [43–45]
Project management, planning and scheduling, top management support, rework	[46–50]
Coordination among all team members, leadership	[51–54]
Rework, Poor supervisor competency, and incomplete drawings	[55–59], [60, 61, 62]
Improper construction method, frequent changes in design, supervision delay, the sequence of activities, overcrowding a job location, and scope of activities	[63–67]
Availability of material, the experience of labor, skill set	[68–74]

Table 2 Reliability analysis

Reliability Cronbach's alpha for the attributes	
Attributes	Cronbach's alpha
All attributes selected for the study	0.78

3 Research Methodology

This research project is done by collecting the data through a structured questionnaire survey. Considering previous research work done on the factors affecting construction productivity, 23 factors are shortlisted which were divided as 9 factors in management group, 6 factors in the technological group, 4 factors in human/labor factors, and 4 factors were categorized under external factors. This structured survey is floated among construction professionals working on site with relevant experience in this field and academicians. The received responses have been analyzed using SPSS 21, and few quantitative tests have been performed on the data [75–77].

4 Data Analysis

4.1 Reliability Analysis

Reliability analysis has been performed using SPSS 21 to check the consistency and reliability of collected data. A value of more than 0.5 has been considered reliable. For the current research, the value is 0.78 which is considered great for the study [78] (Table 2).

4.2 Relative Importance Index

Relative importance index is used to calculate the weighted average impact of the received responses in regard to the questions asked in the structured questionnaire survey. This method is also a good and reliable technique used to rank the attributes on the basis of their relative importance, and it enables us with a ranking list of attributes. The values of RII are given in Table 3.

5 Conclusion and Recommendations

The findings of the study conclude that there were a number of factors affecting construction productivity in construction projects referred to the literature. A total of 23

Table 3 Relative importance index

Rank	Total responses	Total score	RII	Attributes affecting labor productivity of construction projects
1	126	435	0.69	Planning and scheduling
2	126	428	0.68	Availability of material
3	126	421	0.67	Storage areas for materials
4	126	415	0.66	Absenteeism
5	126	408	0.65	Adequate crew and composition
6	126	393	0.62	Poor construction method
7	126	389	0.62	Rework
8	126	386	0.61	Pep talk
9	126	383	0.61	Working condition/confined space
10	126	372	0.59	Type of construction methodology

attributes has been selected for the current study, and top 10 attributes identified using RII are planning and scheduling, availability of material, storage areas for materials, absenteeism, adequate crew and composition, poor construction method, rework, pep talk, working condition/confined space, and type of construction methodology having a RII value of 0.69, 0.68, 0.67, 0.66, 0.65, 0.62, 0.61, 0.61, and 0.59, respectively. The factors which influence construction productivity vary among different countries, region, across projects and might be in similar projects too [79]. Considering this fact, this research project is done by classifying those factors into four categories irrespective of any geographical proximity, any type of work environment, and any built environment project, and various subfactors are allocated to all those four categories which are namely:

I. Management factors
II. Technological factors
III. Human or workforce or labor factors
IV. External factors

Ethical approval: "*For this type of study, formal consent is not required.*" The present research there is no direct involvement of human/respondents. All the data were collected using structured questionnaire survey, and there is no test/procedure/observation is conducted with the respondents while collecting the data.

Informed consent: "*Informed consent was obtained from all individual participants included in the study.*" A statement of formal consent was added in the introductory part of the questionnaire while sharing with the respondents.

References

1. Anvari, B., Angeloudis, P., & Ochieng, W. Y. (2016). A multi-objective GA-based optimisation for holistic Manufacturing, transportation and Assembly of precast construction. *Automation in Construction, 71*(Part 2), 226–241.
2. Kossek, E. E., & Hammer, L. B. (2011). Mixed messages to move from the margin to the mainstream*, 63*(1), 1–16.
3. Yuan, Z., Bi, J., & Moriguichi, Y. (2006). The circular economy: A new development strategy in China. *Journal of Industrial Ecology, 10* (1–2), 4–8.
4. Ma, G., Gu, L., & Li, N. (2015). Scenario based proactive robust optimization for critical chain project scheduling. *Journal of Construction Engineering and Management, 141*(10), 1–12.
5. Powl, A., & Skitmore, M. (2005). Factors hindering the performance of construction project managers. *Construction Innovation Information, Process Management*, 5(1), 41–51.
6. Molavi, J., & Barral, D. L. (2016). A construction procurement method to achieve sustainability in modular construction. *Procedia Engineering, 145,* 1362–1369.
7. Renault, B. Y., & Agumba, J. N. (2016). Risk management in the construction industry: A new literature review. *MATEC Web of Conferences, 66,* 00008.
8. Sathishkumar, V., Ragunath, P. N., & Sugana, K. (2015). Critical factors influencing financial risk in construction projects. *International Journal of Applied Engineering Research, 10*(3), 7033–7047.
9. Mostafa, S., Chileshe, N., & Abdelhamid, T. (2016). Lean and agile integration within offsite construction using discrete event simulation. *Construction Innovation, 16*(4), 483–525.
10. Enshassi, A., Mohamed, S., Mustafa, Z. A., & Mayer, P. E. (2007). Factors affecting labour productivity in building projects in the Gaza strip. *Journal of Civil Engineering and Management, 13*(4), 245–254.
11. Zhang, L., & Fan, W. (2013). Improving performance of construction projects. *Engineering, Construction and Architectural Management, 20*(2), 195–207.
12. Centre, P. G. (2012). BC model for inclusive growth—Study on performance of SKDRDP. *International Journal of Social Sciences and Interdisciplinary Research, 1*(10): 254–262.
13. Lieder, M., & Rashid, A. (2016). Towards circular economy implementation: A comprehensive review in context of manufacturing industry. *Journal of Cleaner Production, 115,* 36–51.
14. Muhwezi, L., Acai, J., & Otim, G. (2014). An assessment of the factors causing delays on building construction projects in Uganda. *Construction Engineering Management, 3*(1), 13–23.
15. Hahn, M. H., Lee, K. C., & Jo, N. Y. (2015). Scenario-based management of individual creativity. *Computers in Human Behavior, 42,* 36–46.
16. T. F. Burgess, P. Grimshaw, L. Huaccho Huatuco, and N. E. Shaw, "Mapping the operations and supply chain management field: a journal governance perspective," *Int. J. Oper. Prod. Manag.*, vol. 37, no. 7, pp. 898–926, 2017.
17. da C, T., Milberg, C., & Walsh, K. D. (2012). Exploring lean construction practice, research, and education. *Engineering, Construction and Architectural Management, 19*(5): 512–525.
18. Pandey, A. K., Dixit, S., Bansal, S., Saproo, S., & Mandal, S. N. (2017). Optimize the infrastructure design of hospital construction projects to manage hassle free services. *International Journal of Civil Engineering and Technology, 8*(10), 87–98.
19. Marhani, M. A., Jaapar, A., Bari, N. A. A., & Zawawi, M. (2013). sustainability through lean construction approach: a literature review. *Procedia-Social and Behavioral Sciences, 101,* 90–99.
20. Ganesan, S. (1987). Construction productivity. *Habitat International, 8*(34), 29–42.
21. Gatti, U. C., Migliaccio, G. C., Schneider, S., & Fierro, R. (2010). Assessing physical strain in construction workforce: A first step for improving safety and productivity management. *Proceedings* of *the 27th International Symposium on Automation and Robotics in Construction (ISARC 2010)* (Isarc), 255–264.
22. Rashid, H. (2015). Construction management : A professional approach of factors affecting the labor productivity. *International Journal of Engineering and Technical Research (IJETR), 3*(1), 283–287.

23. O'Grady, J., & McCabe, B. (2009). *Productivity in the construction industry : Concepts, trends, and measurement issues prism economics and analysis* (pp. 1–26), Department of Civil Engineering, University of Toronto.
24. Faheem, M. I., Khalique, M. A., Kalam, M. A., & Haq, S. S. (2010). Productivity management of workers in construction Industry. *International Journal of Multidisciplinary Research and Advances in Engineering, 2*(II), 7074.
25. Ruddock, L., & Ruddock, S. (2011). Evaluation of trends in the UK construction industry using growth and productivity accounts. *Construction Management and Economics, 29*(12), 1229–1239.
26. Best, R. (2012). International comparisons of cost and productivity in construction: A bad example. *Australasian Journal of Construction Economics and Building, 12*(3), 82–88.
27. U.S. Department of Labor. (2014, October). Productivity growth in construction. *Construction* Engineering *and Management* (Working Paper 478), *142*, 86.
28. Wang, X., Chen, Y., Liu, B., Shen, Y., & Sun, H. (2013). A total factor productivity measure for the construction industry and analysis of its spatial difference: A case study in China. *Construction Management and Economics, 31*(10), 1059–1071.
29. Best, R. (2010). Using purchasing power parity to assess construction productivity. *Construction Economics and Building, 10*, 1–10.
30. Zakeri, M., Olomolaiye, P. O., Holt, G. D., & Harris, F. C. (1996). A survey of constraints on Iranian construction operatives' productivity. *Construction Management and Economics, 14*(5), 417–426.
31. Chau, K. W. (2009). Explaining total factor productivity trend in building construction: Empirical evidence from Hong Kong. *International Journal of Construction Management, 9*(2), 45–54.
32. Dixit, S., Mandal, S. N., Sawhney, A., & Singh, S. (2017). Relationship between skill development and productivity in construction sector: A literature review. *International Journal of Civil Engineering and Technology, 8*(8), 649–655.
33. Safa, M., Cardenas, J. G., Leblanc, D. G., Rose, D., & Shahi, A. (2016). Improving construction labor productivity using automatic rebar tying gun. *33rd International Symposium on Automation and Robotics in Construction (ISARC 2016)* (Isarc), 1–5.
34. Abbott, M. (2013). A comparative approach to determining the growth of productivity of the New Zealand construction industry. *Australasian Journal of Construction Economics and Building, 13*(4), 65–77.
35. Fulford, R., & Standing, C. (2014). Construction industry productivity and the potential for collaborative practice. *International Journal of Project Management, 32*(2), 315–326.
36. Dacy, D. C. (1965). Productivity and price trends in construction since 1947. *Review of Economics and Statistics, 47*(4), 406–411.
37. Santosh, V., & Apte, M. R. (2014). Productivity in building construction. *Journal of Mechanical and Civil Engineering, 10*(5), 64–71.
38. Dixit, S., Pandey, A. K., Mandal, S. N., & Bansal, S. (2017). A study of enabling factors affecting construction productivity: Indian scnerio. *International Journal of Civil Engineering & Technology*, *8*(6), 741–758.
39. Chia, F. C., Skitmore, M., Runeson, G., & Bridge, A. (2012). An analysis of construction productivity in Malaysia. *Construction Management and Economics, 30*(12), 1055–1069.
40. Lee, E.-B., Lee, H., & Ibbs, C. W. (2007). Productivity aspects of urban freeway rehabilitation with accelerated construction. *Journal of Construction Engineering and Management, 133*(10), 798–806.
41. Yung, P., & Agyekum-Mensah, G. (2012). Productivity losses in smoking breaks on construction sites: A case study. *Engineering, Construction and Architectural Management, 19*(6), 636–646.
42. Arashpour, M., Wakefield, R., Blismas, N., & Lee, E. W. M. (2014). Analysis of disruptions caused by construction field rework on productivity in residential projects. *Journal of Construction Engineering and Management, 140*(2), 04013053.

43. Chancellor, W., & Abbott, M. (2015). The Australian construction industry: Is the shadow economy distorting productivity? *Construction Management and Economics, 33*(3), 176–186.
44. Tsehayae, A. A., & Fayek, A. R. (2016). System model for analysing construction labour productivity. *Construction Innovation, 16*(2), 203–228.
45. Sezer, A. A., & Bröchner, J. (2014). The construction productivity debate and the measurement of service qualities. *Construction Management and Economics, 32*(6), 565–574.
46. Pekuri, A., Haapasalo, H., & Herrala, M. (2011). Productivity and performance management—Managerial practices in the construction industry. *International Journal of Performance Measurement, 1,* 39–58.
47. Chia, F. C., Skitmore, M., Runeson, G., & Bridge, A. (2014). Economic development and construction productivity in Malaysia. *Construction Management and Economics, 32*(9), 874–887.
48. Sezer, A. A. (2015). Contractor use of productivity and sustainability indicators for building refurbishment. *Built Environment Project and Asset Management, 5*(2), 141–153.
49. Nguyen, L., & Watanabe, T. (2017). The Impact of Project Organizational Culture on the Performance of Construction Projects. *Sustainability, 9*(5), 781.
50. Thomas, A. V., & Sudhakumar, J. (2013). Critical analysis of the key factors affecting construction labour productivity—An Indian perspective. *International Journal of Construction Management, 13*(4), 103–125.
51. Abdel-Wahab, M. S., Dainty, A. R. J., Ison, S. G., Bowen, P., & Hazlehurst, G. (2008). Trends of skills and productivity in the UK construction industry. *Engineering, Construction and Architectural Management, 15*(4), 372–382.
52. Karimi, H., Taylor, T. R. B., & Goodrum, P. M. (2017). Analysis of the impact of craft labour availability on North American construction project productivity and schedule performance. *Construction Management and Economics, 35*(6), 368–380.
53. Afifi, M., Al-hussein, M., Abourizk, S., & Fotouh, A. (2016). Discrete and continuous simulation approach to optimize the productivity of modular construction element. *Proceedings of the International Symposium on Automation and Robotics in Construction, 33*(1), 1–6.
54. Guntuk, C. R., & Koehn, E., (2010). Construction productivity and production rates : Developing countries. *Challenges, Opportunities and Solutions in Structural Engineering and Construction* (pp. 687–692). Leiden, The Netherlands: CRC Press.
55. Mahamid, I. (2013). Contractors perspective toward factors affecting labor productivity in building construction. *Engineering, Construction and Architectural Management, 20*(5), 446–460.
56. Ruddock, L., & Ruddock, S. (2009). Reassessing productivity in the construction sector to reflect hidden innovation and the knowledge economy. *Construction Management and Economics, 27*(9), 871–879.
57. Nasirzadeh, F., & Nojedehi, P. (2013). Dynamic modeling of labor productivity in construction projects. *International Journal of Project Management, 31*(6), 903–911.
58. Vogl, B. (2015). Measuring Construction: Prices, Output and Productivity. *Construction Management and Economics, 33*(9), 775–777.
59. Dixit, S., (2018, November). Analysing enabling factors affecting the on-site productivity in Indian construction industry. *Periodica Polytechnica Architecture, 49*(2), 185–193.
60. Dixit, S., & Saurabh, K. (2019, April). Impact of construction productivity attributes over construction project performance in Indian construction projects. *Periodica Polytechnica Architecture, 50*, 89–96.
61. Dixit, S., Mandal, S. N., Thanikal, J. V., & Saurabh, K. Evolution of studies in construction productivity: A systematic literature review (2006–2017). *Ain Shams Engineering Journal, 10*, 555–564.
62. Chancellor, W., & Lu, W. (2016). A regional and provincial productivity analysis of the Chinese construction industry: 1995 to 2012. *Journal of Construction Engineering and Management, 142*(11), 05016013.
63. Jarkas, A. M. (2015). Factors influencing labour productivity in Bahrain's construction industry. *International Journal of Construction Management, 15*(1), 94–108.

64. Ballesteros-Pérez, P., Rojas-Céspedes, Y. A., Hughes, W., Kabiri, S., Pellicer, E., Mora-Melià, D., & del Campo-Hitschfeld, M. L. (2017, December). Weather-wise: A weather-aware planning tool for improving construction productivity and dealing with claims. *Automation in Construction, 84*, 81–95.
65. Gurmu, A. T., & Aibinu, A. A. (2017). Construction equipment management practices for improving labor productivity in multistory building construction projects. *Journal of Construction Engineering and Management, 143*(10), 04017081.
66. Pheng Low, S. (2001). Quantifying the relationships between buildability, structural quality and productivity in construction. *Structural Survey, 19*(2), 106–112.
67. Aziz, R. F., & Hafez, S. M. (2013). Applying lean thinking in construction and performance improvement. *Alexandria Engineering Journal, 52*(4), 679–695.
68. Dunlop, P., & Smith, S. D. (2004). Planning, estimation and productivity in the lean concrete pour. *Engineering, Construction and Architectural Management, 11*(1), 55–64.
69. Durdyev, S., & Mbachu, J. (2011). On-site labour productivity of New Zealand construction industry: Key constraints and improvement measures. *Australasian Journal of Construction Economics and Building, 11*(3), 18–33.
70. Karim, N. A., Hassan, S., Yunus, J., & Hashim, M. (2013, August). Factors influence labour productivity and the impacts on construction industry. *Caspian Journal of Applied Sciences Research, 2*, pp. 349–354.
71. Ok, S. C., & Sinha, S. K. (2006). Construction equipment productivity estimation using artificial neural network model. *Construction Management and Economics, 24*(10), 1029–1044.
72. Dozzi, S. P., & AbouRizk, S. M. (1993). *Productivity in Construction*. Ottawa: Institute for Research in Construction, National Research Council.
73. Moselhi, O., & Khan, Z. (2012). Significance ranking of parameters impacting construction labour productivity. *Construction Innovation, 12*(3), 272–296.
74. Dixit, S., Singh, S., Singh, S., Varghese, R. G., Pandey, A. K., & Varshney, D. (2018). Role of solar energy and issues in its implementation in the Indian context. In *MATEC Web of Conferences* (Vol. 172).
75. Singh, A., Agarwal, P., Dixit, S., Singh, S., & Sahai, S. (2018). The transition towards sustainable supply chain management: An empirical study. In *MATEC Web of Conferences* (Vol. 172).
76. Singh, S., Dixit, S., Sahai, S., Sao, A., Kalonia, Y., & Kumar, R. S. (2018). Key benefits of adopting lean manufacturing principles in Indian construction industry. In *MATEC Web of Conferences* (Vol. 172).
77. Singh, S., Bala, A., Dixit, S., & Varshney, D. (2018). Critical analysis of causes of delay in residential construction projects in India. *International Journal of Civil Engineering and Technology, 9*(1), 330–345.
78. Dixit, S., Mandal, S. N., Sawhney, A., & Singh, S. (2017). Area of linkage between lean construction and sustainability in Indian construction industry. *International Journal of Civil Engineering and Technology, 8*(8), 623–636.

Strength and Durability Studies of Cement Concrete M45 Fine Aggregate Partially Replaced with Waste Crushed Glass

G. Lalitha, C. Ramachandrudu and Ch. Sashidhar

Abstract Concrete is widely used by entire world in the construction field. As depletion of river sand is being taking place due to urbanization and construction developments, this experimental work focused on using sustainable materials in the construction practice as well as reducing the usage of natural resources. Using glass waste as construction material, the place natural resource usage will be reduced. Another advantage is that greenhouse gases and dumping waste on open land have been reduced. The pollution levels coming out from concrete materials will be reduced. This experimental work focused on aggregate replacement with 10, 20, 30, and 40% of crushed glass. It was observed that durable and mechanical properties were increased with replacement of fine aggregate up to 30% in addition with super plasticizer Conplast SP430. The compressive strength was increased by 11.35%, tensile strength by 18.97%, and flexural strength by 20%.

Keywords Concrete · Fine aggregate · Waste crushed glass · Strength · Durability

1 Introduction

With the increasing demand of naturally available resources, researchers have thought that technological improvements are required for the society by raising affluence levels in the infrastructure world and depletion in the global pollution. One among

G. Lalitha (✉)
Ph.D Scholor, JNTU Anatapuramu, Ananthapuramu, Andhra Pradesh, India
e-mail: lalithagcivil@gmail.co

C. Ramachandrudu
Civil Engineering Department, Chiranjeevi College of Engineering, Ananthapuram, Andhra Pradesh, India
e-mail: chittariram@gmail.com

Ch. Sashidhar
Civil Engineering Department, JNTU University College of Engineering, Ananthapuram, Andhra Pradesh, India
e-mail: sashigunt@gmail.com

is recycling of glass waste which is used for production of glass to use in various fields. Glass in construction is strong and safe. It is also used as alternative to the sand in concrete. The sustainable material developments in construction field are waste crushed glasses usage as aggregates in concrete. The crushed glass usage in the place of aggregates is most interested by the researchers as waste glass material in the place of aggregate reduces absorption of water, drying shrinkage, and high in resistance to abrasion (2). Excellent properties of glass lead to think about waste glass in concrete. Researchers worked on the influence of size of the glass particle and color used in production of concrete and on alkali silica reaction (ASR) expansion. In general, the ASR expansion decreases with reduction in particle size of glass aggregate (3). Waste crushed glass in construction reduces urban solid waste dumping. LCD panels are becoming majorly used ones in televisions, personal computers, smart phones, tablets, cameras, and so on because they are thin, energy-saving, and lightweight (5). The limitations of glass remanufacturing is not allowing to reproduction of glass from waste glass. As glass remanufacturing is difficult, during sorting preventive measures are to be taken, during sorting as it has composite materials and contaminants which are not feasible technically (6). Generally, waste crushed glass (WCG) increases the resistance against chloride penetration of concrete which gives more advantage in protecting the RCC exposed to seawater and deicing salts. In most of the literature, it was understood that absorption water by the concrete could be minimized by using crushed glass additionally; replacement of natural aggregates with WCG affected the density. The literature reviewed reported that concrete aggregates are the material reducing shrinkage and important constituent impart economy to concrete production (7). Crushed glass usage also converts unused to value-added product and reduces transportation cost as it may be make used of locally (9). If waste glass concrete will reduce water absorption and shrinkage, resistance to abrasion will be increased.

2 Materials

2.1 Cement

53 Grade cement was used in this research work. Cement properties were found and given in the Table 1 (Fig. 1).

Table 1 Cement properties

S. No	Description of Test	Test results	IS limits
1	Fineness of cement	98%	>90%
2	Specific gravity	3.1	3.15
3	Standard consistency	32%	26-33%
4	Initial setting time	43 min	>30 min
5	Final setting time	420 min	<600 min
6	Soundness of cement	3 mm	Should be less than 3 mm.
7	Compressive strength	35.51 N/mm^2	>27 N/mm^2

Fig. 1 Cement

2.2 Grading of Crushed Waste Glass

2.2.1 Glass

The waste glass used is procured from glass manufacturing company in Hyderabad. The collected and crushed waste glass is used in the place of fine aggregate and was analyzed in terms of fineness modulus of crushed glass (Fig. 2 and Table 2).

2.2.2 Fine Aggregate

IS Code for fine aggregate is IS 2386 Part-II Fine aggregate of (River sand of Zone II) with specific gravity 2.6 was used for concrete mix (Fig. 3).

Fig. 2 Waste crushed glass

Table 2 Grading of crushed waste

Size of sieve (mm)	Mass of glass on sieve (gm)	Mass of glass sieve on sieve %	Mass of glass passing %	Cumulative % mass of glass on sieve	ASTM standard specification
4.75	0	0	100	0	95–100
2.36	1.7	0.17	99.83	0.17	80–100
1.18	357.7	35.77	64.04	35.94	50–85
0.6	230.9	23.09	40.97	59.03	25–60
0.3	200.2	20.02	20.95	79.05	5–30
0.15	111.2	11.2	9.75	88.8	0–10
Pan	97.5	9.75	0	0	0

Cumulative % retained = 264.56
Fineness modulus of crushed waste glass ε F/100 = 264.56/100 = 2.64

2.2.3 Coarse Aggregate

Coarse aggregate of maximum size 20 mm and relative density 2.7 was utilized in this research work. The coarse aggregate used is locally available aggregate. Various tests were conducted to determine its physical properties.

3 Water

Locally available potable water is used.

4 Super Plasticizer

These are high range water reducers. The functions are

Avoiding particle segregation.
Improving the flow characteristics.

Fig. 3 Fine aggregate

Reducing water–cement ratio, which implies higher strength.
Improving the workability of concrete.

4.1 *Experimental Investigation*

Five mix proportions were prepared using IS10262. The grade of concrete used was
M45 with water-to-cement ratio is 0.40. The controlled concrete mix ratio came out
as 1: 1.7623: 2.977: 0.4 with cement: fine aggregate: coarse aggregate with water–
cement ratio 0.40. The mixes were tabulated, three specimens were prepared for each
one time testing for compression, split tensile, and flexure and 3 specimens for each
trail for durability tests (Tables 3 and 4).

5 Workability Test

Code: IS 1199-1959

Table 3 Mixes of concrete with crushed waste glass

S. No.	Mix designation	Cement content kg/m^3	Fine aggregate kg/m^3	Coarse aggregate kg/m^3	W/C ratio	Super plasticizer kg/m^3	Crushed glass kg/m^3
1	Nominal	400	702.468	1190.21	0.4	6	0
2	MC10	400	632.22	1190.21	0.4	6	70.2
3	MC20	400	561.97	1190.21	0.4	6	140.5
4	MC30	400	491.73	1190.21	0.4	6	210.74
5	MC40	400	421.48	1190.21	0.4	6	280.98

Table 4 Samples and tests

S. No.	Test NAME	Standard	Specimen Size
1	Slump	BS1881.Part-II-1970	Slump cone bottom 200 mm, height 300 mm, top 100 mm
2	Compressive strength	B.S 1610-Part I-1992	Cube of 150 × 150 × 150 mm
3	Splitting tensile Strength	ASTM-C-496-96	Cylinder 150 × 300 mm
4	Flexural strength	B.S 1610-Part-1-1992	Prism 100 × 100 × 500

In this study, the concrete workability was determined by slump cone method (Fig. 4, Table 5, and Graph 1).

Fig. 4 Slump test

Table 5 Slump values

S. No.	Mix	Slump (mm)
1	Nominal mix	100
2	MC10	153
4	MC20	150
5	MC30	148
6	MC40	139

Graph 1 .

Slump (mm)
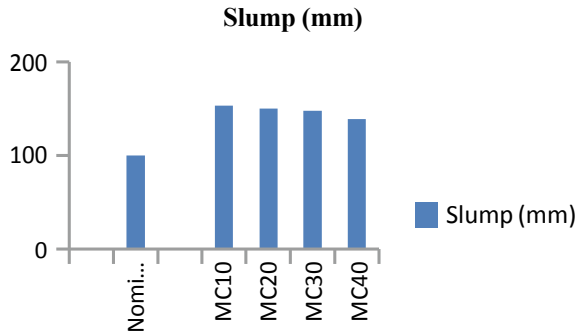
5.1 Casting and Testing

Grease was applied to inner surface of moulds to prevent the cement paste adhesion to the moulds. Cube mould of $150 \times 150 \times 150$ mm (compression test) and prism of $100 \times 100 \times 500$ mm (flexure test), cylinder of 150 mm $\times 300$ mm (split tensile test), and cylindrical moulds of 100×150 mm (RCPT) were used for various samples.

Casting and curing were done according to BS 1881:1952. After filling the moulds, prepared concrete was placed in 3 layers compacted with tamping rod giving 35 blows for each layer. Again the moulds were kept on the vibrating machine and vibrated for 3 min. The slump values reduced as crushed waste glass percentage increases (Figs. 5 and 6).

Fig. 5 Specimen moulds

Fig. 6 Casted specimen

Fig. 7 Specimens in curing tank

Fig. 8 Specimen in compression testing machine

5.2 Curing

Curing process maintains the dampness to take care of heat of hydration. Curing is done in water curing tank as shown in Fig. 7.

6 Compressive Strength Test

Compressive strength is the most common of all tests on hardened concrete, and compressive strength is the most important parameter in structural design. The compressive strength of concrete is obtained by testing cube specimen of size $150 \times 150 \times 150$ mm (Fig. 8, Table 6, and Graph 2).

7 Split Tensile Strength Test

Cylindrical specimen of 100 mm $\times$ 300 was used for split tensile strength (Fig. 9, Table 7, and Graph 3).

Table 6 Compressive strength values

S. No.	Type of mix	Compressive strength (N/mm^2)		
		7 Days	14 Days	28 Days
1	Nominal mix	44.77	52.8	53.3
2	MC10	45.33	47.11	55.66
3	MC20	46.22	52.44	57.22
4	MC30	57.33	57.77	62.20
5	MC40	51.11	54.66	56.44

compressive strength vs Mix design

	Nomina mix	MC10	MC20	MC30	MC40
■ Compressive strength(N/MM2) 7 Days	44.77	45.33	46.22	57.33	51.11
■ Compressive strength(N/MM2) 14Days	52.8	47.11	52.44	57.77	54.66
■ Compressive strength(N/MM2) 28Days	53.3	55.66	57.22	62.2	56.44
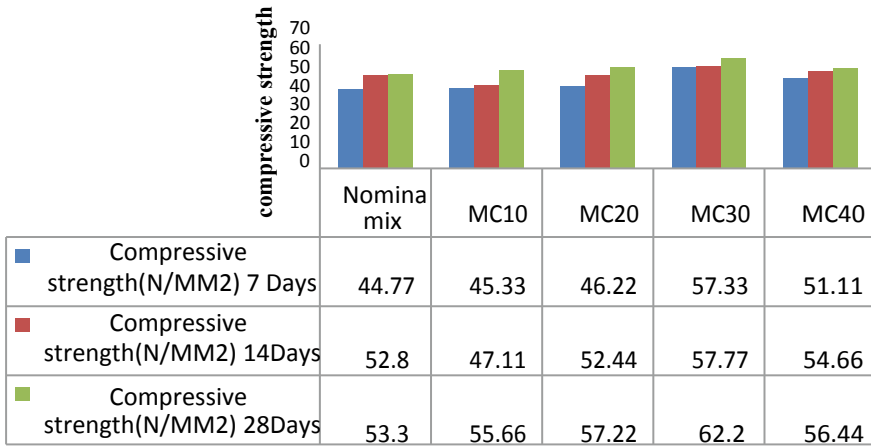
Graph 2 .

Fig. 9 Specimen under split tensile strength test

Table 7 Tensile strength values

S. No.	Type of Mix	Tensile strength (Nmm^2)		
		7 Days	14 Days	28 Days
1	Nominal	2.55	2.75	3.11
2	MC10	2.83	2.97	3.80
3	MC20	2.97	3.11	3.96
4	MC30	3.25	3.85	4.50
5	MC40	2.82	2.62	3.70

Tensile strength vs Mix design

	Nominal 1	MC10 2	MC20 3	MC30 4	MC40 5
■ Tensile strength(Nmm2) 7 Days	2.55	2.83	2.97	3.25	2.82
■ Tensile strength(Nmm2) 14Days	2.75	2.97	3.11	3.85	2.62
■ Tensile strength(Nmm2) 28 Days	3.11	3.8	3.96	4.5	3.7
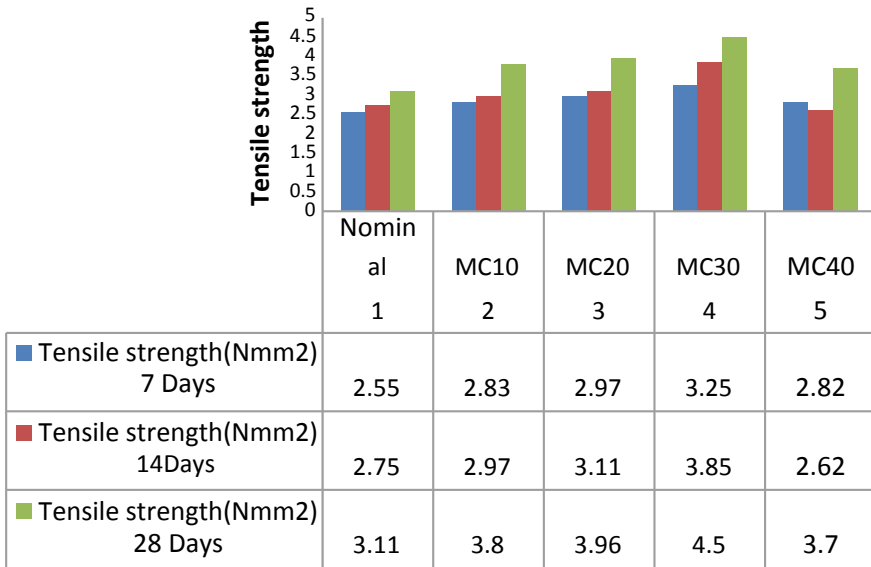
Graph 3   .

Formula: $f = 2P/(\pi \times D \times L)$
where f = Split tensile strength
P = Load at which specimen failed
D = Diameter of specimen
L = Length of specimen

Fig. 10 Specimen under flexural test

Table 8 Flexural strength values

S. No.	Type of Mix	Flexural strength (Nmm^2)		
		7 Days	14 Days	28 Days
1	Nominal	4.4	5.2	6
2	MC10	5.1	5.8	6.5
3	MC20	5.6	6.1	6.8
4	MC30	6.5	6.9	7.2
5	MC40	5.3	5.8	6.1

8 Flexural Tensile Strength

Flexural strength is one measure of the tensile strength of concrete (Fig. 10, Table 8 and Graph 4).

9 Durability Tests: Acid Test

In this research work, the concrete durability was found out by immersing cube specimens in both acids such as HCL and H_2SO_4 (Fig. 11 and Table 9).

Flexural strength vs Mix design

	Nominal	MC10	MC20	MC30	MC40
■ Flexural strength(Nmm2) 7 Days	4.4	5.1	5.6	6.5	5.3
■ Flexural strength(Nmm2) 14Days	5.2	5.8	6.1	6.9	5.8
■ Flexural strength(Nmm2) 28 Days	6	6.5	6.8	7.2	6.1
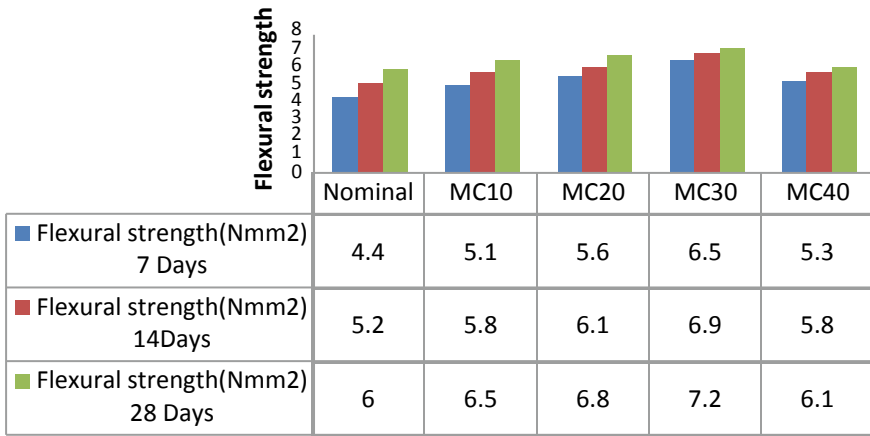
Graph 4 .

Fig. 11 Specimens in HCL and H_2SO_4 after 28 Days

10 Conclusions

The following conclusions are drawn from the detailed experimental investigations conducted on the behavior of M45 grade concrete fine aggregates which are partially

Table 9 Weights of cube specimen immersed in HCL

S. No.	Type of Mix	Average weight of cubes (kg)		Average % loss of weight (%)
		Before immersion in HCL solution	After immersion in HCL solution	
1	Nominal	8.47	8.38	1.06
2	MC10	8.42	8.37	0.59
3	MC20	8.39	8.35	0.47
4	MC30	8.25	8.22	0.36
5	MC40	8.23	8.210	0.36

replaced by crushed glass in comparison with the conventional concrete of same grade.

Crushed glass added to the concrete showed the following changes in the strength parameters of concrete.

1. It is observed that with 30% replacement of fine aggregates with crushed glass to the M45 grade concrete improved the compressive strength of concrete by 11.75% at 28 days compared to the conventional concrete of M45 grade.
2. It is also observed that with 30% replacement of fine aggregates with crushed glass to the M45 grade, there is a great increase in the split tensile strength of concrete—18.97%.
3. It is also observed that with 30% replacement of fine aggregates with crushed glass to the M45 grade, there is a great increase in the flexural strength of concrete—20%.

References

1. Ling, T. C., Poon, C. S., & Wong, H. W. (2012). Management and recycling of waste glass in concrete products: Current situations in Hong Kong. *Resources, Conservation and Recycling, 70*, 25–31.
2. Meyer, C., Egosi, N., & Andela, C. (2001, March 19–20). Concrete with waste glass as aggregate. In *"Recycling and Re-use of Glass cullet"—International Symposium Concrete Technology Unit of ASCE and University of Dundee*.
3. Meyer, C., Baxter, S., & Jin, W. (1996). Alkali-silica reaction in concrete with waste glass as aggregate. In *Proceedings of ASCE Materials Engineering Conference* (pp. p. 1388–1394). Washington, DC.
4. IS 10262 Code Book for MIX Design.
5. From book Designing the renewable energy parks in order to reduce the environmental crisis in the framework of ecological design, case of renewable energy park of Manjil—Iran (pp. 743–746).
6. Mohajerani, A., Vajna, J., Cheung, T., Kurmus, H., Arulrajah, A., & Horpibulsuk, S. (2017). Practical recycling applications of crushed waste glass in construction materials: A review. *Construction and Building Materials, 156*, 443–467.

7. Darshita, T., & Anoop, P. (2014, June). Study of strength and workability of different grades of concrete by partial replacement of fine aggregate by crushed brickand recycled glasspowder. *International Journal of science and Research, 3*(6). www.ijsr.net.
8. Rajabipour, F., Fischer, G., Sigurdardottir, P., Goodnight, S., Leake, A., & Smith, E. (2009). Recycling and utilizing waste glass as concrete aggregate. In *Transportation Research Board (TRB) 88th Annual Meeting*. Washington, DC.
9. IS 456 Code Book.
10. IS 10262 Code Book.

Study on Microstructure of High-Strength (M100) Hybrid Fiber Self-Compacting Concrete Containing Quartz Materials Subjected to Corrosion and Chloride Ingression

G. Vishnupriya, R. K. Tharun Thej and P. Sanketh

Abstract The porous and complex microstructure of reinforced concrete is responsible for its deterioration from external agents attacking its surface. Corrosion of reinforcement bars in concrete deteriorates concrete over a period of time and thus affects its durability. Corrosion of reinforcement bars is affected by quality of concrete, proper design and construction, and environmental conditions. Chloride-induced corrosion of reinforcement is a common phenomenon for concretes subjected to marine environment or de-icing salts. The resistance of concrete to chloride-induced corrosion depends mainly on chloride permeability and compounds present in the microstructure of concrete. In this paper, an effort has been made to study the microstructure of high-strength (M100) self-compacting concrete (HSSCC) with and without adding hybrid steel fibers subjected to accelerated corrosion. Chloride permeability and microstructure of HSSCC with and without fibers is also studied. Though several test methods are there to measure durability of concrete subjected to various chemical attacks, the actual behavior of concrete and its compounds can be found only by studying its microstructure, which will be useful to develop better concretes. X-ray diffraction (XRD) analysis has been carried out to determine the phase amounts of various compounds in multiple phase mixture of HSSCC with and without hybrid steel fibers. Scanning electron microscope (SEM) is used to visualize the elements in the microstructure of the HSSCC concrete.

G. Vishnupriya
Dept. of Civil Engineering, Narsimha Reddy Engineering College, Maisammaguda, Dhulapally, Secunderabad 500100, Telangana, India

R. K. Tharun Thej (✉)
Dept. of Civil Engineering, Srinivasa Ramanujan Institute of Technology, Ananthapuramu 515001, Andhra Pradesh, India
e-mail: tharunthej55@gmail.com

P. Sanketh
Dept. of Civil Engineering, Malla Reddy Institute of Technology and Science, Secundrebad 500100, Telangana, India

1   Introduction

The structure and properties of concrete can change over a period of time. The degradation of concrete due to environment is a common and serious problem. Corrosion of reinforcement bars in reinforced concrete is one such problem [1]. The process of corrosion is studied in detail by Rosenberg et al. [2]. Corrosion is an electrochemical process where self-generated electrochemical activity results from differences in potentials that develop when metals are placed in an electrolyte [3]. In reinforced concrete, the non-uniformities in steel or chemical compounds in concrete will cause potential differences. Due to high alkalinity of concrete compounds, a passive protective layer will be developed on the steel surface, which consists of γ-Fe_2O_3 [4]. This oxide film will protect steel from any chemical reaction, but the ingression of chloride ions into concrete will destroy this layer, exposing steel for chemical reactions. The part at which steel corrodes is termed as anode, where steels attempt to free electrons because of potential difference with cathode region (Fig. 1).

$$Fe \rightarrow Fe^{++} + 2e^- \, (\text{at Anode})$$
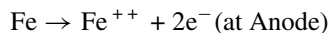
These electrons move inside the steel towards cathode where there are absorbed by oxygen and water in concrete to form hydroxyl ions (OH^-).

$$4e^- + O_2 + 2H_2O \rightarrow 4OH^- \, (\text{at Cathode})$$
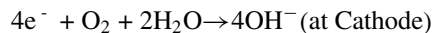
These ions travel towards anode through electrolyte (concrete pores) and react with ferrous ions to form ferric hydroxide, which on further oxidation becomes rust.

$$Fe^{2+} + 2OH^- \rightarrow 4Fe(OH)_2$$
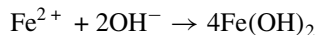
This process of forming rust continues as a cyclic process. The iron oxides or rust formed will have expansively increased volume which induces tensile stresses in concrete leading to cracks and ultimately failure of the member [5, 6]. The cracking of concrete will boost the corrosion process further [7, 8]. The durability of reinforced concrete will depend also on reinforcement type [9], cover to reinforcement [10], and free and bounded chloride contents in cementitious materials [11]. The use of galvanized steel, stainless steel, and coated reinforcements will prevent corrosion [12]. Also increase in cover, modifications, and delamination will reduce corrosion of reinforcement in concrete [13].

Fig. 1 Corrosion cell in a reinforced concrete member [3]
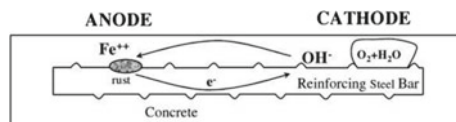
In the present work, concrete cylinder specimens of 100 mm × 200 mm embedded with rebar of 10 mm are prepared and tested after 28 days of curing. The specimens are placed in NaCl solution of 1.2 molarity, and the corrosion process is initiated by applying a constant voltage of 6 volts to the system. The test is terminated when cracks appear on the specimen. Chloride permeability and microstructure of HSSCC with and without fibers is also studied. This involves casting of cylindrical specimens of 100 mm diameter and 50 mm height, cured for 28 days. The passage of chloride ions is done by applying a constant voltage of 60 volts for a period of 6 h with specimen placed between NaCl and NaOH solution reservoirs as per ASTM C1202. Total charge passed through concrete gives the chloride permeability of concrete.

To determine the qualitative and quantitative phases of different compounds of microstructure in the HSSCC with and without hybrid fibers subjected to chloride-induced corrosion, X-ray diffraction analysis is carried out. To identify various compounds visible in the microstructure of HSSCC corroded samples, scanning electron microscope is used.

2   Materials Used

Cement: Ordinary Portland cement of 53 grade is used in this investigation. The cement used has been tested for various proportions as per IS 4031-1988 and found to be confirming to various specifications of IS 12269-1987. The specific gravity of cement is 3.1, and fineness is 2800 cm^2/gm.

Fine and Coarse Aggregates: Quartz sand of sizes 0.3–0.8 mm which has a hardness of 7 on Mohr's scale is used as fine aggregate. Quartz sand has a specific gravity of 2.46 and bulk density of 1526.8 kg/m^3. A coarse aggregate of sizes ranging from 10 mm to 20 mm with specific gravity of 2.68 and bulk density of 1483.66 kg/m^3 is used in the preparation of concrete.

Quartz Powder: Quartz powder serves as an excellent mineral admixture which improves self-compatibility, deformability, and stability in self-compacting concrete (SCC). This is commonly used to improve and maintain the workability, as well as to regulate the cement content and to reduce the heat of hydration. Quartz powder of order 0–10 μm and with a specific gravity of 2.635 is used in this study.

Microsilica: Microsilica is a pozzolanic material which is the by-product in the manufacture of silicon and ferro silicon alloys from high-purity quartz and coal in a submerged arc electric furnace. Due to its versatile properties, it is used as the cement replacement material. Microsilica addition reduces the content of viscosity modifying admixture (VMA), which is even more costly than microsilica. Usually in SCC, the allowable limit of microsilica is 2–3% of cement. Microsilica acts has both filler material and pozzolanic material. The combination of these two actions leads to development of very high strength, and thereby the porosity is reduced and

the structure is more durable. Also the bleeding is reduced through microsilica. The characteristics of microsilica are as shown Table 1.

Fibers: Hooked end steel fibers of length 30 mm, aspect ratio 60:1, and diameter 0.5 mm and Cem-FIL anticrack glass fibers of length 6 mm, aspect ratio 857:1, and diameter 14 μm are used.

Master Glenium ACT 30: Master Glenium ACT 30 is a high-performance concrete superplasticizer based on modified polycarboxylic ether. It has been primarily developed for application in high-performance concrete, where the highest durability and performance are required. It is compatible with all Portland cements that meet recognized international standards.

Glenium Stream 2: Glenium Stream 2 is used as a viscosity modifying admixture. Superplasticizer admixture gives high fluidity, but alone it does not guarantee the necessary properties to ensure a good degree of self-compacting. That is why Glenium Stream 2 is a fundamental admixture when making self-compacting concrete in combination with the other superplasticizer admixtures of the Glenium range in order to guarantee maximum efficiency.

3 Mix Proportions

As shown in Table 1, coarse aggregate content of 48% by volume of the mix is used. Fine aggregate is taken as 52% by the volume of the mix. 1.5% of cementations material is used as superplasticizer, and 0.25% of cementations material is used as viscosity modifying agent. Fibers are tuned to 1.5% of cementations material.

Table 1 Mix proportions used

Materials	HSSCC	HSHFSCC
Cement (kg/m3)	640	640
Microsilica (kg/m3)	64	64
Quartz powder (kg/m3)	160	160
Quartz sand (kg/m3)	887	887
Coarse aggregate (kg/m3)	797.53	797.53
SP (% of P.C)	1.5	1.5
VMA (% of P.C)	0.5	0.5
W/P ratio	0.20	0.21
Steel fibers (% of P.C)	–	0.75
Glass fibers (% of P.C)	–	0.75

4　Preparation of Test Specimens

The self-compacting concrete mixes are checked for the fresh properties of self-compacting specifications, i.e., flow table, L-box and V funnel tests as per EFNARC [14].

Accelerated Corrosion Test:　For ACT, the SCC is poured into cylindrical moulds of 100 mm × 200 mm. The reinforcing rod of 225 mm length and 10 mm diameter is placed concentrically in each cylinder with a cover of 25 mm at bottom and 50 mm projection at top. The specimens are then allowed to harden for 48 h. Epoxy coating is applied to the 50 mm projection of reinforcement bars and is cured for 28 days in the curing tank.

Rapid Chloride Permeability Test:　For RCPT, the SCC is poured into cylindrical moulds of 100 mm diameter and 50 mm height. The concrete is then allowed to harden for 48 h. Then, the specimens are cured for 28 days in the curing tank.

5　Experimental Program and Methodology

Accelerated Corrosion Test:　The accelerated corrosion test setup is shown in Fig. 2. The equipment consists of a precision voltage source which feeds current to the concrete specimens with rebar. The specimens can be kept inside the acrylic container with perforated stainless steel cathode of suitable diameter. NaCl solution of 1.2 M is poured inside the container for penetration into the concrete specimen. Stable DC voltage of 6 volts is applied between the SS cathode and the steel rod. The data acquisition monitors the voltage and current of each concrete specimen. The readings are acquired at regular intervals of time. The test is terminated when cracks appear

Fig. 2　Test setup for ACPT rapid chloride permeability test

Fig. 3 Test setup for RCPT
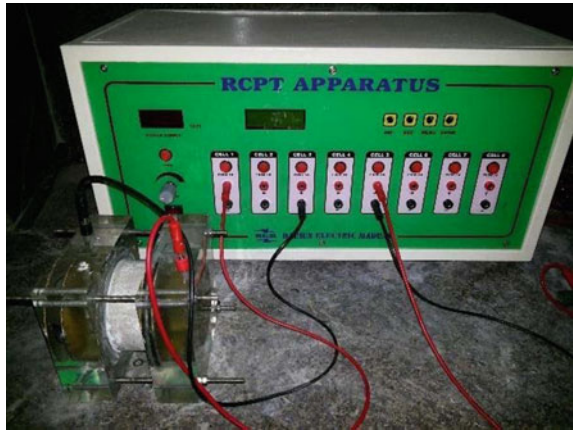
on the specimen. At the end of test, the data can be transferred to a PC which will provide all the readings. Graphical plot can be done current with respect to time.

Rapid Chloride Permeability Test: The RCPT equipment confining to ASTM C-1202 standards is shown in Fig. 3. It consists of a regulated DC power supply of 60 volts. The RCPT specimens are placed in the grooves provided. The NaCl solution with a concentration of 2.4 M is filled in one of the two diffusion cell chambers, while other chamber is filled with 0.3 M NaOH solution. The chloride ions were forced to migrate through the specimen under an impressed voltage of 60 volts. The total current flowing over a period of 6 h is measured. The charge computed in coulombs is then related to chloride ion permeability of concrete.

Concrete samples are taken from the specimens of ACT and RCPT. The sample taken is from the corroded portion in ACT. The samples are crushed to a size of around 5 mm crystals for SEM analysis. For XRD analysis, the samples are powdered and sieved through 90 micron sieve and the powder passing the sieve is considered for testing.

The X-ray diffraction analysis is carried out on samples using Panalytical X' Pert Powder diffractometer using Cu-Kα radiation with a step size of $0.02^{\circ}/2\theta$ for scanning, and raw data of X-ray diffraction patterns of samples are obtained. The raw data obtained from powder diffraction analysis are processed, and compounds are found using QualX2 and Crystallography Open Database. The SEM analysis is carried out using TESCAN scanning electron microscope.

6   Results and Discussion

Accelerated Corrosion Test: The current response is continuously monitored and recorded by the data logger. In addition, the specimens are daily inspected visually for the onset of cracks. The data logger is set at a sampling frequency of 24 h for recording the corrosion current of the circuit. The accelerated corrosion test is terminated after cracking of the specimen when the rate of increase of corrosion current with time was negligible. The failed specimens of HSSCC and HSHFSCC are as shown in Figs. 4 and 5, respectively.

The currents in five channels, i.e., concrete specimens in channel 1 to channel 5 at the corresponding days are given in Tables 2 and 3 for HSSCC and HSHFSCC, respectively. The results are presented using a current–time graph and also the failure time and crack observed are represented in the Figs. 6 and 7 for HSSCC and HSHFSCC, respectively.

Fig. 4 HSSCC specimens after failure

Fig. 5 HSHFSCC specimens after failure

Table 2 Current at the corresponding day for HSSCC

Time in days	Current in μA				
	CH-1	CH-2	CH-3	CH-4	CH-5
1	51	57	69	53	64
2	47	60	68	50	68
3	51	66	68	53	75
4	59	73	64	61	71
5	60	70	67	63	71
6	64	72	73	72	72
7	72	70	72	73	67
8	78	68	72	80	66
9	83	69	73	80	66
10	92	67	75	89	64
11	**82**	**61**	**67**	**95**	**62**
12	**110**	**86**	**89**	**116**	**92**
13	106	78	80	110	75
14	101	72	80	103	65
15	93	63	76	101	62

The HSSCC specimens failed on 11th day where the HSHFSCC specimen took 16 days to fail under the same electrochemical reaction. After the failure of specimens, the time taken for the crack observed in HSHFSCC was delayed when compared HSSCC. Inspection of specimens after concluding the test showed that there are two to three small cracks on the tensile surface of HSHFSCC specimens, whereas only single crack of slightly more width was observed on HSSCC specimens.

7 Rapid Chloride Permeability Test

The corrosion process is initiated by applying a constant voltage of 60 Volts to the system. The current response is continuously monitored and recorded by the data logger for a period of 6 h with an interval of 30 min. The current in five cells, i.e., concrete specimens in channel 1, channel 2, channel 3, channel 4, and channel 5 are shown in Tables 4 and 5 for HSSCC and HSHFSCC, respectively. The results in the form of current vs time for both concretes are shown in Fig. 8.

Table 3 Current at the corresponding day for HSHFSCC

Time in days	CURRENT in µA				
	CH-1	CH-2	CH-3	CH-4	CH-5
1	81	83	97	93	84
2	79	90	94	89	83
3	81	91	106	94	81
4	84	92	103	103	78
5	82	97	114	107	83
6	87	101	128	108	89
7	93	95	126	114	91
8	98	93	119	116	94
9	96	93	119	119	98
10	103	87	117	120	101
11	106	88	122	119	109
12	107	90	123	121	104
13	113	93	119	123	107
14	118	96	121	122	108
15	123	101	125	124	114
16	**116**	**94**	**119**	**113**	**109**
17	139	121	149	147	129
18	**154**	**137**	**157**	**152**	**145**
19	141	131	132	136	134
20	132	124	129	139	126

Fig. 6 Corrosion current versus time graph for HSSCC
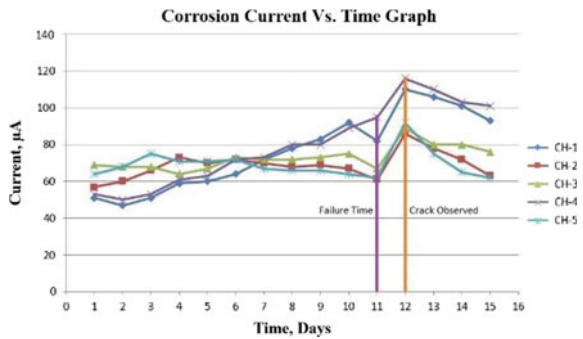
The resistivity or conductivity can be determined for the initial current reading and is calculated from ohms law.

R = V/I

where R is resistance, V is voltage and, I is current. The resistivity is determined from

Fig. 7 Corrosion current versus time graph for HSHFSCC
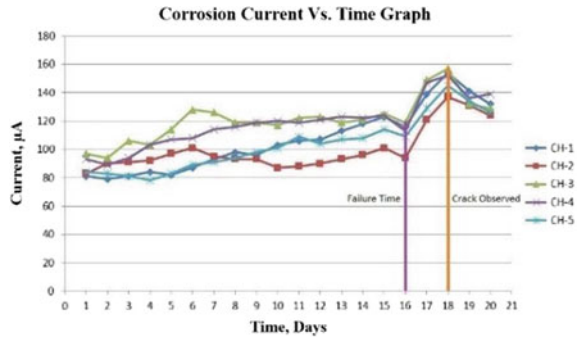
Table 4 Current at the corresponding day for HSSCC

Time in minutes	Current in mA				
	CH-1	CH-2	CH-3	CH-4	CH-5
0	29	25	28	27	29
30	33	27	29	30	30
60	34	27	30	30	30
90	35	29	31	31	31
120	36	31	32	31	31
150	33	31	33	32	32
180	34	33	34	32	34
210	34	33	35	33	34
240	35	34	35	34	35
270	36	34	37	34	36
300	36	35	39	35	37
330	36	35	39	35	39
360	36	37	41	36	41
R.C.P.T in coulombs	804.6	739.8	797.4	756	790.2
Avg. in coulomb	777.6				

Resistivity $= RA/I$

where A is area of the disc and I is thickness of the disc.

The results of resistivity for both the concretes are given in Table 6.

The charge passed in coulombs on an average of 5 samples for HSHFSCC was observed to be 582.84 coulombs.

The charge passed in coulombs on an average of 5 samples for HSSCC was observed to be 777.6 coulombs.

The resistivity in ohm-meters on an average of 5 samples for HSHFSCC is 503.08, and for HSSCC, it was 342.50.

Table 5 Current at the corresponding day for HSHFSCC

Time in minutes	Current in mA				
	CH-1	CH-2	CH-3	CH-4	CH-5
0	19	22	16	21	17
30	21	23	17	21	18
60	21	23	17	22	18
90	23	25	18	23	19
120	25	26	20	25	21
150	26	26	21	25	21
180	27	27	22	27	23
210	27	28	24	27	25
240	28	29	24	28	26
270	28	30	25	29	27
300	29	31	26	30	27
330	30	33	27	31	28
360	31	35	29	32	29
R.C.P.T in coulombs	603	644.4	514.8	613.8	538.2
Avg. in coulomb	582.84				

Fig. 8 Resistivity of HSSFSCC with and without hybrid Fibers
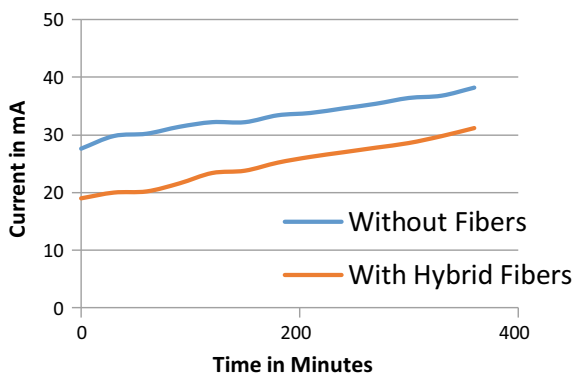
XRD and SEM Analysis: Various types of compounds are found in XRD and SEM analysis of samples. The description of these compounds and their ID's used in this study are as given in Table 7.

The XRD patterns of HSSC concrete samples with and without hybrid steel fibers subjected to corrosion are as shown in Figs. 9 and 10, respectively. These samples are collected at the site of corrosion around reinforcement bar. The quartz peaks in the graphs indicate that quartz materials are very dominant among all compounds, which indicates that these quartz minerals play an important role in attaining high strength (M100). Various feldspar group minerals are found among which microcline

Table 6 Resistivity test results for SCC and HSHFSCC

Mix	Samples	Initial current (mA)	Resistivity at 60 V	Total charge (C)
With HF	CH-1	19	496.040	603
	CH-2	22	428.398	644.4
	CH-3	16	589.048	529.2
	CH-4	21	448.799	613.8
	CH-5	17	554.398	538.2
Without HF	CH-1	29	324.992	804.6
	CH-2	25	376.992	739.8
	CH-3	28	336.599	797.4
	CH-4	27	349.065	756
	CH-5	29	324.992	790.2

Table 7 Description of chemical compounds

ID	Compound name	Chemical formula
AB	Albite	$Na\,Al\,Si_3\,O_8$
CCA	Calcium chloro aluminate (Friedel's salt)	$3CaO.\,Al_2O_3.\,CaCl_2.\,10H_2O$
CCF	Calcium chloro ferrite	$3CaO.\,Fe_2O_3.\,CaCl_2.\,10H_2O$
CH	Calcium hydroxide	$Ca(OH)_2$
D	Dolomite	$Ca\,Mg\,(CO_3)_2$
FD	Feldspar	$K\,Na\,Al\,Si_2\,O_8$
FH	Ferrous hydroxide	$Fe(OH)_2$
FO	Ferrous oxide	FeO
F_2O	Ferric oxide	Fe_2O_3
F_3O	Magnetite	Fe_3O_4
M	Microcline	$K\,Al\,Si_3\,O_8$
Q	Quartz	$Si\,O_2$

amounts more than others. In addition to microcline, albite and feldspar are also found in both concretes samples. The presence of these minerals increases the compressive strength of concrete. Though similar type of minerals found in concretes with and without fibers, the peaks indicate that quantity of these minerals is less in case of concrete without fibers subjected to corrosion. This is because, these minerals are replaced by corrosion resulted compounds more in case of concrete without fiber.

The SEM pictures of HSSC concrete samples with and without hybrid steel fibers subjected to corrosion are as shown in Figs. 11 and 12, respectively. These pictures show a very dense form of concrete with non-porous mineral mass surrounded by C-S-H. This indicates that concrete is well compacted and is rich in minerals that
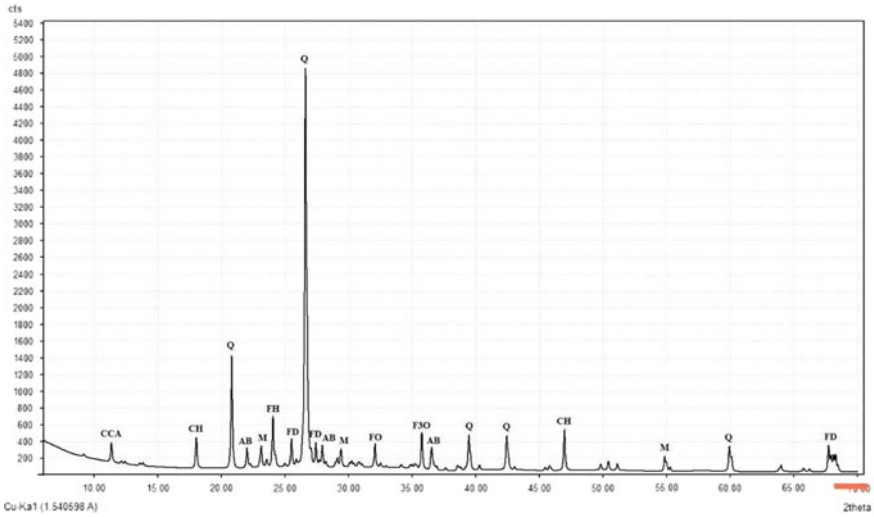
Fig. 9 XRD pattern for HSSCC with fibers subjected to corrosion
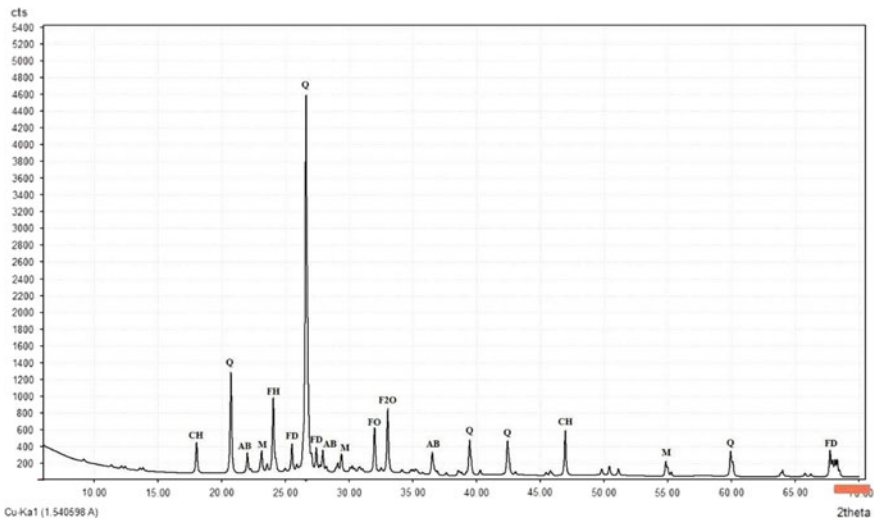
Fig. 10 XRD pattern for HSSCC without fibers subjected to corrosion

contribute to strength and durability. Also we can see more deterioration of concrete microstructure and more iron oxides formed in the case of concrete without fibers.

The basic chemical reactions involved in the corrosion process are as shown in Introduction chapter. However, the formation of various types of corrosion products or oxides are formed due to chemical reactions as shown below.

Fig. 11 Microstructure of HSSCC with fibers subjected to corrosion

Fig. 12 Microstructure of HSSCC without fibers subjected to corrosion

$$Fe^{2+} + 2H_2O \rightarrow Fe(OH)_2$$

$$Fe(OH)_2 \rightarrow FeO + H_2O + 2H^+$$

$$2Fe^{2+} + 3H_2O \rightarrow Fe_2O_3 + 6H^+ + 2e^-$$

$$3Fe^{2+} + 4H_2O \rightarrow Fe_3O_4 + 8H^+ + 2e^-$$
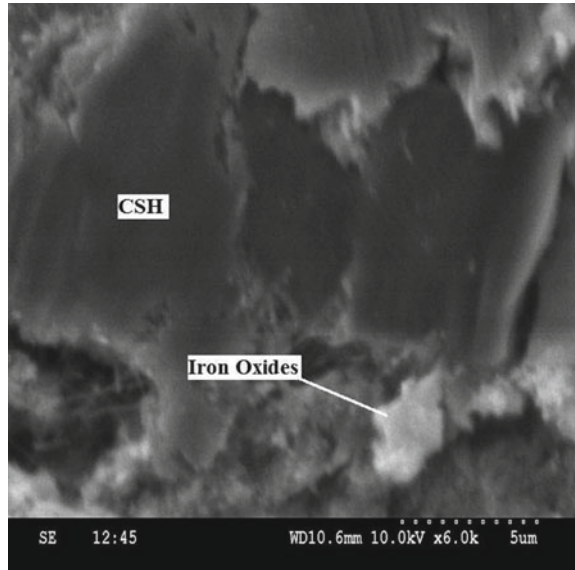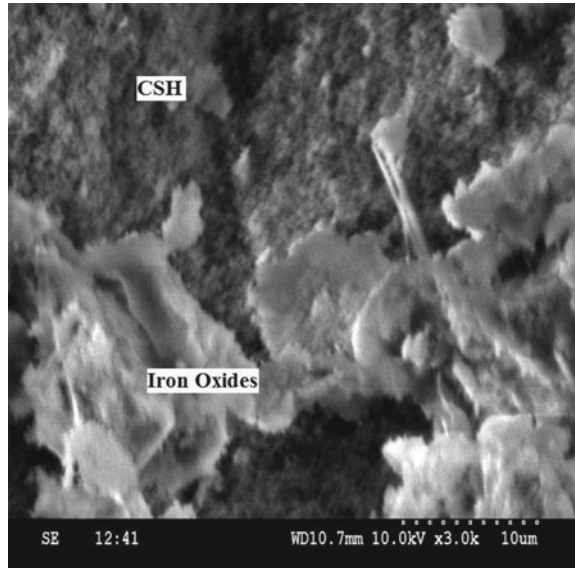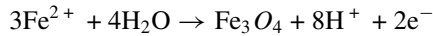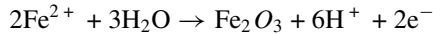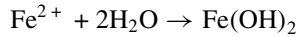
In the XRD patterns of HSSC concrete with and without fibers (Figs. 9 and 10), we can see peaks of iron(II) hydroxide, or ferrous hydroxide (Fe(OH)2). It is observed that the intensity of ferrous hydroxide is more in case HSSC concrete without fiber than concrete with fiber. Further, oxidized corrosion products were also seen in the XRD patterns. Iron(II) oxide or ferrous oxide (FeO) and iron(III) oxide or ferric oxide (Fe_2O_3) are found in HSSC concrete without fibers, whereas ferrous oxide (FeO) and magnetite (Fe_3O_4) are found in HSSC concrete with hybrid steel fibers. FeO and Fe_3O_4 are likely to form in an environment with less dissolved oxygen, whereas Fe_2O_3 favors high oxygen concentrations. This indicates that dissolved or oxygen filled in pores is more in case of concrete without fibers. This leads to more corrosion of reinforcement in concrete without fibers than in case of fibers. The formation of iron oxides on concrete compounds is seen in SEM pictures (Figs. 11 and 12). We can see more concentration of iron oxides in concrete without fiber.

The calcium hydroxide (Ca(OH)$_2$) peaks seen in XRD graphs (Figs. 11 and 12) are responsible for maintaining alkaline environment around reinforcement and formation of passive protective layer containing γ-Fe_2O_3. A small amount bounded chloride in the form of calcium chloro aluminate or Friedel's salt (3CaO. Al_2O_3. $CaCl_2$. $10H_2O$) is found in HSSC concrete with fibers. The reaction of chloride ions with hydrated cement compound C_3A results in the formation of Friedel's salt. This shows that some amount of chloride ions got trapped in concrete without reaching corrosion zone, which is a good sign of corrosion resistance.

The XRD patterns of HSSC concrete samples with and without fibers subjected to chloride ingression are as shown in Figs. 13 and 14, respectively. The quartz peaks in these graphs indicate that it occupies large portion of the concrete microstructure, which indicates that these quartz minerals play an important role in attaining high strength as discussed above. In addition to quartz minerals, feldspar, albite and microcline peaks are seen in both the cases (with and without fibers). As there is no deteriorating effect by the passing chloride ions in concrete, there is no much change in quantities of minerals and compounds found. However, very small amounts of Friedel's salt or calcium chloro aluminate (3CaO. Al_2O_3. $CaCl_2$. $10H_2O$) and calcium chloro ferrite (3CaO. Fe_2O_3. $CaCl_2$. $10H_2O$) are found in case of HSSC concrete with fibers and only calcium chloro ferrite is found in HSSC concrete without fibers. Calcium chloro aluminate is formed due to reaction of chloride ions with C_3A and calcium chloro ferrite is formed due to reaction of chloride ions with C_4AF. In addition to this chemical binding of chloride ions, physical binding may also occur when
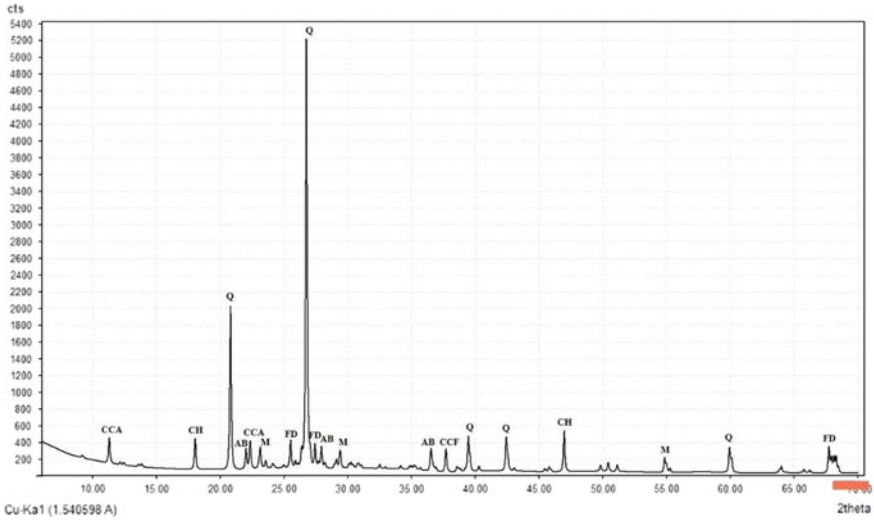
Fig. 13 XRD pattern for HSSCC with fibers subjected to chloride ingression
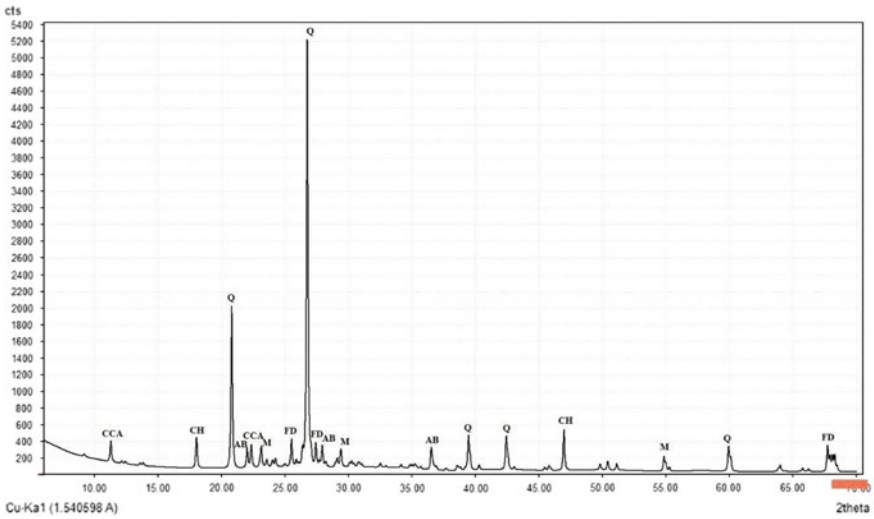
Fig. 14 XRD pattern for HSSCC without fibers subjected to chloride ingression

they get trapped in impervious pores. The binding chlorides will increase the concrete resistance to corrosion of reinforcement. Thus, if we increase the C_3A content, then more binding of chlorides will occur, but this will to increase in sulfate attack. As the XRD graph peaks shown slightly more binding of chlorides in case of concrete with fibers than concrete without fibers, it can be inferred that concrete with fibers offer good resistance to chloride ions in reaching reinforcement zone. There is no visible

change in concretes with and without fibers subjected to chloride ingression as seen in Figs. 15 and 16. These pictures will also represent the dense microstructure of HSSC concretes with and without fibers without any chemical deterioration.

Fig. 15 Microstructure of HSSCC with fibers subjected to chloride ingression
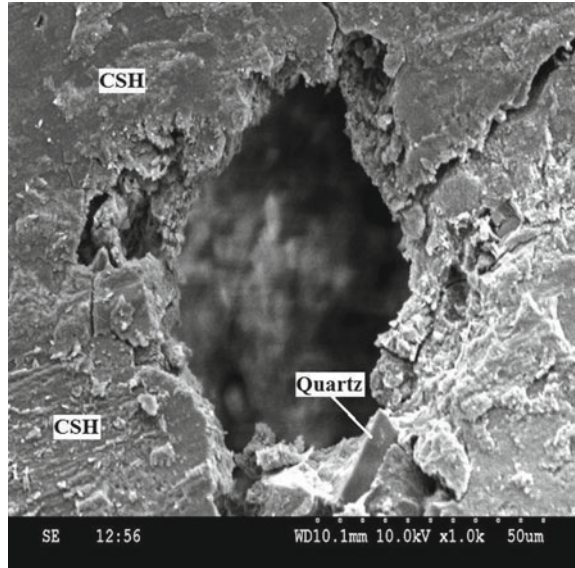
Fig. 16 Microstructure of HSSCC without fibers subjected to chloride ingression
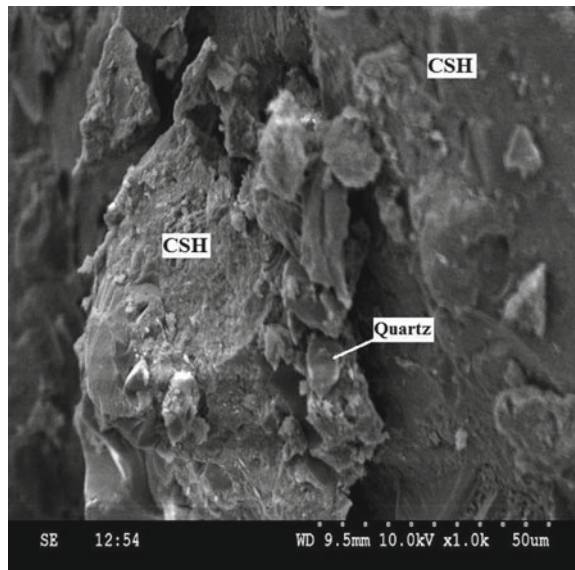
8 Conclusions

The HSHFSC concrete has shown good resistance to chloride permeability and corrosion than HSSC concrete.

The XRD analysis of both HSHFSC and HSSC concretes subjected to corrosion and chloride ingression has shown large amounts of quartz and feldspar minerals which contribute to high compressive strength of concrete.

The presence of high-intensity quartz peaks indicates that very high-strength concretes can be obtained with the use of quartz minerals.

The SEM pictures of both HSHFSC and HSSC concretes subjected to both the tests have shown very dense microstructure, which can offer great resistance to external chemical agents.

The decrease in intensity of quartz minerals and increase in intensity of corrosion products in HSSCC than in the case of HSHFSC explain the reason behind HSFFSC concrete offering more resistance to corrosion than HSSC concrete.

The presence of ferrous oxide and magnetite and absence of ferric oxide in HSHF-SCC indicate less availability of oxygen, which also supports the good resistance offered by HSHFSCC over HSSCC to chloride-induced corrosion of reinforcement.

The increase in chloride binding capacity of HSHFSCC concrete through the formation of more amounts of calcium chloro aluminate and calcium chloro ferrite also adds to the better resistance of HSHFSCC over HSSCC to chloride-induced corrosion.

References

1. Wallbank, E. J. (1989). *The performance of concrete in bridges: A survey of 200 highway bridges*. London: HMSO.
2. Rosenberg, A. Hanson, C. M., & Andrade, C. (1989). Mechanisms of corrosion of steel in concrete. In J. Skalny (ed.) *Material science of concrete* (pp. 285–313). Westerville, OH: American Ceramic Society.
3. Aboutaha R. S. (2004). Guide for maintenance, and rehabilitation of concrete bridge components with FRP composites-research into practice. *TIRC & NYSDOT*, New York, USA.
4. Neville, Adam. (1995). Chloride attack of reinforced concrete: An overview. *Materials and Structures, 28,* 63–70.
5. Silva, N. (2013). *Chloride induced corrosion of reinforcement steel in concrete, threshold values and ion distribution at the concrete steel interface* (thesis for the degree of Doctor of Philosophy). Chalmers University of Technology, Gothenburg, Sweden.
6. Angst, U. (2011, January). Chloride induced reinforcement corrosion in concrete—Concept of critical chloride content-methods and mechanisms (thesis for the degree of Philosophiae Doctor). Norwegian University of Science and Technology-Trondheim.
7. Suzuki, K., Ohno, Y., Praparntanatorn, S., & Tamura, H. (1990). Mechanism of steel corrosion in cracked concrete. In *Proceedings of Third International Symposium on Corrosion of Reinforcement in Concrete Construction*, *The Chemical Industry Society* (pp. 19–28). London, UK.
8. Beeby, A. W. (1981). Cracking, cover and corrosion of reinforcement. In *ACI spring convention*. Dallas, TEX: American Concrete Institute.

9. Fasullo, E. J. (1992). Infrastructure: The battlefield of corrosion. In V. Chaker (ed.), *Corrosion forms and control for infrastructure* (pp. 1–16). ASTM STP 1137. Philadelphia: American Society for Testing and Materials.
10. Gu, P., Beaudoin, J. J., Zhang, M. H., & Malhotra, V. M. (2000). Performance of reinforcing steel in concrete containing silica fume and blast-furnace slag ponded with sodium chloride solution. *ACI Materials Journal, 97*(3), 254–262.
11. M. V. A. Marinescu, & Brouwers, H. J. H. (2010, June). *8th fib PhD Symposium in Kgs*. Lyngby, Denmark.
12. Rober, H. (1982). Reinforcement for concrete structures subject to fatigue. In *Proceedings of Symposium on Fatigue of Steel and Concrete Structures, LABSE, AIPC, IVBH* (pp. 239–245). Lausanne, Switzerland.
13. Babaei, K., & Hawkins, N. M. (1992). Performance of rehabilitated/protected concrete bridge decks. In V. Chaker (ed.), *Corrosion forms and concrete for infrastructure* (pp. 140–154). ASTM STM 1137. 154. Philadelphia: American Society for Testing and Materials.
14. EFNARC. (2005). *Specifications and guidelines for self compacting concrete*. www.efnarc.org.

Thick Section Casting Specifications and Practices in Singapore

Saradhi Babu Daneti, Madhuri Bagadi and Pavan Kumar Dasari

Abstract High peak (curing) temperature caused by the exothermic process of cement–water reaction is one of the concerns in mass concrete elements. In land-scarce Singapore, building and infrastructure constructions are growing at a rapid rate and these constructions are in need of thick (mass) concrete sections to carry or facilitate the transfer loads to responsible elements. Mass concrete elements cast with large pours of concrete helps in enhancing the durability in terms of minimizing the number of construction joints. They are also economical in terms of catching up with tight construction schedules and the use of less manpower and constructional equipment thus leading to resource savings. Yet it is a challenge to carry out large pours with consideration of temperature controlled concrete (TCC) specifications locally. This is partly due to the prevailing tropical weather conditions which have a tendency to rise the concrete temperature more rapidly and the peak temperature in mass concrete elements. It is also very challenging for Ready-Mix Concrete (RMC) suppliers to achieve low fresh concrete temperatures on-site with local weather conditions. Therefore, the selection of right RMC supplier with commitment and due attention to logistical and technical considerations is crucial in terms of consistent concrete supply and optimal TCC performance on strength and heat of hydration. This paper presents one of the recent single largest pours of 18,000 m^3 with C32/40 TCC for casting of the raft foundation at the Marina One (Hyundai-GS JV) Project in Singapore by the Alliance Concrete Singapore Pte Ltd. The parameters that influence temperature rise in mass concrete elements, and the measures taken to control the specifications associated with mass concrete castings in Singapore shall be discussed.

S. B. Daneti (✉)
Alliance Concrete Singapore Pte Ltd., 72 Sungei Kadut Street 1, Singapore, Singapore 729372
e-mail: saradhibabu.daneti@allianceconcrete.com.sg

M. Bagadi
KK Concrete Consultants Pte Ltd., Singapore, Singapore
e-mail: kkconcreteconsultants@gmail.com

P. K. Dasari
Department of Civil Engineering, Madanapalle Institute of Technology & Science, Chittoor, A.P, India
e-mail: drpavankumard@mits.ac.in

165

The in situ thermocouple monitoring and adiabatic temperature rise laboratory testing results associated with this largest pour casting are also presented.

Keywords Mass concrete · Ready mix · Temperature · Insulation · Cracking and DEF

1 Introduction

In view of the increase in infrastructure developments around the world in recent years, mass concrete elements of thickness in the range of 1000–6000 mm are becoming more common. We can see them in different applications such as slabs/beams/columns to pile caps/raft foundations in high rise residential and commercial buildings. ACI 207.1R-05 [1] defines mass concrete as any volume of concrete with dimensions large enough requiring measures to be taken to cope with the generation of heat from hydration of the cement and attendant volume change to minimize cracking. For mass concrete structure, its serviceability performance is generally based on durability, economy, and thermal action; strength requirement is often a secondary concern. Mass concrete member is defined mainly based on its minimum dimension and ACI 301 [2] suggested a minimum dimension of 1.3 m (4 feet) as mass concrete member. Neville [3] reported that the term 'mass concrete' can be applied to any concrete member in which the thermal behavior, arising as a result of the dimensions of the member, may lead to cracking if appropriate actions are not taken. In view of the different definitions, a comprehensive definition was proposed by the Concrete Society Digest No. 2 [4] that a mass pour has to be one of sufficient size to demand special attention to logistical and technical considerations such as concrete supply, casting sequence, cold joints, plastic settlement, heat of hydration and early age thermal cracking. Though it is not generally realistic to define large volume pours in terms of dimension or volume, special considerations may be required in relation to heat of hydration for pours thicker than 500 mm.

The use of temperature controlled concrete (TCC) and the relevant preparations, precautions, and insulations are essential during casting of thick section elements for two reasons:

- To limit the peak (curing) temperature in the element in order to mitigate the possible formation of delayed ettringite formation (DEF) in concrete.

  - Ettringite—calcium sulfoaluminate: $3C_aO.Al_2O_3.3C_aSO_4.32H_2O$ is commonly formed in Portland cement concrete.
  - DEF induced cracking occurs at later ages due to heterogeneous expansion in hardened concrete.

- To prevent cracking resulting from high early differential temperatures between core (center) of the mass element to its surface.

The temperature rise and peak temperature in a section depend on how fast or slow the heat developed during hydration reactions accumulates in the member and/or is

liberated into the surrounding atmosphere. The temperature rise of concrete can be controlled by selecting appropriate materials, construction, and insulation practices. The most important factors that influence the heat rise in thick concrete element, and the measures taken to control the specifications associated with mass concrete castings are discussed as follows:

Ambient temperature: Singapore's prevailing tropical weather conditions have a tendency to increase the rate of heat generated in mass concrete/thick sections and the peak temperatures may be higher due to less heat loss. The ambient temperatures at the time of casting play a role on the resulting peak temperature of concrete. However, under tropical weather conditions, the temperature differential within the concrete element (between the surface and the center) is expected to be lower, which helps to mitigate the prevalence of cracking.

Concrete placing temperature: The rate at which cement reacts and consequently the rate at which it produces heat is a function of the placing temperature of the concrete. The higher placing temperatures of concrete can result in higher rate of temperature rise and in turn higher peak concrete temperature in the mass concrete element. Concrete temperatures can generally be lowered with the use of chilled water and/or ice blocks during batching of concrete. The higher prevailing ambient temperature makes the raw materials even warmer, whereby more efforts are needed during the production to lower the concrete temperatures for supplies to casting large pours. The concrete temperature of a mix T can be estimated from the equation [3] as follows:

$$T = \frac{0.22(T_a W_a + T_c W_c) + T_w W_w}{0.22(W_a + W_c) + W_w} \tag{1}$$

where T = temperatures in °C; W = mass of ingredients per unit volume of concrete; and the subscripts a, c, w refer to aggregate, cement, and water, respectively.

Depth/thickness/short dimension of element: Concrete is a poor conductor of heat; therefore, diffusion of the heat developed at the center of a thick section into the surrounding material is slow. With increase of member thickness, higher heat development is expected, although the rate of heat rise is small when the element thickness exceeds 1.5–2.0 m. When the thickness is large, the behavior of the mass concrete becomes nearly adiabatic condition (where there is no gain or loss of heat) [5].

Mix proportions: For a given binder type and the thickness of the section, binder content in the design mix has a major effect on temperature rise of concrete, which produces heat of hydration when mixed with water. Binder with higher fineness increases the rate and amount of temperature rise. Admixtures have a minor effect on the temperature rise and peak temperature of concrete, except for the rate of alteration of temperature rise based on retarding or accelerating type/performance of admixtures. Aggregates occupy the major volume in concrete and the aggregate temperature affects the fresh concrete temperature. Water content has a small influence on the temperature rise, but water temperature affects fresh concrete temperature. Typically, to lower the fresh concrete temperature by 1 °C requires a 2 °C reduction in aggregate temperature or 4 °C reduction in water temperature [5].

Formwork and insulation: Formwork (type) can influence the temperature rise and differential temperature based on its insulation value for a given thickness of element and concrete type. Use of higher insulation type of formwork can result in higher temperature rise in the mass element due to its longer period of heat retention, but the differential temperatures can be effectively controlled to lower values. Timber formwork provides better insulation than either steel or plastic formwork. Creating air pockets and covering the elements with plastic sheets and polyfoam insulations are some of the recommended insulation measures to reduce differential temperature to minimize early cracking.

The large concrete pours for mass/thick section elements help in enhancing the durability in terms of minimizing the number of construction joints. They are also economical in terms of catching up with tight construction schedules and use of low manpower and constructional equipment thus leading to resource savings. Yet, it is a challenge to carry out large pours with consideration of TCC specifications locally. This is partly due to the prevailing tropical weather conditions which have a tendency to rise the concrete temperature more rapidly and the peak temperature in mass concrete elements. It is also very challenging for Ready-Mix Concrete (RMC) suppliers to achieve low fresh concrete temperatures on-site with local weather conditions. Therefore, the selection of right RMC supplier with commitment and due attention to logistical and technical considerations is crucial in terms of consistent concrete supply and optimal TCC performance on strength and heat of hydration.

This paper presents the recent single largest pour of 18,000 m^3 with C32/40 TCC for casting of raft foundation at the Marina One (Hyundai-GS JV) Project in Singapore supplied by Alliance Concrete Singapore Pte Ltd (ACS). The in situ thermocouple monitoring and adiabatic temperature rise laboratory testing results associated with this largest pour casting are also presented below and discussed.

2   Singapore Scenario and Specifications

Any structural concrete element thickness exceeding 500 mm shall be considered as thick section [6] in local construction industry and in concrete specifications. During the construction of such elements, one or few of the following practices shall be implemented in order to lower the peak temperatures in the section.

1. use of low heat cements like CEM III/B or CEM III/C [7],
2. controlled fresh concrete temperatures during placement by considering chilled water and/or crushed ice flakes/tubes during the production of concrete at ready mixes batching plant,
3. placing of internal heat controlled systems,
4. sandwich layering system with each layer thickness typically limiting to $\leq$ 600 mm,
5. controlled formwork removals or insulations during curing.

- Locally coarse aggregate that is used in concrete is granite, unless specified otherwise.
- All the cements to be in concrete structural works shall be of low alkali type with equivalent $Na_2O \leq 0.60\%$ for cement or the total alkali content of concrete to be ≤ 2.5 kg equivalent Na_2O/m^3.
- The use of CEM III/B cement type with 30% OPC+70%GGBS combination is popular in TCC due to its proven performance in terms of significantly reduced peak temperature and low rate of heat gain in thick section applications.

The reduction/low rate of heat gain depends on the degree of reactivity of the GGBS and some GGBS are more highly reactive, which can result in high rate of heat gain, though the ultimate peak temperatures may be similar or marginally higher. Therefore, TCC of suitable quality and proper insulation measures are essential to mitigate early age cracking caused by the higher differential temperature within the mass element due to temperature effects in terms of heat gain/heat loss after casting.

As the reaction of CEM III/B cement is pozzolanic, a reduction in the rate of (compressive and tensile) strength development, especially at early ages can be expected. Therefore, additional precautions in terms of good insulation practices on-site have to be considered essentially to keep the differential temperatures lower than allowable after a few days of casting until the increase in tensile strength of concrete is able to offer more resistance to cracking against the tensile stresses in the concrete resulting from any restraint. As the granite aggregate is being used locally, the limiting differential temperature proposed to avoid cracking in thick section elements is 27.70 °C. Nevertheless, based on local experiences, no early age thermal cracking was observed/reported in the thick sections like pile caps and raft foundations with differential temperatures of up to 35–40 °C.

Locally, apart from the use of low alkali cements with equivalent $Na_2O \leq 0.60\%$ and CEM III/B cement type with 30% OPC + 70% GGBS combination for the TCC applications in large concrete pours, the considerations of other measures like (1) lower cement contents in design mixes, (2) lower placing temperatures and reducing the pour thicknesses, and (3) use of cooling pipes within the elements (in critical projects) to limit the temperature rise and peak temperatures of concrete within the mass concrete/thick section elements, no risk of DEF induced expansion/damage can be anticipated. Nevertheless, a scrupulous verification of cement type/combination in terms of quality against the compliances/limits and monitoring its performance in TCC is recommended.

3 Largest Pour of TCC for Raft Foundation Casting

Marina One (Hyundai-GS JV) Project is a mixed-used development that is being developed by Malaysia's strategic investment fund, Khazanah Nasional and Singapore's investment company, Temasek. It is planned as two 34-story residential

towers, two 30-story office towers, and a retail podium. Owner: MS Commercial Pte. Ltd./MS Residential 1 Pte. Ltd. /MS Residential 2 Pte. Ltd.

The strength class of C32/40 TCC (with and without waterproof) volume of about 79,200 m^3 was used for the casting of raft foundation, which had a different thickness at different locations typically in the range of 4.0–6.5 m. The overall view of the building and the layout of the raft foundation are shown in Fig. 1. This largest pour of 18,000 m^3 is the last part of the raft foundation, which was casted after completion of successful construction of different volumes like 3000, 5000, and 10000 m^3.

As this largest pour was extremely challenging due to its massive scale and approvals/clearances for construction were confirmed only after the firm commitments by the respective main parties such as construction team, supervision teams, concrete suppliers, and raw materials suppliers. The fresh concrete is chilled to meet the stringent requirement in terms of thick section specifications. A total of 42,000
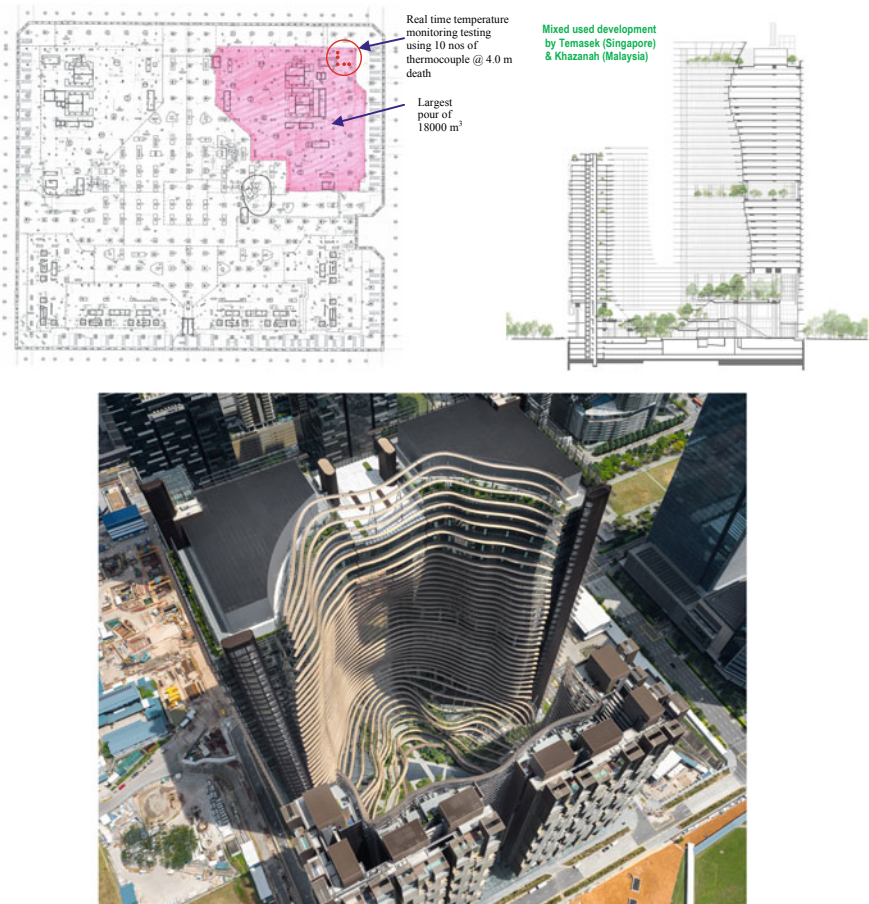
Fig. 1 Typical layout of the raft foundation and overall view of the building

tons of materials was used for this mass pour which is equivalent to 150 empty Airbus A380 passenger airliners. Further details of this largest pour were reported elsewhere [8].

With strong support of Alliance Concrete Singapore (ACS) and commitment in terms of due attention to logistical and technical considerations, Marina One Project team performed the casting for raft foundation with single largest pour of 18,000 m^3 (22.7% of total concrete volume for the casting of raft foundation), including over 2,600 m^3 of integral waterproofed concrete (for top 500 mm thick), using 7 concrete pumps (due to limited space/access for more pumps) in about 57 h while using over 2000 truckloads of continuous concrete pouring. During casting, a smooth supply of concrete was ensured by ACS with our committed support and close monitoring of equipped real-time GPS/GPRS truck tracking system together with effective truck coordination on-site as shown in Fig. 2. This is the largest pour in Singapore and the

Fig. 2 Typical view on-site during casting with lineup of concrete trucks

world, beating the record of earlier large pour casting (16,200 m^3) set in 2014 on the Wilshire Grand project in Los Angeles, USA [9].

This pour was carried out with TCC designed with CEMIII/B cement type with 30% ordinary Portland cement (OPC) and 70% ground granulated blastfurnace slag (GGBS) combinations complying with EN 197 [7]. Additionally, green concrete material of washed copper slag at a replacement level of 10% by weight of fine aggregate was used as part of Building and Construction Authority (BCA) Green Mark requirements toward sustainability in concrete construction [10]. The placing temperature of fresh concrete was limited at 28 °C to control the peak temperatures of concrete at midpoints (under adiabatic condition) of the raft foundation and to limit on the temperature differential in the raft foundation elements with minimum insulation effort so as to prevent any slowdown in the construction progress.

Prior to this largest pour of raft foundation casting, the suitability of TCC mix was verified with adiabatic temperature rise (ATR) test (concrete sample test under no heat loss condition to simulate the core (center) location of the thick section, where the heat is not dissipated). This testing was carried out on sample collected during another large pour (10,000 m^3) of similar thickness cast 5 days earlier to this largest pour, whereby the sample from the center layer of concrete is collected for ATR testing. The ATR test report corresponds to 10,000 m^3 cast sample has recorded a peak temperature of 69.80 °C.

Furthermore, on-site real-time temperature monitoring testing using ten numbers of thermocouple was also carried out during 10,000 m^3 supply and the results were compiled in terms of peak and differential temperatures.

During the actual casting of this largest pour, workability (slump) and fresh concrete temperatures were checked upon arrival of concrete trucks to site. Real-time temperature monitoring within the element using ten numbers of thermocouple was also carried out during this largest pour of 18,000 m^3. The locations of thermocouples installed for raft foundation at 4000 mm depth are given in Figs. 1 and 3. Further to the real-time thermocouple monitoring, concrete corresponding to the center layer
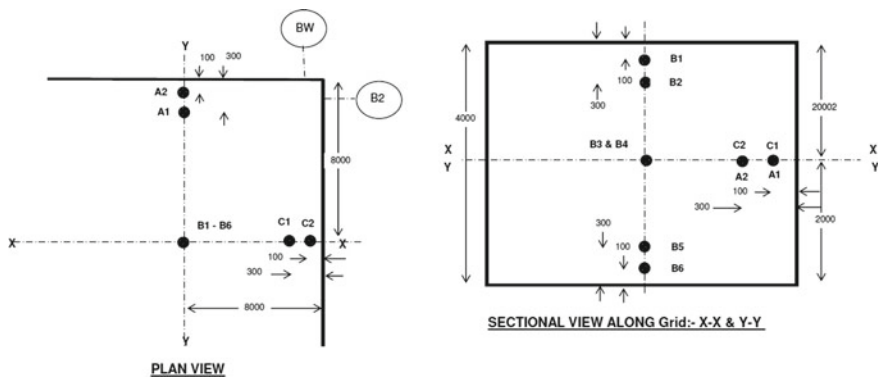
Fig. 3 Thermocouple locations

of casting is also sampled for ATR testing to further verify the quality of concrete supplied to this largest pour of raft foundation casting.

During the real-time monitoring period, concrete was insulated by covering the entire cast area with polyethylene sheet and created an air pocket to act as a heat blanket surrounding the concrete to control the differential temperatures within the element. Apart from the air-pocket insulation measures, a contingency plan with additional insulation in terms of consideration of 50 mm thick polystyrene foam at the respective surface/location to mitigate heat loss from the surface, in the event, the temperature differential is trending toward exceeding the limit (27.7 °C) was also implemented by the site construction team to closely review real-time daily monitoring data.

Furthermore, 150 mm cube samples were made for this TCC for testing at 7-day, 28-day in accordance with the project test sampling requirements as per specifications to test the quality of concrete against the designed strength class for the raft foundation.

4   Results and Discussions

The results of temperature monitoring and the maximum temperature minus 27.70 °C are shown in Fig. 4. The ATR testing peak temperature result of the concrete sample corresponds to this largest pour is shown in Fig. 5.

Largest pour of this casting commenced on March 01, 2015 and the midportion of the casting at the real-time thermocouples monitoring location carried out at about 25 h after the commencement of casting. The highest temperature recorded based on thermocouples monitoring location is 76.0 °C after at about 90 h of casting.
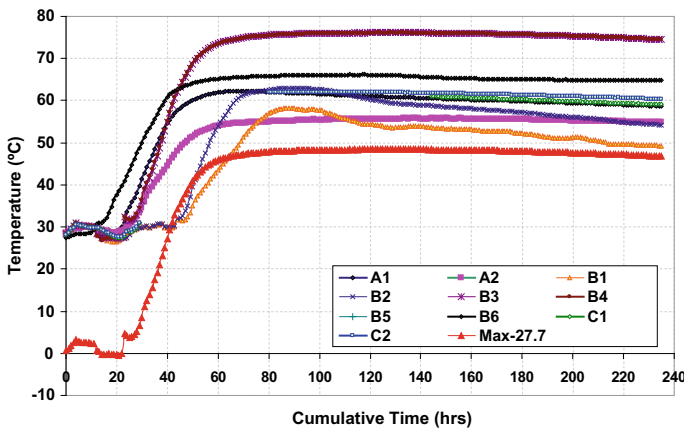
Fig. 4 Real-time thermocouple monitoring results for raft foundation of largest pour of 18000 m^3 casting
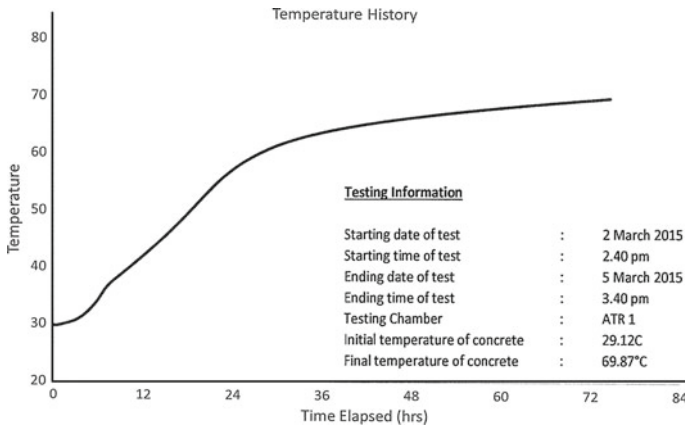
Fig. 5 ATR test result for raft foundation of largest pour of 18000 m³ casting

The differential temperature of concrete is expressed as the maximum temperature (corresponds to B4/B5) minus the limit of 27.70 °C (Max −27.70 °C) and shown in Fig. 5. The adopted insulation measures on-site were found to be effective in limiting the differential temperatures.

The highest temperature result from the ATR testing was found to be 69.87 °C at 73 h after the test commenced. The rate of heat development in the sample was observed to be almost stable at ~ 70 °C and this result coincides with the pre-testing verifications of ATR test result (69.80 °C, corresponds to 10000 m³ of concrete pour) for TCC. The difference on peak temperatures based on real-time monitoring and ATR testing perhaps was due to ambient variations during casting of the midportion of thick section.

The statistical analysis of 76 sets (cube strength results $76 \times 3 = 228$) of samples corresponds to 15,400 m³ of PBFC (excluding ~2600 m³ of PBFC waterproof) concrete are shown in Fig. 6.

The mean (x) and standard deviation (σ) based on 76 sets of samples were found to be 45.60 N/mm², 2.69 N/mm², respectively, for the design strength class of C32/40 TCC used for the raft foundation casting. The statistical results show that quality control of concrete supply was found to be consistent. This largest pour of supply shows that the casting of thick section with consideration of large pour not only helps in minimizing the number of construction joints but also helps to enhance the durability of concrete through consistent quality control of concrete supply, apart from the economy/resource savings.
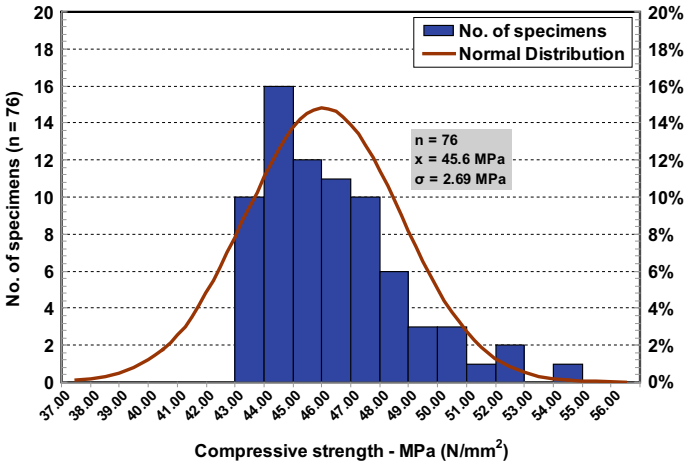
Fig. 6 Statistical analysis of cube strength results

5 Conclusions

- Single largest pour of 18000 m^3 temperature controlled concrete (TCC) supplied by the Alliance Concrete Singapore Pte Ltd was successfully casted at Marina One Project (Hyundai-GS JV) for raft foundation casting with considerations of temperature controlled specifications, and special attention to logistical and technical considerations in terms of quality of concrete.
- Pre and post verifications of TCC quality were verified with relevant temperature controlled laboratory and field testing and the test results were found to be in compliance against the requirements.
- The TCC testing results on temperature controlled parameters and cube strength results show that with careful considerations of large pours for mass concrete/thick section castings a better quality control of concrete can be achieved which in turn enhance the durability of concrete. Further, this leans to the minimization of number of construction joints and significant resource savings in terms of catching up with tight construction schedules and use of low manpower and constructional equipment.
- Based on the review of Singapore concrete specifications and construction practices for mass concrete/thick section castings, no risk of DEF induced expansion/damage can be anticipated with the use of TCC, ensuring the right quality.

References

1. ACI 207.1R-05. (2005). *Guide to mass concrete* (ACI Committee 207 Report).
2. ACI 301-10. (2010). *Specifications for structural concrete* (ACI Committee 301 Report).
3. Neville, A. M. (2011). *Properties of concrete* (5th ed.). London: Pearson.
4. Bamforth, P. (1984). *Mass concrete*. Concrete society digest no. 2. London: The Concrete Society.
5. Harrison T. A. (1992). *Early age thermal crack control in concrete* (CIRIA Report 91).
6. *Land transport authority M&W Specifications for civil & structural works*. (2010). Singapore.
7. *SS-EN 197-1: Cement—Part 1: Composition, specifications and conformity criteria for common cements*. (2011).
8. Daneti S. B. (2015, August 27–28). *Largest pour of temperature controlled concrete for raft foundation casting at marina one project in Singapore by Alliance Concrete*. 40th Conference on Our World in Concrete & Structures (pp. 27–28), Singapore.
9. http://www.guinnessworldrecords.com/news/2014/2/la-construction-workers-break-record-for-largest-concrete-pour-for-new-wilshire-grand-building-video-55376/.
10. https://www.bca.gov.sg/SustainableConstruction/others/sc_materials_book.pdf.

Use of GGBS in Manufacturing of Solid Concrete Blocks

Check for updates

Jagadish Vengala, S. Raju, B. Shiva, L. R. Manjunatha and M. V. Yogananda

Abstract Concrete blocks are produced in large variety of sizes either solid or hollow, dense or lightweight, air cured or steam cured, load bearing or non-load bearing can be produced manually or with the help of machines. Proportioning the mix components for a concrete masonry unit is an important step in producing high-quality units, otherwise it leads to either uneconomical or poor quality. Hence, an attempt was made to address these issues. Although solid concrete blocks are being used abundantly, there are no proper guidelines for the mixture proportioning. Blocks can be used for different purposes like construction of load-bearing walls as well as non-load bearing walls. There has to be proper guidelines to manufacture these blocks in a consistent manner. Blocks produced these days are purely based on experience of the operator or the laborers working at casting yards, which affects the quality of these blocks. Also, there are no proper guidelines for utilizing either mineral or chemical admixtures in the manufacturing of concrete blocks. Sometimes either excess amount or lesser amount of cement in the manufacturing is usually observed, which can be avoided when proper guidelines are provided. Otherwise this leads to an uneconomical mix or affects the quality of the blocks. An effort to provide guidelines for the proportioning of solid concrete blocks was made. Optimum mix for the manufacturing of solid concrete blocks is mix with a cement content of 150 kg/m^3. Mineral admixtures can be used in the manufacturing of solid concrete blocks. However, GGBS has shown very effective in replacement of cement without compromising the quality of the solid blocks. Air-entraining admixtures do not serve their purpose, but plasticizers can be used to reduce w/c for better finish.

J. Vengala (✉)
Department of Civil Engineering, PVP Siddhartha Institute of Technology, Vijayawada, Andhra Pradesh, India
e-mail: jdvengala@yahoo.com

S. Raju · B. Shiva
Civil Engineering Department, BMS Institute of Technology and Management, Bangalore, Karnataka, India

L. R. Manjunatha · M. V. Yogananda
JSW Cement Limited, Vijayanagara, Karnataka, India

1 Introduction

Walls constitute for about 70% of the load that is coming on to the foundation. These walls may be load bearing or non-load bearing elements. Walls usually are constructed using masonry. Masonry is an assemblage of masonry units and mortars. Masonry properties and behavior are controlled by the characteristics of masonry units and mortar as well as the bond between them. Burnt clay bricks and cement mortars are the most commonly used materials for the construction. Nowadays, concrete blocks are being widely used as masonry units.

Concrete blocks are produced in large variety of sizes either solid or hollow, dense or lightweight, air cured or steam cured, load bearing or non-load bearing can be produced manually or with the help of machines. Proportioning the mix components for a concrete masonry unit is an important step in producing high-quality units, otherwise it leads to either uneconomical or poor quality. Hence, an attempt was made to address these issues.

Although solid concrete blocks are being used abundantly, there are no proper guidelines for the mixture proportioning. Blocks can be used for different purposes like construction of load-bearing walls as well as non-load bearing walls. There has to be proper guidelines to manufacture these blocks in a consistent manner. Blocks produced these days are purely based on experience of the operator or the laborers working at casting yards, which affects the quality of these blocks. Also, there are no proper guidelines for utilizing either mineral or chemical admixtures in the manufacturing of concrete blocks. Sometimes either excess amount or lesser amount of cement in the manufacturing is usually observed, which can be avoided when proper guidelines are provided. Otherwise this leads to an uneconomical mix or affects the quality of the blocks.

1.1 Objective of the Study

The study was conducted with the following objectives:

The main objective of this study is to provide proper guidelines for the manufacturing of solid concrete blocks.

- To optimize mixture proportioning for solid concrete blocks so as to avoid wastage or excess utilization of materials.
- To incorporate mineral and chemical admixtures into solid concrete blocks to enhance the performance and also to achieve economy.
- Produce lightweight blocks using chemical admixtures so as to reduce overall load on the structure.

- To assess the performance of these blocks by conducting laboratory to field studies and implementing the same at the site.

  The scope is limited to the use of the following materials.
  The materials used in the project are:

- OPC 53 Grade cement
- Ground-granulated blast-furnace slag (GGBS) (upto 70% replacement)
- Fine Aggregate—Crushed stone sand
- Coarse Aggregate—12.5 mm down and 6 mm down sized crushed aggregates
- Chemical Admixture—Air entrainers and plasticizers.

2 Experimental Program

The experimental programme aimed at developing a mixture proportioning procedure to produce solid concrete blocks. It involved in re-proportioning of cement with different percentages of GGBS and also using commercially available chemical admixtures. The experiments were conducted at ambient temperatures, which ranged from 25–30 °C.

The details of materials used in this study are presented below, and same has been represented as Fig. 1.

Ordinary Portland Cement 53 grade, conforming to the requirements of Indian Standards IS 12269: 2013 [1], was used in the study. Ground-granulated blast-furnace slag is obtained by quenching molten iron slag (a by-product of iron and steel-making) from a blast furnace in water or steam, to produce a glassy, granular product that is then dried and ground into a fine powder. GGBS used in the study satisfies the requirements of IS 16714: 2018. Table 1 gives the characteristics of cement and GGBS.

Crushed stone sand was used as fine aggregate, and crushed granite stone was used as coarse aggregate. A combination of 12.5 mm down and 6 mm down coarse
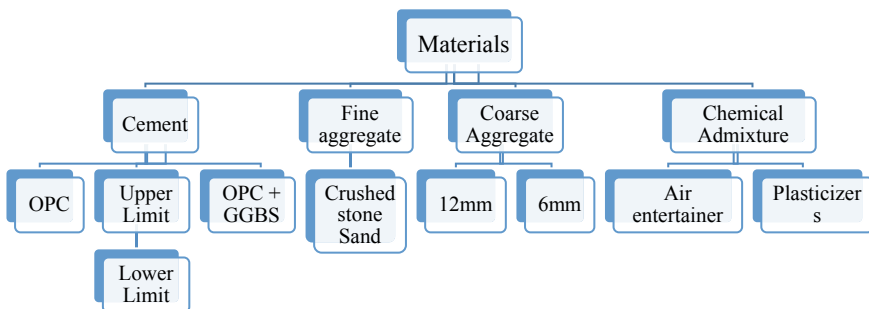
Fig. 1 Materials used in this study

Table 1 Characteristics of cement and GGBS

S. No.	Physical characteristics	Cement	GGBS
1.	Specific gravity	3.15	2.89
2.	Consistency (in %)	27	–
3.	Slag activity index in % 7 days 28 days	– – –	– 68 91
4.	Fineness (m²/kg) (Blaine)	279	372
5.	Setting time (minutes), 1. Initial setting time 2. Final setting time	165 295	– –
6.	Compressive strength (MPa) 3 days 7 days 28 days	35.0 48.0 65.5	– – –

aggregate was used, and 12.5 mm down passed through 12.5 mm sieve and retained on 4.75 mm sieve. The grading and physical properties of coarse aggregate and fine aggregate are shown in Tables 2 and 3.

Potable water was used for mixing and wet curing. Commercially available naphthalene-based plasticizer was used as chemical Admixture. This was formulated to attain high dispersion of cement particles for effective water reduction and slump retention in mixes.

Commercially available air-entraining admixture confirms to the requirements of IS 9103: 1999 was used. This was based on surface-active surfactants which create ultra-stable air bubbles that are strong, small and closely spaced.

Table 2 Sieve analysis of coarse aggregate and fine aggregate

Coarse aggregate		Fine aggregate					
Sieve size (mm)	% passing	Sieve size	Cumulative % passing	Zone—Specifications as per IS 383: 2016 for % passing [2]			
				I	II	III	IV
20	100						
16	100	4.75 mm	100	90–100	90–100	90–100	95–100
12.5	96	2.36 mm	91.6	60–95	75–100	85–100	95–100
10	55.4	1.18 mm	60.8	30–70	55–90	75–100	90–100
4.75	2.4	600 μ	42.5	15–34	35–59	60–79	80–100
Pan	–	300 μ	24.4	5–20	8–30	12–40	15–50
		150 μ	11.5	0–10	0–10	0–10	0–10
		Pan	–	–	–	–	–
The fine aggregate tested conforms to Zone-II							

Table 3 Physical characteristics of aggregates

S. No.	Details	Crushed stone sand	Coarse aggregate
1.	Specific gravity	2.60	2.70
2.	Fineness (by sieve)	Passing 4.75 mm Retained 150 μm	Passing 12.5 mm Retained 4.75 mm
3.	Water absorption (%)	3.10	0.30
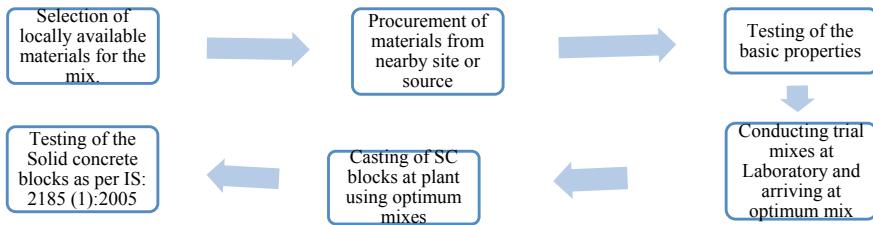
Fig. 2 Work flow of the methodology adopted

A methodology to arrive at optimum mixture proportioning for achieving solid concrete blocks by using both chemical and mineral admixtures is presented. The workflow of the same has been represented in Fig. 2.

2.1 Mix Proportioning

- Concrete was first designed by the IS method of mix design as per IS 10262: 2009, which usually gives a basic guidelines to calculate the mix constituents based on the material properties.
- The programme consisted of four series; For the first series, initially, a nominal mix was designed for > 5 MPa with a high cement content of 200 kg/m^3 and followed by mixes with a medium cement content of 150 kg/m^3 and a low cement content of 100 kg/m^3.
- The optimum mix which satisfied the density and strength criteria is taken as the reference mix to carry out the further experiments. In the second series, cement was replaced with GGBS at 10, 13, 20, 27, 33, 37, 43, 50, 57, 63 and 67% intervals without altering the W/C ratio to achieve economy in the mix while satisfying all the properties.
- In the third series, mixes were also cast with different percentages of air-entraining agent (0.5, 1, 1.5 and 2%) to reduce the density.

- Further in the fourth series, trials were conducted with the different super plasticizer dosage by reducing W/C ratio to ascertain the properties.
- Mixes from series 1 and series 2 are taken further to cast the solid concrete blocks at site and tested for different properties.
- All the mixes were tested for block density, water absorption and compressive strength. The compressive strength tests were conducted on 100 mm×100 mm× 100 mm concrete cubes (except the full-scale blocks cast at site) on 7, 14 and 28 days along with accelerated curing test to know the projected 28 days strength. All the cubes were cured until the day of testing.

Actual mixes, which were arrived, based on the methodology adopted with proportions were as shown in Tables 4 and 5.

3   Results and Discussions

The test results of different cubes and blocks of varying mixes were discussed below. Tests such as compressive strength, water absorption and density of cubes and solid concrete blocks have been tabulated. This also includes discussions based on results obtained.

3.1   Series 1, Mixes Without Admixtures

A total of 25 mixes were produced, out of which three were cast without admixture to arrive at optimum cement content. The mixes namely M1C, M2C and M3C prepared with a cement content of 200, 150 and 150 kg/m^3 respectively. The amount of cement content was decided based on the information gathered from various manufacturing plants in and around Bangalore.

Table 6 gives the result of compressive strength, water absorption and density of blocks of the series 1. From the table, it can be seen that Mix M1C has very high compressive strength of 24 MPa at 28 days, whereas the requirement for solid concrete blocks should have a compressive strength greater than 5 Mpa. Mix M2C has good initial strength of 9 Mpa at 7 days and 10.6 Mpa at 28 days. Mix M3C has low compressive strength of 4.1 Mpa at 7 days which is below the requirements. Hence, Mix M2C was chosen as optimum mix and taken as a control mix to carry out further trials. Density and water absorption values have satisfied the requirements of IS 2185(1): 2005 [3].

Table 4 Mix proportioning for cubes using mineral and chemical admixtures

S. No.	Mix design	Mix proportions		Coarse aggregates	W/C ratio	Cement in kg/m^3	GGBS in kg/m^3	Air entrainer (%)	Plasticizers (%)	Remarks
		Cement	Fine aggregates							
1.	M1C	1	4.888	5.32	0.65	200	–	–	–	High cement content
2.	M2C	1	6.9	7.1	0.85	150	–	–	–	Medium cement content
3.	M3C	1	6.1	6.33	0.72	100	–	–	–	Low cement content
4.	M1G2C	1	6.9	7.1	0.85	135	15	–	–	10% replacement
5.	M2G2C	1	6.9	7.1	0.85	75	75	–	–	50% replacement
6.	M3G2C	1	6.9	7.1	0.85	85	65	–	–	43% replacement
7.	M4G2C	1	6.9	7.1	0.85	95	55	–	–	37% replacement
8.	M5G2C	1	6.9	7.1	0.85	100	50	–	–	33% replacement
9.	M6G2C	1	6.9	7.1	0.85	110	40	–	–	27% replacement
10.	M7G2C	1	6.9	7.1	0.85	120	30	–	–	20% replacement
11.	M8G2C	1	6.9	7.1	0.85	130	20	–	–	13% replacement

(continued)

Table 4 (continued)

S. No.	Mix design	Mix proportions				W/C ratio	Cement in kg/m³	GGBS in kg/m³	Air entrainer (%)	Plasticizers (%)	Remarks
		Cement	Fine aggregates	Coarse aggregates							
12.	M9G2C	1	6.9	7.1		0.85	65	85	–	–	57% replacement
13.	M10G2C	1	6.9	7.1		0.85	55	95	–	–	63% replacement
14.	M11G2C	1	6.9	7.1		0.85	50	100	–	–	67% replacement
15.	M1A2C	1	6.9	7.1		0.85	150	–	1.00	–	with 0.85 W/C
16.	M2A2C	1	6.9	7.1		0.85	150	–	1.50	–	with 0.85 W/C
17.	M3A2C	1	6.9	7.1		0.85	150	–	2.00	–	with 0.85 W/C
18.	M4A2C	1	6.9	7.1		0.85	150	–	0.50	–	with 0.85 W/C
19.	M5A2C	1	6.9	7.1		0.65	150	–	1.00	–	reduced W/C to 0.65
20.	M6A2C	1	6.9	7.1		0.65	150	–	1.50	–	reduced W/C to 0.65
21.	M7A2C	1	6.9	7.1		0.65	150	–	2.00	–	reduced W/C to 0.65

(continued)

Table 4 (continued)

S. No.	Mix design	Mix proportions			W/C ratio	Cement in kg/m³	GGBS in kg/m³	Air entrainer (%)	Plasticizers (%)	Remarks
		Cement	Fine aggregates	Coarse aggregates						
22.	M1P2C	1	6.9	7.1	0.65	150	–	–	0.50	with 0.85 W/C
23.	M2P2C	1	6.9	7.1	0.65	150	–	–	1.00	with 0.85 W/C
24.	M3P2C	1	6.9	7.1	0.65	150	–	–	1.50	with 0.85 W/C
25.	M4P2C	1	6.9	7.1	0.65	150	–	–	2.00	with 0.85 W/C

Table 5 Mix proportions for solid concrete blocks cast at site

S. No.	Mix design	Mix proportions						Remarks
		Cement	Fine aggregates	Coarse aggregates	W/C ratio	Cement in kg/m^3	GGBS	
1.	M1S2C	1	4.88	5.32	0.65	200	–	High cement content
2.	M2S2C	1	6.9	7.1	0.85	150	–	Optimum cement content
3.	M3SG2C	1	6.9	7.1	0.85	130	20	13% replacement
4.	M4SG2C	1	6.9	7.1	0.85	100	50	33% replacement
5.	M5SG2C	1	6.9	7.1	0.85	75	75	50% replacement
6.	M6SG2C	1	6.9	7.1	0.85	65	85	57% replacement
7.	M7SG2C	1	6.9	7.1	0.85	40	110	73% replacement

3.2 Series 2, Mixes with GGBS

In series 2, GGBS was used as partial replacement of cement. Total 11 numbers of trial mix with replacement of GGBS ranging between 10 and 70% namely M1G2C to M11G2C without altering the W/C ratio, i.e., 0.85. Table 7 gives the result of compressive strength, water absorption and block density of the series 2 with GGBS. From Table 7, it was found that cubes cased with GGBS showed good early strength in case of all the mixes. Compressive strength values at 28 days for these mixes range between 6 and 16 MPa. Hence, GGBS is an ideal material as a part replacement of cement in the manufacture of solid concrete blocks. Density and water absorption values for all the mixes satisfy the requirements of IS 2185(1): 2005 [3]. Further, from series 2, five mixes were taken it for casting the blocks at site.

3.3 Series 3 and 4, Mixes with Chemical Admixtures

Chemical admixtures like air entrainers and plasticizers were also introduced in the mix to check strength properties in cubes. Air entrainer dosage ranging from 0.5 to 2% was used in the control mix, and four mixes were casted, namely M1A2C to M4A2C. The blocks cast had very wet mix which is not suitable for casting of solid blocks using egg-laying machines. Hence, water–cement ratio was reduced from 0.85 to 0.65, and cubes were cast in this series namely M5A2C to M8A2C.

Table 6 Test results of series 1 mixes

S. No.	Mix	Compressive strength				Water absorption				Density (Kg/m^3)
		Accelerated curing (MPa)	7 days (MPa)	14 days (MPa)	28 days (MPa)	Dry weight (Kg)	Wet weight (Kg)	Water absorption (%)		
1.	M1C	14.2	19.5	23.3	23.9	2.42	2.55	5.50		2415
2.	M2C	7.4	9.2	10.1	10.6	2.21	2.40	8.89		2206
3.	M3C	3.3	4.1	6.5	9.8	2.24	2.44	9.07		2240

Table 7 Test results of series 2 mixes

S. No.	Mix	Compression strength					Water absorption			Density (Kg/m³)
		Accelerated curing [4] (MPa)	7 days (MPa)	14 days (MPa)	28 days (MPa)	Dry weight (Kg)	Wet weight (Kg)	Water absorption (%)	
1.	M1G2C	3.66	3.58	6.45	9.63	2.23	2.45	9.95	2230
2.	M2G2C	2.17	2.20	8.25	7.55	2.05	2.17	5.94	2047
3.	M3G2C	3.24	4.08	7.20	7.93	2.07	2.24	8.37	2067
4.	M4G2C	3.73	3.86	5.56	6.49	1.97	2.12	7.57	1974
5.	M5G2C	2.44	6.61	6.80	7.17	2.07	2.23	7.71	2071
6.	M6G2C	2.54	3.88	4.01	8.75	2.01	2.19	8.82	2012
7.	M7G2C	2.74	3.02	3.12	6.17	2.02	2.19	8.60	2015
8.	M8G2C	4.54	4.51	3.94	10.97	2.09	2.22	6.47	2088
9.	M9G2C	11.56	10.31	18.19	10.57	2.21	2.37	7.17	2207
10.	M10G2C	4.38	5.07	4.06	16.27	2.04	2.17	6.19	2042
11.	M11G2C	5.20	4.21	5.35	13.62	2.02	2.15	6.13	2022

Table 8 Test results of series 3 and 4 mixes

S. No.	Mix	Compressive strength			Water absorption			Density
		7 days (MPa)	14 days (MPa)	28 days (MPa)	Dry weight (kg)	Wet weight (kg)	Water absorption (%)	
1.	M1A3C	7.33	8.25	9.42	2.16	2.36	9.67	2155
2.	M2A3C	4.55	6.03	7.54	2.00	2.18	9.00	2003
3.	M3A3C	5.16	6.55	8.53	1.87	2.02	7.78	1871
4.	M4A3C	7.89	9.28	10.78	2.20	2.34	6.54	2198
5.	M5A2C	4.28	6.35	7.93	2.03	2.18	7.78	2025
6.	M6A2C	2.21	4.06	5.25	1.97	2.12	7.95	1968
7.	M7A2C	3.05	5.12	5.91	1.95	2.10	7.24	1953
8.	M1P2C	2.96	5.75	7.08	1.77	1.90	7.71	1768
9.	M2P2C	2.50	4.76	6.81	1.84	1.98	7.64	1838
10.	M3P2C	3.20	4.90	6.20	1.86	2.00	7.87	1859
11.	M4P2C	3.20	4.93	6.04	1.90	2.06	8.37	1903

Plasticizers dosages ranging from 0.5 to 2% were also used in the control mix to enhance workability and water reduction. Mixes M1P2C to M4P2C are the mixes with varying dosages of plasticizers.

Table 8 gives the result of compressive strength, water absorption and block density of the series 3 and 4 mixes with air entrainer and plasticizer, respectively.

It was found that air entrainer increased the workability of concrete (mix M1A2C to M4A2C) with the same W/C ratio as that of optimum mix, and this led to segregation of materials. When cast using egg-laying machines, it may not be feasible to mold the material due to segregation in the mixes. Hence, water content was further reduced to 0.65, and mixes M5A2C to M7A2C are cast with reduced water content. Based on the results from density, it was observed that air-entraining admixture does not contribute in weight reduction in the solid concrete blocks. However, compressive strength results of the cubes are within the limits.

Plasticizers increased the workability of concrete, and this increase in workability may give a homogeneous mix of materials at site and can give a better surface finish. The results indicated even though there is a better surface finish, there is a slight reduction in the compressive strength.

3.4 Solid Concrete Blocks Cast at Manufacturing Plant

Based on the trail mixes conducted on cubes, a total number of seven mixes were taken to conduct the trials at solid block manufacturing plant. Solid concrete blocks cast using the different amount of GGBS as part replacement for cement from, i.e.,

10 to 70% are tested for compressive strength, water absorption and block density have been tabulated in Table 9 (Plates 1, 2, 3 and 4). Blocks cast using all the mixes satisfied the requirements of water absorption and compressive strength. It can also be observed that blocks cast with 70% replacement gave good results. As we can see that GGBS has proven to a good option for part replacement of cement up to 70%.

3.5 Outcome of Results

- Optimum mix for production of concrete blocks is M2C which has a cement content of 150 kg/m^3 and a W/C ratio of 0.85.
- GGBS can be used as part replacement of upto 70% which may bring down the cost of each block, without compromising on the quality of the block.
- Air-entraining admixture can be used to reduce water and increase workability of the mix. Air may not be entrapped in the blocks as the blocks structure possesses porous voids.
- Plasticizers can be used in the manufacturing to reduce water content and also to ensure homogeneous mix of all the ingredients.
- Full-scale blocks were cast using GGBS as replacement for cement and proven that it can be utilized. This is not only being economical but also profitable.
- More work on utilization of chemical admixture in the manufacturing of blocks needs to be carried out.

Plate 1 Egg-laying machine

Plate 2 Blocks during production at site

Plate 3 Blocks cast at casting yard

Plate 4 Capping of blocks before compression test

Table 9 Test results blocks cast at site

S. No.	Mix	Compressive strength			Water absorption			Density
		7 days (MPa)	14 days (MPa)	28 days (MPa)	Dry weight (kg)	Wet weight (kg)	Water absorption (%)	
1.	M1S1C	6.59	7.25	8.175	27.4	29.65	8.21	2283
2.	M2S2C	4.06	5.60	7.18	26.77	28.78	7.52	2230
3.	M3SG2C	6.82	7.80	9.23	25.58	27.36	6.98	2131
4.	M4SG2C	3.93	6.20	7.71	26.66	28.49	6.86	2221
5.	M5S2GC	3.31	5.10	6.90	27.34	29.23	6.91	2278
6.	M6SG2C	2.84	4.98	6.54	26.88	28.84	7.27	2240
7.	M7S2GC	5.52	7.25	8.72	27.74	29.64	6.82	2311

4 Conclusions

The following conclusions have been drawn from the above study.

1. GGBS can be utilized as part replacement of cement in the manufacturing of solid concrete blocks.
2. Plasticizers can be used to reduce water content and to increase the homogeneity of the mix, but excess dosage of plasticizers may lead to sticking of the concrete onto the inner surface of the molds in the egg-laying machine.
3. Cement of about 150 kg/m^3 is sufficient to produce required amount of strength in the solid concrete blocks.
4. Even up to the 70% of the cement can be replaced with GGBS.

References

1. IS 12269: 2013. Specifications for 53 grade Ordinary Portland cement, Bureau of Indian Standards, New Delhi.
2. IS 383: 1970. Specification for coarse and fine aggregate, Bureau of Indian Standards, New Delhi.
3. IS 2185 (Part 1): 2005. Concrete masonry units—Specifications, Bureau of Indian Standards, New Delhi.
4. IS 9013: 1978. Method of making, curing and determining compressive strength of accelerated cured concrete test specimens, Bureau of Indian Standards, New Delhi.

Dr. Jagadish Vengala is currently working as Associate professor, PVP Siddhartha Institute of Technology, Vijayawada. He was a former Head, Department of Civil Engineering, BMSIT, Bangalore. He has got more than 18 years of industry, research and teaching experience. He was recipient of Professor V. Ramakrishnan's Young Scientist award for the year 2008–2009 by Indian Concrete Institute. He has published more than 30 publications in various journals and conferences.

Mr. S. Raju completed his Bachelor of Engineering in Civil Engineering from BMS Institute of Technology, Bangalore in 2017.

Mr. B. Shiva completed his Bachelor of Engineering in Civil Engineering from BMS Institute of Technology, Bangalore in 2017.

L. R. Manjunatha is presently working as Deputy General Manager at JSW Cement Limited. He completed BE in Civil Engineering from UVCE, Bangalore, MBA, PGDFM, PGDM (Lean Operations) from Alliance University, Bengaluru and PG Program in Concrete Technology-CGLI (UK). He has got 24 years of industry experience and research experience of ten years and has published over 18 research papers in national and international journals and presented 20 conferences papers in India and abroad in his research field.

Er. M. V. Yogananda is currently working as Concrete Technologist in JSW Cement Limited. He has got more than seven years of industry, research and teaching experience. He has published more than nine publications in various journals and conferences.

Assessment of Wind Loads on Lattice Towers Using Various National Standards

Srinivas Tanuku and K. Rama Mohana Rao

Abstract In this paper, critical review on the estimation of wind load on lattice towers is undertaken using IS 875 (Part 3) through comparative study by referring ANSI/TIA-222G standard which is specially dealt for analysis of lattice tower. Further, it is concluded that the ultimate wind load is reduced by 19–22% using ANSI/TIA-222G standard compared to generalized structural wind loading standard of IS 875 (Part 3)–2015. Therefore, the specific standard for wind load assessment of lattice tower is essential for realistic and accurate estimation of wind loads through referring other national standards specially dealt for lattice towers.

1 Introduction

In the contemporary era, the telecom industry plays a major role in technological development, and thus much more attention is now being paid to telecommunication towers than it was in the past. The functional requirement of telecommunication towers is enhancing both coverage and network reliability and is governing factors on defining height of structure and antenna characteristics. Self-supporting lattice tower is being the effective structural system by considering simple, lightweight, easy fabrication and installation and these are normally square or triangular in plan, made up of steel angle or hollow sections. Wind is predominant load for analysis of these slender structures; therefore, an in-depth understanding on wind loads is essential for structural analysis of telecommunication towers. In India, general wind loading standards are being referred for assessment of wind load on these special structures which may lead to conservative approach and sometimes underestimation of critical

S. Tanuku (✉)
Post Graduate Student in Civil Engineering, JNTU College of Engineering,
Hyderabad, India
e-mail: srinivastanuku1983@gmail.com

K. Rama Mohana Rao
Department of Civil Engineering, Jawaharlal Nehru Technological University, Hyderabad,
Telangana, India

parameter which are affecting the safety of such structure. In this paper, an attempt is made to review current practice by comparing with American national standards specially dealt on analysis of telecommunication towers and basic comparative study on assessment of wind loads are presented in subsequent sections.

2 Wind and Influencing Parameters

Wind means the motion of air in the atmosphere with respect to the surface of the earth is fundamentally caused by variable solar heating of the earth's atmosphere. The earth surface exerts on the moving air a horizontal drag force, whose effect is to retard the flow. This effect is diffused by turbulent mixing throughout a region referred as atmospheric boundary layer. The depth of boundary layer depends upon the wind intensity, roughness of terrain and angle of latitude. Within boundary layer, the wind speed increases with elevation its magnitude at the top of boundary layer is often referred to as a gradient speed. Therefore, the parameter such as risk level of structure, terrain influences, topographical features, shape factor, direction factor and as well structural response to wind all are contributing wind effects on lattice towers.

2.1 Basic Wind Speed

Basic wind speed is defined as the peak gust velocity averaged over short time duration and corresponds to mean height above ground level in open terrain. Basic wind speed shall be extracted from respective country wind map, and duration of basic wind speed given in both code, i.e., IS 875 (Part 3), ANSI/TIA-222G observed as 3-second duration. The suggested life period to be assumed in design and corresponding risk coefficient shall considered in the design. Four categories of return period given in IS 875 (Part 3) based on the importance of structure and is shall be multiplied with basic wind speed to obtain design wind speed, whereas three risk categories are classified in ANSI/TIA-222G and factor shall be multiplied with overall design wind pressure instead of basic wind speed. Due to this, the substantial reduction of design wind pressure on structure is observed using ANSI/TIA-222G compared to IS 875 (Part 3)–2015.

2.2 Terrain and Height Multiplier

The wind speed varies with height due to ground friction and amount of friction varies with ground roughness and is characterized by terrain/exposure categories based on surrounding obstruction. Three categories are defined in ANSI/TIA-222G against
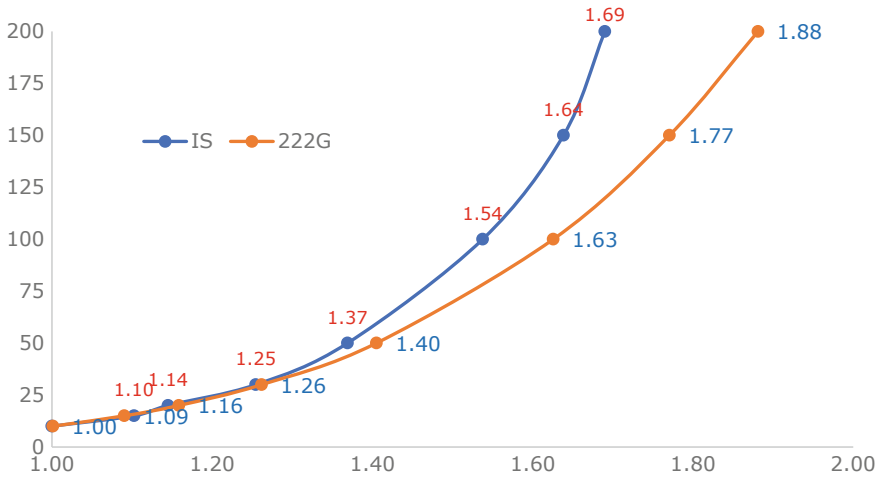
Fig. 1 Terrain height multiplier (open terrain)

four categories in IS 875 (Part 3). An average of 4 and 10% values are increased at 50–100 m and 150–200 m height, respectively, in ANSI/TIA-222G compared to IS 875 (Part 3) for open terrain with scattered obstruction having heights less than 10 m (Fig. 1).

2.3 Topography Influence

Topography influence that has some affects are—funnelling of winds (occurs when there is natural flow of air from an unrestricted area through restricted area, such as mountain pass), mountains (flow over the crest of hill ridge when the wind is normal to edge is considerably less turbulent than the flow of upwind of hill and wind velocity is increased. The effect of topography is to accelerate wind near the summits of hills or crests or cliffs, escarpments or ridges and decelerate the wind in valleys or near the foot of cliffs, steep escarpment, or ridges. As per IS 875 (Part 3), the detailed methodology is given for calculation of topographical factor based on up-wind slop of hill/ridge with maximum factor of 1.36. In ANSI/TIA-222-G, four categories are defined based on structure location on hill and empirical formulae are given for calculation of topographical effects against each category.

2.4 Force Coefficient

Force coefficient is the ratio of resulting force per unit area in the direction of wind to the applied wind pressure. It accounts for the effect of member characteristics (shape, size, solidity, shielding and surface roughness) also it accounts for both wind-ward and lee-ward faces including shielding of lee-ward face by members in wind-ward faces. Force coefficient is given for different types of tower configurations (square/equilateral triangular towers) and type of member such as flat or tubular member based on frame solidity ratio (ratio of projected area of members and total area of panel under considered). Reference to Table 1, force coefficient is reduced by 9 and 4% for square and triangular towers, respectively, in ANSI/TIA-222G (Table 2).

3   Structural Response to Wind

Wind force is essentially dynamic in nature even through it is treated as steady force for simplicity in analysis. Due to the turbulent nature of wind velocities, the wind loads acting on structure also highly fluctuating. The back-ground response made up of largely low-frequency contribution below the lowest natural frequency of vibration is the largest contributor for along-wind loading. The resonant contribution becomes more significant, which will eventually dominate as structure becomes taller in relation to their width and their natural frequencies become lower. The resonant response will be significant when the structure frequency is less than 1.0 Hz. When structure experiences resonant dynamic response, counteracting structural forces come into play to balance wind forces are—inertia force proportional to mass of structure, damping or energy absorbing force and elastic or stiffness force proportional

Table 1 Force coefficient—Tower

Solidity ratio	Square		Triangular	
	IS	222G	IS	222G
0.1	3.80	3.45	3.1	2.96
0.2	3.30	2.98	2.7	2.60
0.3	2.80	2.59	2.3	2.30
0.4	2.30	2.28	1.9	2.06
0.5	2.10	2.05	1.5	1.90

Table 2 Force coefficient—Flat appurtenances

Aspect ratio	IS	222G
≤ 2.5	1.25	1.2
7	1.34	1.4
≥ 25	1.65	2.0

to deflection. As per IS 875 (Part 3), flexible slender structures (defined as first mode frequency is less than 1.0 Hz) and structural elements shall be investigated to ascertain the importance of wind-induced oscillations or excitations along-wind and across-wind directions. Static wind loading is recommended for rigid structure whose first mode frequency is less than 1.0 Hz, where maximum self-supporting lattice towers are fall in this category, i.e., rigid structure by considering first mode frequency. As per ANSI/TIA-222G, a factor of 0.85–1.00 is recommended as gust effect factor which accounts for loading effects in the along-wind direction due to wind turbulence—structure interaction for self-supporting structure (rigid structure) which shall be multiplied to design wind pressure obtained from basic wind speed of 3-second duration. While deciding the frequency of structure, separate empirical formula is given in ANSI code which can reasonably estimate the frequency of lattice towers compared to generic formula given in IS 875 (Part 3).

4 Design Wind Pressure

The design wind pressure at any height above mean ground level shall be calculated as per below against each standard.

As per IS 875 (Part 3)–2015, design wind pressure is given by,

$$\rho_z = \left[0.6\,(V_b\,K_1 K_2 K_3 K_4)^2\right] \times K_d\,K_a\,K_c \tag{1}$$

As per ANSI/TIA-222G, design wind pressure is given by,

$$\rho_z = 0.613\,K_z\,K_{zt}\,K_d\,V^2\,I \tag{2}$$

Ultimate design wind pressure (with load factors, 1.5 for IS 875 and 1.6 for ANSI/TIA-222G) including force coefficient (solidity ratio assumed as 0.2) using both standards are summarized in Figs. 2 and 3.

5 Parametric Study

Two different configurations (square—composed of angle sections; triangular—legs with pipes and others with angular bracings) are considered for parametric study for a basic wind speed of 47 m/s (3-second gust) with open terrain with well-scattered obstruction of 1.5–10 m. Basic tower details are listed below along with tower elevation drawing (Tables 3 and 4; Fig. 4).

Fig. 2 Design wind
pressure, kN/m^2 (face wind)
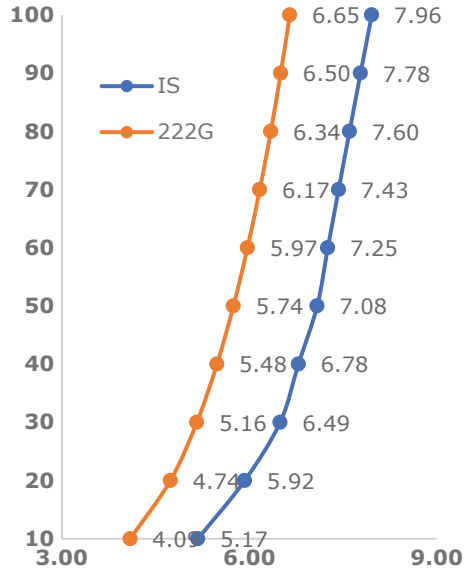
Fig. 3 Design wind
pressure, kN/m^2 (corner
wind)
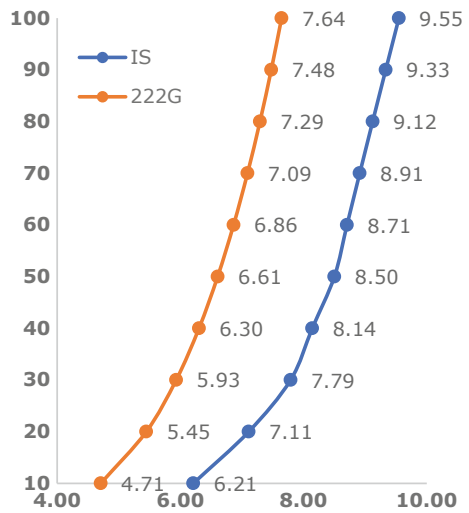
Table 3 Basic tower details

#	Description	Case 1	Case 2
a.	Tower configuration	Square	Triangular
b.	Legs	Steel angles	Steel—CHS
c.	Bracings	Steel angles	Steel angles
d.	Bottom face width	7.35 m	9.15 m
e.	Top face width	1.80 m	2.00 m
f.	Vertical portion	15 m	10 m

Table 4 Antenna details

Antenna type		Square/triangular
GSM antenna	Size (m)	$2.58 \times 0.262 \times 0.116$
	Quantity (Nos.)	12
MW antenna	Size (m)	1.2 m Dia.
	Quantity (Nos.)	3

6 Comparison Summary

From the above, the following summary is observed from the wind load calculation on both cases using IS 875 (Part 3)–2015, ANSI/TIA-222G standard with load factors, i.e., 1.5 for Indian standard and 1.6 for American standard.

6.1 Square Tower

See Table 5.

6.2 Triangular Tower

See Table 6.

6.3 Appurtenance

See Table 7.

7 Conclusion

Following conclusions drawn from the detailed calculation as mentioned above.

- Force coefficient of square tower/triangular towers are lesser in ANSI/TIA-222G.
- Terrain height multiplier is higher in ANSI/TIA-222G compared to IS 875 (Part 3).
- Gust effect factor of 0.85 for self-supporting structures is mainly contributing for lesser wind load compared to IS 875 (Part 3).
- For square towers, wind direction factor for corner wind is estimated using panel solidity ratio compared to 1.2 of IS 875 (Part 3).

Fig. 4 Tower elevation drawing—both options

Table 5 Section-wise wind load comparison—square tower

Section Ht. (m)	Cum. Ht (m)	Exposed area (m²)	Solidity ratio (Φ)	Force coefficient		Design wind pressure (KPa)		Ultimate wind load (kN) (0°)		Ultimate wind load (kN) (45°)	
				IS	222G	IS	222G	IS	222G	IS	222G
4.5	60.00	1.42	0.17	3.43	3.09	1.85	1.67	13.4	9.9	16.1	11.2
5.25	55.50	1.62	0.17	3.44	3.10	1.83	1.64	15.3	11.2	18.4	12.7
5.25	50.25	2.32	0.20	3.30	2.98	1.80	1.60	20.6	15.0	24.7	17.3
6	45.00	3.58	0.21	3.26	2.94	1.75	1.56	30.6	22.3	36.8	25.8
4.5	39.00	2.31	0.18	3.39	3.06	1.71	1.52	20.1	14.5	24.1	16.5
4.5	34.50	2.54	0.17	3.47	3.13	1.68	1.47	22.1	15.9	26.6	17.9
5	30.00	3.03	0.15	3.53	3.19	1.62	1.43	26.1	18.7	31.3	20.9
5	25.00	3.17	0.14	3.61	3.26	1.55	1.37	26.6	19.2	31.9	21.2
5	20.00	3.44	0.13	3.64	3.29	1.49	1.30	27.9	19.9	33.5	21.9
5	15.00	3.78	0.13	3.65	3.30	1.39	1.21	28.8	20.5	34.5	22.5
5	10.00	3.98	0.12	3.68	3.33	1.33	1.08	29.1	19.5	35.0	21.4
5	5.00	4.26	0.12	3.69	3.34	1.33	0.98	31.3	19.0	37.6	20.7

Table 6 Section-wise wind load comparison—triangular tower

Section Ht. (m)	Cum. Ht (m)	Exposed area (m²)		Solidity ratio (Φ)	Cf—pipes		Cf—angles		Design wind pressure (KPa)		Ultimate wind load (kN) (0°)	
		Pipes	Angles		IS	222G	IS	222G	IS	222G	IS	222G
5	60	0.889	0.79	0.17	1.63	1.481	2.83	2.70	1.85	1.67	10.2	7.8
5	55	0.889	0.88	0.18	1.62	1.472	2.79	2.67	1.83	1.63	10.7	8.1
3	50	0.688	0.67	0.21	1.60	1.337	2.68	2.58	1.80	1.61	7.8	5.8
3	47	0.688	0.64	0.17	1.63	1.375	2.83	2.71	1.78	1.59	7.8	5.8
6	44	1.681	1.45	0.16	0.98	1.260	2.86	2.74	1.75	1.55	15.2	12.9
6	38	1.986	1.87	0.16	0.97	1.159	2.88	2.75	1.70	1.50	18.7	15.2
6	32	2.025	2.11	0.14	0.91	1.164	2.949	2.82	1.65	1.44	20.0	16.3
6	26	2.330	2.69	0.14	0.93	1.162	2.928	2.80	1.56	1.38	23.6	19.2
5	20	2.197	2.55	0.14	0.93	1.162	2.929	2.80	1.49	1.30	21.2	17.1
5	15	2.197	3.02	0.14	0.93	1.163	2.933	2.80	1.39	1.21	22.8	18.1
5	10	2.737	3.45	0.15	0.96	1.159	2.887	2.76	1.33	1.09	25.0	18.8
5	5	3.247	3.96	0.16	0.99	1.160	2.844	2.72	1.33	0.98	28.8	19.3

Table 7 Section-wise wind load comparison—triangular tower

Antenna type	Description	IS	222G
GSM antenna	Area (m^2)	0.68	0.68
	Elevation (m)	57.75	57.75
	Force coefficient	1.389	1.495
	Antenna—Qty	12	12
	Total EPA (m^2)	11.27	12.13
	Ultimate wind load (kN)	31.27	27.54
MW antenna (with radome)	Diameter (m)	1.2	1.2
	Elevation (m)	57.75	57.75
	Force coefficient	1.2	0.863
	EPA/Antenna	1.36	0.98
	Antenna—Qty	3	3
	Total EPA (m^2)	4.07	2.93
	Ultimate wind load (kN)	11.29	6.65

- Force coefficient for different MW antenna given in ANSI standard which leads to the accurate assessment of wind load on these antennae.

From the parametric study, ultimate wind load on bare tower are overestimated by 41% (0°), 52% (45°) for square tower and 29% (0°) in triangular hybrid tower configuration using IS 875 (Part 3)–2015. In addition, wind load on flat appurtenance overestimated by 14% compared to ANSI/TIA-222G. Therefore, the specific standard for assessment of wind loads on lattice towers is essential for realistic estimation of wind loads compared to other national standards.

References

1. American National Standard Institute, ANSI/TIA-222-G-2005. (2005, August). Structural standard for antenna supporting structures and antenna, telecommunication industry association.
2. Simiu, E., & Scanlan, R. H. (1996). *Wind effects on structures, fundamentals and application to design* (3rd ed.). New York: Wiley.
3. IS: 875 (Part 3) 2015. Wind loads—Code of practice for design loads (other than earthquake) for buildings and structures.
4. Subramanian, N. (2008). *Design of steel structures*. India: Oxford University Press.
5. Durfee R. H. (1986, May). Review of triangular cross section truss systems. *Journal of Structural Engineering, 112*(5).
6. Venkateswarlu, B., HariKrishna, P., Rajan, S. S., & Kumar, M. S. R. (1994). Stochastic gust response of microwave lattice towers. *Computers & Structures, 52*(5), 1031–1041.

Review of Source Apportionment of Particulate Matter for Indian Scenario

S. A. Nihalani, A. K. Khambete and N. D. Jariwala

Abstract Heavy metals accompanying ambient particulate matter having the size less than 10 μm can infiltrate the lungs in a deeper portion and be retained there. They are not washed out easily and can lead to various health problems. Heavy metals may be released from anthropogenic sources like fossil fuel combustion, solid waste incineration, metallurgical process, and soil dust blown by the wind which gets distributed in the air over a large area. Heavy metals if present in air, even at smaller concentrations are lethal. They are associated with numerous health effects like cancer, cardiotoxicity, neurotoxicity, immunotoxicity causing a rise in disease/death. Therefore, the study of heavy metals in ambient air is significant in air pollution analysis. Further, it is essential to gather data regarding sources and their corresponding contributions, to devise active pollution control programmes and policies for a reduction in ambient air particulate matter concentration. An inclusive evaluation for particulate SA studies has been made in the Indian context, bearing in mind most appropriate particulate sources and their temporal variations.

Keywords Particulate · Receptor model · Source apportionment

1 Introduction

Particulate matter (PM) in the atmosphere is a complex mixture of organic as well as inorganic particles, like soot, pollen, dust, smoke, and liquid droplets. Particles of particulate matter differ significantly in terms of size, source, and composition.

S. A. Nihalani (✉) · A. K. Khambete · N. D. Jariwala
Civil Engineering Department, Sardar Vallabhbhai National Institute of Technology, Surat, India
e-mail: seemanihalani@yahoo.com

A. K. Khambete
e-mail: anjali_khambete3@yahoo.co.in

N. D. Jariwala
e-mail: ndj@ced.svnit.ac.in

It originates from a natural source like dust storms, wind erosion, volcanic eruptions, attrition of surface, re-suspension of soil particles, and anthropogenic sources, namely industrial processes, traffic sources, coal combustion, etc. Particulate matter has detrimental effects on the environment such as climate change, changes in biogeochemical cycles in ecosystems, reduced visibility, and harmful effect on the health of human beings.

Size, concentration, composition, and toxicity of particulate matter are vital features that greatly affect the possible human health problems related to their exposure. It is, particularly, the fine and ultra-fine PM that harbours the capacity to outsmart the natural defence functions within our respiratory system. The particle size appears to have a carrying capacity for associated chemicals. The fine and ultra-fine particles with their potential of entering the bloodstream carry along with them their constituents enabling them to cause all sorts of systemic effects. Among those constituents, metals such as iron, zinc, copper, cadmium, and lead have toxicological and carcinogenic effects. In last years, rigorous programs, monitoring heavy metals in ambient air have been taken up globally that focus on the chemical characteristics and continuing temporal trends. Many studies involve quantification of particulate matter, evaluating mass concentrations, and apportionment of sources using multivariate statistical methods.

2   Source Signature Selection

Source apportionment of airborne particulate matter basically involves information about particulate classification and composition. This information is evaluated crucially to ascertain the occurrence of particular species that are assumed to evolve from acknowledged sources, travel due to atmospheric turmoil and in due course assessed in the receptor site.

Selecting a source profile or source signature is one of the most significant parameters in receptor modelling analysis. Source signature denotes a combination of trace markers or molecule elements that are utilised for source categorisation. An extensive array of source markers are utilised by the researchers, across India for source classification. The crucial markers used for source apportionment studies in India are almost similar to those used worldwide. Different researchers have inferred different sources in a different manner. This is one of the significant considerations in synchronisation of source profiles for source recognition and apportionment. Based on literature studies, for various emission sources in India, the key source signatures are discussed below.

2.1 Crustal Re-suspension/Soil/Road Dust

Road dust is a composite mixture of vehicular exhaust emissions, industrial emissions, soil dust, coal combustion, and construction material; from several anthropogenic and biogenic sources. Al, Ca, Fe, Mg, Na, Si, and Ti are the crustal element markers that are classically used as soil dust or crustal re-suspension tracers. A complete range of element tracers such as Al, Cu, Cr Co, Ca, Fe, Ni, Mg, Pb, Si, T, and V have been utilised in India for recognition of crustal re-suspension or road dust.

The choice of tracer elements for crustal re-suspension category is slightly inconsistent in India. Extensive range of markers like Al, Na, Ni, Pb, Si Ba, Ca, Cu, Fe, K, Mg, Mn, and Zn have been assembled as tracers for the crustal re-suspension group. Few authors have counted re-suspended or road dust in crustal segment, whereas few others have isolated it. Some of the studies associate road re-suspension dust or crustal dust with construction and vehicular activity while some consider them independently. These uncertainties in the selection of source profiles significantly limit the evaluation of results and consequently regulate policy resolutions.

2.2 Traffic Emissions

Traffic profiles normally have Cu resulting from brake liners, Pb from gasoline extracts, and Zn resulting from tyre abrasion. The vehicular source may be further augmented with Al, Ba, Ca, Fe, and K, from diesel usage and brake liners. It may also contain Al from wear and tear of engine pistons, Ba from fuel additives, Fe from the exhaust, Mn from unleaded gasoline, Ni from heavy oil combustion, and Zn from combustion in two-stroke engines. Various basic molecules in different permutations have also been used as signature molecules. Presence of Mg, Fe, Ba, and Zn in major concentration and negligible amounts of Al, Ca Cr, and Mn indicate discharge from wear and tear of brake lining, whereas the incidence of Ba, Fe, and Cu reveal release from brake pad [7]. Lead is used as one of the most conventional markers of vehicular sources. The use of leaded petrol is completely forbidden since the year 2000, but its extended residual lifecycle renders it pertinent for ambient particulates. Concentrations of Pb are found to be gradually decreasing after the use of unleaded petrol; therefore, Pb alone is not used as a sole indicator for vehicular sources. In India, for identification of vehicular emissions, the commonly used tracer element is Pb in addition to elements like V, Mn, Co, and Zn.

2.3 Industrial Emissions

Industrial emissions are usually discharged related to various industrial processes like ceramics, pharmaceutical, petrochemical, metallurgy, etc. A range of elemental

markers such as As, Cd, Co, Cr, and Ni have been used for source apportionment studies of particulate matter in India. Moreover, various diverse trace elements have been used to recognise explicit industrial releases, especially Cu, Ni, and Mn and from iron and steel industries of Mumbai; Cr and Zn from metal industries of Delhi; Cd, Pb, and V from battery wear and refuse oil-burning units of Delhi; Cr from electroplating units of Kolkata; Cu, Ni, and Zn, from metallurgical industries, galvanising, and electroplating while, Cr from tanneries in Kolkata; Cu, Ni, Pb, and Zn from various industries of Agra; Fe, Mn, Pb Zn, and SO_4 from smelting units of Ahmedabad; Ba from oil-fired power plants. Furthermore, an SA study was taken up by Negi [26] in India segregated V, Br as emissions from textile industry; S, Cu, Ni, and V emissions from oil refineries and Zn, Cu, and Mn emissions from non-ferrous industries of Bombay, Bangalore, Nagpur, and Jaipur [30].

2.4 Fuel Combustion

Combustion of fuel is a generic terminology comprising of the burning of a substance that piles up potential energy and which is liberated on burning. Chemical configurations of coal are substantially different in diverse geographical localities that control the picking of explicit marker elements. The coal from the majority of India has lower sulphur content while coal from north-east India being of naval source normally contains a greater amount of Te. Sulphur is one of the major impurities in north-eastern coal, while As is a major contaminant in coal from western India. General element markers of coal ignition are As, S, Se, and SO_4. As per the literature survey, among the various markers used for combustion of coal, Cr, Cu, Ni, V, K, PAH, Cd, Se, Pb, Zn, and As are the most prominent ones [2].

2.5 Marine Aerosols

A significant percentage of ordinary aerosols in the oceanic environment is controlled by marine aerosols. Key markers of marine aerosol contain Na, K, Cl-, and Mg. Normally, the marine aerosol is outlined due to the incidence of Cl^-, K^+, Na^+, and Mg^{2+}. The constituents, however, go through chemical alterations due to the reaction of SO_4^{2-} and NO_3^- releasing Cl^- and Br^- to the atmosphere. The fine particulate matter may have an incidence of NO_3^- due to condensation of HNO_3 from marine origin. Various elements like K^+, Mg^{2+}, Na^+, Cl- with Ca^{2+}, Mg^{2+}, SO_4^{2-}, and HCO_3 are utilised to identify marine aerosols. Identification of certain marker elements are slightly conflicting and might be swayed by different sources like Cl^- and SO_4^{2-} due to fuel burning; K^+ due to garbage combustion; Mg^{2+} and Ca^{2+} from crustal suspension; In India, the majority of the studies related to origin distribution have been done for inland places, hence marine aerosols may not be used as one of the

key sources, except in case of Mumbai. Using K leads to a mix-up of wood with biomass burning and Cl with coal combustion.

2.6 Biomass and Refuse Burning

In India burning of biomass is generally termed as burning of a mixture of cow dung and fuelwood, forest fire and combustion of farming residue. Potassium is one of the most commonly used inorganic markers for biomass incineration in absence of organic tracers. For crustal dust in coarse range, K is used as a tracer element and finer ranges of particulate matter soluble K from biomass burning is used as a tracer element. Zn, Cr, and Ni are the crucial markers for biomass and refuse burning. Few researchers have linked biomass burning with hazardous waste incineration while few have used only incineration or refuse burning as a source. Therefore, establishing a precise influence of various activities is not very easy. Also in Indian cities, waste management is often carried out randomly; hence, it is challenging to predict the precise nature and influence of individual source.

3 Source Apportionment for Indian Cities

For different cities in India, receptor model studies are carried out using diverse techniques like CMB or multivariate analysis models. Bandu [1] performed a source apportionment study for Chandigarh by applying microscopic methods and concluded soil dust as the main source of particulate matter concentration including industrial emissions, traffic emissions, and refuse burning. For two different traffic intersections in Mumbai, Kumar et al. [22] investigated particulate matter present and used factor analysis-multiple regression to identify possible sources as industrial emissions, traffic emissions, road or soil dust, coal burning, and marine aerosols. Tripathi [37] recognised crustal suspension or road dust contributing 69.41%, industrial emissions contributing 11.76% and fuel oil combustion contributing 6.52% to the total particulate emissions. Sharma and Maloo [34] analysed PM10, PM2.5, benzene, and metals in the PM of Kanpur and reported high concentrations. Karar and Gupta [17] monitored ninety PM10 samples for heavy metals Cr, Cd, Fe, Ni, Mn, Pb, and Zn in Kolkata. For the residential site at Kasba, PCA identified traffic emissions linked with road dust and soil dust and solid waste dumping, as possible sources of trace metals. For the industrial site at Cossipore, traffic emissions linked with soil or road dust, tannery industry, galvanising or electroplating units were reported as possible sources of trace metals.

Haritash and Kaushik [16] analysed heavy metals in RSPM for different locations in Hisar, Haryana. The assessment of enrichment factor analysis showed As, Cu, Pb, Ni, and Mn are discharged, primarily from artificial sources and Fe and Mg

are linked with natural sources. Gupta [15] monitored SPM and RSPM at residential and industrial locations in Kolkata. He used CMB for source distribution and predicted coal burning and traffic emissions as main sources of PM10 at residential and industrial spots, respectively. PCA study by Basha and Gaur [3] revealed the greatest variance (80.8%) for steel having a greater presence of Cd, Cu, Cr, and Co linked with ship-breaking events for Alang–Sosiya (Gujarat, India). Srivastava [35] used CMB and PCA for source apportionment of SPM and heavy metals for Delhi. Results from CMB showed that in fine range vehicular pollutants contributed 62%, followed by crustal dust as 35%; while in the coarse range; crustal dust showed 64% contribution and vehicular pollution contribution of 29% while PCA reported vehicular emissions and crustal suspension as one of the major sources in both coarse and fine size ranges. Chelani [10] monitored samples from diverse locations and reported the main sources of particulate emissions as a crustal suspension, traffic emissions, industrial emissions, and marine aerosols.

Kothai et al. [19] used FA-MLR to carry out source distribution of PM2.5 in Navi Mumbai (Maharashtra) and reported the various contributions as 29% from motor vehicles, 23% from industrial emission, 18% from two-stroke vehicles along with fugitive dust, 9% from sea salts, and 3% from the soil. Lakhani and Parmar [23] identified various trace markers like Al, Ca, Cd, Cr, Cu, Fe, Ni, Mg, Mn, Pb, Si, Sn, V, and Zn in size fractioned aerosols in urban air of Agra. Kulshrestha [20] used PCA for source distribution of particulate matter for urban and rural sites in Agra. For urban sites, he identified key contributors to be re-suspended dust, solid waste burning, and industrial emissions while for rural locations the main contributors of PM were identified to be re-suspension, construction activities, and industrial emissions. Khare and Baruah [18] monitored PM2.5 for Jorhat, Assam and used enrichment factor and absolute PCA for source apportionment study. He testified the contribution of traffic generated crustal source to be 38%, coal combustion contribution as 26%, industrial and vehicular emissions to be 19%, wood-burning emissions to be 9%, and secondary aerosol as 8%. Basha and Jhala [4] investigated the presence of heavy metal in particulate matter and source apportionment for Mithapur, Gujarat. Source distribution study using EFs and PCA assisted to recognise industrial emissions, traffic emissions, oil burning, incineration, and soil dust to be the diverse sources of trace metals in the local atmosphere.

Bhattacharya [6] studied heavy metal levels in street dust from main roads in Anand, which showed that road dust carried a higher concentration of heavy metals. PCA and correlation coefficient analysis revealed that the most likely source for the contamination of these dust was vehicle emissions supplemented by local industrial activities. At traffic intersections in Hyderabad, Gummeneni et al. [4] observed PM10 and PM2.5 and testified vehicular pollution, industrial emissions, combustion, re-suspended dust, and refuse burning as main sources of particulate emissions. Tyagi [38] monitored PM10 and heavy metals Ni, Cr, Mn, and Zn at six different sites in Roorkee and identified coal combustion, soil dust and vehicular exhaust as key sources of particulate pollution. Chaudhari [8] carried out sampling and monitoring of PM10 and heavy metals for Nagpur and predicted the poor association between lead and PM10 which pointed out that automobile exhaust is not the key source of

heavy metals in air. Gajghate [13] carried out the correlation and source allotment study for Chennai. The studies showed oil emissions, waste incineration, and road dust suspension as chief contributors of PM10. Roy [33] analysed elemental concentrations of PM10 for Talher, Orissa. Soil dust from mining, automobile emissions, thermal power plant emissions, and non-ferrous smelting were the four key factors, isolated as possible sources by principal components analysis.

Dubey et al. [12] analysed metals in ambient particulates for mining and non-mining zones of Dhanbad in Jharkhand and used principal component analysis for source apportionment. PCA identified the dominance of crustal source as 31.64 and 28.62%, respectively, for mining and non-mining zones. Bhattacharya [5] analysed Zn and Cr concentration in a particulate matter of dust for Anand city. Mohammed [25] investigated the presence of heavy metals like As, Ba, Cd, Cr, Co, Cu, Mn, Ni, Pb, Sc, V, and Zn in ambient particulates of Kakinada city. PCA established that trace elements were principally generated from road dust contributing 52.5% and anthropogenic sources contributing 39.5% mainly involving heavy metals like Cu, Cd, Mn, Ni, and Pb. Pal [27] analysed PM10 and heavy metal concentration at different sites in Moradabad. Pandey [29], studied air quality deviations involving particulate matter and heavy metal concentrations. PCA predicted coal mining and mine fires having 57.71% variance as the chief sources of air contaminants followed by traffic emissions having 17.85% variance and overburdens showing 7.54% variance. Pal and Kumar [28] assessed the concentration of PM10 and trace metals for Moradabad. PCA multivariate techniques identified the chief source of ambient trace metals as automobile emissions, combustion processes, brassware industries, and illegal e-waste. Rajaram and Suryawanshi [31] applied multivariate statistical approach PCA to identify the probable contributors of heavy metals in the Delhi road dust, which indicated that industrial emissions and traffic emissions are the two chief contributors of trace metals in PM10.

Kumar [21] assessed heavy metals in the air concentration and the possible environmental hazard of trace elements in Tamilnadu, India. Chaudhari and Gajghate [9] testified construction activity, vehicular emissions, dust arising from heavy traffic, and industrial emissions as accountable for air pollution in Delhi. Rao et al. [32] analysed 96 RSPM samples from Gajuwaka Industrial Hub of Visakhapatnam and used PCA and CA for source apportionment to report vehicular exhaust, industrial emissions, and construction activities as main contributors. Das and Khezri [11] measured PM2.5 and PM10 along with heavy metals at different locations in Kolkata. As per factor analysis road dust due to vehicles, traffic emissions, biomass burning, industrial emissions, coal burning, and smelting of non-ferrous metals are probable sources of PM10 as well as PM2.5. Meena [24] investigated average concentrations of metals for Kota by using Pearson's correlation, enrichment factor, and principal component analysis and indicated that the contribution from industrial activities was 36–37% and from crustal emissions was 27–31% for coarser particulates where for fine particulates the impact was 33–35% from industrial activities and 28–31% from crustal emissions. Suryawanshi [36] analysed heavy metal concentration in road dust using atomic emission spectroscopy for Delhi. Correlation study along with

PCA predicted association of Pb, Cd, Cr, and Ni with industrial emissions while traffic emissions principally generated Zn and Cu.

4 Discussion and Conclusions

In India receptor models are used for source distribution study of particulate matter across various cities, however, the studies have shown contradictory conclusions. Majority of the studies have recognised vehicular emissions and soil or road dust as significant contributors of fine and coarse particulates, respectively, but separating of these emissions from industrial discharge and construction activity has been meagre. The demonstrative know-how of source apportionment for any PM size in an Indian city does not instigate any degree of confidence based on the studies undertaken to date. Most of the studies have applied multivariate statistical methods to generate diverse factors, characterised by elemental and ionic constituents. These factors, however, can not be explicitly accredited to a single precise source. The probable reasons include honest collinearity of sources and insufficient samples compared to a number of analytes causing uncertainty of the statistical model. The use of PCA which is an unweighted model causes less acceptable factor resolution as compared to PMF which is a recent weighted model.

To differentiate vehicular emissions from non-exhaust vehicular emissions, principally road dust suspension or incompetence to distinguish locally between crustal contributors like desert dust from local blown wind or re-suspended road dust is categorically difficult. It can be challenging to distinguish road dust from local soils if the soils are contaminated by vehicular emissions or if the road dust comprises substantial soil content. It is critical to segregate these sources, quantify the vehicular emissions alone, and finally separate local crustal sources from local soils or road dust. There is a lack of literature study on the multi-site scenario. If multi-site studies occur, multiple sites within a city have been studied rather than studying urban or rural sites to demonstrate the significance of emissions in the city in relation to its local background.

References

1. Bandhu, H. K., Puri, S., Garg, M. L., Singh, B., Shahi, J. S., & Mehta, D. (2000). Elemental composition and sources of air pollution in the city of Chandigarh, India, using EDXRF and PIXE techniques. *Nuclear Instruments and Methods, 160*, 126–138.
2. Banerjee, T., Murari, V., Kumar, M., & Raju, M. P. (2015). Source apportionment of airborne particulates through Receptor Modeling: Indian Scenario. *Atmospheric Research, 164*, 167–187.
3. Basha, S., & Gaur, P. M. (2007). Heavy metal content of suspended particulate matter at world's largest ship-breaking yard, Alang-Sosiya, India. *Water Air Soil Pollution, 178*, 373–384.

4. Basha, S., & Jhala, J. (2010). Assessment of heavy metal content in a suspended particulate matter of coastal industrial town, Mithapur, Gujarat, India. *Atmospheric Research, 97*, 257–265.
5. Bhattacharya, T. (2013). Zinc and Chromium load in road dust, suspended particulate matter and foliar dust deposits of Anand city, Gujara. *Open Journal of Metal, 2013*(3), 42–50.
6. Bhattacharya, T., & Chakraborty, S. (2011). Heavy metal concentrations in street and leaf deposited dust in Anand city, India. *Research Journal of Chemical Sciences, 1*(5), 61–66.
7. Belis, C. A., Karagulian, F. Larsen, B. R., & Hopke, P. K. (2013). Critical review and meta-analysis of ambient particulate matter source apportionment using receptor models in Europe. *Atmospheric Environment, 69*, 94–108.
8. Chaudhari, P. R., & Gupta, R. (2012). Heavy metal pollution of ambient air in Nagpur City. *Environmental Monitoring and Assessment, 184*, 2487–2496.
9. Chaudhari, P. R., & Gajghate, D. G. (2015). Studies on respirable particulate matter and heavy metal pollution of ambient air in Delhi, India. *American Journal of Engineering Research, 4*(12), 45–57.
10. Chelani, A. B., Gajghate, D. G., & Devotta, S. (2008). Source apportionment of PM10 in Mumbai, India using CMB model, *Bull Environ Contam Toxicol,* 190–195.
11. Das, R., & Khezri, B. (2015). Trace element composition of PM2.5 and PM10 from Kolkata—a heavily polluted Indian metropolis. *Atmospheric Pollution Research, 6*, 742–750.
12. Dubey, B., Pal, A., & Singh, G. (2012). Trace metal composition of airborne particulate matter in the coal mining and non–mining areas of Dhanbad region, Jharkhand, India. *Atmospheric Pollution Research, 3*, 238–246.
13. Gajghate, D. G, & Talwar, B. (2012). Chemical characterization of PM10 for metals in ambient air of Chennai, India. *Journal of hazardous, toxic, and radioactive waste, 16*, 169–174.
14. Gummeneni, S., Yusup, Y. B., Chavali, M., & Samadi, S. Z. (2011). Source apportionment of particulate matter in the ambient air of Hyderabad city, India. *Atmospheric Research*. https://www.doi.org/10.1016/j.atmosres.2011.05.002.
15. Gupta, A. K., Karar, K., & Srivastava, A. (2007). Chemical mass balance source apportionment of PM10 and TSP in residential and industrial sites of an urban region of Kolkata, India. *Journal of Hazardous Materials, 142*, 279–287.
16. Haritash, A. K., & Kaushik, C. P. (2007). Assessment of seasonal enrichment of heavy metals in respirable suspended particulate matter of a sub-urban Indian city. *Environmental Monitoring and Assessment,* 257–265.
17. Karar K., & Gupta, A. K. (2006). Characterization and identification of the sources of chromium, zinc, lead, cadmium, nickel, manganese and iron in PM10 particulates at the two sites of Kolkata, India. *Environmental Monitoring and Assessment, 120*, 347–360.
18. Khare, P., & Baruah, B. P. (2010). Elemental characterization and source identification of PM2.5 using multivariate analysis at the suburban site of north-east India. *Atmospheric Research, 98*, 148–162.
19. Kothai, P., Saradhi, I. V., Prathibha, P., Pandit, G. G., & Puranik, V. D. (2008). Source apportionment of coarse and fine particulate matter at Navi Mumbai, India. *Aerosol and Air Quality Research, 8*, 423–436.
20. Kulshrestha, A., Satsangi, P. G., Masih, J., & Taneja, A. (2009). Science of the total environment metal concentration of PM 2.5 and PM 10 particles and seasonal variations in urban and rural environment of Agra, India. *Science*.
21. Kumar, M., Tiwari, S., Murari, V., Singh, A. K., & Banerjee, T. (2015). Wintertime characteristics of aerosols at middle Indo-Gangetic Plain: Impacts of regional meteorology and long range transport. *Atmospheric Environment, 104*, 162–175.
22. Kumar, A. V., Patil, R. S., & Nambi, K. S. V. (2001). Source apportionment of suspended particulate matter at two traffic junctions in Mumbai, India. *Atmospheric Environment, 35*, 4245–4251.
23. Lakhani, A., & Parmar, R. S. (2008). Size distribution of trace metals in ambient air or Agra. *Indian Journal of Radio and Space Physics, 37*, 434–442.
24. Meena, N. K., Maiti, S., & Shrivastava, A. (2011). Discrimination between anthropogenic (pollution) and lithogenic magnetic fraction in urban soils (Delhi, India) using environmental magnetism. *Journal of Applied Geophysics, 73*, 121–129.

25. Mohammed, M. P. (2013). Trace elemental composition in the atmospheric aerosols of Kakinada city, India. *Sustainable Environment Research, 23*(5), 315–324.
26. Negi, B. S., Sadasivan, S., & Mishra, U. C. (1987). Aerosol composition and sources in urban areas in India. *Atmospheric Environment, 21*(6), 1259–1266.
27. Pal, R., & Gupta, M. (2013). Assessment of heavy metals in suspended PM in Moradabad, India. *Journal of Environmental Biology, 35*, 357–361.
28. Pal, R., & Kumar, A. (2014). Source Identification and Distribution of Toxic Trace Metals in Respirable Dust (PM10) in Brass city of India-Global. *Journal of Human-Social Science, 14*(5), 1–12.
29. Pandey, B., Agrawal, M., & Singh, S. (2014). Assessment of air pollution around coal mining area: Emphasizing on spatial distributions, seasonal variations and heavy metals, using cluster and principal component analysis. *Atmospheric Pollution Research, 5*, 79–86.
30. Pant, P., & Harrison, R. (2012). Critical review of receptor modeling for particulate matter: A case study of India. *Atmospheric Environment, 49*, 1–12.
31. Rajaram, B. S., & Suryawanshi, P. V. (2014). Heavy metals contamination in road dust in Delhi city, India. *Environmental Earth Sciences.* Berlin, Heidelberg: Springer-Verlag.
32. Rao, S. S., Rajamani, N. S., & Reddi, E. U. (2015). Assessment of Heavy Metals in RSPM at Residential Colonies of Gajuwaka. *International Journal of Geology, Agriculture, and Environmental Sciences, 3*(5), 56–64.
33. Roy, P. (2012). Source apportionment of ambient PM10. A case study from a mining belt of Orissa. *Amosfera, 25*(3), 311–324.
34. Sharma, M., & Maloo, S. (2005). Assessment of ambient air PM10 and PM2.5 and characterization of PM10 in the city of Kanpur, India. *Atmospheric Environment, 39*, 6015–6026.
35. Srivastava, A. (2008). Source apportionment of total suspended particulate matter in coarse and fine size ranges over Delhi. *Aerosol and Air Quality Research, 8*(2), 188–200.
36. Suryawanshi, P. V., & Rajaram, B. S. (2016). Determining heavy metal contamination of road dust in Delhi. *India Atmósfera, 29*(3), 221–234.
37. Tripathi, R. M., Vinod Kumar, A., Manikandan, S. T., Bhalke, S., Mahadevan, T. N., & Puranik, V. D. (2004). Vertical distribution of atmospheric trace metals and their sources at Mumbai, India. *Atmospheric Environment, 38*, 135–146.
38. Tyagi, V., Gurjar, B. R., Joshi, N., & Kumar, P. (2012). PM10 and heavy metals in sub-urban and rural atmospheric environments of Northern India. *ASCE Journal of Hazardous, Toxic & Radioactive Waste, 16*, 175–182

Shape of Shear Reinforcement Influence Shear Strength Parameters in Rc Beam

Jonna Rohan Reddy, Y. Naga Satyesh and Sonti Girish Babu

Abstract Every load is converted into shear and bending stress. Every load produces compression and tension, compression produced by load in flexure is taken up by concrete, and tension is taken up by reinforcement. Shear force at cross section of the beam may be defined on unbalanced vertical force to the right (or) left of section. In a reinforced concrete beam, shear is taken up by stirrups, which are normally oriented transverse to longitudinal axis. The shape of typical stirrup is a box (or) a rectangle. As a part of experimental research, many researchers sound out that different shaped stirrups can be adopted in place of convention one of which some is spiral. However, in our project, we are preparing different orientation, which is provided, throughout the beam and comparing with conventional beam. We are comparing different parameters such as (1) Load vs deflection, (2) Ultimate load, (3) First crack, (4) Ultimate deflection, etc.

Keywords Shear reinforcement · Orientation · Stirrups

1 Introduction

Our main objective of providing reinforcement in concrete is to improve member properties. Designing of reinforced concrete member is to impart desired load-carrying capacity within serviceability limits and ductile failure which gives necessary indication. When designing a beam or a structural member, usually flexural strength is considered first and then comes shear strength. Shear failure is undesirable

J. R. Reddy (✉)
Vardhaman College of Engineering, Hyderabad, India
e-mail: jonnarohanreddy222@gmail.com

Y. Naga Satyesh
Srinivasa Ramanujan Institute of Technology, Anantapur, India
e-mail: satyesh.yts92@gmail.com

S. G. Babu
Ellenki College of Engineering and Technology, Hyderabad, India
e-mail: sontigirishbabu@gmail.com

since member fails to take specified load. The design of shear should be such that shear strength for every member in structural member must exceed the shear load. The mechanism of shear failure depends upon the structural member's dimensions, geometry, type of loading, and member properties.

The reinforced concrete beam must have the adequate safety margin against bending and shear forces so that it will perform effectively during its lifetime. At the ultimate limit, the combined effects of bending and shear may exceed the resistance capacity of the beam causing cracks. The shear failure is difficult to predict accurately despite extensive experimental research. Whenever applied, shear force exceeds the permissible limits of concrete used in member shear reinforcement has to be provided, otherwise beam fails upon formation of cracks near the support, i.e. high shear region. Diagonal cracks are the main mode of shear failure in reinforced concrete beams propagating from load towards supports causing reduction in load-carrying capacity. Hence, shear reinforcement has to be provided to prevent failure in shear and to increase beam ductility and subsequently increasing load-carrying capacity.

Generally, diagonal cracks start at point of application of load and propagate in 45 degree. Any form of effectively anchored or welded reinforcement which intersects with these cracks will arrest shear cracks up to certain extent. There are three ways of providing the shear reinforcement to the structural member in general practice. They are

1. Stirrups.
2. Inclined bent up bars.
3. Combination of both stirrups and inclined bent up bars.

In reinforcement construction, stirrups are most commonly used shear reinforcement due to its simplicity in fabrication and installation. In the region of high shear, stirrups are closely spaced leading to congestion near the supports due to the presence of closely spaced stirrups will increase the cost and time required for installation. Bent up bars are also used in the provision of shear reinforcement, but due to the difficulty in availability of skilled labour in recent years, less importance given to these bent up bars these type of bars are generally avoided, which also include lot of risk in installation and cost factor. Combination of both stirrups and inclined bent up bars is also not preferred these days. In this research, an experimental investigation on performance of shear reinforcement provided in four different patterns coded as

 I. Control beam(CB), having conventional pattern,
 II. Shear reinforcement oriented towards centre (OSBC),
 III. Shear reinforcements oriented towards end direction (OSBE),
 IV. Spiral reinforcement beam (SB).

This study compares different possible patterns of shear reinforcement, which may replace traditional way of providing stirrups effectively.

2 Literature Review

Moayyad M. Al-Nasra and Naiem M. Asha (2013) in his research paper titled "Shear Reinforcements in the Reinforced Concrete Beams" focuses on use of different types of shear reinforcement in reinforced concrete. Shear failure in reinforced concrete beams is one of the most undesirable modes of failure due to its rapid progression. This sudden type of failure made it necessary to explore more effective ways to design these beams for shear. The reinforced concrete beams show different behaviour at the failure stage in shear compared to the bending, which is considered to be unsafe mode of failure.

Sneed and Julio (2008) discussed the results of experimental research performed to test the hypothesis that the effective depth does not influence the shear strength of reinforced concrete flexural members that do not contain web reinforcement. The beams were designed such that the effective depth is the variable, while the values of other traditionally considered parameters proven to influence the shear strength (such as the compressive strength of concrete, longitudinal reinforcement ratio, shear span-to-depth ratio, and maximum aggregate size) were held constant.

Noor (2005) presented several results of experimental investigation on six reinforced concrete beams in which their structural behaviour in shear was studied.

Piyamahant (2002) showed that the existing reinforced concrete structures should have stirrup reinforcement equal to the minimum requirement specified the code.

3 Material and Its Properties

Materials used in this research were discussed include cement, aggregates (fine and coarse), water, and steel. Material plays a key role in deciding the strength, durability, safety, serviceability of the structural member. Hence, selection of good quality of materials is essential. In order to know the materials quality, preliminary tests were conducted on the samples.

3.1 Cement

Cement is a material which imparts binding properties to concrete. It binds the mineral aggregates. It reacts with water forming (C–S–H gel) compounds for binding of aggregates. There are many basic preliminary tests on cement such as chemical composition test, normal consistency, initial and final setting times, soundness test, etc. Among these, normal consistency test and initial and final setting tests were done.

For this work, we have used "SAGAR PPC CEMENT" (PPC: Portland Pozzolona Cement) with grade as 53 conforming to IS 1489: PART 1 specifying to 1991. The

initial setting time is more than 30 minutes, the final setting time is less than ten hours, and normal consistency of cement is 31%.

3.2 Portland Pozzolona Cement

Portland pozzolona cement is a fly ash-based or calcined clay-based, conforming, respectively, to part 1 and part 2 of IS 1489: 1991, involves the addition of pozzolona (fly ash or calcined clay)—a mineral additive containing silica.

3.3 Fine Aggregate

Aggregates account about three quarters of the total volume of concrete. Here, we have conducted various tests such as zoning, specific gravity specifying to the IS: 383. Specific gravity of chosen fine aggregate is 2.33. Zoning of fine aggregates is done to know which zone the fine aggregate belongs to.

3.4 Coarse Aggregate

In this project, we have taken the locally available crushed angular aggregates, passing through 20 mm sieve and retaining on 16 mm sieve, and some basic tests have done on this aggregates such as specific gravity. Specific gravity of taken coarse aggregate is 3.0.

3.5 Water

According to IS: 3025 (parts 17–32), pH value of water should not be less than 6. Concentration of solids in water should be within certain permissible limits that are specified in code (clause. 5.4), in particular, the content of sulphates (so_3) is limited to 400 mg/l, and chlorides are limited to 500 mg/l in reinforced concrete.

3.6 Concrete Mix Design

Mix design is a process where we are going to select relative quantities of ingredients in the concrete with a main objective to impart required strength, durability, and workability as economical as possible. Mix design is designated as M10, M15, M20,

Table 1 Proportions of ingredients

Water	Cement	Fine aggregate	Coarse aggregate
186	420	658.8	1195.15
0.44	1	1.56	2.84

M25, M30 as m refers to mix design, where number denotes the strength attained at the end of 28 days of curing in N/MM2.

There are many types of mix design which many people follows like ACI practice, British practice, Indian Standard recommendation, etc., but here, we followed Indian standard code of mix design. Here, in this project, for casting, we adopt for M30 grade of concrete (Table 1).

4 Testing and Methodology

4.1 Specimen

The experimental program consists of total eight beams which are of size $700 * 150 * 150$, with a varied configuration in the transverse reinforcement. In order to check the shear parameters such as shear cracking in the reinforced concrete beam, the specimens used here are normal beams, oriented shear beam towards centre from two sides, oriented shear beam towards the one end, and spiral beams.

Above showed the reinforcement provided in reinforced concrete structure, with a different patterns. The typical detailing drawings of four different types of reinforcement are shown in Figs. 1, 2, 3 and 4.

All the eight beams were cast in a steel mould of size $700 * 150 * 150$. The concrete mix with characteristic strength as M30. In the concrete mix pozzolona, Portland cement is used with water–cement ratio as 0.45.

Fig. 1 Normal/traditional beams
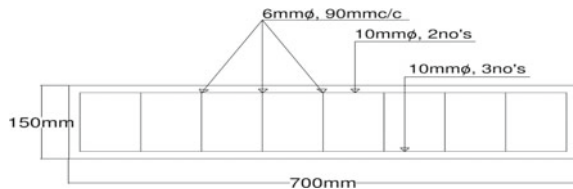
Fig. 2 Oriented shear beam from two sides
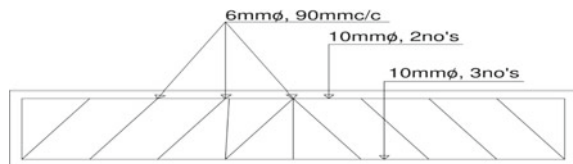
Fig. 3 Oriented shear beam towards one end

6mmø, 90mmc/c
10mmø, 2no's
10mmø, 3no's

Fig. 4 Spherical beams

6mmø, 90mmc/c
10mmø, 2no's
10mmø, 3no's
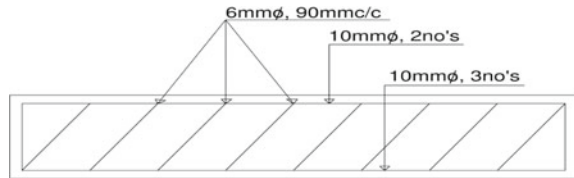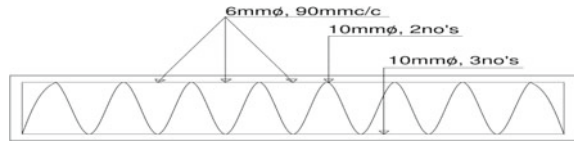
The reinforcement used in the beams is of size 10 mm for main reinforcement and 6 mm for transverse/web reinforcement, and we have considered here the under reinforcement.

The beams are cast and kept on vibrator table in order to undergo compaction. After the compaction, these beams are left inside the mould for ten hours, and after initial setting, these moulds are removed. These beams which are removed from the mould are left for curing about 28 days. After the 28 days of curing, these beams should be surface dried, and after the surface dry, these beams are ready for testing.

4.2 Test Procedure

The main aim of doing the testing of specimen, i.e. beam is to know the ultimate strength of the specimen, and also we can know about at what load the first crack has been absorbed and type of failure that specimen will undergo.

Prior to testing, the surface of specimen is painted with white emulsion for the purpose of making cracks visible and easy to crack.

Here, the specimen is kept in the machine in between grips and extensometer if required can automatically record the change in gauge length during the test. If extensometer is not fitted, the machine itself can record the displacement between its crossheads on which the specimen is held. However, this method not only records the change in length of specimen but also all other extending/elastic components of the testing machine and its drive systems including any slipping of the specimen in grips.

Once the machine is started, it begins to apply an increasing load on specimen. Throughout the tests, the control system and its associated software record the load and extension or compression of the specimen. Load applied here is both in one-point load and two-point load.

Place the beam on the test bench under UTM with proper alignment of gauge length of 600 mm. load is applied in a incremental manner and measure the readings

such as deflection corresponding to the load increment then absorb the first crack on the beam and note it down.

The graph will be displayed in the system connected to the UTM, which can be saved in system itself. When ultimate strength is reached, load valve should be released, and type of failure of beam is absorbed. The load at first crack and ultimate strength in normal beam is compared with other type of beams.

5 Results

The results of all beams were noted down:

Table 2 represents deflection values corresponding to load at for every 5 kN load increment, peak load, and first crack load.

Curve in Graph 1 is graphical representation of deflection corresponding to load values.

Table 2 Normal beam (NB)/control beam (CB) point load

NB1	
Load	Deflection
0	0
5	0.14
10	0.48
15	0.57
20	0.66
25	0.75
30	1.03
35	1.13
40	1.22
45	1.31
50	1.59
55	1.68
60	1.77
65	1.96
70	2.24
75	2.33
80	2.42
85	2.79
90	2.88
95	3.07
100	3.35
105	4.46

(continued)

Table 2 (continued)

NB1	
Load	Deflection
110	9.65
114.3	18.35
Peak load	114.3
Ultimate deflection	−
82	26
First crack	−
74	2.3
Failure	Tension
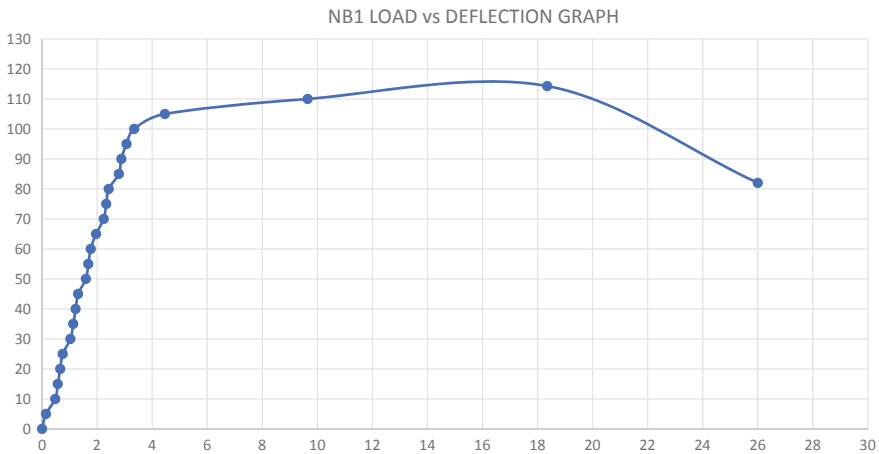
Graph 1 Normal beam (NB) load vs deflection graph

Table 3 represents deflection values corresponding to load at for every 5 kN load increment, peak load, and first crack load.

Curve in Graph 2 is graphical representation of deflection at corresponding to load values.

Table 4 represents deflection values corresponding to load at for every 5 kN load increment, peak load, and first crack load.

Curve in Graph 3 is graphical representation of deflection corresponding to load values.

Table 5 represents deflection values corresponding to load at for every 5 kN load increment, peak load, and first crack load.

Curve in Graph 4 is graphical representation of deflection corresponding to load values.

Table 6 represents deflection values corresponding to load at for every 5 kN load increment, peak load, and first crack load.

Table 3 Normal beam (NB)/control beam (CB) two-point load

NB2	
Load	Deflection
0	0
5	0.2
10	0.4
15	0.52
20	0.64
25	0.76
30	0.98
35	1.14
40	1.22
45	1.31
50	1.36
55	1.59
60	1.66
65	1.75
70	1.79
75	1.85
80	1.95
85	2.05
90	2.1
95	2.15
100	2.38
105	2.47
110	3.52
110.2	4.96
Peak load	110.2
Ultimate deflection	−
90	11.32
First crack	−
76	1.85
Failure	Shear

NB2 LOAD vs DEFLECTION GRAPH
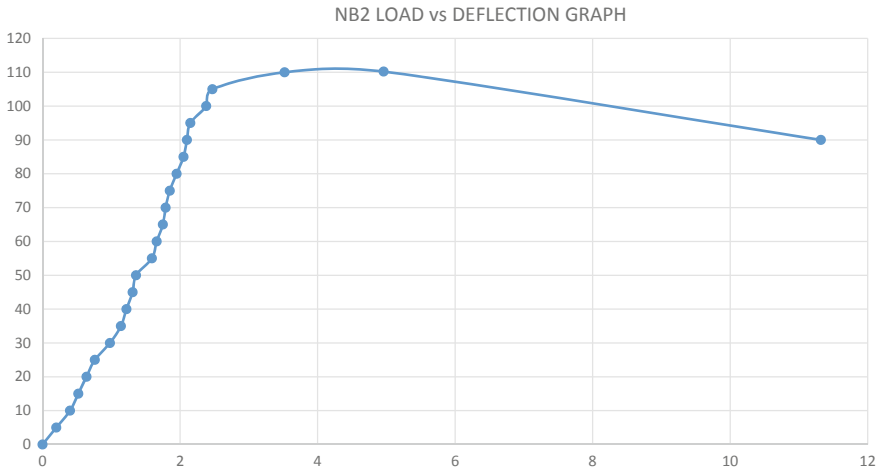
Graph 2 Normal beam (NB) two-point load vs deflection graph

Table 4 Oriented shear beam towards ends (OSBE) point load

OSBE1	
Load	Deflection
0	0
5	0.42
10	0.59
15	0.77
20	0.85
25	0.85
30	0.94
35	1.02
40	1.28
45	1.36
50	1.54
55	1.62
60	1.88
65	1.96
70	2.31
75	2.39
80	2.73
85	2.99
90	3.33
95	3.42

(continued)

Table 4 (continued)

OSBE1	
Load	Deflection
100	3.76
105	4.36
110	6.16
115	7.22
120	8.52
122.7	10.59
Peak load	122.7

OSBE1 LOAD vs DEFLECTION GRAPH
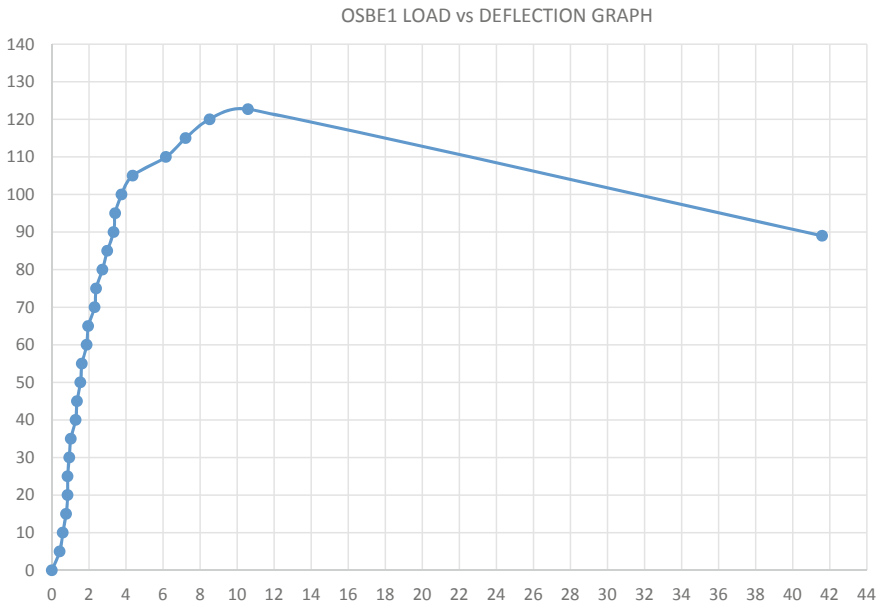
Graph 3 Oriented shear beam towards the end (OSBE) load vs deflection graph

Curve in Graph 5 is graphical representation of deflection corresponding to load values.

Table 7 represents deflection values corresponding to load at for every 5 kN load increment, peak load, and first crack load.

Curve in Graph 6 is graphical representation of deflection corresponding to load values.

Table 8 represents deflection values corresponding to load at for every 5 kN load increment, peak load, and first crack load.

Curve in Graph 7 is graphical representation of deflection corresponding to load values.

Table 5 Oriented shear beam towards ends (OSBE) two-point load

OSBE2	
Load	Deflection
0	0
5	0.2
10	0.42
15	0.73
20	0.85
25	0.99
30	1.14
35	1.29
40	1.41
45	1.56
50	1.73
55	1.85
60	2.05
65	2.14
70	2.35
75	2.53
80	2.61
85	2.79
90	2.94
95	3.12
100	3.32
105	3.47
110	3.68
111.7	3.86
120	4.32
125	5
130	5.65
135	5.95
140	6.71
144.9	7.13
Peak load	144.9
Ultimate deflection	–
120	16.98
First crack	–
134	5.75
Failure	Shear + Tension
% increase in service load	76.315789
% increase in ultimate load	31.488203

OSBE2 LOAD vs DEFLECTION GRAPH
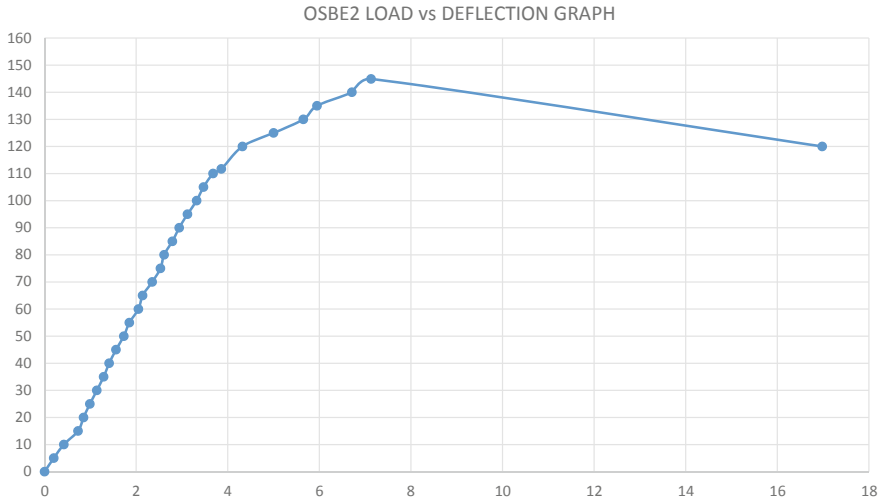
Graph 4 Oriented shear beam towards the end (OSBE) two-point load vs deflection graph

Table 6 Oriented shear beam towards centre (OSBC) point load

OSBC1	
Load	Deflection
0	0
5	0.65
10	0.89
15	1.02
20	1.08
25	1.15
30	1.28
35	1.344
40	1.53
45	1.53
50	1.66
55	1.79
60	1.92
65	2.04
70	2.17
75	2.43
80	2.49
85	2.56
90	2.75
95	2.94

(continued)

Table 6 (continued)

OSBC1	
Load	Deflection
100	3.2
105	3.33
110	3.58
115	4.86
117.8	5.82
Peak load	117.8
Ultimate deflection	—
71	36.86
First crack	—
107	3.48
Failure mode	Tension
% increase in service load	44.5946
% increase in ultimate load	3.06212

OSBC1 LOAD vs DEFLECTION GRAPH
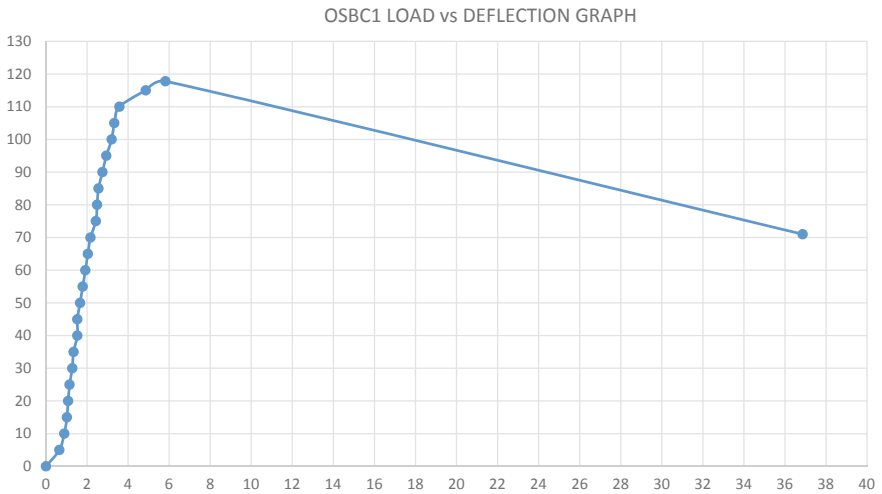
Graph 5 Oriented shear beam towards the centre (OSBC) point load vs deflection graph

Table 9 represents deflection values corresponding to load at for every 5 kN load increment, peak load, and first crack load.

Curve in Graph 8 is graphical representation of deflection corresponding to load values.

Curve in Graph 9 is a graphical representation comparing beams load with deflection graph.

Table 7 Oriented shear beam towards centre (OSBC) two-point load

Load	Deflection
0	0
5	0.2
10	0.4
15	0.52
20	0.64
25	0.76
30	0.98
35	1.14
40	1.22
45	1.31
50	1.36
55	1.59
60	1.66
65	1.75
70	1.79
75	1.85
80	1.95
85	2.05
90	2.1
95	2.15
100	2.38
105	2.47
110	2.57
115	2.7
120	2.98
125	3.1
130	3.19
135	3.33
140	3.49
145	3.62
150	3.78
155	4.14
160	4.6

(continued)

Table 7 (continued)

Load	Deflection
163.2	4.96
Peak load	163.2
Ultimate deflection	–
80	10.62
First crack	–
133	3.25
Failure mode	Tension
% increase in service load	75
% increase in ultimate load	48.0944
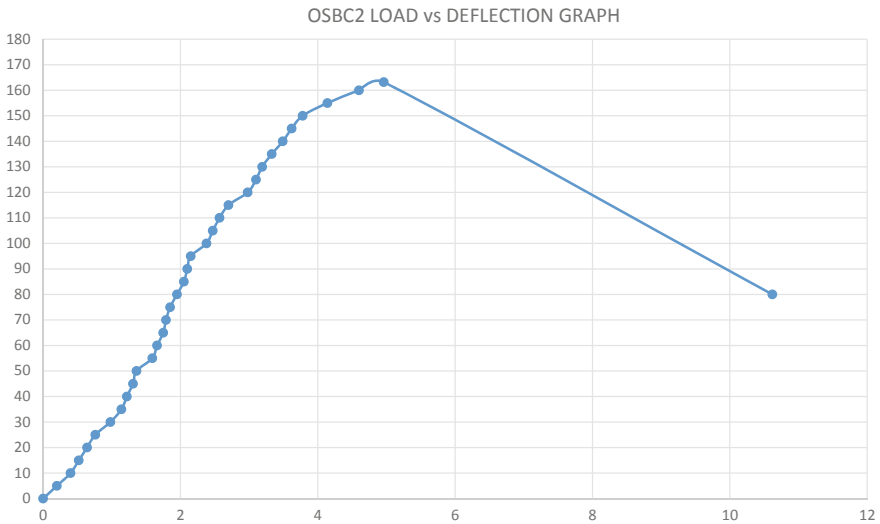
Graph 6 Oriented shear beam towards the centre (OSBC) two-point load vs deflection graph

Curve in Graph 10 is a graphical representation comparing beams load with deflection graph.

Graph 11 graphical representation showing first crack of beams under point load.

Graph 12 graphical representation showing first crack of beams under two-point load.

Graph 13 graphical representation of percentage increase in first crack load for point load when compared to normal beam.

Graph 14 graphical representation of percentage increase in first crack load for two-point load when compared to normal beam.

Graph 15 graphical representation of percentage increase in ultimate load under point load when compared to normal beam.

Table 8 Spiral beam (SB) point load

SB1	
Load	Deflection
0	0
5	0.14
10	0.4
15	0.48
20	0.57
25	0.62
30	0.8
35	0.9
40	1.06
45	1.16
50	1.22
55	1.36
60	1.45
65	1.56
70	1.68
75	1.78
80	1.89
85	2.2
90	2.35
95	2.45
100	2.68
105	3.02
110	4.23
115	5.36
120	6.35
125	7.02
130	7.88
135	8.5
140	9.6
145	11.2
148.3	14.2
Peak load	148.3
Ultimate deflection 90	26.6
First crack 112	4.3
Failure mode	–
% increase in service load	51.3514
% increase in ultimate load	29.7463
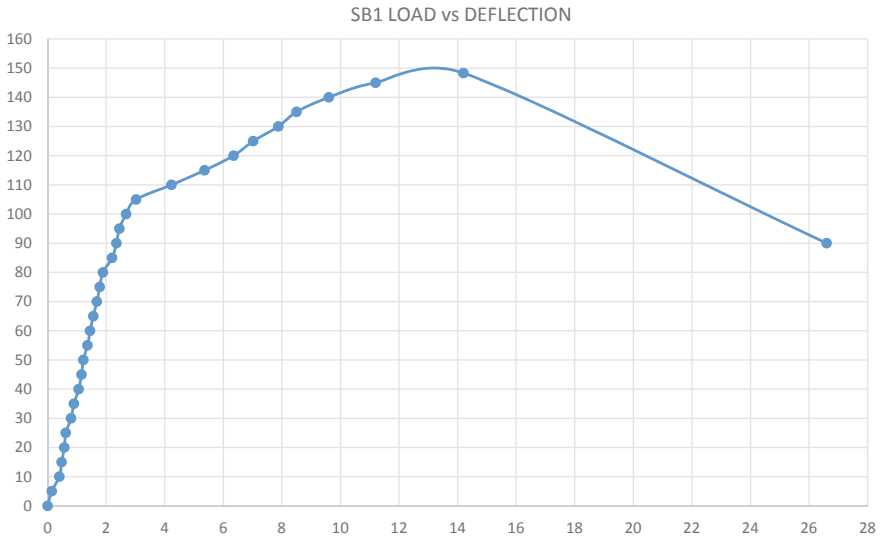
Graph 7 Spiral beam (SB) point load vs deflection

Table 9 Spiral beam (SB) two-point load

SB2	
Load	Deflection
0	0
5	0.32
10	0.49
15	0.58
20	0.8
25	0.82
30	0.93
35	1.01
40	1.1
45	1.19
50	1.28
55	1.365
60	1.49
65	1.54
70	1.67
75	1.76
80	1.84
85	2.02
90	2.1

(continued)

Table 9 (continued)

SB2	
Load	Deflection
95	2.24
100	2.41
105	2.63
110	2.89
115	3.07
120	3.24
125	3.46
130	3.63
135	3.84
140	4.07
145	4.86
150	5.42
152.7	8.22
Peak load	152.7
Ultimate deflection	–
115.47	25.07
First crack	–
142	4.22
Failure mode	Shear + Tension
% increase in service load	86.8421
% increase in ultimate load	38.5662
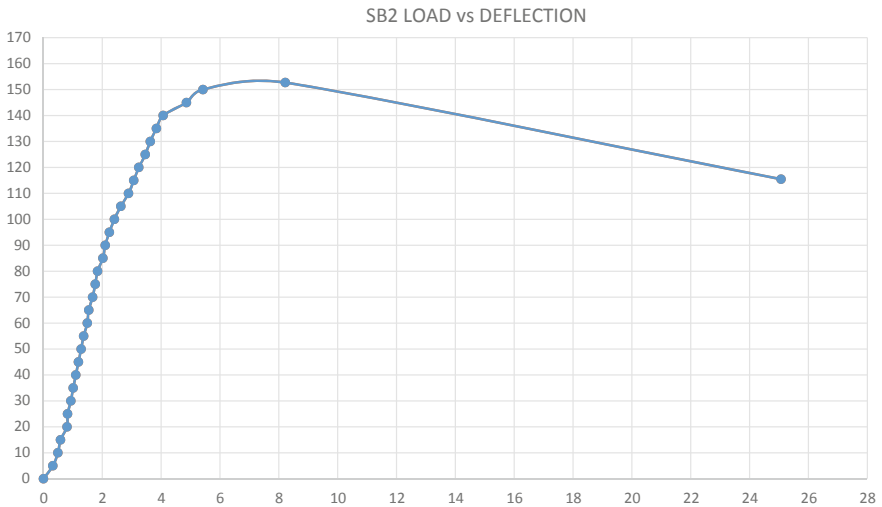
Graph 8 Spiral beam (SB) two-point load vs deflection

BEAMS TESTED WITH POINT LOAD
LOAD vs DEFLECTION GRAPH
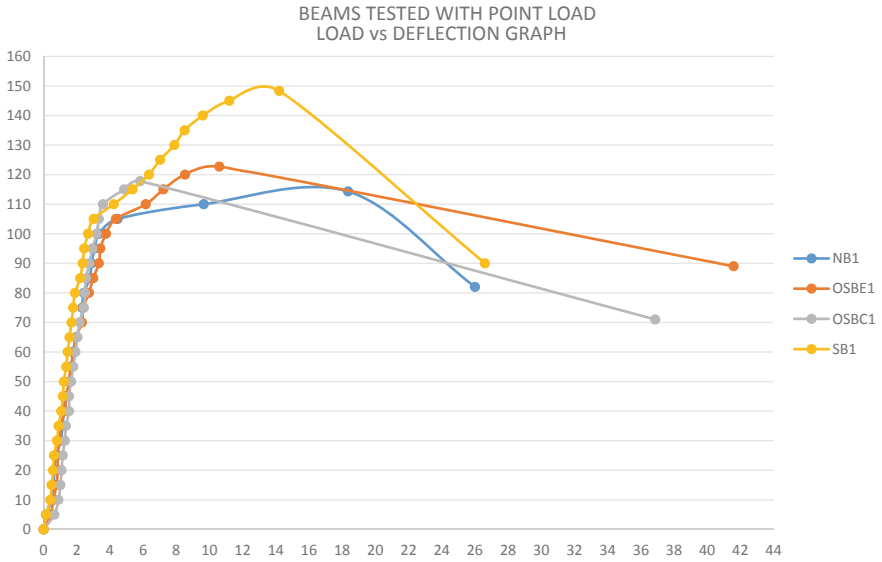
Graph 9 Comparison of all beams with point loads

BEAMS TESTED WITH TWO POINT LOAD
LOAD vs DEFLECTION GRAPH
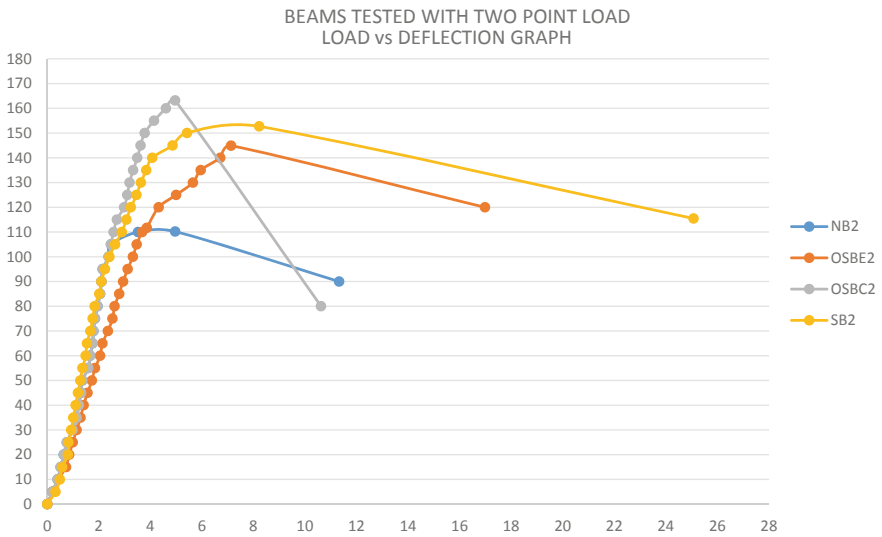
Graph 10 Comparison of all beams with two-point loads

FIRST CRACK LOAD of BEAMS UNDER POINT LOAD
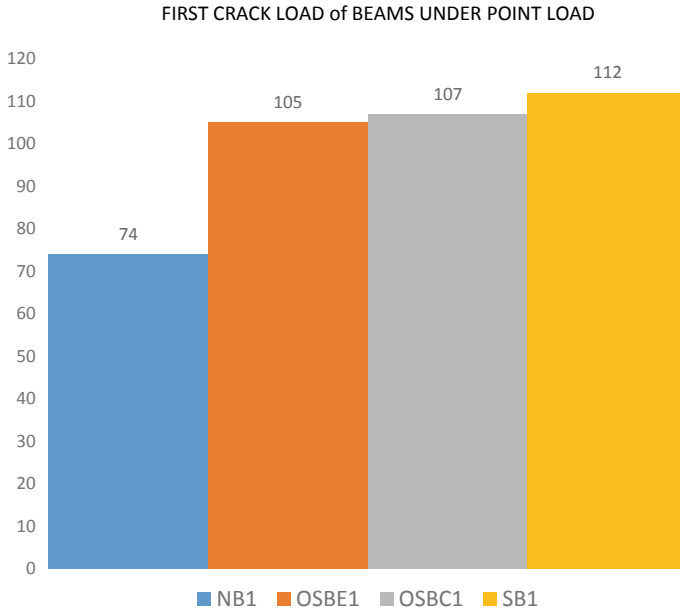
Graph 11 Comparisons of all beams with first crack load under point load

FIRST CRACK LOAD of BEAMS UNDER TWO POINT LOAD
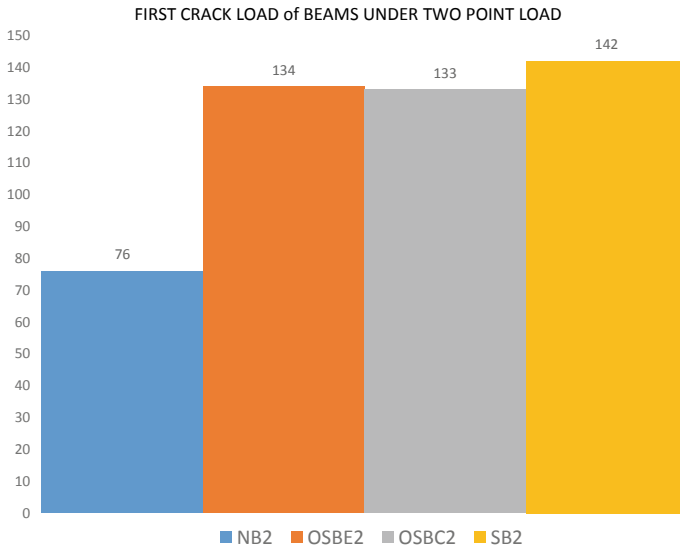
Graph 12 Comparison of all first crack load under two-point load

ULTIMATE LOAD of BEAMS UNDER POINT LOAD
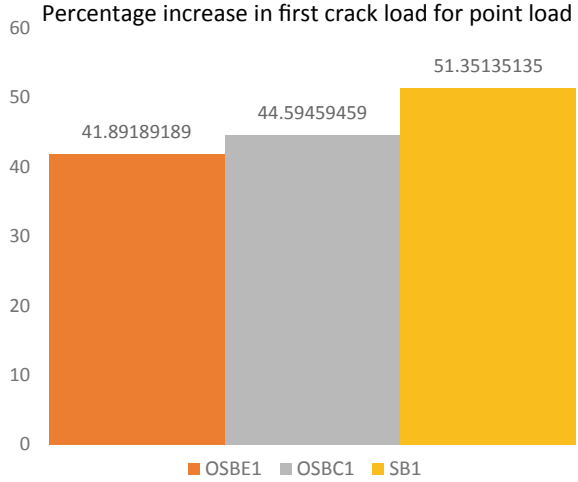
Graph 15 Comparison of all ultimate load under point load

ULTIMATE LOAD Of BEAMS UNDER TWO POINT LOAD
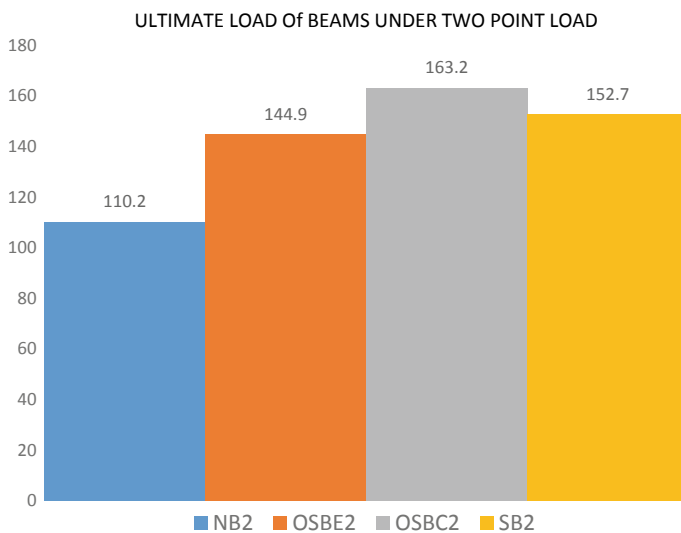
Graph 16 Comparison of all ultimate loads under two-point load

Percentage Increase In ULTIMATE LOAD For Point Load
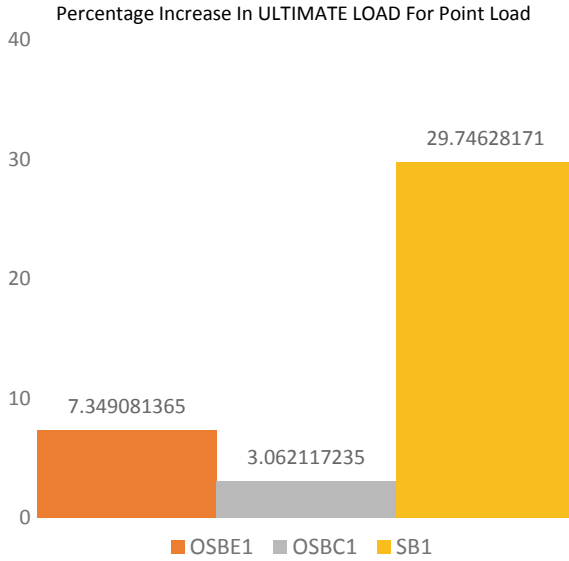
Graph 17 Comparison of all percentage increase in ultimate load under point load

Percentage increase in ULTIMATE LOAD for point load
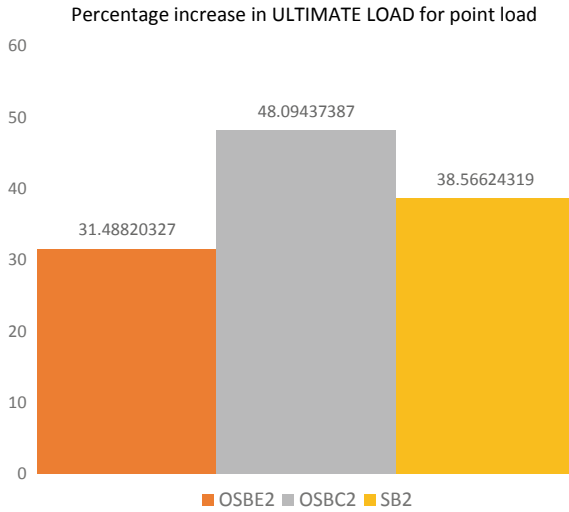
Graph 18 Comparison of all percentage increase in ultimate load under two-point load

Table 10 Load values table

S.No.	Beam notation	F.C load	Def. at F.C	Ultimate load	% increase in F.C load	% increase in ultimate load	Failure mode
1.	NB1	74	2.3	114.3	–	–	Tension
2.	OSBE1	105	4.36	122.7	41.89	7.34	Tension
3.	OSBC1	107	3.48	117.8	44.59	3.06	Tension
4.	SB1	112	4.3	148.3	51.35	29.74	Shear + Tension
5.	NB2	76	1.85	110.2	–	–	Shear + Tension
6.	OSBE2	134	5.75	144.9	76.31	31.48	Shear + Tension
7.	OSBC2	133	3.25	163.2	75	48.09	Tension
8.	SB2	142	4.22	152.7	86.84	38.56	Shear + Tension

F.C = First crack

6 Conclusions

From discussion made, the following conclusions have been drawn:

1. First crack has been increased from 74 kN in CB/NB under point load to105 kN for OSBE, 107 kN for OSBC, and 112 kN for SB.
2. Percentage increase in first crack load under point load is 41.89% for OSBE, 44.91% for OSBC, and 51.35% for SB.
3. First crack has been increased from 76 kN for CB/NB under two-point load to 134 kN for OSBE, 133 kN for OSBC, and 142 kN for SB.
4. Percentage increase in first crack load under two-point load is 76.31% for OSBE, 75% for OSBC, and 86.84% for SB.
5. Peak load has been increased from 114.3 kN for CB/NB under point load to 122.7 kN for OSBE, 117.8 kN for OSBC, and 148.3 kN for SB.
6. Percentage increase in peak load under point load is 7.34% for OSBE, 44.59% for OSBC, and 29.74% for SB.
7. Peak load has been increased from 110.2 kN for CB/NB under two-point load to 144.9 kN for OSBE, 163.2 for OSBC, and 152.7 for SB.
8. Percentage increase in peak load under two-point load is 31.48% for OSBE, 48.09% for OSBC, and 38.56% for SB.

From above, we can conclude that first crack has been reasonably increased for the OSBE, OSBC, and SB when compared to CB/NB under both point loading and two-point loading.

From above, we can conclude that peak load has been increased for OSBE, OSBC, and SB when compared with CB/NB under both point loading and two-point loading.

References

1. Al-Nasra, M. M., & Asha, N. M. Shear reinforcements in the reinforced concrete beams.
2. Bentz, M. P. C. E C., & Xie, E. G. S. L. An adequate theory for the shear strength of reinforced concrete structures.
3. Tompos, E. J., & Frosh, R. J. Influence of beam size, longitudinal reinforcement, and stirrup effectiveness on concrete shear strength.
4. Zakaria, M., Ueda, T., Wu, Z., & Meng, L. Experimental investigation on shear cracking behavior in reinforced concrete beams with shear reinforcement.
5. Unnikrishna, P., & Devdas, M. Reinforced concrete design.

Experimental Study on Bacterial Concrete Using Bacillus Subtilis Micro-Organism

Kunamineni Vijay and Meena Murmu

Abstract Concrete is a homogenous mix in which the cracks are unavoidable. The seepage of water and other salts through the cracks makes concrete weaker and reduces its life. Further, corrosion of steel may also occur due to the seepage of water and salts which weakens the reinforcement in concrete. Hence, it is required to rehabilitate the concrete for economic life of structures. To remediate the cracks in concrete, an inherent biomaterial, a self-healing material, is developed using bacteria. Bacterial concrete is a technique which is highly desirable because the calcium carbonate precipitation is induced as a result of microbial activities that can heal the cracks itself. Provision of suitable conditions and calcium sources to the microbes, a few strains of microbes can prompt the precipitate the calcium carbonates in concrete. This precipitation capability has been evaluated in recent decades to justify the improvement in strength and durability properties of concrete. In this study, Bacillus subtilis bacteria was used and tested for suitability in concrete. This paper shows the impact of Bacillus subtilis bacteria on compressive strength, workability and self-healing of cracks in concrete. Results show that the addition of bacteria can increase the strength of the concrete. And the workability of bacterial concrete depends on the nutrient source, i.e. calcium lactate; addition of calcium lactate may increase the workability of concrete. However, bacteria cultures and spore powder place a minor role in workability of concrete. Both the cultured and spore powder bacteria are giving good results in healing of cracks.

Keywords Bacillus subtilis · Compressive strength · Calcium lactate · Workability · Self-healing of cracks

K. Vijay (✉) · M. Murmu
Civil Engineering Department, National Institute of Technology, Raipur 492010, India
e-mail: vijay.kunamaneni@gmail.com

1 Introduction

Concrete is a widely used construction material that comprises cement, fine and coarse aggregate. It is considered to be the highly consumed material, next to water. In any case, it is vulnerable to the formation of small-scale cracks with pores in it. These small-scale cracks and pores are exceptionally unwanted in concrete, due to the fact that they give an open path for water and different harmful substances to enter. This results in corrosion of reinforcement, thereby reducing the durability and strength of concrete. It is very expensive to repair these cracks in the concrete, and a huge amount is being spent on this throughout the globe. For the purpose of repairing cracks, different methods are available; however, main parts of conventional repair methods are costly, chemical-based and prompt severe environmental and health hazards. Recently, healing of cracks and pores in the concrete utilizing microbiologically initiated calcite precipitation is found to be an effective alternate method. This remedial strategy using bacteria outperforms different procedures due to the advantages like bio-based eco-friendly, durable and cost-effective. The $CaCO_3$ precipitation initiated by Bacillus aerius and Bacillus pasteurii was observed to be effective in healing of cracks with improved compressive strength [1, 2]. A considerable increase in strength and durability of fly ash concrete through self-healing has been observed using Sporoscarcina pasteurii micro-organisms [3]. The similar change has been observed in silica fume concrete using Sporoscarcina pasteurii micro-organisms for self-healing [4]. Bacillus megaterium micro-organisms were utilized as a part of concrete, and this indicated a 24% increase in compressive strength [5]. Bacterial concrete, comprising alkaliphilic micro-organisms and calcium particle solutions, has drawn attention of researchers in the recent era. It depends on microbial-induced $CaCO_3$ precipitation (MICP) around the individual particles and at particle–particle contacts to bond free particles [6]. This MICP procedure relies upon urease delivering micro-organisms that are universal. During this movement of microbial urease, the urea is decomposed by micro-organisms. As a part of digestion, micro-organism species gives urease, which catalyzes urea to ammonium and carbonates. These outcomes in a rise of pH level further improve the carbonate concentration in the bacterial surroundings. These parts aid hydrolyze to ammonia (NH_4^+) and carbonic acid (CO_3^{2-}) for the formation of $CaCO_3$. The process of hydrolysis and precipitation of $CaCO_3$ is as follows [7, 8].

$$CO(NH_2)_2 + H_2O \rightarrow NH_2COOH + NH_3$$

$$NH_2COOH + H_2O \rightarrow NH_3 + H_2CO_3$$

$$H_2CO_3 \rightarrow HCO_3^- + H^+$$

$$2NH_3 + 2H_2O \rightarrow 2NH_4^+ + 2OH^-$$

$$HCO_3^- + H^+ + 2NH_4^+ + 2OH^- \rightarrow CO_3^{2-} + 2NH_4^+ + 2H_2O$$
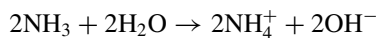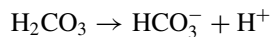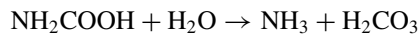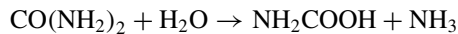
The negatively charged cell wall of the bacteria draws cations from the environment, together with Ca^{2+}, to deposit on their cell surface. The Ca^{2+} ions react with the CO_3^{2-} prime to precipitate calcium carbonate at the cell surface that serves as a nucleation site.

$$Ca^{2+} + Cell \rightarrow Cell{-}Ca^{2+}$$

$$Cell{-}Ca^{2+} + CO_3^{2-} \rightarrow Cell{-}CaCO_3$$
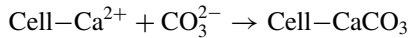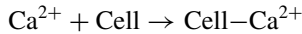
Bacterial concrete has been an alternative and an innovative metabolic product with the scope for research in construction and civil engineering. The durability of building materials is enhanced using this process and is demonstrated [9–13]. This process is also used for healing of cracks on concrete.

Several researchers have reported the effect of bacterial species, Bacillus pasteurii and Bacillus sphaericus on the bacterial concrete. In any case, restricted research has been done on different types of micro-organisms. The current examination deals with the suitability of Bacillus subtilis micro-organism for use in concrete. The impact of micro-organisms on workability and compressive strength of concrete has also been examined. The present examination exhibits that bio-mineralization component in cementitious materials can be a suitable strategy to enhance the strength characteristics.

2 Materials and Methodology

2.1 Cement, Fine and Coarse Aggregate

Ordinary Portland cement tested as per Indian Specifications IS: 4031-1988 [14] has been used. And natural sand tested as per Indian Standard Specifications IS: 383-1970 [15], with 4.75 mm and 20 mm as maximum size of fine and coarse aggregate, respectively, has been used.

2.2 Bacillus Subtilis Bacteria

The Bacillus subtilis microbes are procured and cultured by using liquid medium containing simple nutrient broth medium 13 gm per litre of distilled water to which 1.5% of agar was mixed to attain solid medium per store culture. The bacterial cells are harvested by the method of separation from the 72-h developed cultures. These

Table 1 Test data for identification of bacteria

Test	Indicator used	Observation	Results
Gram staining reaction	Crystal violet	Purple colour	Gram positive
Lactose fermentation test	Phenol red indicator and lactose	Yellow colour	Positive

cultured samples were tested for identification the isolated bacteria. The test data are given in Table 1. In all bacterial concrete mixes 13 gm per litre Nurient broth medium has been added for germination of bacteria.

2.3 Calcium Lactate

Calcium lactate is well known as calcium salt pentahydrate, and the chemical formula is $C_6H_{10}CaO_6$. It is a white powder having efflorescent odour. It is formed by reacting lactic acid with calcium carbonate or calcium hydroxide. The physical properties of calcium lactate are tabulated in Table 2.

3 Concrete Mix Design and Testing

In this examination, control mix was done by BIS: 10262 [16]. The mix proportions of concrete utilized were water: cement: fine aggregate: coarse aggregate: 0.4: 1.0: 1.3: 2.48; four altered mixes have been prepared for this study. Mix 1 (M1) does not contain any amount of bacteria and calcium lactate. Mix 2 (M2) contains 0.5% of calcium lactate. Mix 3 (M3) contains 0.5% of calcium lactate and 0.5% of bacteria in spore powder having a concentration of 2 million cfu/gm. Mix 4 (M4) contains 0.5% of calcium lactate and cultured bacteria of concentration 10^5 cells/ml and in. Concrete cubes of 100 mm size were cast for testing of compressive strength. After casting, these cubes were initially kept in moulds at room temperature for about a

Table 2 Calcium lactate physical properties

Properties	Result
Chemical formula	$C_6H_{10}CaO_6$
Appearance	White powder
Solubility	Soluble in water
Odour	Efflorescent
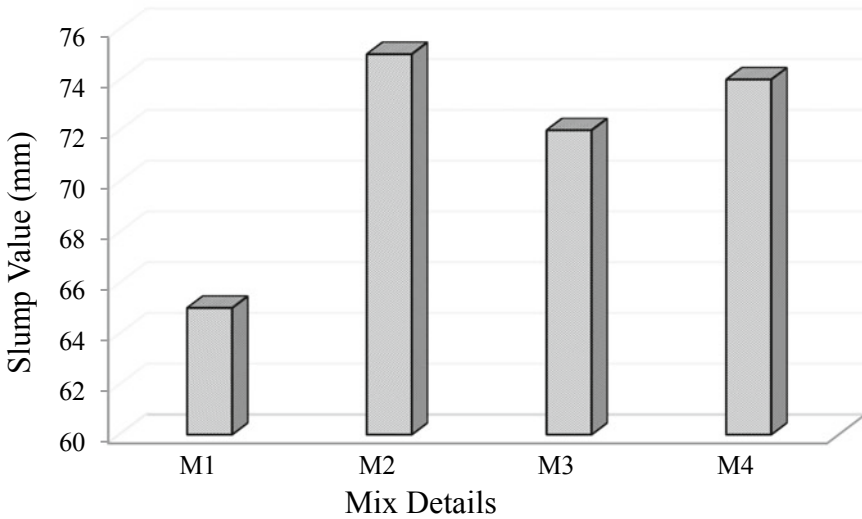
Fig. 1 Slump values of concrete mixes containing bacteria and calcium lactate

day. These are then demoulded and placed in water for curing. These were tested for 7 and 28 days of curing period in triplicate.

4 Results and Discussion

4.1 Workability of Concrete

Workability of concrete means the capacity to work with concrete. A concrete is said to be workable if it can be handled without any segregation. It can be set without the loss of homogeneity. It is the property of freshly blended concrete. In the present examination, the concrete is tested for workability before casting.

From Fig. 1, it is observed that the workability of concrete may increase due to the addition of calcium lactate, and it may delay the setting time of concrete. There is no much influence on workability by the addition of bacteria spores or cultures in concrete.

4.2 Compressive Strength

From Fig. 2, the higher compressive strength of bacterial concrete is observed compared to the normal concrete. Both spore powder and cultured bacteria are good in
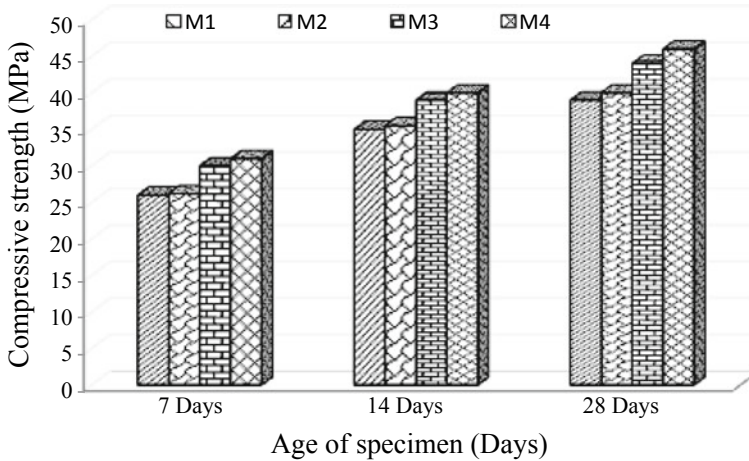
Fig. 2 Compressive strength of concrete

precipitating the calcium carbonate in concrete. It is observed that a maximum of 16% of compressive strength has been increased when comparing with the normal concrete. The concrete containing only calcium lactate will show lower compressive strength results when compared with microbial concrete because calcium lactate is in the same form after curing; also, calcium carbonate does not form only by the addition of calcium lactate; it requires micro-organisms to convert it to calcium carbonate. This may increase the strength of the concrete.

4.3 *Self-Healing of Cracks*

The artificial cracks are developed in concrete samples at the age of 28 days by applying a constant load, and these cube samples are again kept for curing. Both the cultured and spore powder bacterial concretes are giving good results in healing of cracks (Fig. 3).

5 Conclusions

This study presents the effect of Bacillus subtilis bacteria on workability, compressive strength and self-healing of cracks in concrete. The obtained results indicate that the microbial self-healing agent can be used for self-healing of cracks in concrete. The workability of bacterial concrete depends on the nutrient source, i.e. calcium lactate. The addition of calcium lactate may increase the workability of concrete; however, bacteria cultures and spore powder place a minor role in workability of concrete.
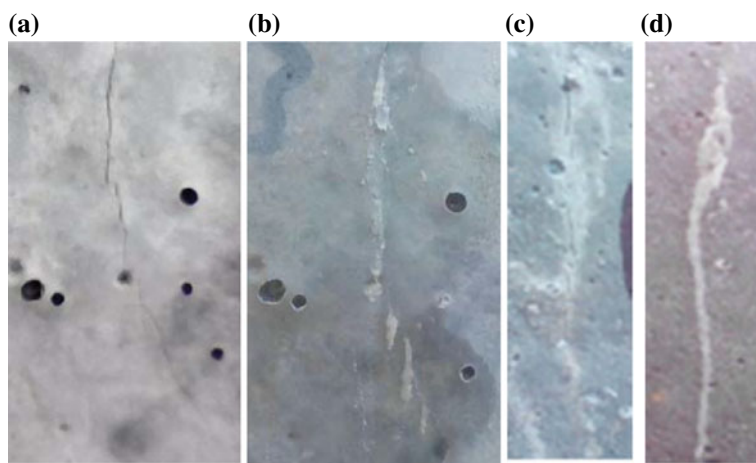
Fig. 3 Test cubes with **a**, **c** Artificially developed cracks in microbial concrete. **b**, **d** Healing of artificially developed cracks in bacterial concrete

Compressive strength of concrete may increase due to the addition of bacteria by converting calcium lactate to calcium carbonate. Only the addition of calcium lactate can reduce the strength of concrete. Both the cultured and spore powder bacteria shows good results in healing of cracks.

References

1. Wang, J., Dewanckele, J., Cnudde, V., Van Vlierberghe, S., Verstraete, W., & De Belie, N. (2014). X- ray computed tomography proof of bacterial-based self-healing in concrete. *Cement and Concrete Composites, 53,* 289–304.
2. Siddique, R., Singh, K., Singh, M., Corinaldesi, V., & Rajor, A. (2016). Properties of bacterial rice husk ash concrete. *Construction and Building Materials, 121*, 112–119.
3. Chahal, N., Siddique, R., & Rajor, A. (2012). Influence of bacteria on the compressive strength, water absorption and rapid chloride permeability of fly ash concrete. *Construction and Building Materials, 28*(1), 351–356.
4. Chahal, N., Siddique, R., & Rajor, A. (2012). Influence of bacteria on the compressive strength, water absorption and rapid chloride permeability of concrete incorporating silica fume concrete. *Construction and Building Materials, 37,* 645–651.
5. Andalib, R., Majid, M. Z. A., & Hussin, M. W. (2016). Optimum concentration of Bacillus megaterium for strengthening structural concrete. *Construction and Building Materials, 118*, 180–193.
6. Kim, H. K., Park, S. J., Han, J. I., & Lee, H. K. (2013). Microbially mediated calcium carbonate precipitation on normal and lightweight concrete. *Construction and Building Materials, 38,* 1073–1082.
7. Vijay, K., Murmu, M., & Deo, S. V. (2017). Bacteria based self healing concrete—A review. *Construction and Building Materials, 152,* 1008–1014.
8. Van Tittelboom, K., De Belie, N., De Muynck, W., & Verstraete, W. (2010). Use of bacteria to repair cracks in concrete. *Cement and Concrete Research, 40*(1), 157–166.

9. Jonkers, H. M., Thijssen, A., Muyzer, G., Copuroglu, O., & Schlangen, E. (2010). Application of bacteria as self-healing agent for the development of sustainable concrete. *Ecological Engineering, 36,* 230–235.
10. De Muynck, W., De Belie, N., & Verstraete, W. (2010). Microbial carbonate precipitation in construction materials: A review. *Ecological Engineering, 36*(2), 118–136.
11. Bachmeier, K. L., Williams, A. E., Warmington, J. R., & Bang, S. S. (2002). Urease activity in microbiologically-induced calcite precipitation. *Journal of Biotechnology, 93*(2), 171–181.
12. Luo, M., Qian, C. X., & Li, R. Y. (2015). Factors affecting crack repairing capacity of bacteria-based self-healing concrete. *Construction and Building Materials, 87,* 1–7.
13. De Muynck, W., Cox, K., De Belie, N., & Verstraete, W. (2008). Bacterial carbonate precipitation as an alternative surface treatment for concrete. *Construction and Building Materials, 22*(5), 875–885.
14. BIS. 1988. 4031, Indian Standard 43 Grade Ordinary Portland Cement—Specification, Bureau of Indian Standards.
15. BIS. 1970. 383, Specifications for Coarse and Fine Aggregates from Natural Sources for Concrete.
16. BIS. 2009. 10262, Guidelines for Concrete Mix Design Proportioning, Bureau of Indian Standards.

Effect of Rice Husk Ash and Silica Fume as Strength-Enhancing Materials on Properties of Modern Concrete—A Comprehensive Review

Shaswat Kumar Das , **Saurabh Kumar Singh** , **Jyotirmoy Mishra** and **Syed Mohammed Mustakim**

Abstract Achieving a concrete with good strength and durability using OPC is quite challenging in the present scenario as per the environmental exposures are concerned. Hence, Geopolymer concrete, concrete without cement, has proved to be a better alternative and qualifies to be a concrete for modern-age constructions. Modern concrete production should promote the idea of sustainable utilization of various industrial by-products such as fly ash, silica fume, Rice Husk Ash, ground-granulated blast-furnace slag (GGBS), and many more which are pozzolanic in nature. And the old conventional method of making concrete using OPC should be minimized gradually as cement production is a potential threat to environment due to huge carbon footprints leading to global warming. So the major challenge of concrete makers is to develop and implement newer construction materials which will enhance strength and durability of concrete. High-strength Geopolymer concrete and blended OPC-based concrete are the most important research areas which need to be encouraged at a higher scale for making durable high-rise structures utilizing strength-enhancing materials. In this review, the effects of incorporation of strength-enhancing materials, i.e., silica fume and Rice Husk Ash on Geopolymer concrete and OPC-based concrete, are discussed with necessary comparisons from various research studies around the world.

S. K. Das (✉)
Department of Civil Engineering, GCE, Keonjhar, Odisha 758002, India
e-mail: shaswatdas_sce@gcekjr.ac.in

S. K. Singh
Department of Mining Engineering, GCE, Keonjhar, Odisha 758002, India
e-mail: ss9983803883@gmail.com

J. Mishra
Department of Civil Engineering, VSSUT, Sambalpur, Odisha 768018, India
e-mail: jmishra0805@gmail.com

S. M. Mustakim
Environment & Sustainability Department, CSIR-IMMT, Bhubaneswar 751013, Odisha, India
e-mail: mustakim@immt.res.in

1   Introduction

From the 3800-year-old Great Pyramid of Giza to the modern architecture marvels
like Burj Khalifa, human's love for high-rise buildings has never changed but as
David Allan Coe said "It is not the beauty of a building you should look at; it's
the construction of the foundation that will stand the test of time." With the ever-
increasing rates of construction, now more than ever the use of cement has increased
and is expected to reach the production rate of 4830 million metric tons by 2030
[1]. As of now cement is the second most widely used material worldwide with
the first being water. The humongous use of ordinary Portland cement (OPC) gives
rise to several problems. The major problems regarding OPC are sustainability, high
CO_2 emissions (5–7% of the world's CO_2 emission is due to the use of OPC), and
wastage of water in the curing process [2]. Geopolymer concrete (GPC) is a concrete
without cement and is made up of industrial wastes containing high content of silicon
and aluminum. It was first introduced by a French chemist named Joseph Davidovits.
Apart from the aggregates, the major constituents of Geopolymer concrete are source
material and alkaline liquids [3]. The major source materials used in Geopolymer
concrete are fly ash and ground-granulated blast-furnace slag (GGBS). Furthermore
to enhance the strength and durability properties of GPC, some strength-enhancing
materials are also used, viz. silica fume, Rice Husk Ash, nano silica, etc. The markets
have an ever-increasing demand for the strength-enhancing materials due to the
significant increase in the quality and life of the modern concrete.

2   Geopolymer Concrete Versus OPC Concrete

Modern construction works require skilled laborers and good machinery which basi-
cally increase the cost of construction naturally. The cost of cement, its effect on
environment due to carbon footprints, water requirements, and durability issues are
now well known. On the other hand, Geopolymer concrete, the concrete without
cement, will give a tough competition in near future to cement manufacturers as it
reduces the dependence on cement and water for making concrete. Highly alkaline
solutions, namely sodium/potassium hydroxide and sodium/potassium silicate along
with industrial waste materials such as fly ash, GGBS, and Rice Husk Ash which are
rich in silicon and aluminum combine to form the Geopolymer matrix which is very
different from C-S-H gel mechanism in OPC-based concrete. Geopolymer concrete
reduces water requirements for mixing and curing. On the other hand, conventional
concrete needs sufficient water both for mixing and curing which increases problems
with respect to water shortage. Extensive research findings from all over the world

suggest that Geopolymer concrete is the third generation concrete. The first and the second are lime-based concrete and cement-based concrete. Researches established that Geopolymer concrete is superior to conventional concrete in terms of setting time, strength, workability, and durability. Though certain behavioral characteristics, proper mix design code has not been established till now. Hence, conventional concrete is preferred by most concrete makers and users.

3 Need for Strength-Enhancing Materials

Wind and seismic load conditions are now implemented in design of every high-rise structures. And particular emphasis should be given on quality and strength of concrete. Therefore, there is a need for strength-enhancing materials in making concrete as we know that a concrete with maximum strength has better mechanical properties too and also it can counter various load conditions. Numerous researches worldwide on the implementation of strength-enhancing materials like silica fume and Rice Husk Ash on making high-strength Geopolymer concrete and OPC-based concrete have proved to be encouraging. As the strength-enhancing materials are pozzolanic in nature, naturally they contribute to high strength and better durability in Geopolymer as well as conventional concrete. Geopolymer concrete needs rich source of silicon/aluminum which will make a high-strength Geopolymer matrix after reaction with alkaline solutions and conventional concrete requires C-S-H gel formation for strength which is enhanced by pozzolanic activity of these strength-enhancing materials such as silica fume and Rice Husk Ash.

4 Strength-Enhancing Materials—Silica Fume (SF) and Rice Husk Ash (RHA)

4.1 Silica Fume

Silica fume (SF) also known as micro-silica is a by-product of ferrosilicon industry. Silica fumes are very fine non-crystalline silica produced as a by-product during the production of elementary silicon or silicon-containing alloys in electric arc furnaces. The silica fumes have unbound potential to be used in conventional cement concrete and Geopolymer concrete due to the high amount of amorphous silica content present in it. ASTM has specified silica fume as pozzolanic material and developed a standard for its use in cementitious mixtures—ASTM C1240. The physical and chemical properties of silica fumes given by some scientists and researchers are given below in Table 1 and Table 2, respectively.

Table 1 Physical properties of silica fume

Physical properties	H. Y. Moon et al.	N. K. Amudhavalli
Specific gravity	2.20	2.20
Mean particle size (μm)	–	0.1
Specific surface area (m^2/Kg)	20,470	20,000
Bulk density (Kg/m^3)	–	576

4.2   Rice Husk Ash

India being the second largest producer of rice has enough resources to produce Rice Husk Ash (RHA) in humongous quantities. RHA is a by-product of the rice milling industries. It is produced by controlled combustion of rice husk in the steam boiler. The heat energy produced in the process is used in processing the rice [6]. Meanwhile, this process produces 55 kg of ash per 1000 kg of husk [7]. The RHA produced can be used as a supplementary cementitious material (SCM) in OPC concrete and as a strength-enhancing material in Geopolymer concrete because of the high percentage of nascent SiO$_2$ present in the ash. The physical and chemical properties of RHA proposed by some researchers are tabulated below (Tables 3 and 4).

5   Effects of Silica Fume on Concrete

5.1   Compressive Strength

Conventional Concrete. Karthikeyan and Arunkumar stated that the compressive strength of conventional concrete increases when silica fume is added although the change in compressive strength is not very significant. They found maximum compressive strength of 65.60 MPa with 10% of silica fume where the normal concrete compressive strength was 61.79 MPa [12]. The compressive strength results have been depicted in Fig. 1.

Geopolymer Concrete. F. N. Okoye et al. stated that the compressive strength of Geopolymer concrete significantly increases with an increase in silica fume content, and they observed the maximum compressive strength of the GPC having 40% of silica fume which was nearly twice of the GPC without the silica fume [5].

A Joshua Daniel et al. studied the behavior of Geopolymeric reactions with OPC as a precursor. They replaced OPC by silica fume in M25 grade concrete with 20, 40, and 60%. They found the maximum compressive strength of 30.1 MPa with 40% of silica fume, and there was a reduction in compressive strength of the mixtures

Table 2 Chemical properties of silica fume

Silica fume	SiO_2	CaO	MgO	Na_2O	K_2O	MnO	Al_2O_3	Fe_2O_3	SO_3	LOI
H. Y. Moon et al. [4]	91.20	0.70	0.30	–	–	–	1.30	0.8	–	2.30
F. N. Okoye et al. [5]	93.67	0.31	0.84	0.40	1.10	0.84	0.83	1.30	0.16	2.10

Table 3 Physical properties of RHA

Physical properties	Mehta et al. [7]	Nagrale et al. [8]
Mean particle size	–	63.8
Specific gravity	2.06	2.11 μm
Fineness passing 45 μm (%)	99	98

containing 20 and 60% silica fume by 30.37 and 19.45% with respect to conventional concrete [13].

5.2 Workability

Conventional Concrete. The workability of cement concrete with different percentage replacements of cement by silica fumes was investigated, and it was found that at increased percentage of silica fume enhanced the concrete workability marginally, the maximum compaction factor and slump were found as 87 and 42 mm at a replacement of 35% of OPC by silica fumes [14].

Geopolymer Concrete. The workability of Geopolymer concrete gradually decreases with the percentage increment of silica fumes. The workability of Geopolymer concrete containing silica fume was measured using slump cone, and it was observed that silica fume-containing mixtures were less workable than that of the mix containing only fly ash [5].

P. Chindaprasirt et al. stated that the Geopolymer mixes are more cohesive as compared to OPC concrete mixes due to the addition of viscous sodium silicate solutions in the fresh Geopolymer concrete [15].

5.3 Durability

5.3.1 Sulfate Attack

Conventional Concrete. The sulfate attack occurs in conventional concrete due to the presence of calcium compounds (free lime) when the silica fume is added to cement concrete mixes as a replacement of cement; it shows pozzolanic activity and utilizes the free lime content to form secondary C-S-H gel. In a 5% sodium sulfate solution, the resistance of mortar specimens with silica fumes showed a greater resistance than the conventional mortar specimens [4].

Geopolymer Concrete. The Geopolymer concrete containing silica fume displayed greater sulfate resistance in comparison to both OPC concrete and Geopolymer concrete without silica fume. The increment in sulfate resistance of silica

Table 4 Chemical properties of RHA

Constituents	SiO$_2$	Al$_2$O$_3$	Fe$_2$O$_3$	CaO	MgO	SO$_3$	Na$_2$O	K$_2$O	LOI
Le et al. [9]	86.81	0.50	0.87	1.04	0.85	–	0.69	3.16	4.6
Lung [10]	91.00	0.35	0.41	–	0.81	1.21	0.08	3.21	8.5
Zerbino et al. [11]	95.04	0.30	0.44	1.25	0.45	0.01	0.09	1.04	0.51
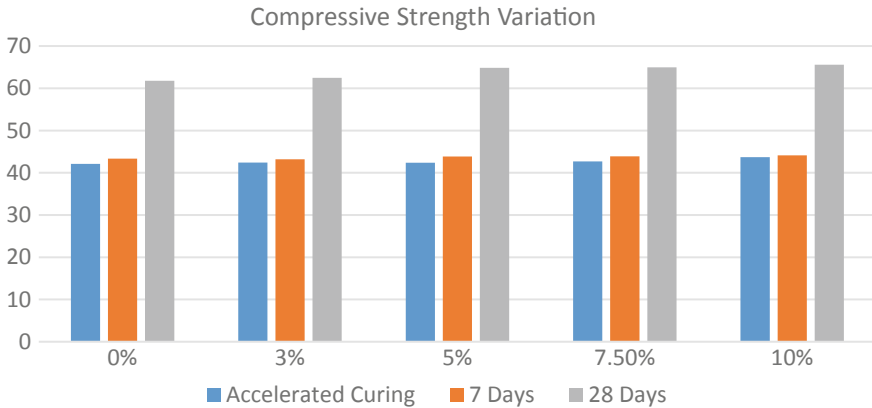
Fig. 1 Variation of compressive strength with % of silica Fume (Karthikeyan et al. [12])

fume incorporated Geopolymer concrete may be due to the denser microstructure development [16].

5.3.2 Chloride Attack

Conventional Concrete. Safwan A. Khedr investigated the performance of mortar specimens with and without silica fume in high concentration of HCl and found a greater resistance to chloride attack in mortar specimens containing silica fumes [17].

Geopolymer Concrete. The experiments by F. N. Okoye et al. on keeping Geopolymer concrete cubes with silica fumes in a chloride environment of 5% NaCl for 56 days depicted that the sample had good chloride resistance [5]. The micro-structural image of the specimens was analyzed by SEM analysis (Fig. 2).

6 Effect of Rice Husk Ash on Concrete

6.1 Compressive Strength

Conventional Concrete. P. Chandan Kumar investigated the effect of Rice Husk Ash in cement concrete by replacing the OPC in various percentages, and he found that the 7.5% replacement of OPC by RHA gives better compressive strength as compared to the conventional one [18].
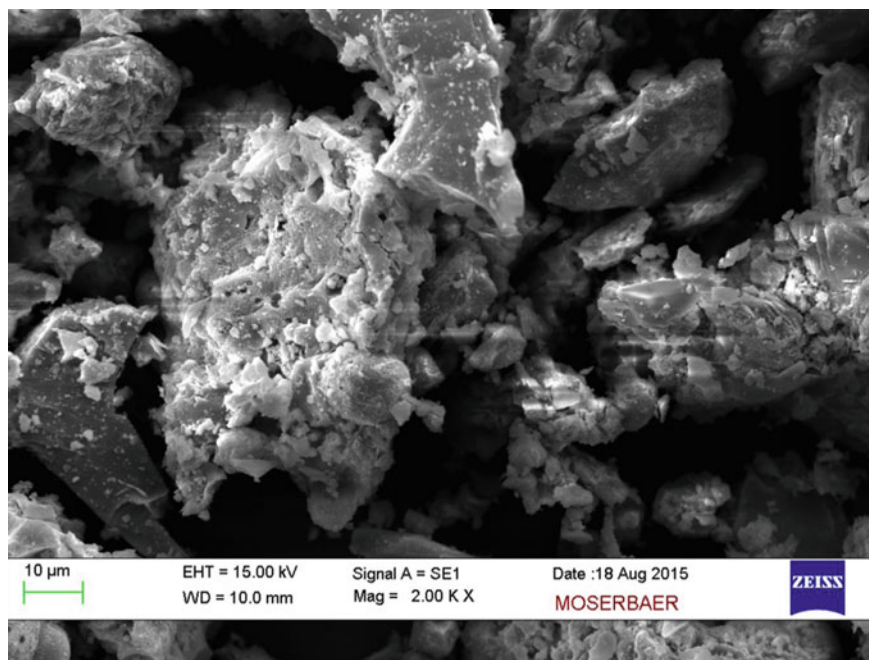
Fig. 2 SEM image of GPC specimen after chloride treatment (F. N. Okoye et al. [5])

Tests on compressive strength were conducted by M. S. Ismail and A. M. Wali-uddin by varying percentages of RHA in cement concrete. They concluded that the replacement of 20% of the mixture with RHA gave the best results in compressive strength tests [19]. Furthermore Arvind Kumar et al. studied the effect of Rice Husk Ash in OPC concrete by replacing 20% of cement by RHA; initially, they found the early strength of RHA-based concrete was less but the final strength was slightly higher as compared to conventional concrete [20] (Fig. 3).

Geopolymer Concrete. Seyed Mahmoud Zabihi et al. conducted experimental investigations on OPC-RHA-based Geopolymer concrete. The results explicitly indicate that a significant enhancement in compressive strength occurs when the OPC is replaced up to 80% by RHA [21].

Howsoever, the results of experiments conducted by P. V. Ramani et al. imply that RHA is a strength-enhancing material when used in place of GGBS in quantities under 10%. Beyond that RHA tends to decrease the compressive strength. When GGBS is replaced by RHA in an optimum doge, compressive strength of 51 MPa was achieved in the span of 28 days [22].

The experiments conducted by D. R. Dara and A. C. Bhogayata on varying RHA percentages from 0 to 25% in fly ash-based Geopolymer concrete depict the increment of compressive strength by 5.40% compared to normal concrete samples at 25% of RHA [23].
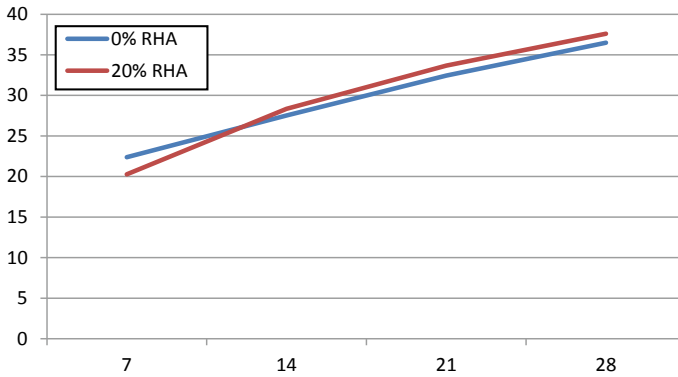
Fig. 3 Variation of compressive strength with time (Kumar et al. [20])

6.2 Workability

Conventional Concrete. RHA has a very large specific surface area due to highly porous nature of the material and fineness. This results in decreased workability of the concrete due to excessive water absorption [17].

Ramakrishnan S. et al. has conducted slump test (as per IS: 1199-1959) to measure workability, and they found a decreasing value of slump with the increment of RHA percentage in the concrete matrix [24]. The slump test results are shown in Table 5.

Geopolymer Concrete. In fly ash-based Geopolymer concrete, the workability gradually decreases with the percentage increase of RHA. At 25 and 30% of RHA content, the Geopolymer concrete shows very less workability [25].

RidhoBayuaji et al. performed an experiment to check the workability of RHA-fly ash-based Geopolymer concrete and found a cohesive and non-workable concrete mix. Thereafter, they added table sugar in a doge of 10.5 kg/m^3 in the Geopolymer concrete. This resulted in a longer setting period enabling the concrete to be workable for a longer time [26].

Table 5 Slump results with different % of RHA (Ramakrishnan et al. [24])

Mix	S. No.	RHA %	Slump value
M40	01	0	71
	02	5	33
	03	10	18
	04	15	5
	05	20	–
	06	25	–

6.3 Durability

6.3.1 Sulfate Attack

Conventional concrete. The sulfate resistance of RHA-based concrete is exceptionally higher as compared to normal concrete. When the RHA specimens were immersed in Na_2SO_4 and $MgSO_4$, the strength decoration of RHA-based concrete was negligible as compared to that of normal concrete specimens [27].

H. K. Venkatanarayanan et al. reported that the sulfate resistance of the RHA-based concrete cubes was greater than the control concrete cubes at 360 days [28].

Geopolymer Concrete. It is being reported that the Geopolymer concrete has greater sulfate resistance than the cement concretes as there is no free lime content. Geopolymer concrete shows greater sulfate resistance with increasing levels of RHA from 0 to 15% [29]. Yun YongKim et al. studied the behavior of Geopolymer mortar made up of RHA in sulfate environment and found the effective resistance of the specimens of RHA-based mortars toward sulfate attack [30].

6.3.2 Chloride Attack

Conventional Concrete. OPC concrete is comparatively porous in nature than RHA-based concrete; hence, it is more prone to the chloride attacks as the chloride ions tend to penetrate the concrete through these voids. RHA reduces the total volume of void ultimately making concrete impervious to chloride ion penetration.

The corrosion performance of concrete was studied with RHA content of 0, 5, 10, 15, 20, 25, and 30%, and it was notified that the concrete with 15, 20, 25, and 30% of RHA showed greater chloride resistance [31].

Geopolymer Concrete. The corrosion resistance of Geopolymer concrete improves when GGBS is replaced with RHA. P. V. Raman et al. conducted rapid chloride permeability tests (RCPTs) on Geopolymer concrete specimens containing 0, 10, 20, and 30% RHA [22]. The results of the experiment are charted below (Fig. 4).

7 Conclusions

Based on the studies and comparisons mentioned in the paper, we can reach on the conclusion that both Rice Husk Ash and silica fume enhance the properties of conventional as well as Geopolymer concrete. However, the impacts on strength and durability of these strength-enhancing materials are more significant in case of
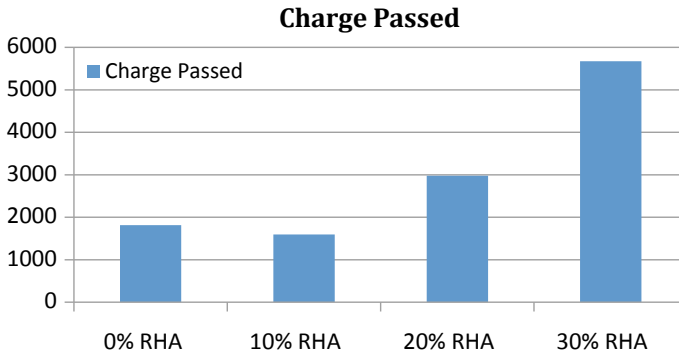
Fig. 4 Rapid chloride permeability test results with different % RHA (Ramani et al. [22])

Geopolymer concrete. These materials improve the properties of conventional concrete but it is not sustainable as concrete uses OPC as the primary binder. Hence, more efforts and extensive research are required to establish and implement Geopolymer concrete to promote sustainable development.

References

1. Global cement production from 1990 to 2013 (in million metric tons), ©Statista 2018.
2. McCaffrey, R. (2002). Climate change and the cement industry. *Global Cement and Lime Magazine* (Environmental Special Issue), 15–19.
3. Davidovits, J. (1988). Soft mineralogy and geopolymers. In *Proceedings of the of Geopolymer 88 International Conference*. Compiègne, France: Université de Technologie.
4. Moon, H. Y. (2003). Seung-Tae Lee, and Seong-Soo Kim, Sulphate resistance of silica fume blended mortars exposed to various sulphate solutions. *Canadian Journal of Civil Engineering, 30*, 625–636.
5. Okoye, F. N., Durgaprasad, J., & Singh, N. B. (2016). Effect of silica fume on the mechanical properties of fly ash based-geopolymer concrete. *Ceramics International*. http://dx.doi.org/10.1016/j.ceramint.2015.10.084.
6. Das, S. K., & Patel, A. (2018). *Potential of Rice Husk Ash in Concrete Production: A Literature Review, Second International Conference on Advances in Concrete*, Structural and Geo-technical Engineering, BITS Pilani, Rajasthan, India. https://www.researchgate.net/publication/324079453.
7. Mehta, P. K. (1992). Rice husk ash—A unique supplementary cementing material. In *Proceedings of the CANMET/ACI International Symposium on Advances in Concrete Technology*, ed. V. M. Malhotra, 407–430. Athens, Greece.
8. Nagrale, S. D., Hajare, H., & Modak, P. R. (2012). Utilization of rice husk ash. *International Journal of Engineering Research, 2*(4), 001–005.
9. Le, H. T. (2015). *Behaviour of rice husk ash in self-compacting high performance concrete* (Ph.D thesis). Institute for Building Materials Science, Bauhaus University Weimar, Germany.
10. Chao-Lung, H., Le Anh-Tuan, B., & Chun-Tsun, C. (2011). Effect of rice husk ash on the strength and durability characteristics of concrete. *Construction and Building Materials, 25*(9), 3768–3772.

11. Zerbino, R., Giaccio, G., & Isaia, G. C. (2011). Concrete incorporating rice-husk ash without processing. *Construction and Building Materials, 25*(1), 371–378.
12. Karthikeyan, A. (2013). *Influence of Silicafume in Self Compacting Concrete Under Its Fresh and Hardened State*, 7th Rilem Conference on Self Compacting Concrete, Paris, France. https://www.researchgate.net/publication/306285931.
13. Joshua Daniela, A., Sivakamasundaria, S., & Nishantha, A. (2017). Study on partial replacement of silica fume based geopolymer concrete beam behavior under torsion. *Procedia Engineering*. https://doi.org/10.1016/j.proeng.2016.12.162.
14. Srivastava, V., Kumar, R., Agarwal, V. C., & Mehta, P. K. (2014). Effect of silica fume on workability and compressive strength of OPC concrete. *Journal of Environment and Nanotechnology*. https://doi.org/10.13074/jent.2014.09.143086.
15. Chindaprasirt, P., & Chalee, W. (2014). Effect of sodium hydroxide concentration on chloride penetration and steel corrosion of fly ash-based geopolymer concrete under marine site. *Construction and Building Materials, 63,* 303–310.
16. Rostami, M., & Behfarnia, K. (2017). The effect of silica fume on durability of alkali activated slag concrete. *Construction and Building Materials*. http://dx.doi.org/10.1016/j.conbuildmat.2016.12.072.
17. Khedr, S. A., & Abou-Zeid, M. N. (1994, August). Characteristics of silica-fume concrete. *Journal of Materials in Civil Engineering, 6*(3), 357–375.
18. Kumar, P. C., & Rao, P. M. (2010). Benefits of use of rice husk ash in concrete. *Journal of Industrial Pollution Control, 26*(2), 239–241.
19. Ismail, M. S., & Waliuddin, A. M. (1996). Effect of rice husk ash on high strength concrete. *Construction and Building Materials, 10*(7), 521–526. https://doi.org/10.1016/0950-0618(96)00010-4.
20. Kumar, A., Tomar, A. K., Gupta, S. K., & Kumar, A. (2016, July). Replacement of cement in concrete with rice husk ash. *SSRG International Journal of Civil Engineering (SSRG-IJCE), 3*(7).
21. Zabihi, S. M., Tavakoli, H., & Mohseni, E. (2018). Engineering and microstructural properties of fiber-reinforced rice husk–ash based geopolymer concrete. *Journal of Materials in Civil Engineering*. https://doi.org/10.1061/(asce)mt.1943-5533.0002379.
22. Ramani, P. V., & Chinnaraj, P. K. (2015). Geopolymer concrete with ground granulated blast furnace slag and black rice husk ash. *Građevinar*. https://doi.org/10.14256/jce.1208,2015.
23. Dara, D. R., & Bhogayata, A. C. (2015). Experimental study of RHA-FA based geopolymer composites. *International Journal for Scientific Research & Development, 3*(4), ISSN (online): 2321-0613.
24. Ramakrishnan, S., Velrajkumar, G., & Ranjith, S. (2014, January). Behavior of cement-rice husk ash concrete for pavement. *International Journal of Emerging Trends in Engineering and Development*, 1(4), ISSN 2249-6149. http://www.rspublication.com/ijeted/ijeted_index.htm.
25. Mohamed Usman, M. K., & Senthil Pandian, M. (2014). Study on Fly Ash and Rice Husk Ash Based Geopolymer Concrete with Steel Fibre. *Civil Engineering Systems and Sustainable Innovations*, ISBN: 978-9383083-78-7.
26. RidhoBayuaji, M. F., Nuruddin, S., Francis, J. J., Ekaputri, T., Triwulan, S., & Subaer, H. (2015). Fansuri, mechanical properties of MIRHA-Fly Ash geopolymer concrete. *Materials Science Forum*. https://doi.org/10.4028/www.scientific.net/MSF.803.49.
27. Kamau, J., Ahmed, A., & Ngong, K. (2018). Sulfate resistance of rice husk ash concrete. *MATEC Web of Conferences 199*, 02006. https://doi.org/10.1051/matecconf/201819902006.
28. Venkatanarayanan, H. K., & Rangaraju, P. R. (2015). Effect of grinding of low-carbon rice husk ash on the microstructure and performance properties of blended cement concrete. *Cement & Concrete Composite, 55*, 348–363. https://doi.org/10.1016/j.cemconcomp.2014.09.021.
29. Bashir, S., & Saharan, S. (2017). Resistance of geopolymer concrete against Sodium Sulfate (Na_2SO_4) Solution. *International Journal of Engineering Research & Technology (IJERT)*, *6*(11). ISSN-2278-0181.

30. Kim, Y. Y., Lee, B. J., Saraswathy, V., & Kwon, S. J. (2014). Strength and durability performance of alkali-activated rice husk ash geopolymer mortar. *Scientific World Journal, 2014,* Article ID 209584.
31. Saraswathy, V., & Song, H. W. (2007). Corrosion performance of rice husk ash blended concrete. *Construction and Building Materials*. https://doi.org/10.1016/j.conbuildmat.2006.05.037.

A Parametric Study on Torsionally Coupled Base-Isolated Structures

Govardhan Bhatt

Abstract Extensive studies on the behaviour of base-isolated symmetrical structures have been carried out everywhere throughout the world. However, limited work has been reported on behaviour of base-isolated asymmetric structures. Because of torsion of stories in asymmetric structures, destructive effects on structures arise, during the earthquake. Consequently, on the grounds that asymmetric structures are progressively helpless against seismic burdens, researchers have given more consideration to the behaviour of such structures. In structures, mass asymmetry is typically present at various floor levels. This mass asymmetry might be because of water tank given at top of the structure, any overwhelming weight machine set at any floor level, etc. Because of this mass asymmetry in structure, the centre of mass does not correspond with the centre of stiffness causing unusualness. As the eccentricity increases, displacement and the torsion in the building will also increase (Colunga 2002). In this paper, torsionally coupled base-isolated buildings of different heights have been analysed for different spectrum compatible time histories of different code standards. A parametric study is presented and is very helpful to define base-isolated structures having torsional irregularity. The empirical equations obtained for structures are useful in estimating the displacement of the asymmetric structure, and further, it is useful for the adjustment required in the stiffness of base-isolated buildings so as to neutralize the effect of torsion.

Keywords Torsion · Base isolation · Eccentricity · Displacement · Earthquake spectrum

1 Introduction

In last two to three decades, examinations have been done on single- and multi-storey asymmetric structural models. A lot of research was carried out by many investigators. From the past examinations on asymmetric base-isolated structures,

G. Bhatt (✉)
Department of Civil Engineering, NIT Raipur, Raipur, Chhattisgarh 492010, India
e-mail: gov.ce@nitrr.ac.in

some conclusions have been drawn. The displacement response amplifications of the base isolation system of an asymmetric structure are compared with the response of a symmetric structure. It was demonstrated that the base displacement demand amplifications are eater for bigger eccentricities of the superstructure, and that they likewise rely upon the period of the isolated structure. It was again inferred that asymmetry decreases the viability of base isolation systems, since the more presented isolators will in general twist plastically, while the despite everything others stay flexible. It was additionally seen that the maximal base displacement is recorded for unidirectional eccentricity and not for bidirectional eccentricity as ay be normal. The impact of base isolation framework eccentricity is contemplated considerably more in detail. It is concluded that a higher eccentricity of base isolation system (>15%) has a negative base displacements effect than the superstructure eccentricity. As the eccentricity increases, results increase of displacement and the torsion in building [1]. Therefore, an eccentric base isolation system should not be utilized in building practice. It is brought up that greater torsional amplifications can be normal on account of a mass eccentric structure than on account of stiffness eccentric structures. Jangid and Datta [2, 3] surveyed the nonlinear reactions of lead elastic isolation systems in uneven structures for 20 world's well-known seismic earthquake records. They have inferred that the viability of base isolation is commonly decreased for higher eccentricities. Colunga and Gomez [1] reported that the torsional reaction of base-isolated structures when eccentricities are in the superstructure. Colunga [4] has investigated the torsional reaction of base-isolated structures when unidirectional and bidirectional eccentricities are in the superstructure. Hashemi et al. [5] have inspected the new technique for control and decrease of torsion with base isolation. They investigated the impact of torsion in seismic behaviour of base-isolated buildings with 5, 10, 15 and 20% mass eccentricities in unidirection. Therefore, the examination exhibited in this briefly outlines how the parameters depicted above effect explicit supportive structure parameters for isolators, such as peak displacements, ductility demands, and displacement. The variation of displacement in the superstructure in terms of ratio of maximum displacement and average displacement on different types of soil is also focused.

2 Modelling and Assumptions

2.1 Structural Model Considered

The three different cases of building models differing in the number of stories (3, 5 and 7) are considered for the study. The model of the building is shown in Fig. 1. The structure is normal in height and symmetric regarding two main orthogonal axes. The structure has four frames in each direction with a typical bay width of 7 m and a storey height of 3 m.
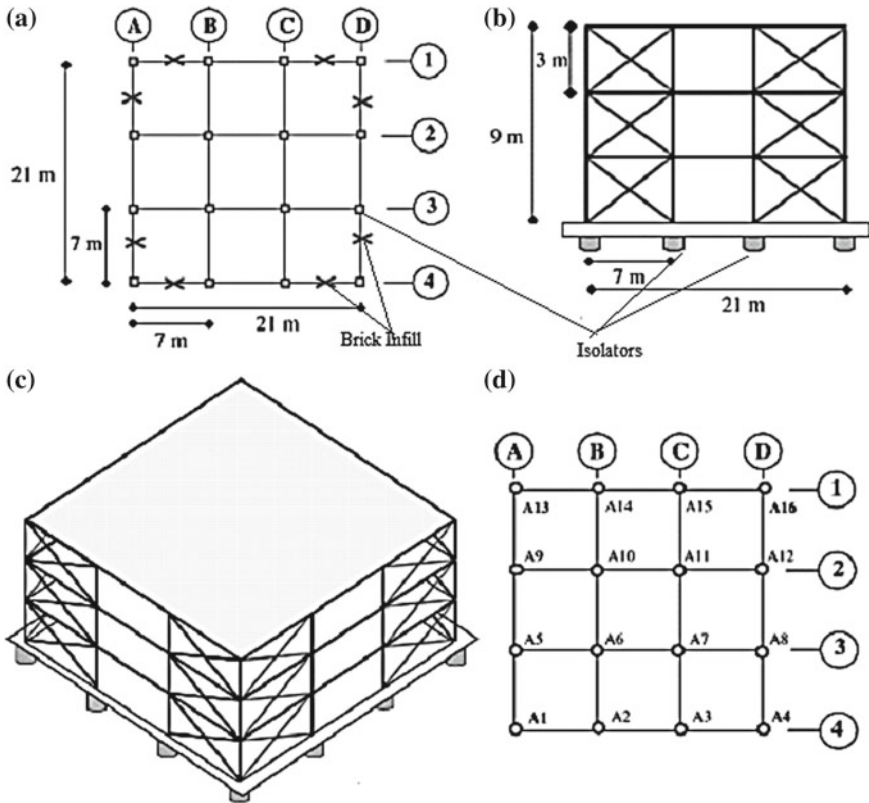
Fig. 1 Benchmark models: **a** plan, **b** elevation, **c** isometric view, and **d** isolation system

Square cross section is provided to typical reinforced concrete (RC) columns, and rectangular cross section is provided to RC beams. The static eccentricities e_s gotten by moving the centres of mass of the superstructure (CMs) from the centre of stiffness of the superstructure (CRs) and centre of stiffness of the isolation system (CS), which are situated in the geometric centre of the plan, as shown in Fig. 2. Static eccentricities (e_s) in the superstructure of 5, 10, 15 and 20% of the floor plan dimension (L = 21 m) were chosen. Configuration of building for five- and seven-storey buildings is maintained the same as in the case of three-storey building shown in Fig. 1. The characteristic strength of concrete is 25 N/mm². URM infill is considered in the modelling and is modelled as a diagonal strut element.

Properties of beams and columns for three-, five- and seven-storey buildings are given in Table 1. At all floor levels, beam elements and column elements are of the same size.
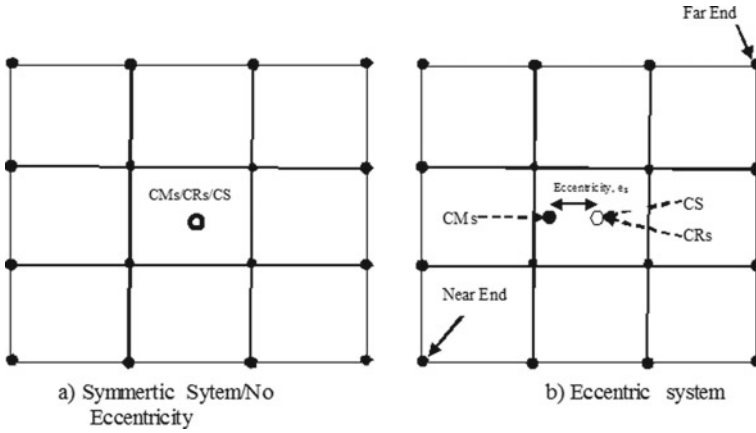
Fig. 2 Unidirectional eccentricity

Table 1 Geometry and material properties of the base-isolated structure

S. No.	No. of storey	Beams (m)	Columns (m)
1	Three	0.30×0.40	0.40×0.40
2	Five	0.35×0.45	0.50×0.50
3	Seven	0.50×0.62	0.62×0.62

2.2 Characteristics of the Bilinear Isolators

In this study, bilinear isolators with a post-yield stiffness ratio (K_e/K_2) of 10 is selected. The isolators are designed following some available recommendations of the ASCE 7, ASCE 41-06, NEHRP and Uniform Building Code (UBC-97). Buildings are supported by 16 elastomeric bearings, just below a rigid slab along each column line. Isolators are grouped into three categories based on the column load with no eccentricity or symmetric system. Isolators A1, A4, A13 and A16 are grouped in category 1, A2, A3, A5, A8, A9, A12, A14 and A15 are grouped in category 2 and A6, A7, A10 and A11 are grouped in category 3. Isolators are designed by considering the effect of soil conditions based on the soil amplification factors given in the code.

2.3 Selected Acceleration Records

Three ground motions of different magnitude and maximum acceleration are selected for the study. The ground motions details are given in Table 2. The ground motion acceleration records are selected based on the variation in the predominant frequencies and other parameters. Spectrum compatible time histories are generated for the

Table 2 Ground motions details selected for the time history analysis

S. No.	Name and year	Magnitude	Maximum acceleration (g)	Predominant period (sec)
1	Chi-Chi 1999	7.62	0.364	0.620
2	Kobe 1995	6.90	0.345	0.160
3	Northridge 1994	6.69	0.568	0.260

(a) IS 1893:2002 Hard soil/Rock   (b) IS 1893:2002 Medium soil
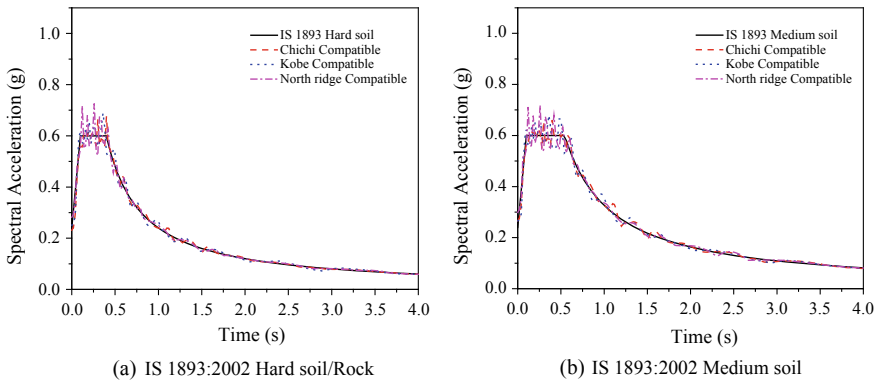
Fig. 3 Response spectra of compatible time histories

response spectra of IS 1893. Each case with two different types of soil scaled to Zone IV (0.24 g) is considered.

For IS 1893:2002, hard soil or rock and medium soil are considered. Spectrum compatible time histories and their response spectra are plotted and as shown in Fig. 3. The WAVEGEN code is utilized for the generation of spectra perfect time accounts. The computer code depends on the wavelet-based algorithm introduced by Mukherjee and Gupta [6].

3 Results and Discussion

By using computer program, SAP2000 response spectrum analysis has been carried out. It is noticed from the response spectrum analysis; the base-isolated periods in both the directions are increased from 2 to 2.5 times with the fixed base period. Nonlinear time history analyses are carried out for three different storey buildings. A total of 270 analysis cases are carried out using SAP 2000 [7] software to study the amplification of the roof displacement in terms of displacement ratio ($\Delta_{max}/\Delta_{avg}$). Displacement is measured at the roof at both ends (i.e. near and far ends, flexible side and stiffer side), and average of two displacements (Δ_{avg}) is taken. The ratio of
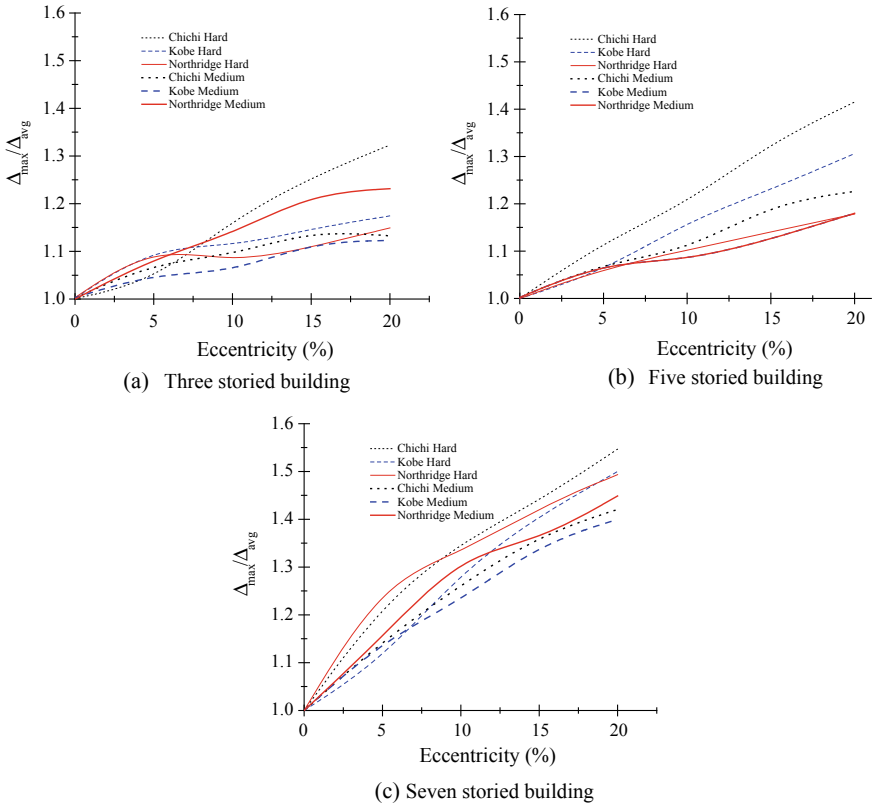
Fig. 4 Plot between the displacement ratio and the eccentricity for different stories

maximum displacement ($\Delta_{\max}$) of flexible end/far end and average displacement is plotted with respect to eccentricity (Fig. 4).

From the above plots, it is noticed that the displacement ratio increases with the increase in the eccentricity. Up to 10% eccentricity, there is not much increase in the displacement ratio and increases to 35 at 20% eccentricity. In all cases, variation of displacement is almost linear. Upper bound values and lower bound values for displacement ratio for different eccentricities are obtained from Eq. (1)

For IS 1893,

$$\Delta_{\max}/\Delta_{\mathrm{avg}} = 0.984 + 0.017\,e$$
$$\Delta_{\max}/\Delta_{\mathrm{avg}} = 1.008 + 0.006\,e \tag{1}$$

For Chi-Chi earthquake ground motion, the displacement ratio is almost linearly varying and is more than other two earthquake ground motions. Upper bound values and lower bound values for displacement ratio for different eccentricities are obtained from Eq. (2)

For IS 1893,

$$\Delta_{max}/\Delta_{avg} = 1.005 + 0.021\,e$$
$$\Delta_{max}/\Delta_{avg} = 1.011 + 0.008\,e \tag{2}$$

For seven-storey building, upper bound and lower bound values of the displacement ratio can be calculated using Eq. (3). Upper bound values of Chi-Chi are higher as compared to other earthquakes.

For IS 1893,

$$\Delta_{max}/\Delta_{avg} = 1.051 + 0.026\,e$$
$$\Delta_{max}/\Delta_{avg} = 1.024 + 0.020\,e \tag{3}$$

4   Concluding Remarks

Literatures on eccentricity of base-isolated building have been studied thoroughly, and some of the important highlights have been presented here. Torsionally coupled base-isolated buildings of different heights have been analysed for different cases. Nonlinear time history analysis using SAP 2000 for three-, five- and seven-storied buildings is carried out. Results are plotted in terms of ratio of maximum displacement to average displacement with respect to eccentricity.

1. It is noticed that the displacement ratio increases with the increase in the eccentricity in the building.
2. There is not much increase in the displacement ratio of three-storied building up to 10% eccentricity, and after that, displacement ratio increases to 35% of the average displacement at 20% eccentricity. In all cases, the variation of displacement is almost linear. In case of medium soil, variation in the displacement ratio of building is the same for Kobe and Northridge earthquakes.
3. In seven-storied building, the variation of displacement ratio, for Kobe and Northridge earthquakes for medium type of soil, is more compared to hard soil.
4. For all the three codes, equations are derived to obtain the upper bound and lower bound values of the displacement ratio.
5. A parametric study is presented in this chapter which is very helpful to define base-isolated structures having torsional irregularity. The empirical equations obtained for structures are useful in estimating the displacement of the asymmetric structure, and further, it is useful for the adjustment required in the stiffness of base-isolated buildings so as to neutralize the effect of torsion.

References

1. Tena-Colunga, A., & Gomez, S. L. A. (2002). Torsional response of base isolated structures due to asymmetries in the superstructure. *Engineering Structures, 24*(12), 1587–1599.
2. Jangid, R. S., & Datta, T. K. (1993). Non-linear response of torsionally coupled base isolated structure to harmonic excitation. *Structural Mechanics and Earthquake Engineering, JSCE, Japan, 10*, 139–148.
3. Jangid, R. S., & Datta, T. K. (1993). Seismic response of a torsionally coupled system with asliding support. *Journal of Structures and Buildings, Institution of Civil Engineers, UK, 99*, 271–280.
4. Tena-Colunga, A., & Cruz, E. J. L. (2007). Torsional amplifications in asymmetric base-isolated structures. *Engineering Structures, 29*(2), 237–247.
5. Hashemi, M. Y., Moghadam, A. S., Ziyaeifar, M., & Hosseini, M. (2008). *The method for control and reduction of torsion with base isolation*. The 14 WCEE, Beijing, China.
6. Mukherjee, S., & Gupta, V. K. (2002). *Wavelet-based generation of spectrum-compatible time-histories (WaveGen)*. IITKanpur, India: Software Reference manual.
7. Computer and Structures, Inc. (CSI). (2005). *CSI analysis reference manual for SAP2000*, Berkeley, CA.
8. IS: 1893 (Part 1)—2002. Criteria for earthquake resistant design of structures. *Bureau of Indian Standards*, 5th Revision, and New Delhi.
9. He, X., & Li, H. (2010). Torsionally coupled dynamic performance analysis of asymmetric offshore platforms subjected to wave and earthquake loadings. *Earthquake Engineering and Engineering Vibration, 9*(2), 247–258.
10. Jangid, R. S., & Datta, T. K. (1992). Seismic behaviour of torsionally coupled base isolated structure. *European Earthquake Engineering, Italy, VI*, 2–13.
11. Jangid, R. S., & Datta, T. K. (1994). Nonlinear response of torsionally coupled base-isolated structures. *Journal of Structural Engineering, ASCE, 120*(1), 1–22.
12. Nagarajaiah, S., Reinhorn, A. M., & Constantinou, M. C. (1993). Torsion in base isolated structures with elastomeric isolation systems. *Journal of Structural Engineering, ASCE, 119*(10), 2932–2951.

Stability Analysis and Bidirectional Vibration Control of Structure

Satyam Paul, Wen Yu and Raheleh Jafari

Abstract In the area of vibration control associated with structures, proportional-integral-derivative (PID) is considered to be an effective controller for the vibration attenuation scheme. Although the researchers prefer the use of PID controller but due to huge uncertainties in the structure, the control actions are not good. This paper depicts the application of combined PID control with Type-1 Fuzzy system for the compensation of the involved uncertainties. The main role of the Type-1 Fuzzy logic model is the identification of the uncertainties in the modeling equation and also to compensate it in an effective way. The methodology of Lyapunov stability criterion is implemented to validate the uniform stability of the closed-loop system. The synergistic combination of active mass damper (AMD), torsional actuator (TA), and Type-1 Fuzzy PID controller resulted in superior vibration attenuation which is validated by the experimental tests.

Keywords PID · Fuzzy logic · Vibration control

1 Introduction

A significant development within the area of structural engineering and control is demonstrated in [1]. The translation-torsion is an important phenomenon that is induced in the building due to the impingement of bidirectional earthquake and causes significant amount of damages to the building [2]. Exhaustive investigation reveals the importance of active devices in attenuation of vibration over the passive

S. Paul (✉)
School of Science and Technology, Örebro University, Örebro, Sweden
e-mail: satyam.controlsystems@gmail.com

W. Yu
Department of Automatic Control, CINVESTAV-IPN, Mexico City, Mexico
e-mail: yuw@ctrl.cinvestav.mx

R. Jafari
School of Design, University of Leeds, Leeds, UK
e-mail: jafari3339@yahoo.com

devices [3]. The important characteristics of PID controller are that it provides the necessary control effect without the background of the model information. PID controller is also favored for its simplicity and can be implemented without complexities [4]. Investigation suggests that PID controller has been used by the researchers working in the area of vibration control related to the structures, but the implications of lateral-torsional vibration were not considered. Even the uncertainty compensation was not given due importance.

In the vibration control of structure, fuzzy logic is considered to be one of the important techniques since it provides effective results with superior nonlinear mapping [5, 6]. In [7], the concept of semi-active control is utilized to achieve vibration attenuation in structure. The magnetorheological (MR) damper with fuzzy approach is implemented for the process. The innovative approach of Type-1 Fuzzy controller for mitigating seismic forces is utilized in the work of [8]. MR dampers in combination with an optimal Type-1 Fuzzy controller for structural vibration mitigation are illustrated in [9]. The application of hybrid mass damper with the Type-1 Fuzzy concept is proposed by [10].

This paper illustrates the effectivity of Type-1 Fuzzy PID control for the compensation of nonlinearity and superior vibration control. The effect of nonlinearity in structural stiffness is given due consideration while carrying out analysis. The Type-1 Fuzzy concept is implemented to deal with the involved nonlinearity, whereas the controller actions are generated using PID. A torsional actuator (TA) is composed of a disk and a motor and is utilized to mitigate structural torsional vibration. An active mass damper (AMD) which generates linear forces is used to mitigate the lateral vibration of the structure. The important conditions are derived using Lyapunov analysis which validates the stability of Type-1 Fuzzy PID controller. The controller gains are designed effectively based on the derived conditions. The experimental setup consists of two-floor structure with AMD and TA place on the top floor for suitable vibration minimization. The experimental results validate that significant vibration attenuation along both lateral and torsional directions can be achieved using Type-1 Fuzzy PID controller.

2   Bidirectional Modeling and Active Control

The mathematical model of n-floor structure can be represented by the equation [11, 12]:

$$M\ddot{X} + C\dot{X} + f_s = f_e \tag{1}$$

where $X \in R^n$, $M \in R^{n \times n}$, $C \in R^{n \times n}$. Also, $f_s = \begin{bmatrix} f_{s,1} \ldots f_{s,n} \end{bmatrix} \in R^n$ signifies structure stiffness force vector, and $f_e \in R^n$ represents external force vector implemented to the structure. The external forces which are bidirectional in nature generate torsional vibrations along with vibrations in x and y axes. The displacements of the

structure under the effect of the bidirectional force $f_e = \begin{bmatrix} f_x, f_y \end{bmatrix}$ have three components, $X = [x, y, \theta]^T$, where θ is the torsional component. Again the diagonal matrix $M = \text{diag}(M_x, M_y, J_t) \in R^{3n \times 3n}$, where $M_x = M_y = \text{diag}(m_1 \ldots m_n)$, m_i is the mass of the i-th floor, and $J_t = \text{diag}(m_1 r_1^2 \ldots m_n r_n^2)$ is illustrated as polar moment of inertia. In the situation where the structure is affected by very strong force resulting in the deformation of the structure beyond its limit of linear elastic behavior, then it is not possible to model the structure stiffness force f_s as a linear model. In this case, the Bouc–Wen model can be utilized to analyze the behavior of the structure. The relationship between forces and displacements can be validated using:

$$f_{\rho,i} = \epsilon_{\rho i} k_{\rho i} x_{\rho i} + (1 - \epsilon_{\rho i}) k_{\rho i} \varphi_{\rho i} \tag{2}$$

where $\rho = (x, y)$, $i = 1 \ldots n$, $\epsilon_{\rho i} > 0$. Equation (2) is comprised of elastic and non-elastic parts.

Figure 1 depicts the position of AMD and TA on the structure for suitable mitigation of external forces f_x and f_y which are bidirectional in nature. The placement of the AMD is favored over the mass center of the structure, whereas the position of the TA is on the structure physical center. $u = \begin{bmatrix} u_x, u_y, u_\theta \end{bmatrix}$ are the control forces along three components. The combination of structural model (1) with control force yields the following closed-loop system:

$$M\ddot{X} + C\dot{X} + f_s - f_e = \Gamma(u - d_u) \tag{3}$$

Here, u is the control signal which follows the condition $u \in R^{3n}$ and is transferred to the dampers for vibration attenuation. The dampers' location matrix is illustrated by Γ. Both AMD and TA have specific functions. The former is utilized to minimize
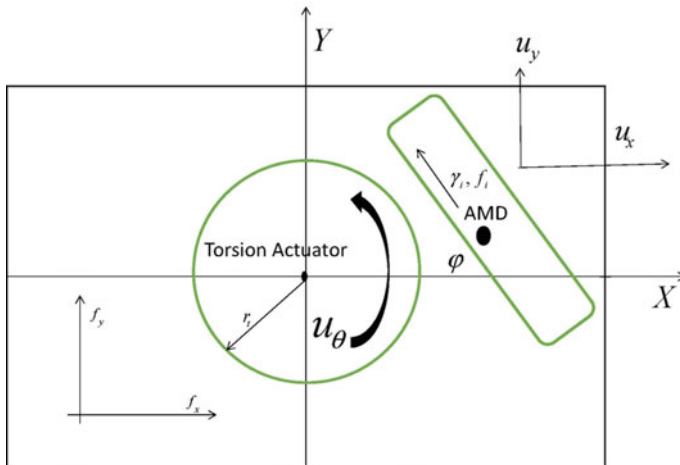
Fig. 1 Active control of bidirectional structures

the acceleration of structure along x and y directions, and the latter is utilized to mitigate the torsional aspects of the structure. The term $\boldsymbol{d_u}$ in Eq. (3) signifies the damping and frictional force vector illustrated as:

$$d_u = \begin{bmatrix} c\dot{x}_{i,x} + \epsilon m_{di} g \tan h\left[\beta \dot{x}_{i,x}\right] \\ c\dot{x}_{i,y} + \epsilon m_{di} g \tan h\left[\beta \dot{x}_{i,y}\right] \\ c\dot{\theta}_t + F_c \tan h\left[\beta \dot{\theta}_t\right] \end{bmatrix}$$

where m_{di} is the mass of the damper. The damping coefficient terms associated with the column friction are represented by c, β, and ϵ. Also, the Coulomb friction torque is represented by F_c. The hyperbolic tangent criteria $\tan h$ is dependent on two factors, namely the speed of motor and β. The velocities of AMD along x and y directions are represented by $\dot{x}_{i,x}$ and $\dot{x}_{i,y}$, whereas the angular velocity of TA is represented by $\dot{\theta}_t$.

3 Control Scheme of Type-1 Fuzzy PID Controller

The feedback criteria are the main aspects of PID controller with three appropriate actions. In order to increase the speed of response, P action is implemented. The D component is implemented for damping. The purpose of implementing I-action is to achieve required steady-state response [13]. The equation illustrating the PID control law:

$$\boldsymbol{u} = -K_p\left(X - X^d\right) - K_i \int_o^t \left(X - X^d\right) d\tau - K_d\left(\dot{X} - \dot{X}^d\right) \tag{4}$$

where K_p, K_i, and K_d are the gains. For the structure control considering $X^d = \dot{X}^d = 0$, (4) becomes

$$\boldsymbol{u} = -K_p X - K_i \int_o^t X d\tau - K_d \dot{X} \tag{5}$$

The mathematical model of the structure with embedded PID control:

$$M\ddot{X} + C\dot{X} + F = \Gamma\left(-K_p X - K_i \int_o^t X d\tau - K_d \dot{X}\right) \tag{6}$$

where the uncertainties are given by

$$F = f_s + f_e + \Gamma d_u \tag{7}$$

The nonlinear functions can be compensated precisely using the technique of fuzzy logic. A fuzzy compensation scheme which is adaptive in nature is utilized for the approximation of unknown nonlinearity. In Eq. (7), $F = [f_x, f_y, f_\theta]$ is not known and so the fuzzy logic technique will be implemented to approximate it. The fuzzy rules can be stated as, $Z = [x, \dot{x}]$.

$$R^l : If\ x\ is\ A_1^l\ and\ \dot{x}\ is\ A_2^l,\ then\ \hat{F}_f\ is\ B^l \tag{8}$$

where $l = 1, 2, 3 \ldots P$ is the rule index, A_1^l, A_2^l denote fuzzy sets assigned to x and $\dot{x}$, respectively, and B^l denotes fuzzy singletons assigned to the output $\hat{F}_f$ of the fuzzy model, where $\hat{F}_f$ is the estimation of F. Also, $\hat{F}_f(Z|W)$ is the fuzzy model output and can be illustrated as [14]:

$$\hat{F}_f = W\Phi(Z) \tag{9}$$

where $W = [W_1, \ldots, W_p]^T$ is the adjustable parameters' vector, $W_l = [W_{l1}, \ldots, W_{lp}]^T$, W_l is the point at which $\mu_{Bl} = 1$, $\Phi(Z) = [\phi_1(Z), \ldots, \phi_p(Z)]^T$.

$$\phi_i(Z) = \prod_{i=1}^{n} \mu_{A_{ji}} \bigg/ \left(\sum_{j=1}^{p} \prod_{i=1}^{p} \mu_{A_{ji}} \right) \tag{10}$$

where $\mu_{A_{ji}}$ is the membership functions of the fuzzy sets A_i^j in (8). For the membership functions, Gaussian functions are selected as

$$\mu_{A_{ji}} = \exp\left(\frac{-\|z_i - c_{ji}\|^2}{\rho_{ji}^2} \right) \tag{11}$$

where c and ρ represent the mean and variance of the Gaussian function, respectively. The modified control law utilizing (5) and (9) can be illustrated as:

$$u = -K_p X - K_i \int_o^t X d\tau - K_d \dot{X} - W_t \Phi(Z) \tag{12}$$

For stability analysis,

$$u = -K_p X - K_d \dot{X} - \xi - W_t \Phi(Z), \xi = K_i \int_o^t X d\tau, \xi(0) = 0 \tag{13}$$

The closed-loop system (3) with the fuzzy PID control (13) becomes

$$M\ddot{X} + C\dot{X} + f_s + f_e + \Gamma d_u = -K_pX - K_d\dot{X} - \xi - W_t\Phi(Z), \dot{\xi} = K_iX \quad (14)$$

In matrix form, the closed-loop system is

$$\frac{d}{dt}\begin{bmatrix} \xi \\ X \\ \dot{X} \end{bmatrix} = \begin{bmatrix} K_iX \\ \dot{X} \\ M^{-1}(C\dot{X} + F + K_pX + K_d\dot{X} + \xi + W_t\Phi(Z)) \end{bmatrix} \quad (15)$$

where F is denoted by (7). In order to estimate F, we will employ $W_t\Phi(Z)$ such as

$$F_t = W_t\Phi(Z)$$
$$F = W\Phi(Z) + \sigma(Z) \quad (16)$$

Using (16) in (15), we have

$$\frac{d}{dt}\begin{bmatrix} \xi \\ X \\ \dot{X} \end{bmatrix} = \begin{bmatrix} K_iX \\ \dot{X} \\ M^{-1}(C\dot{X} + W\Phi(Z) + \sigma(Z) + K_pX + K_d\dot{X} + \xi + W_t\Phi(Z)) \end{bmatrix} \quad (17)$$

The equilibrium of (17) is $[\xi_X, x, \dot{x}] = [\xi_x^*, 0, 0]$. Since at equilibrium point $x = 0$ and $\dot{x} = 0$, the equilibrium is $[\sigma(0), 0, 0]$. In order to move the equilibrium to origin, we
define

$$\hat{\xi} = \xi - \sigma(0) \quad (18)$$

For simplicity, only the analysis of $x-$ component is laid down, where $y-$ component and $\theta-$ component follow the similar trend. The final closed-loop equation considering $x-$ component is

$$M_x\ddot{x} + (C_x + \alpha_fC_{x\theta})\dot{x} + W_x\phi_x(Z_x) + \sigma_x(Z_x)$$
$$= -K_{px}x + K_{dx}\dot{x} - \hat{\xi}_x + \sigma_x(0)$$
$$\hat{\xi}_x = K_{ix}x \quad (19)$$

In order to analyze the stability of (19), we need the following properties

P1. The positive definite matrix $M = M_x = M_y$ satisfies the following condition where

$$0 < \lambda_m(M) \leq \|M\| \leq \lambda_M(M) \leq \bar{m}, 0 < \lambda_{jt}(J_t) \leq \|J_t\| \leq \lambda_{Jt}(J_t) \leq \bar{j}_t \quad (20)$$

where $\lambda_m(M)$ and $\lambda_M(M)$ are the minimum and maximum eigenvalues of the matrix M, respectively, and $\bar{m} > 0$ is the upper bound, $\lambda_{jt}(J_t)$ and $\lambda_{Jt}(J_t)$ are the minimum

and maximum eigenvalues of the matrix J_t, respectively, and $\bar{j}_t > 0$ is the upper bound.

P2. The term $\sigma(\tilde{x})$ is Lipschitz over $\tilde{x}$ and $\tilde{y}$

$$\|\sigma(\tilde{x}) - \sigma(\tilde{y})\| \le k_\sigma \|\tilde{x} - \tilde{y}\| \tag{21}$$

where k_σ is the Lipschitz constant. Most of the uncertainties are first-order continuous functions. Since f_s, f_e, and d_u are first-order continuous functions and satisfy Lipschitz condition, **P2.** can be established.

We calculate the lower bound of $\int \sigma$ as

$$\int_0^t \sigma(Z)dx = \int_0^t f_s dx + \int_0^t f_e dx + \int_0^t d_u dx - \int_0^t W\Phi(Z)dx \tag{22}$$

Here, we define the lower bound of $\int_0^t f_s dx$ as $-\bar{f}_s$, and $\int_0^t d_u dx$ as $-\bar{d}_u$

Compared with f_s and $-\bar{d}_u$, f_e is much bigger in the case of an earthquake. We define the lower bound of $\int_0^t f_e dx$ as $-\bar{f}_e$. Since $\Phi(Z)$ is a Gaussian function, $\int_0^t W\Phi(Z)dx = \frac{W}{2}\sqrt{\pi}\mathrm{erf}(Z)$.

$$k_\sigma = -\bar{f}_s - \bar{f}_e - \bar{d}_u - \frac{W}{2}\sqrt{\pi} \tag{23}$$

Here, $\sigma_x(0)$ is considered to be zero as it is concerned to building structures. The following theorem gives the stability analysis of fuzzy PID controller.

Theorem If the fuzzy PID controller mentioned in (12) is utilized to control the vibration of the structural system (3), then the asymptotic stability of the closed-loop system (19) will be validated at the equilibriums $[\xi_x - \sigma_x(0), x, \dot{x}]^T = 0$, where the updating law for the fuzzy compensator is

$$\frac{\mathrm{d}}{\mathrm{d}t}W_{tx} = -\left[k_w \emptyset_x(Z_x)_w^{-1}\left(\dot{x} + \frac{\gamma}{2}x\right)^T\right]^T \tag{24}$$

where k_w is a positive definite matrix and $\gamma > 0$ is a design parameter and so the control gain satisfies the followings

$$\lambda_m(K_{px}) \ge \frac{3}{2}\left[k_{\sigma_x} + \lambda_M(C_x) + \lambda_M(\alpha_f C_{x\theta})\right] \tag{a}$$

$$\lambda_M(K_{ix}) \le \frac{1}{6}\sqrt{\frac{1}{3}\lambda_m(M_x)\lambda_m(K_{px})}\frac{\lambda_m(K_{px})}{\lambda_M(M_x)} \tag{b}$$

$$\lambda_m(K_{dx}) \geq \frac{1}{4}\sqrt{\frac{1}{3}\lambda_m(M_x)\lambda_m\big(K_{px}\big)}\left[1 + \frac{\lambda_M(C_x) + \lambda_M\big(\alpha_f C_{x\theta}\big)}{\lambda_M(M_x)}\right](c)$$
$$- \lambda_m(C_x) - \lambda_m\big(\alpha_f C_{x\theta}\big) \tag{c}$$

Proof Here, the Lyapunov function is defined as

$$V_x = \frac{1}{2}\dot{x}^T M_x \dot{x} + \frac{1}{2}x^T K_{px}x + \frac{\gamma}{4}\hat{\xi}_x^T K_{ix}^{-1}\hat{\xi}_x + x^T\hat{\xi}_x + \frac{\gamma}{2}x^T M_x\dot{x} + \frac{\gamma}{4}x^T K_{dx}x$$
$$+ \int_0^t \sigma_x dx - k_{\sigma_x} + \frac{1}{2}tr_x\left(\hat{W}_x^T k_w^{-1}\hat{W}_x\right) \tag{25}$$

where $V_x(0) = 0$. Also, $\hat{W}_x = W_{tx} + W_x$. It implies that $\frac{d}{dt}\hat{W}_x = \frac{d}{dt}W_{tx}$. In order to show that $V_x \geq 0$, it is separated into three parts, such that $V_x = V_{x1} + V_{x2} + V_{x3}$.

$$V_{x1} = \frac{1}{6}x^T K_{px}x + \frac{\gamma}{4}x^T K_{dx}x + \int_0^t \sigma_x dx - k_{\sigma_x} + \frac{1}{2}tr_x\left(\hat{W}_x^T k_w^{-1}\hat{W}_x\right) \geq 0 \tag{26}$$
$$\text{Since, } K_{px} \geq 0, K_{dx} \geq 0$$

$$V_{x2} = \frac{1}{6}x^T K_{px}x + \frac{\gamma}{4}\hat{\xi}_x^T K_{ix}^{-1}\hat{\xi}_x + x^T\hat{\xi}_x \geq \frac{1}{2}\frac{1}{3}\lambda_m\big(K_{px}\big)\|x\|^2$$
$$+ \frac{\gamma\lambda_m(K_{ix})^{-1}}{4}\left\|\hat{\xi}_x\right\| - \|x\|\left\|\hat{\xi}_x\right\| \tag{27}$$

when $\gamma \geq \frac{3}{\left(\lambda_m(K_{ix})^{-1}\lambda_m\big(K_{px}\big)\right)}$,

$$V_{x2} \geq \frac{1}{2}\left(\sqrt{\frac{\lambda_m\big(K_{px}\big)}{3}}\|x\| - \sqrt{\frac{3}{4(\lambda_m\big(K_{px}\big))}}\left\|\hat{\xi}_x\right\|\right)^2 \geq 0 \tag{28}$$

And

$$V_{x3} = \frac{1}{6}x^T K_{px}x + \frac{1}{2}\dot{x}^T M_x\dot{x} + \frac{\gamma}{2}x^T M_x\dot{x} \tag{29}$$

also,

$$Y^T A X \geq \|Y\|\|AX\| \geq \|Y\|\|A\|\|X\| \geq \lambda_M(A)\|Y\|\|X\| \tag{30}$$

again when $\gamma \leq \frac{1}{2}\frac{\sqrt{\frac{1}{3}\lambda_m(M_x)\lambda_m\big(K_{px}\big)}}{\lambda_M(M_x)}$

$$V_{x3} \geq \frac{1}{2}\left(\sqrt{\frac{\lambda_m(K_{px})}{3}}\|x\| + \sqrt{\lambda_m(M_x)}\|\dot{x}\|\right)^2 \geq 0 \tag{31}$$

Now we have,

$$\frac{1}{2}\frac{\sqrt{\frac{1}{3}\lambda_m(M_x)\lambda_m(K_{px})}}{\lambda_M(M_x)} \geq \gamma \geq \frac{3}{\left(\lambda_m(K_{ix})^{-1}\lambda_m(K_{px})\right)} \tag{32}$$

The derivative of (25) is

$$
\begin{aligned}
\dot{V}_x = {} & \dot{x}^T\left[-C_x\dot{x} - \alpha_f C_{x\theta}\dot{x} - \sigma_x(Z_x) - K_{px}x - K_{dx}\dot{x} - \hat{\xi}_x + \sigma_x(0)\right] \\
& + \frac{\gamma}{2}x^T\left[-C_x\dot{x} - \alpha_f C_{x\theta}\dot{x} - \sigma_x(Z_x) - K_{px}x - K_{dx}\dot{x} - \hat{\xi}_x + \sigma_x(0)\right] \\
& + \dot{x}^T K_{px} + \frac{\gamma}{2}\hat{\xi}_x^T K_{ix}^{-1}\hat{\xi}_x + \dot{x}^T\hat{\xi}_x + x^T\hat{\xi}_x + \frac{\gamma}{2}\dot{x}^T M_x\dot{x} \\
& + \gamma x^T K_{dx}\dot{x} + \sigma_x(Z_x)\dot{x}^T - tr_x\left[\frac{\mathrm{d}}{\mathrm{d}t}\tilde{W}_x^T k_w^{-1}\left(\dot{x} + \frac{\gamma}{2}x\right)^T \emptyset_x(Z_x)\right]\tilde{W}_x \tag{33}
\end{aligned}
$$

The updating law for the fuzzy compensator is proposed as

$$\frac{\mathrm{d}}{\mathrm{d}t}W_{tx} = -\left[k_w\emptyset_x(Z_x)^{-1}\left(\dot{x} + \frac{\gamma}{2}x\right)^T\right]^T \tag{34}$$

Now if the fuzzy is tuned using (34), then we have

$$
\begin{aligned}
\dot{V}_x = {} & \dot{x}^T\left[-C_x\dot{x} - \alpha_f C_{x\theta}\dot{x} - K_{dx}\dot{x} + \sigma_x(0)\right] \\
& + \frac{\gamma}{2}x^T\left[-C_x\dot{x} - \alpha_f C_{x\theta}\dot{x} - \sigma_x(Z_x) - K_{px}x - \hat{\xi}_x + \sigma_x(0)\right] \\
& + \frac{\gamma}{2}\hat{\xi}_x^T K_{ix}^{-1}\hat{\xi}_x + x^T\hat{\xi}_x + \frac{\gamma}{2}\dot{x}^T M_x\dot{x} \tag{35}
\end{aligned}
$$

Using (30)

$$
\begin{aligned}
-\frac{\gamma}{2}x^T C_x\dot{x} &\leq \frac{\gamma}{2}\lambda_M(C_x)\left(x^T x + \dot{x}^T\dot{x}\right) \\
-\frac{\gamma\alpha_f}{2}x^T C_{x\theta}\dot{x} &\leq \frac{\gamma}{2}\lambda_M(\alpha_f C_{x\theta})\left(x^T x + \dot{x}^T\dot{x}\right) \tag{36}
\end{aligned}
$$

where $\|C_x\| \leq k_{C_x}$ and $\|C_{x\theta}\| \leq k_{C_{x\theta}}$. Since $\hat{\xi}_x = K_{ix}, \hat{\xi}_x^T K_{ix}^{-1}\hat{\xi}_x$ becomes $x^T\hat{\xi}_x$, and $x^T\hat{\xi}_x$ becomes $x^T K_{ix}$. Now using the Lipschitz condition (21)

$$\frac{\gamma}{2}x^T[\sigma_x(0) - \sigma_x(Z_x)] \leq \frac{\gamma}{2}k_{\sigma_x}\|x\|^2 \tag{37}$$

Using (21), (36), (37) in (35),

$$\dot{V}_x \leq -\dot{x}^T\Big[\lambda_m(C_x) + \lambda_m(\alpha_f C_{x\theta}) + \lambda_m(K_{dx}) - \frac{\gamma}{2}\lambda_M(M_x) - \frac{\gamma}{2}\lambda_M(C_x)$$

$$- \frac{\gamma}{2}\lambda_M(\alpha_f C_{x\theta})\Big]\dot{x} - x^T\Big[\frac{\gamma}{2}\lambda_m(K_{px}) - \lambda_M(K_{ix})$$

$$- \frac{\gamma}{2}k_{\sigma_x} - \frac{\gamma}{2}\lambda_M(C_x) - \frac{\gamma}{2}\lambda_M\alpha_f C_{x\theta}]x \tag{38}$$

So, $\dot{V}_x \leq 0$, $\|x\|$ minimizes if two conditions are met:

(1) $\Big[\lambda_m(C_x) + \lambda_m(\alpha_f C_{x\theta}) + \lambda_m(K_{dx}) \geq \frac{\gamma}{2}[\lambda_M(M_x) + \lambda_M(C_x) + \frac{\gamma}{2}\lambda_M(\alpha_f C_{x\theta}).$
(2) $\lambda_m(K_{px}) \geq \frac{2}{\gamma}\lambda_M(K_{ix}) + k_{\sigma_x} + \frac{\gamma}{2}\lambda_M(C_x) + \lambda_M(\alpha_f C_{x\theta}).$

Now using (32) and $\lambda_m(K_{ix}^{-1}) = \frac{1}{\lambda_M(K_{ix})}$, and also $\frac{2}{\gamma}\lambda_M(K_{ix}) = \frac{2}{3}\lambda_m(K_{px})$, we have (a), (b), and (c) which prove the theorem.

4   Experimental Analysis and Results

A two-floor structure is laid down experimentally in order to prove the effectiveness of Type-1 Fuzzy PID controller. The arrangement of building structure mounted on the shake table along with AMD and TA positions is shown in Fig. 2.

There is a requirement of the proposed controller to have knowledge of position and velocity data. From the accelerometer installed in the floors, accelerometer signals are extracted which are then fed to the numerical integrators to obtain the velocity and position signals. The angular accelerations are calculated from the value of positions and velocities along *x* and *y* components. This is achieved by identifying the structural parameters of the two-floor structure. Finally from angular accelerations by utilizing numerical integrator, angular velocity and angular position are

Two Storey Structure   Position of TA and AMD
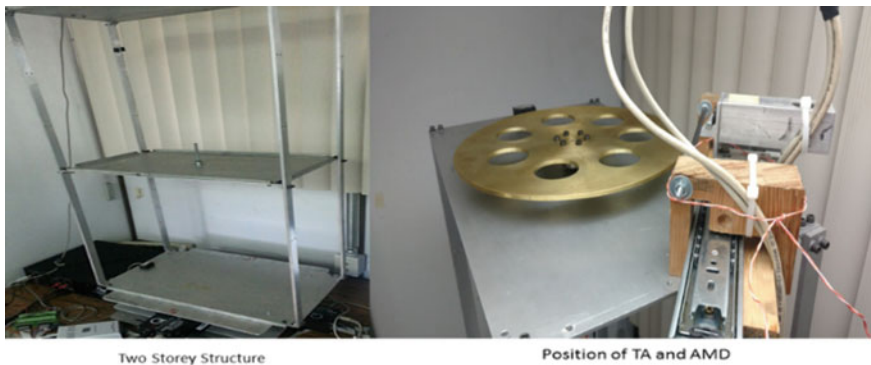
Fig. 2 Experimental setup with the placement of AMD and TA

extracted. It is very important to select the value of $k_{\sigma_x}, k_{\sigma_y}, k_{\sigma_\theta}$. These values are affected by the external force F. It is observed that the maximum force required to actuate the building structure prototype during experiment is 300 N. Therefore, we select the values $k_{\sigma_x}, k_{\sigma_y}, k_{\sigma_\theta} = 400$. Applying these values and from theorem, we have

$$K_{px} = 1800, K_{py} = 2000, K_{p\theta} = 2200, K_{dx} = 160, K_{dy} = 220,$$
$$K_{d\theta} = 300, K_{ix} = 2000, K_{iy} = 2300, K_{i\theta} = 3500 \tag{39}$$

The Northridge earthquake is taken as sample and fed into the shake table for creating the vibration on the two-floor structure. The analysis is carried on the basis of vibration on the structure, and the Type-1 Fuzzy PID controller is used for the control signals which perform superiorly well. The performance of the controller is evaluated on the basis of what extent the controller is able to mitigate vibration on each floor. Gaussian functions are considered for membership function of the fuzzy controller. The design aspect considered in this case is mentioned in the work of Guclu [15]. Three membership functions are utilized in order to convert the position and velocity into linguistic variables. The normalization of position inputs and velocity inputs associated with the fuzzy technique is carried out in the form $Z \in [-1, 1]$. A number of experiments are conducted to establish that minimal regulation error can be maintained with nine rules. In the adaptive rules (24), $\gamma = 6$. In this paper, the attenuation of vibration along x and θ components is shown. The results of the vibration attenuation are shown in Figs. 3 and 4. The signal associated with Type-1 Fuzzy PID control is illustrated by Fig. 5.

From Figs. 3 and 4, it can be observed that the controller is capable enough to reduce vibration to significant level. The combination of AMD and TA with Type-1 Fuzzy PID displays superior performance. The torsional vibration minimization is achieved more efficiently using TA. Finally, it is validated that most effective results were observed when both AMD and TA were utilized in combination for vibration mitigation.
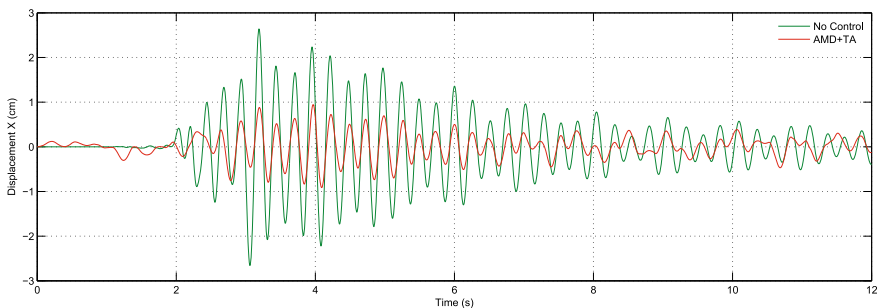
Fig. 3 Vibration attenuation using Type-1 Fuzzy PID (x direction—second floor)
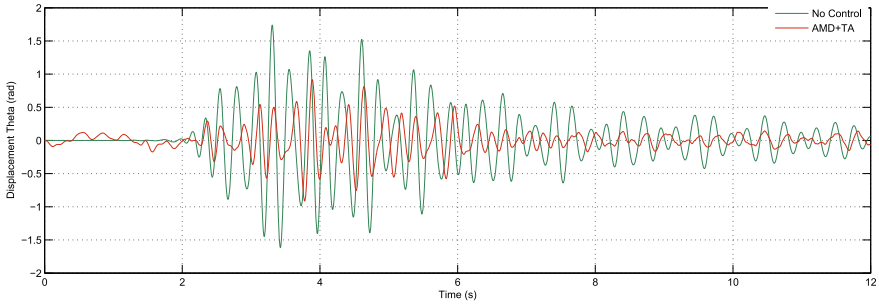
Fig. 4 Vibration attenuation using Type-1 Fuzzy PID (θ direction—second floor)
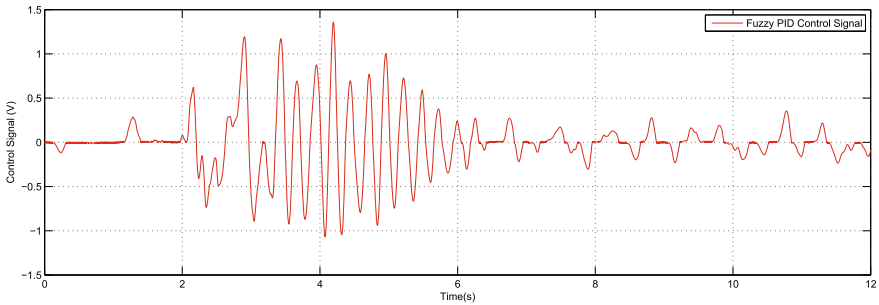
Fig. 5 Type-1 Fuzzy PID control signal

5   Conclusion

In this paper, an active control strategy was implemented and the control of vibration in the two-floor structure model is analyzed. Lyapunov stability analysis is carried to prove that the proposed Type-1 Fuzzy PID controller is within the stable zone and capable enough to suppress the vibration in two-floor structure. Also the illustrated theorem gives the conditions for tuning the Fuzzy and PID gains. Superior vibration attenuation is observed when both AMD and TA worked simultaneously.

References

1. Yao, J. T. P. (1972). Concept of structural control. *Journal of the Structural Division, 98*(7), 1567–1574.
2. Lin, J. L., & Tsai, K. C. (2008). Seismic analysis of two-way asymmetric building systems under bi-directional seismic ground motions. *Earthquake Engineering & Structural Dynamics, 37*(2), 305–328.
3. Soong, T. T. (1999). *Active structural control: Theory and practice*. New York, USA: AddisionWesley.

4. Astrom, K. J., Hang, C. C., Persson, P., & Ho, W. K. (1992). Towards intelligent PID control. *Automatica, 28*(1), 1–9.
5. Chien, Y.-C., & Teng, C.-C. (1993). Fuzzy modeling using neural networks. In J. W. Nieuwenhuis (Ed.), *Proceedings of the European Control Conference* (pp. 503–508). Groningen, The Netherlands: ECC.
6. Mei, F., Man, Z., & Nguyen, T. (2001). Fuzzy modelling and tracking control of nonlinear systems. *Mathematical and Computer Modelling, 33*(6), 759–770.
7. Das, D., Datta, T. K., & Madan, A. (2012). Semiactive fuzzy control of the seismic response of building frames with MR dampers. *Earthquake Engineering and Structural Dynamics, 41,* 99–118.
8. Duc, N. D., Vu, N. L., Tran, D. T., & Bui, H. L. (2012). A study on the application of hedge algebras to active fuzzy control of a seism-excited structure. *Journal of Vibration and Control, 18*(14), 2180–2200.
9. Ali, S. F., & Ramaswamy, A. (2009). Optimal fuzzy logic control for MDOF structural systems using evolutionary algorithms. *Engineering Applications of Artificial Intelligence, 22*(3), 407–419.
10. Ahlawat, A. S., & Ramaswamy, A. (2002). Multiobjective optimal FLC driven hybrid mass damper system for torsionally coupled seismically excited structures. *Earthquake Engineering & Structural Dynamics, 31*(12), 2121–2139.
11. Chopra, A. K. (2011). *Dynamics of structures-theory and applications to earthquake engineering* (4th ed.). Prentice-Hall International Series.
12. Paul, S., Yu, W., & Li, X. (2016). Recent advances in bidirectional modeling and structural control. *Shock and Vibration, 2016* (Article ID 6275307).
13. De Cock, K., De Moor, B., Minten, W., Van Brempt, W., & Verrelst, H. (1997). A tutorial on PID-control, Katholieke Universiteit Leuren Department of Electrical Engineering ESAT-SISTA/TR, 1997–08.
14. Wang, L. X. (1994). *Adaptive fuzzy systems and control: Design and stability analysis.* Englewood Cliffs, NJ: PTR Prentice Hall.
15. Guclu, R., & Yazici, H. (2008). Vibration control of a structure with ATMD against earthquake using fuzzy logic controllers. *Journal of Sound and Vibration, 318*(1–2), 36–49.

Sustainable High-Performance Cementitious Composites

K. Ganesh Babu and B. Chandrasekhar

Abstract The need for an acceptable performance of structural facilities over its entire lifetime need never be overstressed. In fact, the performance of a well-designed structural member is always defined with the performance of the materials of construction in the environmental regime in which it is situated. In addition, it may be too far-fetched to generalize the requirements and still find appropriate material compositions or systems that are suitable for all applications even in the built space. In the present context, it is felt prudent to look for appropriate solutions for the single most ubiquitous construction material, concrete, which could result in high performance in the most severe natural environment of the oceans as well as the highly industrialized and polluted urban localities. It was also felt necessary that one should look at the possible avenues only for the most commonly used structural concretes of normal strength range for construction requirements of small- and medium-range infrastructural facilities which do not have adequate quality assurance and quality control mechanisms in place.

Keywords Concrete · High performance cementitious materials · Environment · Structures · Sustainability

1 Introduction

The performance of structural materials is a matter of paramount importance, not just in the built environment alone, but also to the entire range of fabricated structural systems including in applications related to aerospace and ocean engineering fields. This is because these facilities are all exposed to the vagaries of the environmental forces on which there can be no control like in the case of hermetically sealed or

K. Ganesh Babu (✉)
Mahindra Ecole Centrale, Hyderabad, Telangana, India
e-mail: kgbabu18@yahoo.com

B. Chandrasekhar
GITAM University, Hyderabad, Telangana, India
e-mail: sekharbhojaraju@gmail.com

appropriately controlled environments in other applications. Even the built infrastructure itself may be located in the environmental extremes of hot and humid to the cold and freezing apart from the other extremes of caustic industrial to the ocean environment. In this context, it is only appropriate to look for the right choice of the material that can adequately perform in a given environment over the entire lifespan of the structural facility.

The present paper is an effort to introduce the subject of both performance and sustainability in relation to the most commonly used and conventional normal strength concrete composites. It also presents a general outline indicating how the various aspects that are being discussed will have to be reassessed either for a much higher strength grade, or for the applications in highly aggressive environments of the oceans or the industry. In a way, it lays the foundation for an appropriate recognition of the various parameters that influence the performance and the role of material compositions to address the aspects of sustainability. It also tries to present an outline on a methodology for assessing any specific composition to ensure that it satisfies the requirements of performance and the limitations after having chosen the cementitious material combination to ensure sustainability.

2   Concrete Compositions

Concrete has undergone several changes over the years due to the fact that it can still be made with a very large proportion of locally available materials, while only a small fraction of the factory produced cement is required. This fact is obviously very much underplayed and if not unrecognized by the proponents of the several probable alternatives that were suggested over the years. Moreover, if one takes a glance on the several modifications that occurred over the millennia, starting from the lime compositions one can always observe that not only the cementitious compositions have significantly changed due to the several insights into their hydration mechanism and also the more modern manufacturing technologies that came into existence. Even the appropriate gradation and proportioning methodologies of recent times enabled the concrete strength, a parameter that is often taken to be the yardstick of all its performance and utilization potential. Some of the broad strength ranges for the structural concretes that have come into existence over the past five decades could be listed as the following, particularly to be in line with the different national recommendations that are in vogue today (ACI 211.1-4).

- Normal, Heavyweight, Mass concretes: 15–45 MPa
- Lightweight concretes: 15–40 MPa
- No-slump concretes: 15–50 MPa
- High strength concrete: 50–85 MPa.

Other than these recommendations for conventional concretes, there are guidelines presented for several other types of concretes like polymer concrete, sulphur concrete, ultrahigh-performance concrete, over a wide strength range, apart from the general

"guidelines for reporting details of concrete". Notwithstanding this, there have been several other advancements in concrete technology, with the advent of better cements, superplasticizers and mineral admixtures along with better mixing compaction and curing resulting compositions that exhibit much higher strengths. A broad outline of these, as referred to in literature, could be the following.

- Very high strength concretes: 85–120 MPa
- Super high strength concretes: 120–150 MPa
- Ultrahigh-performance concretes: 150–250 MPa.

There have been several other compositions much higher strength reported in the literature, and most of these use high-efficiency pozzolanic materials and the most modern poly (carboxylic ester)-based superplasticizers of today, along with specially designed high strength microfibers in their production.

Looking back at this broad development strength itself, the marginal strength structural concretes (20–50 MPa) of about half a century back have given way to several options with strengths possible excess of almost a 100 MPa in the constructions of today. In fact, the research community is conventionally talking in terms of almost 200 MPa, compared to the 20 MPa that is most ubiquitous and application even today, though one could make the same with much less cement, the most expensive component in the concrete production. Incidentally, it is the interest of the research community to look for and go into the depths of the mechanisms in the making of high and ultrahigh strength concrete composites, because of the enormous opportunities that it provides for recognition and esteem in professional circles. However, the often-neglected fact is that the marginal strength structural concretes, particularly in the lower range of about 30 MPa, are still the most utilized if not required for a wide range of the constructed facilities.

3   Environmental Regimes and Performance Requirements

An important often much talked about aspects about concretes is also their performance particularly in terms of the life cycle cost. However, it is essential to recognize that the performance of the material is a parameter that is primarily dependent upon the environmental ingress in which it is located. It is often never really necessary to look for the most exotic and expensive compositions for several of the general-purpose applications, but it is essential to ensure that the chosen material should still perform adequately over the complete design life of the structural facility.

At this stage, it is probably be appropriate to understand the environmental exposure classes that are internationally recognized along with their relevance in terms of their effects and possible situations in which they are broadly applicable. While there are several such environmental classifications are available, presented below is the one that was proposed in the Euro standards (Table 1).

Table 1 Outline of the exposure classes and effects on concrete [1]

Exposure class	Environmental attack	Applicable situations	Possible effects
XO	Nil	Foundation levelling course	None
XC	Carbonation	Building structural members, walls, slabs, drains	Corrosion of reinforcement
XD/XS	Chloride ingress/Ocean environment	Bridge railings, ocean atmosphere, inter-tidal, splash and submerged zones	Corrosion of reinforcement
XF	Freeze–Thaw/ + deicing salt	Structural members exposed to frost, Bridge members exposed to deicing salts	Corrosion of reinforcement Sulphate attack, freeze/thaw effect
XA	Chemical attack	Industrial process liquids and gases	Chemical attack
XM	Wear	Roads, industrial floors	Abrasion and erosion

4 General-Purpose Structural Concretes

A more fundamental and broader discussion on the various parameters that affect the strength of concrete as well as the environmental regimes and the methodology of ensuring high-performance cementitious composites was presented earlier [2].

Incidentally, even in the harshest of environmental zones, there are several constructed facilities that probably do not require a very high strength from structural considerations. However, from an environmental perspective there is a need that concretes have to be designed to ensure that the different chemicals do not permeate deep into the concrete to promote the corrosion of steel in concrete or destroy the integrity of the concrete otherwise. Naturally, the primary objective is to limit the environmental ingress through a control on the porosity and permeability of the concrete mass and in particular the cover concrete. It may not be possible to explain, in detail, the extremely complex pore system and its influence on the strength as well as the durability characteristics of concrete in such a short reporter as this. One of the simplest methods of ensuring some level of control is by enforcing the different strength levels required for protection in each environmental zone. It is obvious that such a control is only possible through a limitation on the maximum water–cement ratio permissible. Apart from this to ensure that the concrete serves adequately over the lifetime of the structure inside of the degradation that takes place over the period, the minimum cement content is to be ensured.

In view of this for ensuring the durability of adequately designed structural components in the different environmental zones, the Euro norms [1] prescribe the specific requirements and are also the case with other national recommendations. These are

- maximum water–cement ratio,

- minimum cement content, and
- minimum compressive strength class.

Even so, it is recognized that the parameters are not mutually exclusive though each of them caters to a different aspect of the performance criteria as already discussed above. However, the most important of all these are probably the water–cement ratio which influences directly the permeable porosity of the system that largely controls the durability and performance. Given the fact that the consistency of concrete depends on the water content in most normal concrete compositions which are already specified in the various national recommendations, the cement content is obviously a broad a prescribed quantity. Apart from this even if there are other pozzolanic admixtures permitted in these recommendations, the effective cementitious material content is also quite obvious and thus the compressive strength. It may probably be most appropriate to actually fix the recommendations on the maximum and minimum requirements presented above in consonance with each other. Moreover, an additional requirement which is also known from the various national bodies is the minimum clear cover to reinforcement. It may be appropriate to specify this also along with recommendations for the above for the various environmental zones that are envisaged. It may be appropriate to once again look at the recommendations for these parameters and discusses their relevance as well as specifies how they should be viewed in relation to the wide variety of constituent materials utilized for the making of concretes in practice. Discussions below reflect broadly the well-accepted recommendations of the latest Euro norms which are probably best suited from almost all considerations.

5   Maximum Water–Cement Ratio

The maximum water to effective cement ratio, and not the water to cementitious material ratio as perceived and advocated by a few, is the fundamental parameter on which the porosity of the concrete composite depends. It is essential to recognize the effective cementitious contribution of any pozzolans adopted either in the making of the cement or as a part of the constituent materials in the concrete production. There are specific guidelines available for such an evaluation in at least a few of the national recommendations which could be used appropriately.

6   Minimum Cement Content

The minimum cement content is the one that is often confused with the cementitious material content. The Euro norms specifically require that the values specified are only the cement part of the cementitious materials, and even in case of pozzolanic cements or additions, the minimum cement content required shall be the reduced

effective cementitious material (reduced to the specified lower values prescribed under the effective cementitious material component in [1] considering the efficiency specified therein) in the concrete mixture.

7 Minimum Compressive Strength

The compressive strength in a general way was taken to be the cube compressive strength, which is also used in the Euro norms. The compressive strength in itself is a definite parameter and in the best way to arrive at the probable value is to use the relationship between the compressive strengths and the effective water–cementitious material ratio and not the water–cement ratio or water–cementitious material ratio.

8 Minimum Clear Cover

While the about three parameters primarily related to the cementitious material content, this requirement ensures that there is sufficient time for the environmental front to reach the reinforcement level, particularly chlorides and carbonation, so that reinforcement corrosion does not take place. This in fact is like a barrier coating on the reinforcing steel, and the ingress of the environment, dependent on the porosity and permeability of the concrete cover, defines the appropriate thickness of the cover.

In conclusion, a broad outline of the recommendations for the general-purpose concretes of normal strengths (lower strengths) is being presented, considering both the strength and porosity requirements and the economy. Maybe it is only appropriate to mention at this particular stage that these recommendations are presented as guidelines for general construction practice in field at present. However, it is obvious and is also recognized that there are specialized construction practices relevant to prefabricated constructions, very high strength and high-performance concrete requirements in specific cases, which will all have to be addressed appropriately through a clear delineation of the various requirements to ensure the specific performance requirements of the concrete composites at the various stages of construction, apart from its overall performance over the entire life of structure (Table 2).

Finally, it is only appropriate to look at the present Indian scenario and critically examine how the recommendations in them correlate with the Euro and international norms. In the first place, it is probably just to recognize that the codal recommendations are for practicing engineers who are not to be burdened with the additional task of having to understand why and how these specifications came into existence, while implementing the same scrupulously. A couple of aspects need probably a specific mention at this point, which was already discussed in a previous publication [3].

- Simply put, it is essential that the cement strength should be established at the specific water–cement ratio 0.50 as adopted by most international specifications.

Table 2 Probable recommendations for normal structural concretes [3, 4]

S. No.	Type of concrete	Max.%—Pozzolan (%)	Slump/flow* (mm)	sp[b] (%)	Min. cem.[a] (Kg/m^3)	Max. water	Max.w/c	Cube Strength (MPa)
1. **General-purpose concretes of lower strengths** (generally with fly ash or GGBS) (20–50 MPa; w/cm ~ 0.45–0.75; Low-end pozzolans only; Max. 25 mm graded aggregate)							–	
1.1.	OPC concretes	0	Extremely Dry–150	1.0–2.0	240–320	150–200	0.75/0.45	20–50
1.2.	Plasticized concretes	0	50–150					
1.2.	Pozzolanic concretes	30-F/50-G	Extremely Dry–150					
1.4.	Flowing concretes	30-F/50-G	150–200					
1.5.	HPC	30-F/50-G	100–200					
1.6.	SCC	30-F/50-G	500–650					

[a] Minimum effective cementitious material content corrected taking into account the efficiency prescribed in EN 206-1, 2000 and not the total cementitious materials

[b] Superplasticizer content as a percentage of the total cementitious materials

Note All aggregates should be appropriately graded to ensure good packing characteristics

- Furthermore, the strength to water–cement ratio relationship suggested should also comply with the specifications as given by the Euro norms for the corresponding cement's strengths grades appropriately.
- In this context, the design strength and target strength values essential for structural construction should also not be confused with and be appropriately recognized by both concrete suppliers and RMC manufacturers.
- Some of these problems arise from either in an appropriate interpretation of the available knowledge or maybe sometimes from simple business considerations.

9   Concluding Remarks

The principal aim of the present paper is to look at the broad perspective of the ubiquitous and most general-purpose concrete mixtures for the different mundane and common applications in field today. It tries to take stock of the broad spectrum of structural concretes strengths possible, while limiting its discussions to the requirements of achieving a reasonably economical and performance effective concrete compositions that are relevant to the various environmental zones in which the structures could be situated. It tries to delineate the various parameters that could influence the structural components in the various environmental zones and the effects of such influence itself. Finally, a very brief and comprehensive outline of the recommendations for ensuring a reasonable performance of normal concrete constructions in any of these environmental zones was also attended, particularly while ensuring that these recommendations are in line with the Euro norms that came into existence in the recent past.

References

1. EN 206-1. (2000). Concrete—Part 1: Defnitions, specifcations and quality control, European Committee for Standardization, Brussels, Belgium, 74pp.
2. Ganesh Babu, K. (2018). *High performance self-consolidating cementitious composites*. CRC Press, Taylor & Francis Group, 6000 Broken Sound Parkway NW, Suite 300, Boca Raton, FL 33487-2742, USA, 451pp.
3. Ganesh Babu, K. (2018, August). *Options for the sustainability of cement and concrete composites, All India Seminar on Recent Developments in Concrete Composites (RDCC-2018)* (pp. 24–25). Hyderabad: The Institution of Engineers (India).
4. Grube, H., Kerkhoff, B., & DIN EN 1045-2. (2001). The new German concrete standards DIN EN 206-1 and DIN EN 1045-2 as basis for the design of durable constructions. *Beton, 51*(3), 19–28.
5. ACI 211.1-91. (1997). Standard practice for selecting proportions for normal, heavy-weight, and mass concrete, ACI Manual of Concrete Practice. American Concrete Institute, Farmington Hills, MI, 38pp.

6. ACI 211.2-98. (1998). Standard practice for selecting proportions for structural lightweight concrete, ACI Manual of Concrete Practice, American Concrete Institute, Farmington Hills, MI, 18pp.
7. ACI 211.3R. (1997). Guide for selecting proportions for no-slump concrete, ACI Manual of Concrete Practice, American Concrete Institute, Farmington Hills, MI, 30pp.
8. ACI 211.4R-93. (1998). Guide for selecting proportions for high-strength concrete with Portland Cement and Fly Ash, ACI Manual of Concrete Practice, American Concrete Institute, Farmington Hills, MI, 38pp.

What Makes Concrete a Possible Contender for Sustainable Development?—A Panoramic View

K. Ganesh Babu and Y. Amarnath

Abstract Concrete has served as a rival material of construction not just over the past hundred years alone but also in some format or the other has been in existence from times immemorial. The present effort is to look at the broad panorama of its development, in general, and to look at the various facets of its more recent modulations to see how it is coping up with the requirements of sustainability. One of the objectives is not just to concentrate only on the so-called use of materials like supplementary cementitious materials and demolition wastes, but to look at comprehensively in all different formats to ascertain its capacity to perform as a sustainable material of construction. In principle, this would mean that the concrete composites of high strength or even ultra-high strength apart from the other modulations in between have all got to be carefully analyzed and demarcated, for an appropriate utilization ensuring sustainability, particularly in the Indian scenario.

Keywords Concrete · Durability · High Performance Concrete · Sustainable Development · Ultra High Performance Concrete

1 Introduction

It is not hyperbole if it is said that material science is the engine that drives the advancements in civilization, facilitating at least supposedly the living comfort of human society. There is a lot of telltale evidence about the enormous wealth of knowledge that many of the ancient civilizations exhibited which are still not clearly understood are explained in several cases. The present-day standing of science and technology can be attributed to the seedlings of our forefathers around the eighteenth

K. Ganesh Babu (✉)
Retired Professor, Indian Institute of Technology, Chennai, Tamilnadu, India
e-mail: kgbabu18@yahoo.com

Y. Amarnath
Srinivasa Ramanujan Institute of Technology, Anantapurm, Andhra Pradesh, India
e-mail: y.amarnath@gmail.com

century followed up and nurtured by the efforts in the nineteenth century, culminating in phenomenally rapid advancements during the twentieth century, though a lot attributed to the influence and urgency during the two World Wars. Even so, the two most prominent materials of construction happen to be steel and concrete which often is vie for a position of dominance driven by speed of construction and off-site fabricability in the case of steel compared to the economy and use of locally available materials of concrete. Simply speaking, the carbon footprint of both significances as their use in terms of quantity is phenomenal increasing with the increasing urbanization of society. However, if appropriately assessed and judiciously adopted, the concrete has several advantages over its nearest rival the steel with its different possibilities, particularly the inexpensive maintenance and substantial lifespan of structures built with it.

The need for an appropriate recognition of the characteristics of a material is probably the most important aspect of its sustainable utilization in general. Concrete, accepted to be the largest produced construction material and in a way is considered to be one of the yardsticks of the standard of living of a community, was purported to be a material of the past several times during its long history. However, its resurgence in many other forms and modifications apart from the strides it made it possible strength levels always endeared researchers to look at it with fascination if not admiration. Even so, there are several factors that are often not so clearly understood even in its conventional utilization, naming it to be the primary culprit for all the inadequate and inappropriate practices adopted. This paper tries to project broadly some of the more important aspects of the need for an appropriate understanding of the various concrete alternatives possible and their utilization potential for the diversion needs of society today.

2   Concrete Is Innately Sustainable?

It is often forgotten that in spite of the several significant advancements in materials science, more importantly metals and composites, it is still concrete that occupies the pride of possession as the most preferred construction material for most structures, starting from the mundane to reach the most exalted heights like *Burj Khalifa in* Dubai. Some *simple facts* about the characteristics of *concrete structural members* in comparison with the most preferred alternative *steel* could be simply listed as the following:

- Concrete can be *appropriately reinforced* to account for the tensile stresses, and it can be produced in innumerable *number of strength grades*.
- It can accommodate in its bulk *several different locally available materials* as aggregates apart from a very large variety of *industrial waste materials* as pozzolans or even just as fillers if needed.
- It is possible to mold it into any *intricate shape* without having to weld or bolt.

- The minimum *thickness requirements* of a reinforced concrete alternative for structural members which is essentially the locally produced by and large require no additional *local stiffening* of the webs and flanges as in the case of structural steel fabrications.
- Steel structures *inherently corrode* in the oxygen-rich environment of earth, in fact trying to go back to its native ore status, and need *periodic protection* (almost every 5–10 years) through painting throughout the expected life span of the structure.
- This is the most expensive and *irksome in an operating structural facility* and is the one single factor for the popularity of concrete in general.
- Concrete with its highly alkaline nature ensures *adequate protection* of the reinforcing steel inside almost *throughout the life span* of the structure with minimal maintenance.
- The *several alternatives possible* with the concrete compositions *can also be tailored* to suit the needs of the protection of steel inside, if only addressed before construction.
- The advantages of *offsite fabricability* of large steel components that will weigh significantly less permitting an *easier transportation* even compared to the more recent prefabrication alternatives in concrete is always an advantage in *congested urban locations*. However, with the possible relook at the available alternatives concrete has dominated even these scenarios.
- In this context, the new concrete alternatives like *fiber reinforced concrete, ferrocement, as well as ultra-high performance concrete* compositions have pushed the realms of concrete applications far beyond that of steel in recent years.
- Furthermore, the advantages offered by the *so-called industrial wastes*, which often can impart significant strength and performance characteristics to the mundane concrete composites should be understood appropriately and utilized advantageously.
- This apart, the science and *technology of cement and cementitious compositions* in conjunction with their *reinforcement and fibrous reinforcements* are advancing significantly in recent years.
- Finally, with the depletion of suitable raw materials in adequate quantities (particularly the aggregates) for the manufacture of concrete, the use of *construction and demolition waste materials* (CDMs) has become a matter of urgent necessity for sustainability.
- One should not be unaware of the fact that even in this context of CDMs, the use of construction *wastes other than the recycled aggregates* alone is advancing.
- Last but not the least is to assess any project viability in terms of its total *lifetime cost* as well as its *fire safety* and *reliability* requirements.
- The advancements in materials science, the avenues for the repair and rehabilitation of concrete structural facilities have also seen a significant diversification in terms of newer chemical and mineral compositions, FRPs, etc., apart from the technology associated with their application.

One can go on further into several other details of *manufacture, construction, processing, fabrication, erection, maintenance apart from the repair and rehabilitation*

characteristics of each of the major construction materials. But, a brief understanding of the above parameters will probably reinforce the idea that *concrete has come to stay* as one of the most preferred construction materials for the foreseeable future and is certainly in line with the sustainability doctrines of environmental protection.

   Having understood at least cursorily the various parameters and aspects that impact and encourage the adoption of concrete as the most preferred construction material in the present-day scenario, one has to be explicitly clear that there are several misconceptions due to the huge volume of information that is available on the enormous variations possible with concrete composites. Apart from this, one has to vary the fact that there is a lot of misinformation floating and public primarily driven by highly competitive business considerations. There is also a significant need to collate information available in its proper perspective and present verifiable facts coherently at this stage. The often perceived new, newer and newest innovations are many a time since the old wine in new bottles, though there may be a very small factor that is often faithfully and systematically concealed to ensure its recognition as a significant innovation. In light of this, the following few paragraphs try to project some of the primary aspects that need to be recognized for an appropriate and satisfactory application of the various cementitious compositions in the different environmental as well as construction scenarios. To simplify and not to elaborate in a brief report, most of these aspects are presented as bullet points which could help the reader to focus on these primary aspects explicitly, while keeping in mind that there is a lot more that was not said but needs be understood implicitly.

3   Effective Use of Concrete

To begin with, there is a need to recognize that the specifications of concrete for any particular application should be defined based on both the functional characteristics of the structural member as well as the environmental characteristics in which it is supposed to perform. The structural characteristics include primarily as follows:

- The size and shape intricacies of the member, the depth of casting, the reinforcement congestion—to ascertain the maximum size aggregate and the consistency in the concrete required,
- The thickness of the structure—to understand the heat of hydration, its dissipation and probable effects of thermal cracking,
- The strength requirements in terms of the design strength of the member and the target strength of the concrete that is required to ensure a satisfactory minimum strength at all locations based on the statistical variance possible,
- The environmental zone in which it is situated—to ensure that the type of cement, minimum strength, cement content, cover thickness as well as the maximum water cement ratio and air entrainment requirements are all mat adequately.

An appropriate mixture design ensuring that the above parameters are satisfied adequately is an absolute must. More important over and above such a recognition is

the fact that the concrete satisfies these needs in place through a well orchestrated quality assurance and quality control mechanism. Some of the parameters that may need to be appropriately checked and enforced could be listed as follows:

- the maximum size and gradation of both coarse and fine aggregates, the presence of deleterious materials and super fine dust, silt or clay,
- the minimum and maximum consistency levels as delivered and placing the structure and not as ordered and transported to the site,
- the adequacy of filling and compaction, particularly in corners and the cover regions,
- the appropriate curing regimes to ensure proper strength development and to avoid possible cracking, etc.

There is a lot at this missing many a time in what was envisaged, recommended and ordered and the final product that is actually in place in the structural member. While there is a definite record of both the concrete as expected to be in the structure and also sometimes the apparently systematic (sporadic) quality assurance that goes along with it, the resultant material in place is not what was envisaged. Needless to say that, it should be recognized that the idea of quality assurance and quality control is not to prescribe tests and their frequency alone, but to ensure that the final product is indeed what was indeed desired and appropriate by all concerned with the construction. This includes all including the facility owners, planners, designers, contractors and other associated finishing and furnishing suppliers.

4   Further Avenues for Sustainability Are Not Farther

While many of the efforts are focused on the realization of better concrete composites through research and developmental avenues primarily on the cementitious materials, be it the cement or pozzolans and associated modulators called chemical admixtures, the need for ensuring the efficacy of these materials for realizing the desired effects is paramount. Without going in depth into each of these materials one by one, a few broad outlines for an effective utilization of both the normal concrete constituents as well as the chemical and mineral admixtures are presented.

5   Aggregate Modulations

The increasing strain on natural resources particularly in the construction scenario necessitates the utilization of not just the locally available materials, but also encourages the use of construction and demolition wastes products. In specific, there is an urgent need for the supply of appropriately characterized aggregate fractions and even aggregate combinations for ensuring the realization of the highest possible compressive strength and the concretes produced. This means

- There is an urgent need and also a large scope for the supply of well characterized aggregate compositions from both coarse and fine aggregates.
- The need for understanding manufactured sand as an alternative for natural river sand, in terms of modifications in mixture designs is still not adequately understood.
- The above efforts could pave the way for ensuring the utilization of recycled concrete aggregate as a farther measure toward sustainability.
- Simple and effective techniques for utilization of both recycled aggregates and manufactured sand in general building construction are needed.

6 Pozzolanic Additions

With phenomenally large consumption of coal for thermal power production, the availability of fly ash can be taken for granted for the foreseeable future. The production of steel and the associated blast furnace slag as a waste by-product is also a reality. These are two low-end pozzolanic materials that can help significantly in reducing the consumption of cement in most general-purpose applications of concrete. The high-end pozzolanic materials like silica fume, metakaolin, RHA and zeolite could be utilized most advantageously for the production of high strength and ultra-high strength compositions.

- While the use of fly ash and GGBS is positively recognized as an advantage by the industry, there is an urgent need to curb the inappropriate and over-enthusiastic utilization of overtures by many should be regulated.
- For equations related to concretes of strengths below 50 MPa, the low-end pozzolanic materials like fly ash and GGBS could be used. This also helps in preventing the cementitious pines required for an appropriate flexibility and compaction and achieving a void-free mass without much difficulty that will ensure a significantly higher performance.
- In line with this, it is also obvious that the high-end pozzolanic materials listed earlier could be used for achieving strengths up to almost 120 MPa. The higher pozzolanic efficiency of these materials helps in limiting the total cementitious materials content to acceptable limits, which helps in reducing the wetting water requirements of mix as well as the plasticizer and other chemical admixtures utilized.

7 Chemical Admixtures

The use of chemical admixtures even in the routine construction practices has become a reality, but it would be greatly beneficial to have a fundamental understanding of their behavior for limiting them the minimum required from cost considerations also.

- It is suggested that for concretes below 50 MPa, the plasticizer requirements can easily be limited to about 1% in most cases.
- Even for very high strength concretes of almost 100 MPa, the required plasticizer levels could be limited to about 2–2.5%. In fact, in the case of much higher superplasticizer contents it appears that the water in the superplasticizer liquid is probably the one that is responsible for the higher fluidity rather than the solid complement of the superplasticizer chemical with in.

8 Cement Modifications

There are two very specific observations that could be with regard to the need for an understanding of the cement and its various modifications.

- The simplest one is to ensure that the cement confirms to the international norms in terms of the various strength grades, which is almost all codes in the world is the strength of an appropriate mortar at the water cement ratio of 0.5. The specific change is essentially relevant to the Indian scenario, as the so-called higher-grade cement of 42.5 and 52.5 can be utilized with confidence. It may be noted that the higher grade of cement is achieved through an appropriate modulation of the particle size distribution in the grinding if only the chemical characteristics are ensured appropriately. The amount of saving in cement accruing out of these simple yet monumental change could result in such a huge saving of cement that it could be the equivalent of doubling the cement production without any additional investment, if only one considers the use of pozzolanic admixtures, be it the lower end or the higher end types.
- This would also help in ensuring that the water cement ratio to strength relationships presented in the Euro norms can be advantageously utilized. The reduction and appropriate utilization of cement itself through ensuring conformity of the cement to international regulations will not only help economizing the cost of concrete, but will also help in reducing its reactivity to the environment thus achieving a higher performance.

9 Concluding Remarks

In fact, if one chooses to look at the intricate details of each of the constituent materials including the pozzolanic and chemical admixtures with a view to enhance sustainability, there is a lot that can be achieved. It is important to realize, orchestrate, enunciate, state and even indoctrinate these facts for the vibrant future of our economy as well as the protection of our environment.

Assessment of Groundwater Contamination with Emphasis on Sulfates, Barites Mining Area, Mangampeta, Andhra Pradesh, India

Check for updates

Veeraswamy Golla, Balaji Etikala, Nagaraju Arveti, S. R. Sradha, N. Janardhan, M. Rajasekhar and M. Subbarao

Abstract In the Mangampeta mining area, 15 groundwater samples were collected in a polyethylene bottles, measuring pH and EC at the same time water samples were sent to the laboratory to analyze the various physicochemical properties of water. On this basis, the quality of drinking water and irrigation water was estimated. Parameters including PH, EC, TDS, hardness and certain cations and anions were observed in drinking water quality. These are fairly suitable for drinking purposes in concentrated area, and the second part measures the parameters such as sodium percentage, Kelly ratio, sodium absorption ratio, potential salinity, non-carbonated hardness and magnesium ration. The concentrations of sulfate in mining region ranged from 447 to 1880 mg/l in drinking water. The vicinity of Mangamapeta, which is highly polluted by sulfate ions due to the existence of natural barite ore deposits, interacts with groundwater.

Keywords Physicochemical parameters · USSL diagram · Concentration of sulfates diagram · Wilcox diagram · Gibb's diagram · Chadha's and correlation diagram

V. Golla (✉) · B. Etikala · N. Arveti
Department of Geology, Sri Venkateswara University, Tirupati, Andhra Pradesh, India
e-mail: veeraswamygolla33@gmail.com

S. R. Sradha · N. Janardhan
Department of Civil Engineering, Annamacharya Engineering College, Tirupati, Andhra Pradesh, India

M. Rajasekhar
Department of Geology, Yogivemana University, Cuddapah, Andhra Pradesh, India

M. Subbarao
Department of Geography, Sri Venkateswara University, Tirupati, Andhra Pradesh, India

1 Introduction

Water is one of the main commodities for the survival of living organisms on the surface of the Earth. Human destiny for various needs, for instance, agriculture, drinking and irrigation practices, where there is no life on earth even without water, and it is an elixir for all living organisms [1–3]. The caliber of water plays a key role in surviving countries across the globe. The contamination of groundwater during sulfide oxidation in the carbonate environment causes an increase in sulfate levels, i.e., for drinking water. In agriculture, which has been widely used as fertilizer, pesticide and rapidly increasing industries, the reliability of groundwater with sulfate contamination is increased. Sulfide oxidation carbonate contamination in groundwater leads to unsuitable for drinking. The increasing of the urban population may lead to the pollution and increase in chloride in groundwater. The exploitation of barites ($BaSO_4$) minerals with a large amount of mining rock and tailing in Obulavaripalli Mandal, Managampeta village, contaminated with sulfates. Barite was mined near Mangampeta village in Andhra Pradesh. The place is the world largest barite deposits with reserve of >65 million tonnes [4–6]. The natural occurrence and commercial exploitation of barite even in Mangampeta threaten local groundwater resources because of waste leachate. Most of the people depend on groundwater resources for drinking and agriculture. The presence of chemical elements in the study area groundwater represents dissolution of geological material (various rocks) which the water flows in aquifer [7]. Several researchers have paid attention on the geological aspects of the barites region of Mangampeta to a certain extent than its environmental and groundwater contamination [8–11].

2 Study Area

The mining area is a small village with the name of the Mangamapeta located between the latitude: N 14° 01′ and the longitude 79° 19 E. It extends over 160.691 ha in the Cuddapah district, and it is encircled by Kodur Mandal to the south, Pullampeta Mandal to the west, Chitvel Mandal to the north, Rajampet Mandal to the east, which is in south-eastern India. The workplace in the area is partially filled with water and contains minerals such as barites, quartz, calcite, bentonite clay, gypsum and feldspars. The large ore body with $BaSO_4$ forms granular barite. The barite-type replacement occurs along the quartz and pyrite grain boundaries in the black shale. Vein-type barite is limited to underlying dolomites of barite beds (Fig. 1).
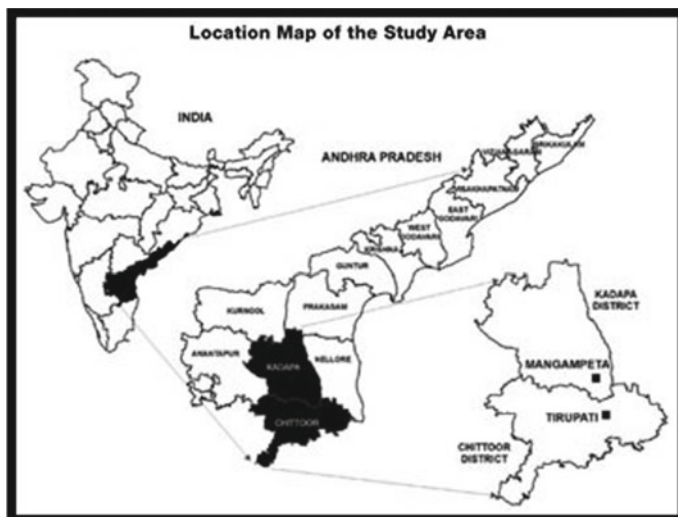
Fig. 1 Location map of the study area

3 Materials and Methods

A total sample of 15 groundwater samples were collected to analyze the physico-chemical parameters. The samples have been collected in 1000 ml pre-washed and pre-conditioned polyethylene bottles with 5% HNO_3 and then thoroughly cleaned with deionized water. The polyethylene sampling bottles were cleaned three times at each sampling site before the sampling [12–15]. The samples were analyzed for physicochemical and major ion of chemistry parameters with standard methods such as pH, electrical conductance, total dissolved solids, total hardness (TH), calcium (Ca), sodium (Na), magnesium (Mg), potassium (K), bicarbonates (HCO_3), carbonates, sulfates (SO_4), and chlorides (Cl).

4 Results and Discussion

4.1 Assessment of Water for Drinking Purpose

The suitability of groundwater for drinking was discussed below (pH):

pH measures the relative quantity of water loose hydrogen and hydroxyl ions. Water pH determines solubility (the amount that can be dissolved in water) and biological availability (the amount that may be utilized by aquatic life). The pH values meta-analysis range from 7.4 to 8.10 with a mean of 7.7. In keeping with BIS

Table 1 The statistics of physicochemical specifications of groundwater samples

Sample No.	Min	Max	Average	SD	Median	SE
EC	830.00	2370.00	1321.333	432.581	1270.000	61.176
pH	7.40	8.10	7.707	0.194	7.700	0.027
TDS	531.00	1517.00	845.800	276.877	813.000	39.156
Ca (mg/l)	118.00	423.00	233.133	86.130	228.000	12.181
Mg (mg/l)	110.00	346.00	178.333	62.680	171.000	8.864
Na (mg/l)	18.00	41.00	28.467	6.621	28.000	0.936
K (mg/l)	8.00	29.00	14.267	5.175	14.000	0.732
HCO_3 (mg/l)	204.00	381.00	283.067	52.325	284.000	7.400
Cl (mg/l)	204.00	381.00	283.067	52.325	284.000	7.400
SO_4 (mg/l)	447.00	1880.00	830.733	358.198	794.000	50.657
Hardness as $CaCO_3$ (mg/l)	269.00	769.00	411.400	123.010	399.000	17.396
Percent sodium	2.88	9.13	6.040	1.713	5.890	0.242
Potential salinity	11.87	27.56	16.622	4.114	15.440	0.582
Residual sodium carbonate	−43.34	−11.84	−21.678	7.550	−20.951	1.068
Non-carbonate hardness	591.77	2166.93	1083.918	377.501	1047.545	53.387
CaI 1	0.64	0.88	0.792	0.064	0.810	0.009
CaI 2	0.14	0.48	0.287	0.104	0.309	0.015
GR I	0.63	0.63	0.634	0.000	0.634	0.000
GR II	0.06	0.22	0.130	0.039	0.129	0.005
Kelly's ratio	0.02	0.08	0.050	0.017	0.050	0.002
Mg ratio	37.60	77.87	55.765	10.399	55.267	1.471
SAR	0.19	0.49	0.351	0.094	0.341	0.013
PI	6.82	19.38	12.988	3.222	12.836	0.456

[21], the ideal pH limit in drinking water is 6.5–8.5. In this study, all the groundwater samples fall inside the preferred limits.

The statistics of physicochemical specifications of groundwater samples are presented in Table 1.

4.2 Electrical Conductivity

Electrical conductance (EC) measures the degree of water mineralization, which depends on interaction between rock and water and thus the residence point of time of the water with the rock [16]. Water can be classified as tasteless, sweet, brackish,

salty and brine on the basis of EC. Complete ionized water components described by EC have been noticed to greatly determine the quality of water for drinking. The EC values for this study range from 830 to 2370 µmhos/cm, with a mean value of 1321.33 µmhos/cm. Groundwater less than 750 µmhos/cm with EC is advisable to drink. The majority of the samples are not suitable for drinking.

4.3 Total Dissolved Solids (TDS)

All the ions dissolved in water such as calcium (Ca^{2+}), sodium (Na^+), magnesium (Mg^{2+}), potassium (K^+), bicarbonate (HCO_{3-}), chloride (Cl^-) sulfate ($SO4^{2-}$), etc., increase the TDS values. The total dissolved solids of groundwater were classified. In this study, TDS in all groundwater samples with an average value of 845.80 mg/l varied from 531.0 to 1517.00 mg/l. According to the above classification, eight groundwater samples are within the range of drinking water permissible and can be used for irrigation as the TDS was <1000 mg/l and the remaining four groundwater samples are brackish. In this study, TDS in all groundwater samples with a mean value of 845.80 mg/l varies from 531.0 to 1517.00 mg/l.

4.4 Total Hardness

Water hardness relies on the water content of Ca^{2+} and Mg^{2+} [17]. It occurs naturally in most groundwater due to the weathering of calcareous rock and calcium-rich minerals. Ca^{2+} and Mg^{2+} together with their SO_4^{2-}, Cl^-, HCO_{3-} and CO_3^{2-} make nature's water hard. The safe hardening limit of 300 mg/l proposed for drinking water. Hard water causes urolithiasis, parental anencephalic mortality, certain cancers and cardiovascular disorders [18]. More cardiovascular disease incidences are reported to be more limited to soft water than hard water [19–22]. Groundwater hardness in this study ranges from 269.0 to 769.0 mg/l. In the study area, 99% of the samples are shown to be very difficult in nature. The values are depicted in Table 2.

4.5 Major Cations and Anions

Ca^{2+} and Mg^{2+} concentrations vary from 118.0 to 423.0 mg/l and 110.0–346.0 mg/l (Table 1.4). Calcium results from calcium-enriched minerals such as pyroxenes, amphiboles and feldspars. In this study, all the samples surpassed the allowable limit of 200 mg/l [21]. The major source of magnesium ions in groundwater is the ion exchange in aquifers. The majority of samples within the study area exceed the maximum allowable limit of 150 mg/l. The ionic concentrations of sodium and potassium in groundwater ranged from 18 to 41 and from 8.0 to 29 mg/l. Feldspar and

Table 2 Classification of groundwater for the irrigation

Classifications	Categories	Range	Number of samples
IDS	Fresh water	<1000	
	Brackish water	1000–10,000	11
	Saline water	10000–100,000	4
	Brine water	>100,000	
	Soft	0–75	
	Moderatelyhard	75–150	
Total hardness	Hard	150–300	2
	Very hard	>300	13
Electrical conductivity	Excellent	<250	All
	Good	250–750	
	Remissible	750–2250	
	Doubtful	2250–5000	
	Unsuitable	>5000	
Sulphate (SO_4)	Mild	<150	
	Moderate	150–1500	
	Severe	1500–10,000	14
	Very severe	>10,000	1
Chloride (meq/l) [27]	Excellent	<4	
	Good	4–7	
	Remissible	7–12	5
	Doubtful	12–20	10
	Unsuitable	>20	
Percent sodium (%Na)	Excellent	0–20	All
	Good	20–40	
	Permissible	40–60	
	Doubtful	60–80	
	Unsuitable	>80	
Sodium absorption ratio (SAR)	Very low	<2	All
	Low	2–12	
	Medium	12–22	
	High	22–32	
	Very high	>32	
Permeability inbox (PI)	Suitable	<75	All
	Unsuitable	=75	
Residual sodium carbonate (R5C) (meq/l)	Permissible	<1.25	All
	Unsuitable	=1.25	

<div align="right">(continued)</div>

Table 2 (continued)

Classifications	Categories	Range	Number of samples
Magnesium absorption ratio (MAR)	Permissible	0–50	4
	Unsuitable	>50	11
Raghunath [32] Kelly's ratio	Suitable	<1	All
	Unsuitable	=1	

clay weathering are a source of sodium and potassium in groundwater. According to the WHO [22], the maximum allowable limit of sodium for drinking is 200 mg/l. Most groundwater samples fall below the permissible limit. Bicarbonate concentrations varied between 204.0 and 381.0 mg/l with a mean of 283.067 mg/l (Table 2). There is no clear evidence of health effects because bicarbonate is present. Bicarbonate levels below 200 mg/l are suggested to be appropriate for drinking purposes [23]. The water was not suitable for drinking because it exceeded the bicarbonate limits. The chlorides concentration ranges from 168.1 to 230.1 mg/l [22]. The sulfate ranges from 447.0 to 1880.0 mg/l.

In this area, sulfate ion is present extensively due to mineral sources of barite ($BaSO_4$) (Fig. 2). All groundwater samples surpassed the allowable limit of 250 mg/l for drinking water. The major ion abundance in groundwater is as follows:

$$Ca^{2+} > Mg^{2+} > Na^+ > K^+ \text{ and } SO_4^{2-} > HCO_{3-} > Cl^- > CO_{3-}$$
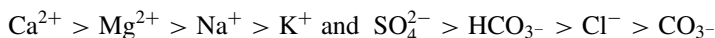
Fig. 2 Shows concentration of sulfate diagram
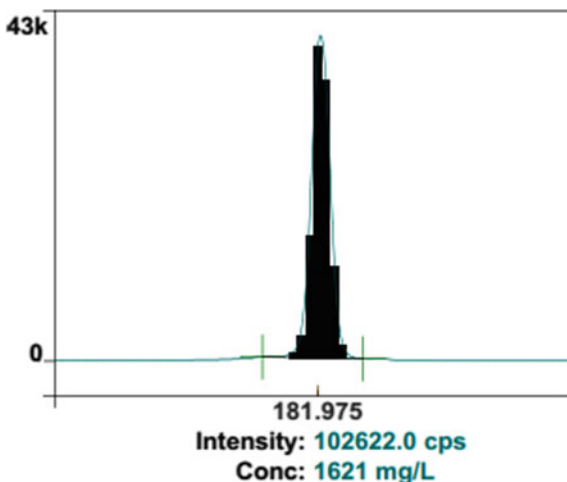
5 Assessment of Water Quality for Irrigation Use

5.1 Sodium Absorption Ratio (SAR)

The SAR is used to predict the risk of sodium accumulation in the soil. Excess sodium changes soil properties and reduces soil structure and its permeability [22]. It is the combination of calcium and magnesium (beneficial elements) in relation to soil dispersibility known effects, while high electrical conductivity in waters leads to increase in soil salinity, and high sodium content leads to increase in alkalinity in soils. SAR values can be calculated using the below equation [24]

$$SAR = \frac{Na^+}{\left[(Ca^{2+} Mg^{2+})/2\right]^{1/2}} meq/l$$

It measures the potential dangers in irrigation water of excess sodium. SAR values for groundwater samples in the study area ranged from 0.19 to 0.49 with a mean value of 0.351. The SAR values of the water samples are less than 10 and are rated as good for irrigation [25, 26] (Table 1.2).

5.2 USSL Classification

The USSL classification gives the mixed effect of the salinity and sodium hazard. It can be plotted by taking (SAR) on the *Y*-axis and EC values on *X*-axis. Low sodium absorption high conductivity C3 and S1 in this study area indicates useful for irrigation use.

5.3 Non-carbonate Hardness (NCH)

NCH values ranged from 591.77 to 2166.93 mg/l. According to ICMR, the majority samples are within the allowable limits of <600 [27].

5.4 Kelly's Ratio

The water quality for irrigation was classified by Kelly's ratio [28], which is the Na^+ level measured against calcium and magnesium. The Kelly's ratio calculation formula is as follows:

$$KR = \frac{Na^+}{(Ca^{2+} + Mg^{2+})}$$

Kelly's ratios are calculated for all groundwater samples and ranged between 0.02 and 0.08 with a mean of 0.05 mg/l. The ratio value of Kelly is <1 is useful for irrigation. Kelly's ratio of all the samples is within allowed limits. The water is therefore suitable for irrigation.

5.5 Magnesium Hazard

Ca^{2+} and Mg^{2+} generally maintain a balance in most of the waters. Elevated Mg^{2+} ions in waters soil structure, by converting it into alkaline which reduces the yield of crops. Szabolcs and Darab [29] found the calculation method for assessing irrigation water in terms of magnesium hazard (MH) as listed below

$$MH = Mg^{2+}/(Ca^{2+} + Mg^{2+}) \times (meq/l)$$

The magnesium ratio in Table 1.2 varied from 37.60 to 77.87 with an average value of 55.765. Passage of water through calcareous rock formation can result in a high magnesium ratio [30]. In this study, about six water samples with >50% affect the crops by making the soils into alkaline [31].

5.6 Residual Sodium Carbonate (RSC)

Elevated levels of RSC in water result increase in sodium adsorption of the soil. Eaton has demonstrated the concept of calculating of RSC as follows [32]:

$$RSC = (CO_3^{2-} + HCO_{3^-}) - (Ca^{2+} + Mg^{2+})(meq/l)$$

The RSC water classification shows minimum values of -43.34 and maximum values of -11.84. Almost all the groundwater samples fall under safe limit of <1.25 and only all samples within the maximum permissible level of 2.5.

5.7 Percent Sodium (%Na)

The excess sodium ion in water has ability to react with soil which reducing soil permeability [2, 33]. It is used to know the water suitability for irrigation [34].

Fig. 3 USSL classification
(after USSL, 1854)
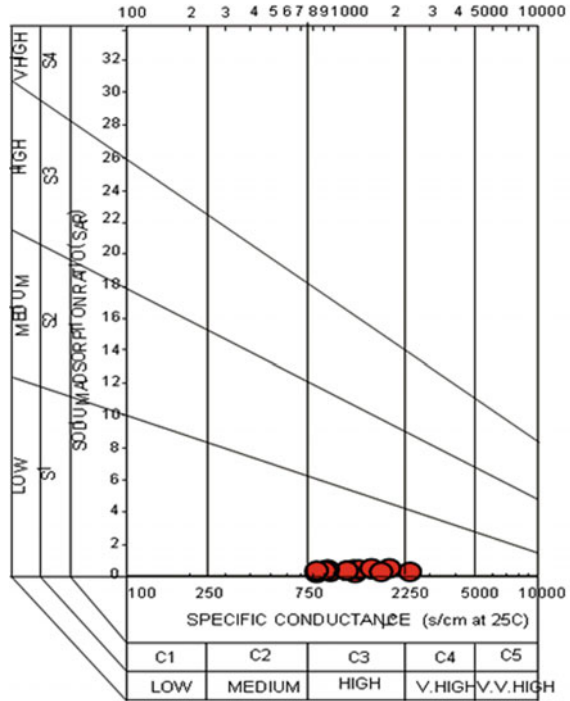
Todd (1980) defined the proportion of sodium soluble as

$$\%\text{Na} = \frac{(\text{Na}^+ + \text{K}^+)}{(\text{Ca}^{2+} + \text{Mg}^{2+} + \text{Na}^+ + \text{K}^+)} \times 100\,(\text{meq/l})$$

The sodium percentage value determined is between 2.88 and 9.13 with a mean of 6.04 meq/l. (Table 1). In this study, almost 56% of samples fall in good range (20–40), and approximately 60% of the samples are allowed (40–60). The water quality is shown in Fig. 3.

5.8 Wilcox Diagram

Wilcox diagram is used to classify the groundwater for irrigation use by plotted EC in the X-axis and the %Na in Y-axis in [35] . The presence of excess salts of sodium in the soil–plant system that causes osmotic effects (Fig. 4). 14 samples were fallen to allowable, and one sample is inappropriate for irrigation.

Fig. 4 Wilcox diagram
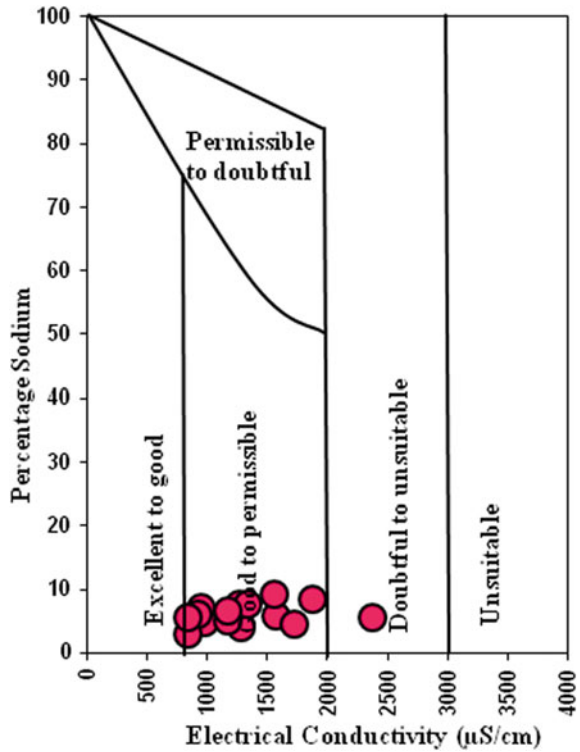
5.9 Potential Salinity

The potential salinity values vary between 11.87 and 27.56 with an average of 16.622 (Table 1.4). It suggests that the potential salinity of a groundwater sample in the studied area is almost high (>10), makes the water unsuitable for irrigation purposes, and the remaining water falls within the safe category.

6 Hydrochemical Facies of Groundwater

The general purpose of studying hydrochemical facies is to correlate the chemistry of groundwater with the lithological and hydrological environment.
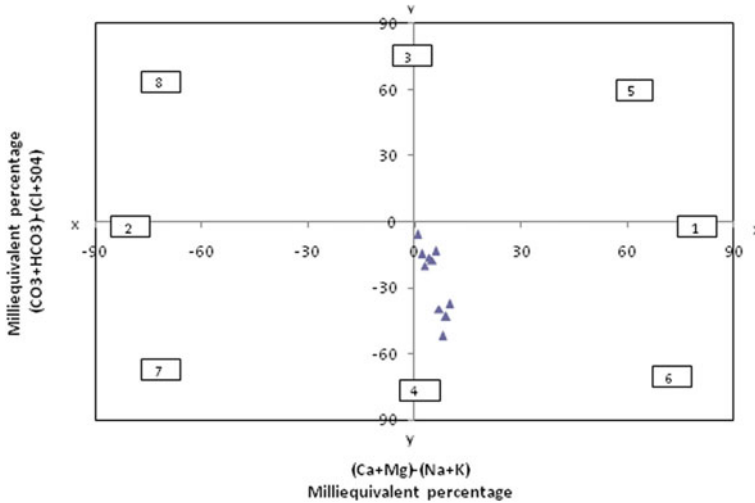
Fig. 5 Chadha's diagram

6.1 *Chadha's Diagram (Modified Piper)*

The groundwater facies were categorized from Chadha's diagram [36], to know the hydrochemical facies. It is a modified Piper diagram and Durov diagram [37]. From the results, it is found that all samples fall in Ca–Mg–Cl facies type (Fig. 5).

7 Correlation

The correlation and trend line analysis refers to the relationship between the parameter as shown in the diagram below. In this analysis, EC and TDS have a strong relationship between the R^2 value is one and the mg and the R^2 hardness value is 0.77, 0.57, respectively (Fig. 6).

8 Gibbs Classification

The Gibbs classification is used to determine the correlation between water and lithology of the aquifer [38]. Groundwater quality changes significantly owing to weathering and human activities. The controlling mechanisms of groundwater are evaporation dominance, rock-weathering dominance and precipitation dominance which are evaluated by plotting the data as a function of TDS according to the variation in the ratios of $Na^+ + K^+/(Na^+ + K^+ + Ca^{2+})$ and $Cl^-/(Cl^- + HCO_{3-})$. Even though it
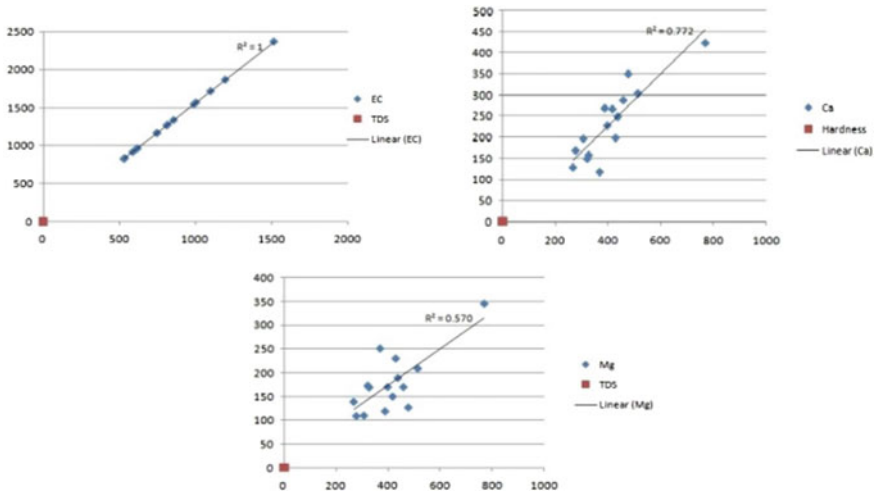
Fig. 6 Correlation diagrams between TDS and EC, Ca and Mg

is controversial for rivers with elevated $Na^+ + K^+/(Na^+ + K^+ + Ca^{2+})$, Gibbs [39], it gives a comprehensive method to identify rivers waters which are governed by precipitation or rock–water interaction or evaporation-crystallization.

$$\text{Gibbs Ratio I} = \frac{Cl^-}{(Cl^- + HCO_{3^-})}$$

$$\text{Gibbs Ratio II} = \frac{(Na^+ + K^+)}{(Na^+ + K^+ + Ca^{2+})}$$

From Fig. 7, it can be found that all the water samples fall under the rock–water interaction area. The water chemistry is influenced by the rock–water interaction, rock weathering such as barites, dolostone and quartzite and shale group of rocks.

9 Conclusions

The groundwater analysis shows that the area of Mangamapeta is quite suitable for dirking, particularly surrounding villages of mining area. The concentration of sulfates in the study area exceeds due to leaching and weathering of barites ($BaSO_4$) minerals. Due to the presence of dolomite, the carbonate group of minerals was responsible, and the dissolution of minerals leads to an increase in the TDS in waters of the study area. Brackish water should also be unfit for drinking. The connection between EC and TDS, Ca and Mg was strong. Chadha's diagram shows that water type Ca–Mg–Cl. Majority samples are suitable for irrigation. Moreover, the Gibbs
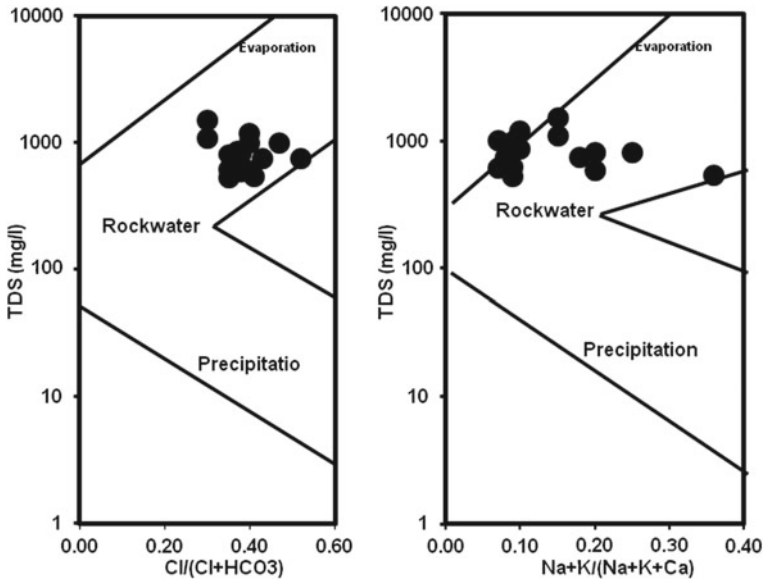
Fig. 7 Gibbs classification

diagram indicates the water polluted with interaction of the barites ($BaSO_4$), due to this reason the sulfate levels in higher in the concentrated area.

References

1. Nagaraju, A., Veeraswamy, G., Sridhar, Y., & Thejaswi, A. (2017). Assessment of groundwater quality in Gudur area of Andhra Pradesh, South India. *Fresenius Environmental Bulletin, 26*(5), 3597–3606.
2. Nagaraju, A., Suresh, S., Killham, K., & Hudson-Edwards, K. (2006). Hydro geochemistry of waters of Mangampeta barite mining area, Cuddapah basin, Andhra Pradesh, India. *Turkish Journal of Engineering and Environmental Sciences, 30,* 203–219.
3. Veeraswamy, G., Nagaraju, A., Balaji, E., Sreedhar, Y., & Rajasekhar, M. (2018). Water quality assessment in terms of water quality index in Gudur area, Nellore District, Andhra Pradesh. *International Journal of Technical Research & Science, 3*(I), 34–39.
4. Toran, L. (1987). Sulfate contamination in groundwater from a carbonate-hosted Trans. *Washington, DC, 25*, 914–923.
5. Satapathy, S., Singh, R. K., Kumar, C., Negi, R., Mishra, K., & Bhuyan, K. (2017). Biostrategic removal of sulphur contamination in groundwater with sulphur-reducing bacteria: A review. https://doi.org/10.1177/1178622117690777.
6. Subba Rao, M. V. (2004). A case study of mining environmental activities of the Andhra Pradesh Mineral Development Corporation Limited, APMDC, Hyderabad, Andhra Pradesh, India (Unpublished report).
7. Balai, E., Nagaraju, A., Sreedhar, Y., Thejaswi, A., & Sharifi, Z. (2014). Hydrochemical characterization of groundwater in around Tirupati area, Chittoor District, Andhra Pradesh. *Applied Water Science, 7*(3), 1203–1212.

8. Basu, P. K. (1997). On Archaean and Proterozoic barite deposits of Cuddapah Basin. *Indian Mineral, 51,* 169–178.

9. Kurien, T. K., Setti, D. N., Neelakantam, S., Suthanandam, P., & Roy, S. (1977). Baryte mineralization and its origin, Mangampeta, Cuddapah District, Andhra Pradesh. *Indian Mineral, 18,* 1–6.

10. Neelakantam, S. (1987). Mangampeta Barites deposits, Cuddapah District, Andhra Pradesh. *Memorial Geological Society of India, 6,* 429–458.

11. Viswanadh, K., & Sastry, A. V. R. (1983). Volcanogenic rocks from Mangampeta Area, Andhra Pradesh. *Indian Journal of Earth Science, 10*, 142–151.

12. Veeraswamy, G., Balaji, E., Veeranjaneyulu, A., Subbarao, M., Surekha, A., & Narasimhlu, K. (2018). Data sets on delineation of groundwater potential zones identified by geospatial tool in Gudur area, Nellore district, Andhra Pradesh, India. *Data in Brief, 20*, 1984–1991. https://doi.org/10.1016/j.dib.2018.09.054.

13. Trivedy, R. K., & Geol, P. K. (1986). *Chemical and biological methods for waste pollution studies* (pp. 35–96). Karad: Environmental Publication.

14. APHA. (2005). Standard methods for the examination of water and wastewater. In A. D. Eaton, L. S. Clesceri, E. W. Rice, A. E. Greenberg, & M. H. Franson (Eds.). Washington, DC: American Public Health.

15. Mishra, U. K., Tripathi A. K., Tiwari, S., & Mishra, A. (2012). Assessment of quality and pollution potential of groundwater around Dabhaura area, Rewa District, Madhya Pradesh. *Earth Sciences Research Canada, 1*(2), 249–261.

16. Tripathi, A. K., Mishra, U. K., Ajay, Mishra, & Parul, Dubey. (2012). Assessment of groundwater quality Gurh Tehseel, Rewa District Madhya Pradesh, India. *International Journal of Scientific and Engineering Research, 3*(9), 1–12.

17. Eaton, E. M. (1950). Significance of carbonate in irrigation water. *Soil Science, 69*, 123–133.

18. Sawyer, C. N., & McCarty, P. L. (1967). *Chemistry for sanitary engineers* (2nd ed., 405 p.), McGraw-Hill Series in Sanitary Science and Water Resources Engineering. Toronto, CA: McGraw-Hill.

19. Crawford, M. D., Gardner, M. J., & Morris, J. N. (1972). Water hardness, rainfall and cardiovascular mortality. *Lancet, 1,* 1396–1397.

20. Sawyer, C. N., & McCarty, P. L. (1978). *Chemistry for environmental engineering* (3rd ed.). New York: McGraw-Hill.

21. BIS. (2012). Indian standard drinking water specification, Second Revision ISO: 10500:2012, Bureau of Indian Standards, Drinking Water Sectional Committee, FAD 25. New Delhi, India.

22. WHO. (2011). *Guidelines for drinking water quality* (2nd ed.). Geneva: World Health Organization Geneva.

23. Bhardwaj, V., & Singh, D. S. (2011). Surface and groundwater quality characterization of Deoria District, Ganga Plain, India. *Environmental Earth Sciences, 63*(2), 383–395.

24. Kelley, W. P. (1957). *Alkali soils—Their formation, properties and reclamation*. New York: Reinhold.

25. Alagbe, S. A. (2006). Preliminary evaluation of hydrochemistry of the Kalambaina formation, Sokoto Basin, Nigeria. *Environmental Geology, 51,* 39–45.

26. Gupta, P. K. (2005). Methods in environmental analysis: Water, soil and air. *Agrobios*, Jodhpur, India, pp. 1–127.

27. Ayers, R. S., & Westcot, D. W. (1985). Water quality for agriculture. *FAO Irrigation and Drainage Paper, 29*, 37–70.

28. Kaur, Rajdeep, & Singh, R. V. (2009). Analysis of water quality parameters of ground water near Bichhwal industrial area, Bikaner in post-monsoon season, November 2008. *International Journal of Chemical Sciences, 7*(4), 2519–2534.

29. Szabolcs, I., & Darab, C. (1964). The influence of irrigation water of high sodium carbonate content of soils. In *Proceedings of 8th ISSS, Trans* (Vol. 2, pp. 802–812).

30. Pandian, K., & Sankar, K. (2007). Hydrogeochemistry and groundwater quality in the Vaippar river basin, Tamilnadu. *Journal of Geological Society of India, 69,* 970–982.

31. Paliwal, K. V. (1972). Irrigation with saline water. Monogram No. 2 (New series). IARI, New Delhi, p. 198.
32. Raghunath, H. M. (1987). *Groundwater*. New Delhi: Wiley Eastern.
33. Todd, D. K., & Mays, L. W. (2005). *Groundwater hydrology* (3rd ed., p. 656). Hoboken, NJ: Wiley.
34. Sundaray, S. K., Nayak, B. B., & Bhatta, D. (2009). Environmental studies on river water quality with reference to suitability for agricultural purposes: Mahanadi river estuarine system, India—A case study. *Environmental Monitoring and Assessment, 155,* 227–243.
35. Wilcox, L.V. (1948). The quality of water for irrigation. U.S. Department of Agriculture Technical Bulletin No. 962, pp. 1–40.
36. Maoui, A., Kherici, N., & Derradji, F. (2010). Hydrochemistry of an Albian sandstone aquifer in a semi arid region, Ain Oussera, Algeria. *Environmental Earth Sciences, 60,* 689–701.
37. Tijani, J. (1994). Hydrochemical assessment of groundwater in Moro area, Kwara State, Nigeria. *Environmental Geology, 24,* 194–202.
38. Chadha, D. K. (1999). A proposed new diagram for geochemical classification of natural waters and interpretation of chemical data. *Hydrogeology Journal, 7*(5), 431–439.
39. Gibbs, R. J. (1971). Mechanisms controlling world water chemistry: Evaporation-crystallization process. *Science, 172,* 871–872.

Statistical and Analytical Evaluation of Groundwater Quality of Atmakur Area, SPSR Nellore District, Andhra Pradesh, South India

Balaji Etikala, Veeraswamy Golla, Nagaraju Arveti, Sreedhar Yenamala, Prasad Mannala and P. L. Keshava Kiran Kumar

Abstract A statistical approach for instance cluster and factor modes was performed to categorize 21 wells in the Atmakur area of SPSR Nellore District based on groundwater hydrochemistry. The collected groundwater samples were examined for physico-chemical specifications and major ion chemistry like pH, electrical conductivity, TDS, Ca^{2+}, Na^+, Mg^{2+}, K^+, Cl^-, HCO_3- and SO_4^{2-} using standard methods. Additionally, chloro-alkaline indices and Gibbs ratio were executed to the analysed data to assess the dominant processes controlling groundwater chemistry of the region. $Ca–Mg–HCO_3$ was the main hydrochemical facies in Chadha's classification. The end results showed that silicate weathering (which is further endorsed by scatter diagram of HCO_3-, SO_4^{2-} versus Ca^{2+}, Mg^{2+}, dissolution of sulphates and chlorides due to the fertilizers and intense agricultural activities, water–rock interaction and reverse ion exchange are responsible for the groundwater chemistry in this region.

Keywords Cluster analysis · Factor analysis · Groundwater · Gibbs ratio · Indices of base exchange · Atmakur · SPSR Nellore · Andhra Pradesh

1 Introduction

Groundwater is one of the indispensable characteristic assets essential for human beings, house assistance, manufacturing industry, cultivation and allied activities [1]. Diversity in groundwater chemistry of a region is related to physico-chemical parameters that are significantly affected by geological processes and human activities [2].

B. Etikala (✉) · V. Golla · N. Arveti · S. Yenamala
Department of Geology, Sri Venkateswara University, Tirupati, Andhra Pradesh, India
e-mail: balajiyvu@gmail.com

P. Mannala
Centre for Earth, Ocean and Atmospheric Sciences, University of Hyderabad, Hyderabad, Telangana, India

P. L. Keshava Kiran Kumar
Department of Geology, Yogi Vemana University, Kadapa, Andhra Pradesh, India

Moreover, some other factors that influence groundwater quality are precipitation, surface water availability, nature of recharge water and hydrochemical processes regulating groundwater hydrochemistry [3, 4]. While devising developmental undertakings, monitoring of water quality, quantity and information on factors regulating water chemistry is very important since water is being used for various purposes. Thus, hydrochemical investigation of the groundwater has turned into a high need concern.

The multivariate statistical approach intends attaining reliable data reduction from large data sets and to obtain comprehensive information which helps in the elucidation of the geochemical source. In the most recent decades, multivariate statistical practices like factor and cluster have been using to know the correlation and distinguished geochemical behaviour of water and their sources of contaminants among the studied wells [5]. This could be the successful way of interpreting, organizing and deciphering geochemical data. Earlier, a number of researchers have been used the approach of statistical techniques in India and around the world for sustainable utilization of groundwater [6–13].

2 Study Area

The study was carried out in Atmakur Mandal (14°33′ N and 14°47′ N latitudes 79° 26′ E and 79°42′ E longitudes) located in SPSR Nellore district, Andhra Pradesh state, South India (Fig. 1). It is encircling in the survey of India (SOI) toposheets no. 57 N/9, N/10, and it has an elevation of 15 m above sea level. A minor tributary Boggeru joins other minor streams flows eastwards and joining the Penna River near Varlagudipadu. The geology of Atmakur lies within the Migmatized garnetiferous Quartz-mica schist with amphibolite bands of Archaean age to alluvium (sand, silt and clay dominant) of Quaternary age. The mean yearly rainfall of the Mandal is 936 mm. The groundwater level varies between 3 and 8 m.

3 Materials and Methods

Twenty-one representative groundwater samples were collected in pre-cleaned well-dried polyethylene bottles from Atmakur area in the month of May 2015. Sampling localities were traced using a portable GPS tracker, and they were portrayed in Fig. 1. Then, the samples were investigated for both physico-chemical specifications and major ion chemistry by adopting established procedures [14, 15]. Analytical results were then processed for factor and cluster (both Q and R-modes) analysis with assisting MINITAB 18 program. Moreover, Chadha's, Gibbs and scatter plots were plotted for identifying the key factors governing hydrochemistry.
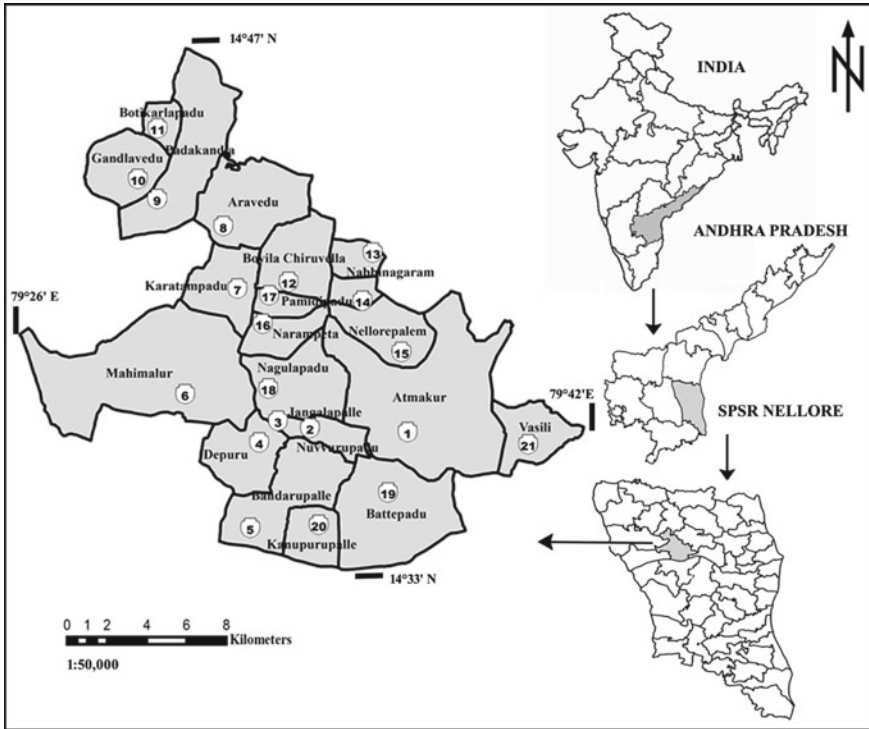
Fig. 1 Location map of the study area with water sample points

4 Results and Discussion

The summary statistics of the analysed parameters and the samples surpassing the acceptable limits were shown in Table 1. The abundance of major ion chemistry of water is as follows: $Ca^{2+} > Na^+ > Mg^{2+} > K^+$ and $HCO_3{-} > Cl^- > SO_4{}^{2-}$.

4.1 Hydrochemical Facies

The general principle of a hydrochemical facies study is to relate the chemistry of groundwater to the geological and hydrological environment. In this study, the groundwater nature was assessed by Chadha's classification and found that the dominant hydrochemical facies was $Ca–Mg–HCO_3$ water type (Fig. 2).

Table 1 Minimum, maximum, average and suitability categorization for drinking according to the guidelines of different components of groundwater

S. No.	Constituents	Min	Max	Mean	AL[a]	SSAL[b]
1	Calcium (Ca) (mg/l)	64	314	172	200	0
2	Magnesium (Mg) (mg/l)	11	105	48	150	0
3	Sodium (Na) (mg/l)	20	217	97	200	1
4	Potassium (K) (mg/l)	3	15	8	NG[c]	–
5	Bicarbonate (HCO_3) (mg/l)	276	859	551	NG	–
6	Sulphate (SO_4) (mg/l)	27	107	71	250	0
7	Chloride (Cl) (mg/l)	35	355	198	250	8
8	Specific conductance (μmhos/cm)	570	3120	1765	NG	–
9	Total dissolved solids (TDS) (mg/l)	365	1997	1130	1000	10
10	pH	7.2	8.1	8	6.5–8.5	0
11	CAI-I	−1.02	0.56	0.08	–	–
12	CAI-II	−0.15	0.37	0.09	–	–
13	Gibbs ratio-I	0.17	0.48	0.36	–	–
14	Gibbs ratio-II	0.20	0.52	0.34	–	–

[a]Acceptable limits; [b]Samples surpassing the acceptable limits; [c]No Guideline
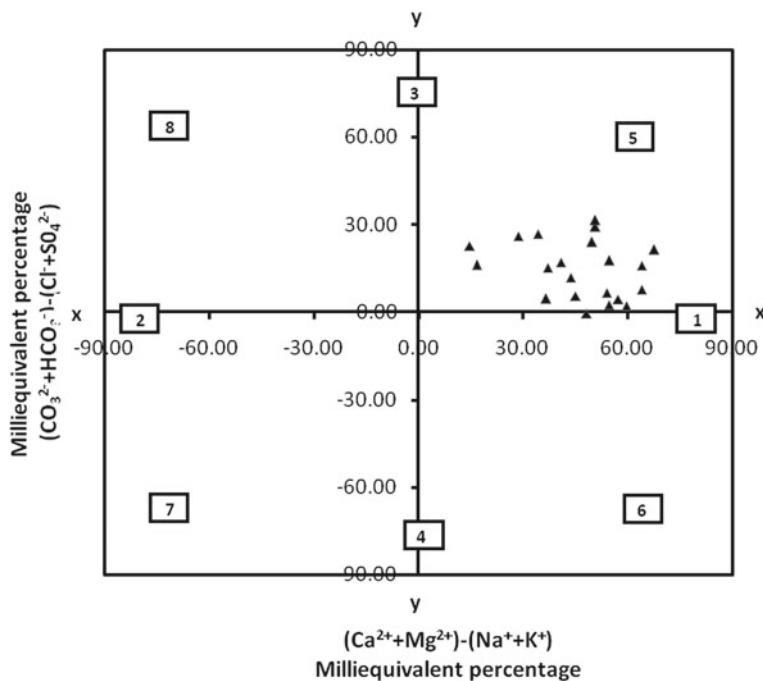
Fig. 2 Chadha's classification

4.2 Hierarchical Cluster Analysis (HCA)

The wards linkage squared Euclidean distance hierarchical algorithm extracted two clusters with a similarity index of 50% between the parameters among the wells (Fig. 3). The first cluster is composed of the wells 1–4, 6, 11–14, 16 and 21 which represent 52% of the studied wells. Basically, this cluster shows negative loadings with all the parameters except SO_4^{2-} ions which point to the dissolution of sulphate mineral (e.g. gypsum) and sulphate-rich fertilizers [16], whereas the cluster two is composed of the wells 5, 7–10, 15 and 17–20 which represent the remaining 48% of the studied wells. This cluster was dominated by concentrations of electrical conductivity (EC), total dissolved solids (TDS), HCO_3-, Ca^{2+}, Cl^-, Mg^{2+}, Na^+ and K^+ ions among the studied wells which point the silicate weathering minerals such as pyroxene, mica and hornblende.

Cluster analysis of variables using ward linkage squared distance hierarchical algorithm produced two clusters (Fig. 4). Cluster one has two contributively parameters with negative correlation such as pH and SO_4^{2-} which represents the inverse relationship of pH with SO_4^{2-} ions in groundwater. Cluster two consists of electrical conductivity (EC), total dissolved solids (TDS), HCO_3-, Ca^{2+}, Cl^-, Mg^{2+}, Na^+ and K^+ which may be representative of overall effects of water–rock interactions, silicate weathering (Ca^{2+}, Mg^{2+}, Na^+ and K^+), dissolution of atmospheric carbon dioxide (HCO_3-), due to fertilizers and intense agricultural activities (Cl^-) and parameters which are influenced by each and every ion in groundwater (EC and TDS). This cluster includes virtually every ion of groundwater.
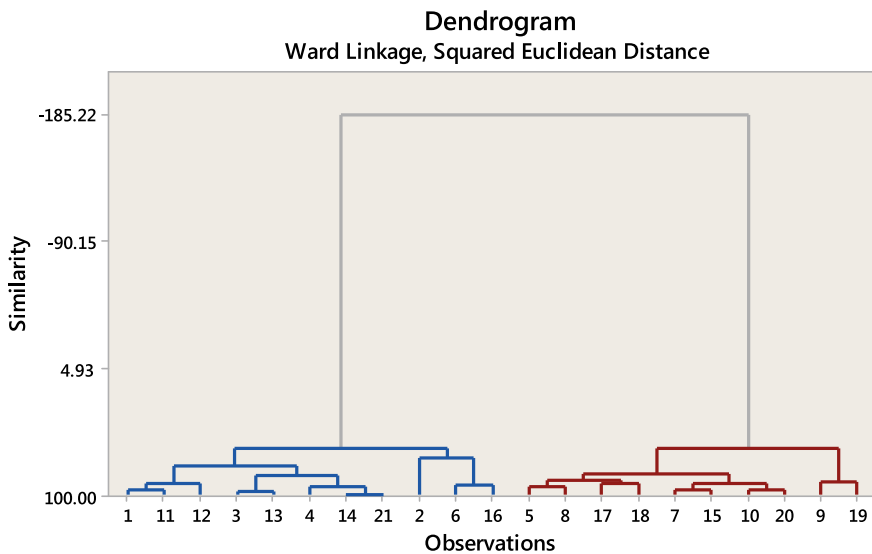
Fig. 3 Dendrogram of Q-mode cluster analysis
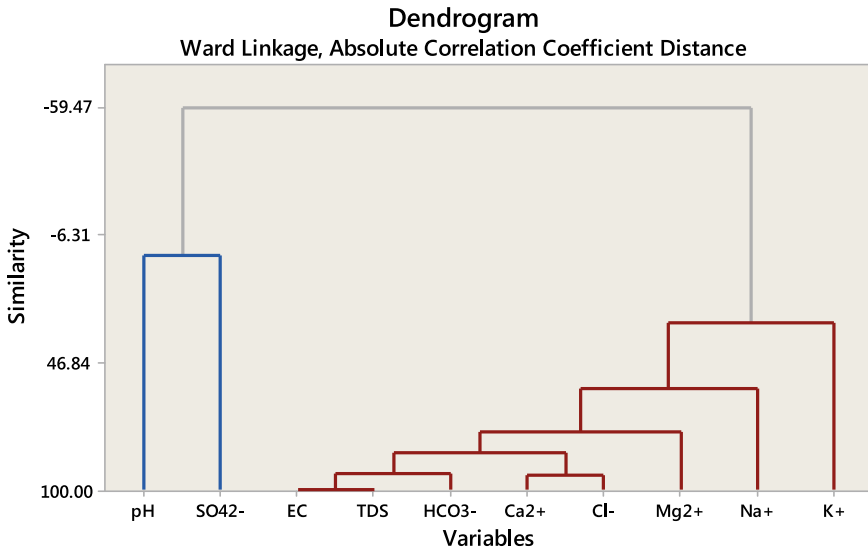
Fig. 4 Dendrogram of variables from R-mode cluster analysis

4.3 Factor Analysis

Varimax rotated factor loading was performed to the analysed data, and it has given nine factors to represent the variation of water chemistry (Table 2). Moreover, the scree plot was drawn by taking eigenvalue on *Y*-axis and factor on *X*-axis to comprehend the factors which have a considerable effect on the chemistry of water (Fig. 5).

Table 2 Varimax rotation factor loading matrix with values of variance and % variance

Variables	Factor-1	Factor-2	Factor-3
pH	0.048	0.103	**0.990**
EC	**0.940**	0.208	0.102
Ca^{2+}	**0.871**	0.389	−0.049
Mg^{2+}	0.769	0.140	0.129
Na^+	**0.549**	0.130	0.123
K^+	0.357	**0.914**	0.140
HCO_3-	**0.914**	0.093	0.071
Cl^-	**0.919**	0.238	−0.068
$SO_4{}^{2-}$	−0.093	−0.061	0.015
TDS	**0.940**	0.207	0.102
Variance	5.2367	1.1883	1.0650
% variance	0.524	0.119	0.106
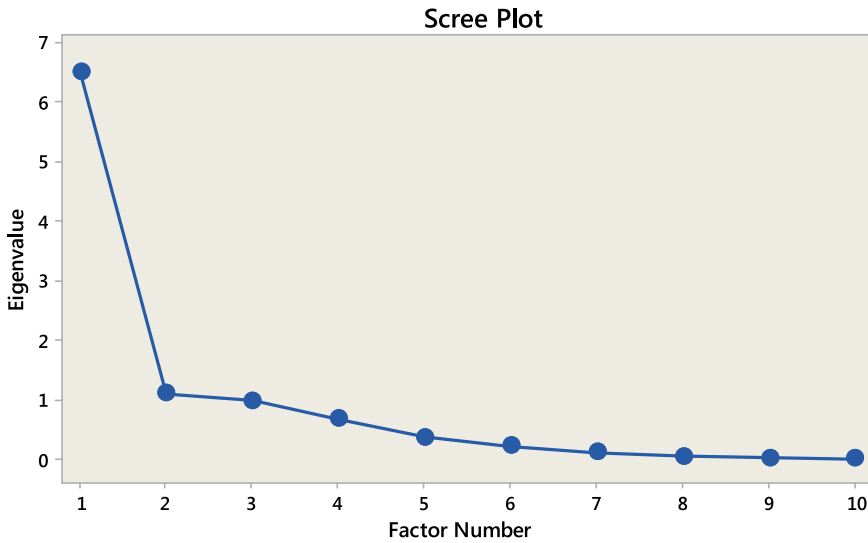
Fig. 5 Scree plot of eigenvalue versus factor number

Only factors with >1 or equivalent to 1 will be considered as potential sources of variance explained by each factor in the data [17]. Accordingly, the first three factors were taken into consideration as they explain 90% of the total variance of hydrochemistry (Table 2).

The first factor shows significant positive loaded values with EC, calcium, magnesium, sodium, bicarbonates, chloride and TDS (Table 2). The constituents such as Ca^{2+}, Mg^{2+} and Na^+ represent that these parameters were loaded into the aquifers due to weathering silicate minerals. The constituent such as Cl^- in aquifer possibly caused by using fertilizers and intense agricultural activities, whereas HCO_3- was possibly attributable to the role of carbonic acid in the weathering of silicate minerals. EC and TDS represent that the parameters were influenced by all these major ions. The second factor shows significant positive loadings with K^+ which represents that the ions probably loaded into the aquifers attributable to the silicate weathering minerals, for instance, biotite and muscovite [18], whereas the third factor shows positive loadings with the parameter pH only which is likely influenced by the alkaline nature of the water.

4.4 Processes Governing Groundwater Chemistry

Gibbs classification and water–rock interaction

Gibb's recommended two diagrams like (i) TDS versus $Cl^-/(Cl^- + HCO_3-)$ and (ii) TDS versus $(Na^+ + K^+)/(Na^+ + K^+ + Ca^{2+})$ [19]. Most samples fall under rock dominance zone reveals that rock–water interaction process prevails followed

by evaporation dominance (Fig. 6). The silicate weathering prevails if HCO_3- and SO_4^{2-} dominate over Ca^{2+} and Mg^{2+} [20]. The scatter diagram of $Ca^{2+} + Mg^{2+}$ versus $HCO_3- + SO_4^{2-}$ (Fig. 7) showed that the samples lie beneath the equiline, indicates silicate weathering and the points above the equiline point to carbonate weathering [21].
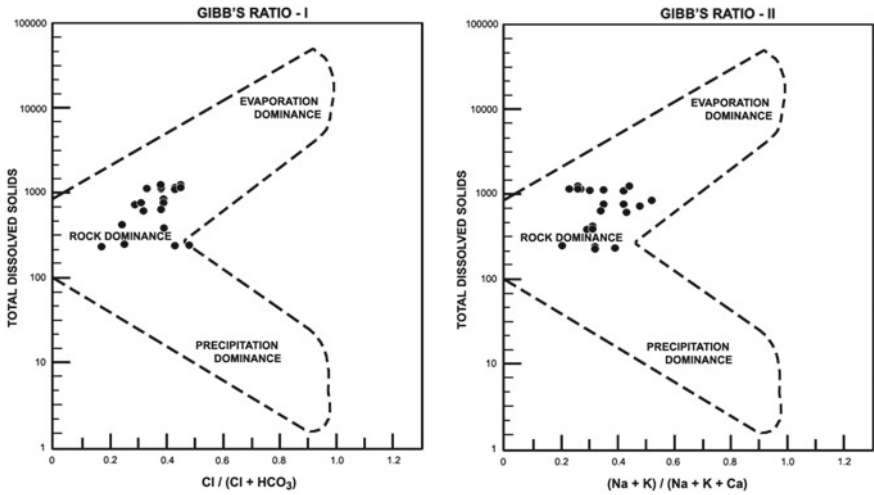
Fig. 6 Gibbs diagram
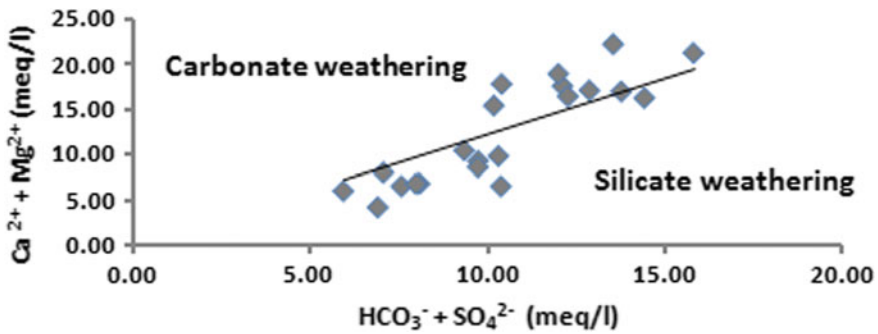
Fig. 7 Scatter plot of $Ca^{2+} + Mg^{2+}$ versus $HCO_3- + SO_4^{2-}$

4.5　Indices of Base Exchange

Schoeller [22] has demonstrated the method of ion exchange within groundwater and its host environs through its travel and residence time in an aquifer [22]. The CAI-1 and CAI-2 were calculated by the following formulas:

$$\text{Chloro-alkaline index (CAI) 1} = \left(Cl^- - \left(Na^+ + K^+\right)\right)/Cl^-$$

$$\text{Chloro-alkaline Index (CAI)2} = \left(Cl^- - \left(Na^+ + K^+\right)/\left(SO_4^{2-} + HCO_3^- + CO_3^{2-} + NO_3^{2-}\right)\right)$$

If CAI is negative, there will be an ion exchange between Na^+ and K^+ with Ca^{2+} and Mg^{2+} in water. If the ratio is positive, the ion exchange is reversed, and about 57% of groundwater samples showed positive ratios illustrate the reverse type of base exchange.

5　Conclusions

Multivariate statistical techniques, Chloro-alkaline indices and Gibbs ratio were executed to the analysed data to know the processes governing the groundwater chemistry. The abundance of major ion chemistry of water is as follows: $Ca^{2+} > Na^+ > Mg^{2+} > K^+$ and $HCO_3- > Cl^- > SO_4^{2-}$. The Q-mode cluster analysis which has resulted two distinctive clusters, cluster 1 (1–4, 6, 11–14, 16 and 21), cluster 2 (5, 7–10, 15 and 17–20), two variable clusters in R-mode such as cluster 1 (pH and SO_4^{2-}), cluster 2 electrical conductivity (EC), total dissolved solids (TDS), HCO_3-, Ca^{2+}, Cl^-, Mg^{2+}, Na^+ and K^+), three two distinctive factors, factor 1 (with significant positive loaded values with EC, calcium, magnesium, sodium, bicarbonates, chloride and TDS), factor 2 (with high positive loadings with K^+ only) and factor 3 (with high positive loadings with pH only) has demonstrated the sources that controlling groundwater hydrochemistry are silicate weathering, dissolution of sulphates and chlorides due to the fertilizers and intense agricultural activities. $Ca–Mg–HCO_3$ was the major hydrochemical facies in Chadha's classification. The scatter diagram showed that silicate weathering prevails in the study area as HCO_3- and SO_4^{2-} dominate over Ca^{2+} and Mg^{2+}. Moreover, the Gibbs ratio showed that rock–water interaction followed by evaporation, whereas the CAI-1 and CAI-2 indicate reverse ion exchange is responsible for the groundwater chemistry in this region.

References

1. Papaioannou, A., Mavridou, A., Hadjichristodoulou, C., Papastergiou, P., Pappa, O., Dovriki, E., et al. (2010). Application of multivariate statistical methods for groundwater physicochemical and biological quality assessment in the context of public health. *Environmental Monitoring and Assessment, 170,* 87–97.

2. Subramani, T., Elango, L., & Damodarasamy, S. R. (2005). Groundwater quality and its suitability for drinking and agricultural use in Chithar River Basin, Tamil Nadu, India. *Environmental Geology, 47,* 1099–1110.

3. Nagaraju, A., Balaji, E., Thejaswi, A., & Sun, L. (2015). Quality evaluation of groundwater in Mulakalacheruvu area, Chittoor district, Andhra Pradesh, South India based on hydrogeochemistry. *Fresenius Environmental Bulletin, 24,* 4496–4503.

4. Zahedi, S., Azarnivand, A., & Chitsaz, N. (2017). Groundwater quality classification derivation using multi-criteria-decision-making techniques. *Ecological Indicators, 78,* 243–252.

5. Nagaraju, A., Balaji, E., Sun, L. H., & Thejaswi, A. (2018). Processes Controlling groundwater chemistry from Mulakalacheruvu area, Chittoor District, Andhra Pradesh, South India: A statistical approach based on hydrochemistry. *Journal of the Geological Society of India, 91,* 425–430.

6. Belkhiri, L., Boudoukha, A., & Mouni, L. (2010). A multivariate statistical analysis of groundwater chemistry data. *International Journal of Environmental Research, 5,* 537–544.

7. Olsen, R. L., Chappell, R. W., & Loftis, J. C. (2012). Water quality sample collection, data treatment and results presentation for principal components analysis-literature review and Illinois River Watershed case study. *Water Research, 46*(9), 3110–3122.

8. Dhakate, Ratnakar, Mahesh, J., Sankaran, S., & Gurunadha Rao, V. V. S. (2013). Multivariate statistical analysis for assessment of groundwater quality in Talcher Coalfield Area, Odisha. *Journal of the Geological Society of India, 82,* 403–412.

9. Ranmanesh, A., Locke, R. A., & Wimmer, B. T. (2014). Multivariate statistical evaluation of groundwater compliance data from the Illinois Basin-Decatur project. *Energy Procedia, 63,* 3182–3194.

10. Viswanath, N. C., Dileep Kumar, G., Ammad, K. K., & Usha Kumari, E. E. (2015). Ground water quality and multivariate statistical methods. *Environmental Processes, 2,* 347–360.

11. Boateng, T. K., Opoku, F., Acquaah, S. O., & Akoto, O. (2016). Groundwater quality assessment using statistical approach and water quality index in Ejisu-Juaben municipality, Ghana. *Environmental Earth Sciences, 75,* 1–14.

12. Kumar, M., Ramanathan, A. L., Tripathi, R., Farswan, S., Kumar, D., & Bhattacharya, P. (2017). A study of trace element contamination using multivariate statistical techniques and health risk assessment in groundwater of Chhaprola Industrial Area, Gautam Buddha Nagar, Uttar Pradesh, India. *Chemosphere, 166,* 135–145.

13. Gulgundi, M. S., & Shetty, A. (2018). Groundwater quality assessment of urban Bengaluru using multivariate statistical techniques. *Applied Water Science, 8*(43), 1–15.

14. Tripathi, A. K., Mishra, U. K., Mishra, A., & Dubey, P. (2012). Assessment of groundwater quality Gurh Tehseel, Rewa District Madhya Pradesh, India. *International Journal of Scientific & Engineering Research (IJSER), 3,* 1–12.

15. APHA. (2012). *Standard methods for the examination of water and wastewater* (22nd ed.). New York: American Public Health Association.

16. Nosrati, K., & Van Den Eeckhaut, M. (2012). Assessment of groundwater quality using multivariate statistical techniques in Hashtgerd Plain, Iran. *Journal of Environmental Earth Science, 65,* 331–344.

17. Cattell, R. B. (1966). The scree test for the number of factors. *Multivariate Behavioral Research, 1*(2), 245–276.

18. Davis, S. N., & Dewiest, R. J. (1966). *Hydrogeology* (p. 463). New York: Wiley.

19. Gibbs, R. J. (1970). Mechanisms controlling world water chemistry. *Science, 17,* 1088–1090.

20. Elango, L., Kannan, R., & Senthil Kumar, M. (2003). Major ion chemistry and identification of hydrogeochemical processes of groundwater in part of Kancheepuram district, Tamil Nadu, Indian. *Journal of Environmental Geosciences, 10,* 157–166.
21. Khan, Rubia, & Jhariya, D. C. (2018). Hydrogeochemistry and groundwater quality assessment for drinking and irrigation purpose of Raipur City, Chhattisgarh. *Journal Geological Society of India, 91,* 475–482.
22. Schoeller, H. (1977). Geochemistry of groundwater. In *Groundwater studies—An international guide for research and practice* (Vol. 15, pp. 1–18). Paris: UNESCO.

Corrosion Performance Evaluation of Rebar in Metakaolin Blended Concrete

U. Raghu Babu and B. Kondraivendhan

Abstract Reinforcement corrosion is of obvious importance in reinforced structures in harsh environments. The presence of sulfates may influence the chloride-induced corrosion of rebar in concrete. In this paper, the results of an experimental investigation are presented wherein the influence of chloride and chloride plus sulfate ions on the corrosivity of rebar embedded in ordinary Portland cement (OPC) and OPC blended with metakaolin (MK) concretes has been investigated. In this investigation, concrete mixtures have been prepared with four replacement levels of OPC (0, 5, 10, and 15%) with MK and water to cementitious material ratio 0.5. Reinforced concrete specimens were exposed to pure chloride solution. Further, to investigate the influence of sulfate concentration on chloride-induced corrosion, the samples were exposed to the composite solution of chloride and sulfate ions of various concentrations. The corrosion performance of rebar has been monitored by the half-cell potential values. Besides, an impressed voltage technique for accelerated corrosion test has also adopted to investigate the optimum replacement level of cement with MK as a short-term technique. Results of accelerated corrosion test indicated that beyond 10% MK, the concrete was found to be less corrosion resistant. From potential measurements, it was observed that the presence of magnesium sulfate with chlorides influences the time to initiation of corrosion in both plain and MK blended concretes.

Keywords Impressed voltage · Corrosion · Metakaolin · Sulfates · Chlorides

U. Raghu Babu (✉) · B. Kondraivendhan
Applied Mechanics Department, Sardar Vallabhbhai National Institute of Technology, Surat, Gujarat 395007, India
e-mail: ammaraghubabu@gmail.com

B. Kondraivendhan
e-mail: kondraivendhan78@gmail.com

1 Introduction

Concrete structures such as bridges, offshore platforms, and tunnels are required to perform in aggressive environments. Most of structural failures are mainly due to the reinforcing steel corrosion due to chlorides and sulfate attack. Structural failures not only have resulted in loss of economy, but it also resulted in loss of human life. Many researchers have been investigated and believed that the incorporation of pozzolana materials like fly ash, silica fume, etc. plays a vital role in enhancing the strength and durability of the structures.

In recent years, many of the researchers [1–6] have been focused on the metakaolin (MK) as a supplementary cementitious material due to its high capability to react with $Ca(OH)_2$ present in cement. MK is alumina–silicate type pozzolana, which is obtained from the calcination of the kaolin clay at the temperatures range of 500–800 °C. Brooks and Johari [7] reported that the incorporation of MK increased the compressive strength measurements. Li and Ding [8] suggested from their experimental results that the maximum compressive strength can be achieved with concrete made with 10% cement replacement. In contrast, Khatib and Wild [9] reported that 20% replacement of cement with MK gives the maximum strength. The studies conducted by Poon et al. [10] are shown that the paste specimens containing 10% MK perform better in terms of strength.

The addition of MK led to resist the ingress of aggressive ions into the concrete due to its potential to decrease the porosity of the concrete [11]. The permeability of concrete and chloride binding is the key factors for resistance to the penetration of chlorides into concrete. It is believed that the incorporation of MK helps to decrease chloride diffusion due to refined pore structure and reduced electrical conductivity [12]. Parande et al. [2] concluded that the addition of 15% MK with the replacement of cement performs better in corrosion resistance, water absorption and resistivity, and ultrasonic pulse velocity values. Shi et al. [5] observed from an experimental investigation that the addition of MK helps to reduce the disadvantages with seawater in concrete by enhancing properties of compressive strength, pore structure, and microstructure.

This present work forms part of a research work, which aims to exploit the optimum level of metakaolin as a cement replacement in reinforced concrete to enhance the durability. In the current work, one set of experimental studies has been undertaken for performance evaluation of the cylindrical concrete specimens made with various replacement levels of metakaolin with water to cementitious material (w/cm) ratio 0.5 under accelerated conditions. In accelerated corrosion test the concrete samples were immersed in 2.5% NaCl solution, and the corrosion process was initiated by applying the voltage of 12 V D.C. to the reinforcement. Another set of experimental investigation has been undertaken on the influence of the sulfate concentration on chloride-induced corrosion of reinforced concrete with different replacement levels of metakaolin. Further, the probability of corrosion was checked by carrying out half-cell potential test as per ASTM C 876 [13] on the specimens at the end of wetting period of every wetting and drying cycle.

2 Experimental Method

2.1 Materials and Specimen Preparation

In the experimental study, ordinary Portland cement of 53 grade, river sand confirming zone II from local sources, tap water, and the natural coarse aggregate of size 20 mm were used. The specific gravity of the fine and coarse aggregate was 2.70 and 2.75, respectively. The metakaolin was supplied by Kaolin Techniques Pvt. Ltd. The chemical composition of cementitious material used in this work is shown in Table 1. All concrete mixtures were prepared by the w/cm ratio 0.5.

Cylindrical concrete specimens with diameter of 100 mm and length of 200 mm were prepared with a centrally embedded thermally mechanically treated (TMT) steel reinforcement of diameter 12 mm. Reinforcement bars were cut to the required length of 200 mm. One end of the rebar was drilled and threaded to fit the stainless steel (SS) screw for connections. To remove surface scale, each bar was wire brushed and cleaned by soaking in hexane then allowed to air dry. An SS screw and two nuts were attached to the rebar. Both ends of the rebar were taped with insulating tape after coating with insulating paint so that a 150 mm portion of the bar is bare as described in Fig. 1. The cement was replaced by the MK in the replacement level of 0, 5, 10, and 15% by weight of cement. Slumps were kept constant 50–75 mm for all mixtures. The concrete specimens were cast in three layers, using a vibrating table to produce superior compaction.

2.1.1 Exposure Conditions

After 24 h of casting, the cylindrical specimens were demolded and placed in water for 27 days of moist curing. After moist curing, the specimens were exposed to cyclic wetting and drying using three different aggressive test solutions prepared with

Table 1 Chemical composition of cementitious materials

Chemical compound	OPC	MK
Al_2O_3 (%)	5.32	40–42
Fe_2O_3 (%)	4.23	1.3 (max)
SiO_2 (%)	20.65	52–54
MgO (%)	1.13	1.0
TiO_2 (%)	–	0.5 (max)
CaO (%)	64.12	1.0
SO_3 (%)	2.16	–
Na_2O (%)	–	–[a]
LOI (%)	2.39	1.5

[a]Na_2O K_2O: 0.5–2.5%

Fig. 1 Schematic representation of accelerated corrosion test
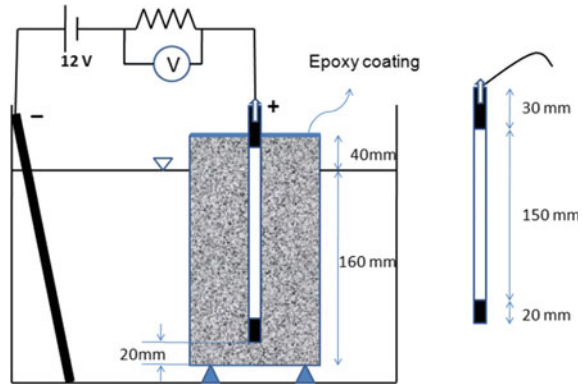
sodium chloride (NaCl) and magnesium sulfate ($MgSO_4$) as the sources of chlorides and sulfate, respectively. Each cycle consists of ten days wetting and twenty days drying. The composition of exposure solutions is as detailed below:

Solution 1: 2.5% NaCl
Solution 2: 2.5% NaCl + 1.5% $MgSO_4$
Solution 3: 2.5% NaCl + 3% $MgSO_4$.

2.2 Techniques Adopted

2.2.1 Impressed Voltage Technique

The short-term accelerated corrosion technique named as impressed voltage technique is adopted to evaluate the optimum replacement level of cement with MK. The system was prepared with the rebar embedded in concrete as an anode, externally placed SS rod as a cathode, and the electrolyte is 2.5% NaCl solution. The diagram of the test setup is shown in Figs. 1 and 2. By using an external DC source, a constant voltage of 12 V is applied between rebar and SS rod up to the cracking of the specimen. The anodic current was noted for every two hours and the time to initiate a first crack on the concrete was observed (see Fig. 3), and the corresponding anodic current was noted. This short-term accelerated technique was adopted on only the specimens made with MK concrete replacement levels of 0, 10, and 15%. The cylindrical specimens after completion of water curing were kept in the laboratory condition for two months, after that they were subjected to the accelerated corrosion test.

Fig. 2 Test setup for
accelerated corrosion test

Fig. 3 Typical cracked
specimen

2.2.2 Half-Cell Potential Measurements

The half-cell potential measurements of the concrete mixtures made with OPC and
OPC blended with MK exposed to different aggressive environments were deter-
mined. The potential measurements were taken at the end of each wetting cycle
with respect to saturated calomel electrode (SCE). The positive terminal of the high
impedance multimeter was connected to the reinforcing bar, and the common ter-
minal was connected to the SCE. The potential values were taken at six different
locations of the specimen parallel to rebar. The average of these values was recorded
and interpreted based on the ASTM C 876-91, as shown in Table 2.

Table 2 ASTM C 876 [13, 14] criterion for corrosion

Potential, mV versus SCE	Probability of corrosion
More negative than −275	>90% (active corrosion)
Between −275 and −125	Uncertain
More positive than −125	>10% (passive corrosion)

3 Results and Discussion

3.1 Impressed Voltage Technique

The variation of corrosion current response with time for MK replacement levels of 0, 10, and 15% is shown in Fig. 4. From Fig. 4, it is observed that the reinforcement embedded in the concrete mix made with OPC and OPC blended with 15% MK exhibited a rapid increase of current as compared to the concrete with 10% MK. From this, it is clear that the MK addition beyond 10% is less resistive to corrosion and the service life of this concrete will be less. The results of the impressed voltage technique for plain and blended concretes are reported in Table 3. The anodic current of the concrete blended with 10% MK is less than the plain concrete and 15% MK blended concrete. This rise in the corrosion resistance of specimens prepared with

Fig. 4 Corrosion current versus time of various dosages of MK
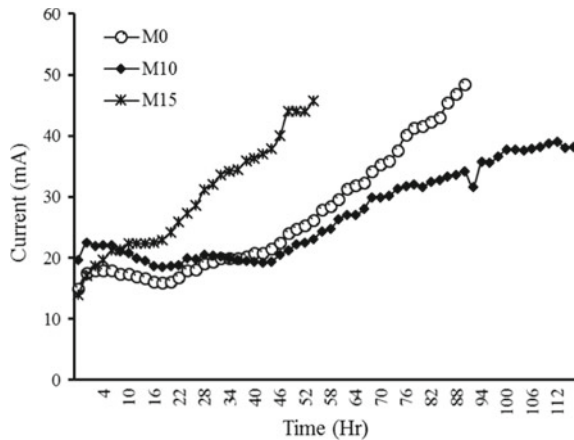
Table 3 Impressed voltage data for OPC and MK admixed systems

System	Time to crack (h)	Maximum current (mA)
OPC	92–107	36–37
OPC + 10% MK	116–119	20–32
OPC + 15% MK	56–62	34–35

10% of MK is due to the pore structure refinement and stronger paste matrix of pozzolanic reactivity of MK [15].

3.2 Half-Cell Potential Measurements

The plots of time corrosion potentials of the rebar embedded in OPC and OPC blended with MK concretes exposed to different aggressive solutions are shown in Figs. 5, 6 and 7. The data on corrosion initiation time for both plain and blended concretes is shown in Table 4. The corrosion initiation time was observed to be more for the concretes blended with MK as compared to that of plain concrete. The

Fig. 5 Half-cell potential versus time for specimens exposed to NaCl
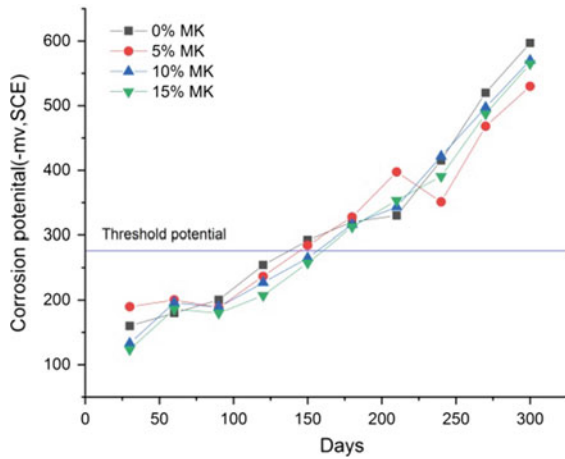
Fig. 6 Half-cell potential versus time for specimens exposed to a composite solution of NaCl with 1.5% magnesium sulfate
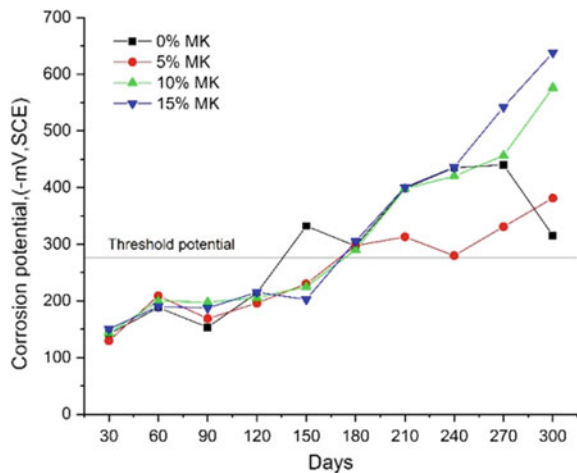
Fig. 7 Half-cell potential versus time for specimens exposed to a composite solution of NaCl with 3% magnesium sulfate
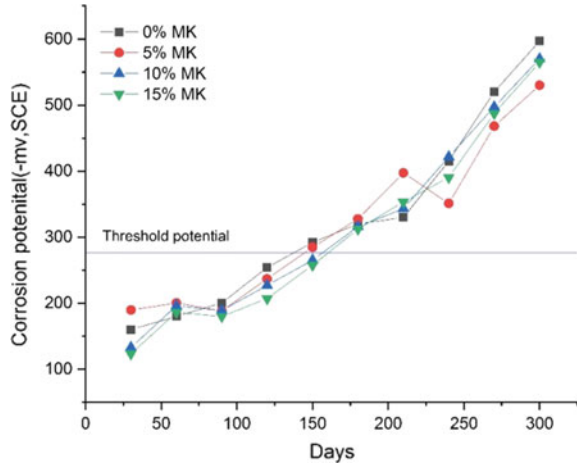
Table 4 Time to corrosion initiation of rebar of OPC and OPC blended with MK

Exposure solution	OPC	MK 5%	MK 10%	MK 15%
2.5% NaCl	136	144	156	158
2.5% NaCl + 1.5% MgSO$_4$	135	170	173	171
2.5% NaCl + 3% MgSO$_4$	156	162	167	170

addition of 1.5% magnesium sulfate to chloride increased the time to initiation of corrosion about 26, 17, and 13 days for the concretes 5, 10, and 15% MK blended concrete, respectively. For concretes exposed to a composite solution of 2.5% sodium chloride and 3% magnesium sulfate, the corrosion initiation times were observed to be increased about 20, 18, 11, and 12 days for cement replacement level of 0, 5, 10, and 15% with MK, respectively as compared to pure chlorides. The increment of corrosion initiation time with the addition of sulfates to chlorides is attributed to the influence of Mg^{+2} cation associated with sulfate. The formation of Mg(OH)$_2$ from the reaction of Mg^{+2} ions with calcium hydroxide clogs the pores and resist further ingression of chlorides into concrete. While observing the influence of sulfate concentration with the fixed chloride concentration on corrosion of rebar in plain and metakaolin blended concrete, no systematic results have been observed. In normal OPC concrete, the corrosion initiation time increased from 135 to 156 days, with the increment of sulfate content in the fixed chloride solution from 1.5 to 3%. On the other hand, the concrete blended with metakaolin up to 10% shows the decrement of corrosion initiation time with the increment of sulfate content. However, it remains the same for the concrete with a 15% MK addition.

From Table 4, it is also observed that the corrosion initiation time increased with the incorporation of metakaolin to concrete. There is a significant increment in corrosion initiation up to the replacement level of 10% of MK, but slight increment is observed beyond 10% replacement of MK.

4 Conclusions

From the present experimental investigation, the following conclusions were drawn:

- The addition of 10% MK as a replacement of cement is beneficial than higher replacement levels for improving the chloride-induced corrosion performance of rebar in concrete.
- The incorporation of MK helps to delay the corrosion initiation compared to OPC concrete in the presence of both chloride and chloride–sulfate solutions.
- The potential measurements did not indicate a clear trend on the influence of the sulfate percentage level of chloride-induced corrosion.
- The time to corrosion initiation was found to be more in the specimens exposed to the combined solution of NaCl and $MgSO_4$.

References

1. Rashad, A. M. (2015). A synopsis about the effect of metakaolin on the durability of Portland cement—An overview. *Scientia Iranica. Transaction A, Civil Engineering, 22*, 579–604.
2. Parande, A. K., Ramesh Babu, B., Aswin Karthik, M., Deepak Kumaar, K. K., & Palaniswamy, N. (2008). Study on strength and corrosion performance for steel embedded in metakaolin blended concrete/mortar. *Construction and Building Materials, 22,* 127–134.
3. Antoni, M., Rossen, J., Martirena, F., & Scrivener, K. (2012). Cement and concrete research cement substitution by a combination of metakaolin and limestone. *Cement and Concrete Research, 42,* 1579–1589.
4. Li, Q., Geng, H., Huang, Y., & Shui, Z. (2015). Chloride resistance of concrete with metakaolin addition and seawater mixing: A comparative study. *Construction and Building Materials, 101,* 184–192.
5. Shi, Z., Shui, Z., Li, Q., & Geng, H. (2015). Combined effect of metakaolin and sea water on performance and microstructures of concrete. *Construction and Building Materials, 74,* 57–64.
6. Wang, G. M., Kong, Y., Shui, Z. H., Li, Q., & Han, J. L. (2014). Experimental investigation on chloride diffusion and binding in concrete containing metakaolin. *Corrosion Engineering, Science and Technology, 49,* 282–286.
7. Brooks, J. J., & Johari, M. M. (2001). Effect of metakaolin on creep and shrinkage of concrete. *Cement and Concrete Composites, 23*(6), 495–502.
8. Li, Z., & Ding, Z. (2003). Property improvement of Portland cement by incorporating with metakaolin and slag. *Cement and Concrete Research, 33*(4), 579–584.
9. Khatib, J. M., & Wild, S. (1996). Pore size distribution of metakaolin paste. *Cement and Concrete Research, 26*(10), 1545–1553.
10. Poon, C. S., Kou, S. C., & Lam, L. (2002). Pore size distribution of high performance metakaolin concrete. *Journal of Wuhan University of Technology-Materials Science Edition, 17,* 42–46.
11. Güneyisi, E., Gesoğlu, M., & Mermerdaş, K. (2008). Improving strength, drying shrinkage, and pore structure of concrete using metakaolin. *Materials and Structures, 41,* 937–949.
12. Khatib, J. M., & Wild, S. (1998). Sulphate Resistance of metakaolin mortar. *Cement and Concrete Research, 28*(1), 83–92.
13. ASTM C 876. (1999). Standard test method for half-cell potentials of uncoated reinforcing steel in concrete.

14. Vedalakshmi, R., Balamurugan, L., Saraswathy, V., Kim, S. H., & Ann, K. Y. (2010). Reliability of galvanostatic pulse technique in assessing the corrosion rate of rebar in concrete structures: Laboratory vs field studies. *KSCE Journal of Civil Engineering, 14,* 867–877.

15. Sudheer, S., Babu, U. R., & Kondraivendhan, B. (2019). Influence of metakaolin and red mud blended cement on reinforcement corrosion in presence of chloride and sulfate ions. In B. B. Das & N. Neithalath (Eds.), *Sustainable construction and building materials*. Lecture Notes in Civil Engineering (pp. 717–725). Singapore: Springer.

Effect of Pond Ash on Black Stone Waste Aggregate Concrete

U. Raghu Babu, N. Venkata Ramana, Sakevalla Vinay Babu
and Piantee Pavithra

Abstract During the energy generated from the thermal power plants, the waste generated in large quantities is a serious environmental concern due to its disposal. Many researchers have well documented the utilization of fly ash as a mineral admixture among the different wastes generated from the thermal power plant. However, limited studies have investigated the effect of the other wastes, including pond ash on the mechanical properties of concrete. In this context, the investigation on the effect of pond ash in the construction industry is required. In addition, this paper also investigates the utilization of black waste stone as coarse aggregate in concrete, which helps to reduce the consumption of natural resources. An attempt has been made to investigate the compressive strength and splitting tensile strength, and the performance of concretes made with partial replacement of cement with pond ash and coarse aggregate with black stone aggregate. For this, concrete specimens were prepared with two different w/cm (water to cementitious) material ratios, four different replacement ratios (0, 5, 15, and 25%) of cement, and four different replacement levels of coarse aggregate (0, 25, 50, and 75%). The experimental results concluded that the potential applicability of pond ash and waste stone aggregate in concrete leads to the active utilization of waste products from both thermal power plants and

U. Raghu Babu (✉)
Applied Mechanics Department, Sardar Vallabhbhai National Institute of Technology,
Surat, Gujarat 395007, India
e-mail: ammaraghubabu@gmail.com

N. Venkata Ramana
Construction Technology Department, Visvesvaraya Technological University,
Center of PG Studies, Kalaburagi, Karnataka 585105, India
e-mail: rccramana@gmail.com

S. Vinay Babu · P. Pavithra
Department of Civil Engineering, G. Pullaiah College of Engineering and Technology,
Kurnool, Andhra Pradesh 518002, India
e-mail: vinaysake@gmail.com

P. Pavithra
e-mail: pavithra137.civil@gmail.com

stone polishing industry. In addition, the relation between the compressive and tensile strength measurements was carried out by statistical analysis.

Keywords Pond ash · Concrete · Compressive strength · Tensile strength · Statistical analysis · Industrial waste

1 Introduction

Currently, the industrial waste products are being used in the construction industry as mineral admixtures like rice husk ash, silica fume, ground granulated blast furnace slag, coal bottom ash and fly ash, etc. The incorporation of industrial waste as a partial replacement of cement is beneficial to improve the quality, strength, and durability of construction. However, it also ensures cost and energy.

The generation of electricity through thermal route involves combustion of pulverized coal/lignite has been the backbone of the power capacity of India. In comparison with imported coals which have low ash content of the order of 10–15%, Indian coal is of low grade with ash content of the order of 30–45%. Normally, the two types of ashes (fly ash and bottom ash) are thus being generated at thermal power stations mixed thoroughly with large quantities of water and sluiced to on-site storage ponds called ash ponds. The unused fly ash and bottom ash slurry are known as pond ash. The ash is not only required large areas of land for its disposal but is also one of the sources of pollution of both air and water. This disposal and environmental problems can be minimized by effective utilization of ash in the concrete industry.

In India, during the year 2016–17 Andhra Pradesh, Chhattisgarh, Madhya Pradesh, Maharashtra, Odisha, Uttar Pradesh, and West Bengal have generated more than 10 million-ton of ash. Uttar Pradesh has occupied the first place among states generating highest ash residuals with the maximum generation of 28.27 million tons. Central Electricity Authority (CEA) has been monitoring the generation and utilization of ash at coal/lignite-based thermal power stations in the country. In order to utilize the ash generated from the thermal power plants, a huge research work has been carried out on the effective utilization of fly ash in the construction industry. However, several studies [1–8] have been performed on the application of bottom ash to construction material as fine aggregate [1] and as a cement replacement material. But limited literature was available on pond ash, which is the mixture of unused fly ash [2] and bottom ash.

Andhra Pradesh is a home to varieties of construction stones, including Tadipatri, Bethamcherla, Cuddappah, and such others, which make excellent floors. The stone industries produce a large quantity of marble waste in the form of powder/slurry and pieces of irregular size of stones. However, the stones obtained from the quarries are usually dumped in empty pits in the forest area and beside the roads, thereby creating huge amounts of waste which is a serious environmental concern.

Binici et al. [3] investigated the effect of marble and limestone dust as fine aggregate on the different properties of concrete. The concrete mixtures were prepared with

5, 10, and 15% marble and limestone dust replacement of fine aggregate. Results indicated that modified concretes containing made with marble and limestone dust have good workability, abrasion resistance, and sulfate resistance. As an extension of the previous work, Binici et al. [4] studied the durability of the concretes made with granite and marble as coarse aggregate, river sand, and ground blast furnace slag as fine aggregate. The results indicated that concretes with marble and GBFS were shown superior performance in terms of durability and bonding strength. The experimental work conducted by Venkata Ramana et al. [5] showed that 50% replacement of natural aggregate by stone waste aggregate is desirable for concrete works. Kore and Vyas [6] were carried out an experimental study to examine the possibility to use marble waste as a coarse aggregate in concrete by replacing natural coarse aggregate with marble aggregate in different percentages in the range of 0–100% by weight. It was observed that the concretes made with marble aggregate showed the increase in compressive strength by 40 and 18% at 7 and 28 days, respectively, as compared to concrete with natural aggregate.

In the current experimental study, the compressive and split tensile strength of concrete made with various replacement levels of cement and coarse aggregate were investigated. In order to investigate the effect of pond ash, the concrete specimens were prepared with various replacement levels (0, 5, 15, and 25%) of cement by the pond ash. Further, to investigate the utilization of Bethamcherla black stone in concrete, the concrete was made with Bethamcherla black stone waste aggregate (BSWA) with replacement levels of 0, 25, 50, and 75% of the natural aggregate (NA).

2   Materials and Experimentation

For the preparation of the test specimens, ordinary Portland cement of 53 grade conformed to IS 12269 [9] was used as a basic binding constituent of the concrete. The specific gravity of cement was observed as 3.05. The values of initial and finally setting of time were found as 45 and 360 min, respectively. Locally available river sand was used as fine aggregate. Normal crushed aggregate from local sources was used as natural coarse aggregate. The specific gravity of sand and natural coarse aggregate is determined as 2.58 and 2.66, respectively. The raw stone waste material collected from the stone polishing industry, Bethamcherla, Kadapa District (Andhra Pradesh). The material was transported to the crusher unit and converted the waste stone as coarse aggregate of size 20 mm maximum sizes of aggregate (MSA) and 10 mm MSA. The specific gravity of the combined 20 and 10 mm aggregate in the proportion of 60 and 40%, respectively, is determined as 2.68. For each mix, three concrete cubes of size $150 \times 150 \times 150$ mm for compressive strength and three cylindrical specimens of size 150 mm diameter and 200 mm height were prepared.

Total 96 concrete cube specimens and 96 cylindrical specimens were prepared with two water cementitious materials (w/cm) ratio of 0.45 and 0.48, four cement replacement levels, four aggregate replacement levels, and three replicates.

For concrete mixing and curing, the laboratory tap water, which is free from the concentration of acid and organic substances, was used. While casting the specimens, mixing was carried out as an electrically operated mechanical mixer, and both cube and cylinder specimens were vibrated mechanically by using table vibrator. Concrete was poured into the molds in three uniform layers. After 24 h, the specimens were demolded and transferred into the curing tank until the test age.

3   Test Setup

3.1   *Compressive Strength Test*

As per IS: 516-1959 [10] compression test on concrete cube specimens was conducted with a compression testing machine of 2000 kN capacity and a least count of 1.0 kN. As per IS: 516-1959 [10], this test was conducted on three replicates of cube specimens of concrete made with various replacement levels of pond ash and black stone waste aggregate. The average of compressive strength of three replicates is reported as the compressive strength of the concrete mixture.

3.2   *Split Tensile Strength Test*

As per IS: 5816-1999 [11], a split tensile strength test was conducted on three cylindrical specimens for each concrete mix. The cylindrical specimen was carefully placed in the jig with packing strip and loading pieces and the jig was placed in the machine so that the specimen is located centrally. The average value of three replicate specimens was considered as the split tensile strength of that concrete group.

4   Results and Discussion

Figures 1 and 2 depict the compressive strength variation of BSW concrete with pond ash content for w/cm 0.45 and 0.48, respectively. From Fig. 1, it was observed that compressive strength decreased continuously with increasing pond ash content for concretes with coarse aggregate substitution of 25 and 50%. However, the rapid decreasing trend was observed in the compressive strength of BSW-25 and BSW-50 concretes from 15% pond ash substitution. But for BSW-75 concrete the rapid decreasing trend was started from 5% pond ash content onwards. From Fig. 2, it was observed that the concrete with pond ash replacement of more than 15% decreases the compressive strength rapidly in all BSW concretes which include BSW-25, BSW-50, and BSW-75 at the w/cm 0.48. Figure 3 shows the effect of w/cm ratio on compressive strength of the concrete with 0% aggregate substitution. The same trend was observed

Fig. 1 Compressive strength variation of concrete specimens with w/cm 0.45
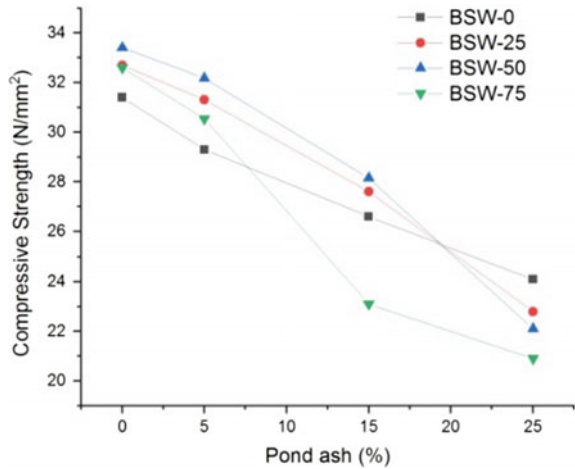
Fig. 2 Compressive strength variation of concrete specimens with w/cm 0.48
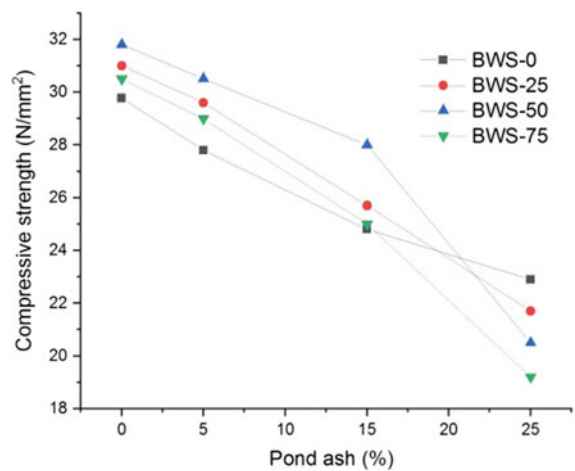
in all BSW concretes. From Fig. 3, it was also observed that the concrete specimens made with w/cm 0.48 have shown lower compressive strength values as compared to that of made with w/cm 0.45. It is due to the fact that as w/cm ratio increases the porosity of the concrete increases, which results in a decrease in compressive strength. It is important to note that at 5% pond ash dosage, the concrete with 25 and 50% BSW aggregates were showing more compressive strength values than the control concrete (0% pond ash and 0% BSW aggregate).

From Figs. 4 and 5, it was observed that the split tensile strength of specimens made with pond ash decreases as the dosage of pond ash increases. However, specimens made with lower w/cm ratio result higher tensile strength as compared to that of higher w/cm ratio. It can be observed that the substitution of BSW aggregates increases the split tensile strength at all replacement levels. As the pond ash addition increases the

Fig. 3 Compressive strength
variation with w/cm ratios
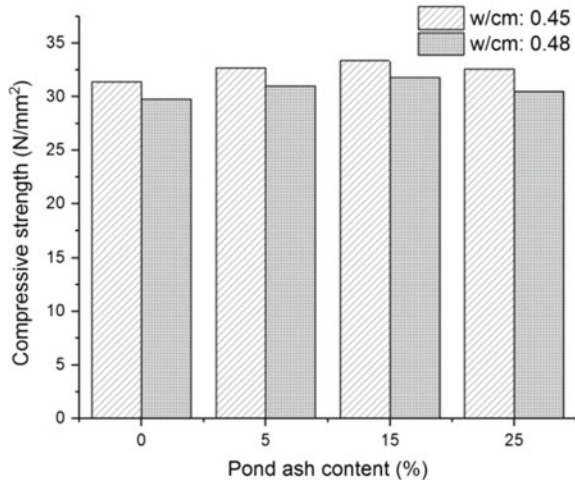
Fig. 4 Split tensile strength
variation concretes with
w/cm 0.45
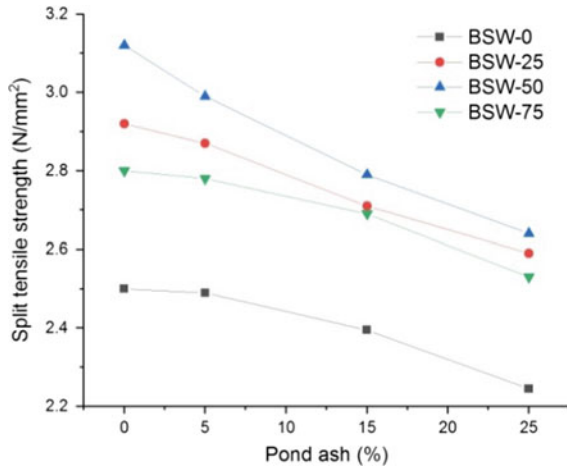
performance of BSW concretes decreasing in terms of strength values. However, it is
observed that the concrete with 50% replacement of BSW stone aggregate showing
greater strength values as compared to other replacement levels.

From the available literature [12–22], it is observed that concrete splitting tensile
strength is closely related to that of compressive strength. Nonlinear equation can
represent the relationship between tensile strength and compressive strength of con-
crete, due to the increase in tensile strength and decrease in the ratio of compressive
and tensile strength of concrete with an increase in compressive strength. For the
purpose of evaluating the empirical relationship between splitting tensile and com-
pressive strength of BSW aggregate concrete, the following relationship was adopted
in this study

Fig. 5 Split tensile strength variation of concretes with w/cm 0.48
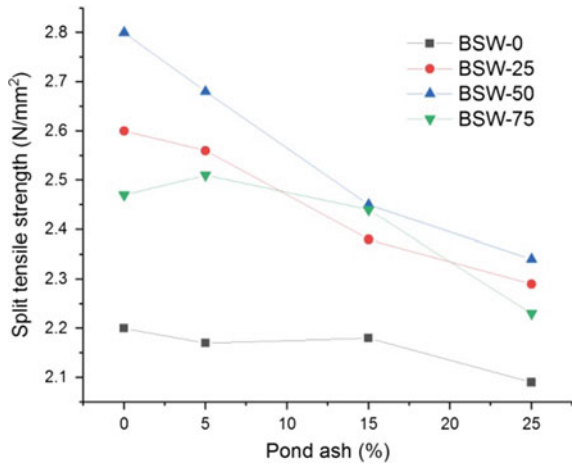
$$f_t = a(f_c)^b$$

where

a and b are fitting parameters.

The above-adopted equation is in agreement with the relations proposed by many researchers for compressive and tensile strength relationship. The models proposed by other authors are listed in Table 1. From the obtained test results, the relationship between the compressive strength and tensile strength was obtained through nonlinear curve fitting (Fig. 6):

$$f_t = 0.7(f_c)^{0.38}$$

The proposed relation between tensile and compressive strength of concretes was remarkably in agreement with the functions proposed by the authors, ACI 318-99 [18], Mokhtarzadeh et al. [19], ACI 363R-92 [20], etc.

Table 1 Proposed models by several authors

S. No	Reference	Proposed function
1.	ACI 363R-92	$f_t = 0.59(f_c)^{0.5}$
2.	ACI 318-99	$f_t = 0.56(f_c)^{0.5}$
3.	Mokhtarzadeh et al.	$f_t = 0.3(f_c)^{0.66}$
4.	Oluokun et al.	$f_t = 0.294(f_c)^{0.69}$
5.	Neville	$f_t = 0.23(f_c)^{0.67}$
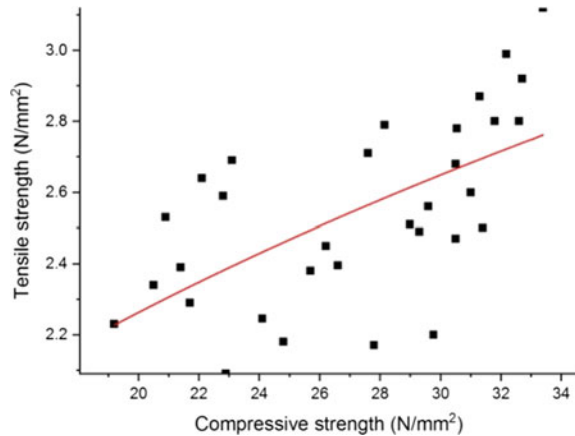
5   Conclusion

From the outcome of the present experimental investigation, the following observations were drawn:

1. Up to 50% replacement of coarse aggregate with BSW aggregates is beneficial to enhance the strength properties of concrete.
2. While increasing the pond ash dosage, both compressive and split tensile strength measurements were decreasing.
3. With the replacement of natural aggregates up to 50% by BSW aggregates, the pond ash can be utilized in concretes by 5% of cement replacement.
4. As the w/cm ratio increases, the both compressive and tensile strength measurements decreases.
5. The proposed model is very beneficial for the prediction of the splitting tensile strength of BSW concrete from compression strength.

References

1. Arumugam, K., Ilangovan, R., & James, M. D. (2011). A study on characterization and use of pond ash as fine aggregate in concrete. *International Journal of Civil and Structural Engineering, 2,* 466–474.
2. Phanikumar, B. R., & Sofi, A. (2016). Effect of pond ash and steel fibre on engineering properties of concrete. *Ain Shams Engineering Journal, 7,* 89–99.
3. Binici, H., Kaplan, H., & Yilmaz, S. (2007). Influence of marble and limestone dusts as additives on some mechanical properties of concrete. *Scientific Research and Essay, 2*(9), 372–379.
4. Binici, H., Shah, T., Aksogan, O., & Kaplan, H. (2008). Durability of concrete made with granite and marble as recycle aggregates. *Journal of Materials Processing Technology, 208*(1), 299–308.

5. Venkata Ramana, N., Reddy Babu, G., & Raghu Babu, U. (2018). Bearing strength of steel fibre reinforced black marble stone waste aggregate concrete. *Materials Today: Proceedings, 5*(1), 1201–1210.

6. Kore, S. D., & Vyas, A. (2016). Impact of marble waste as coarse aggregate on properties of lean cement concrete. *Case Studies in Construction Materials, 4,* 85–92.

7. Jung, S. H., & Kwon, S. J. (2013). Engineering properties of cement mortar with pond ash in South Korea as construction materials: From waste to concrete. *Central European Journal of Engineering, 3,* 522–533.

8. Kulkarni, V., Kandekar, S., Mehetre, A., & Dashrath, K. B. (2014). Compression and split tensile strength of concrete containing different aggregates. *International Journal of Engineering Research & Technology (IJERT), 3,* 469–474.

9. Bureau of Indian Standards (BIS), IS 12269: 53 grade ordinary Portland cement.

10. Bureau of Indian Standards (BIS), IS 516-1959 (Reaffirmed 2004): Methods of tests for strength of concrete.

11. Bureau of Indian Standards (BIS), IS: 5816-1999 (Reaffirmed 2004): Splitting tensile strength of concrete—Method of test.

12. Lavanya, G., & Jegan, J. (2015). Evaluation of relationship between split tensile strength and compressive strength for geopolymer concrete of varying grades and molarity. *International Journal of Applied Engineering Research, 10,* 35523–35529.

13. Arioglu, N., Canan Girgin, Z., & Arioglu, E. (2006). Evaluation of ratio between splitting tensile strength and compressive strength for concretes up to 120 MPa and its application in strength criterion. *ACI Materials Journal, 103,* 18–24.

14. Adriano, D. C., Page, A. L., Elseewi, A. A., Chang, A. C., & Straughan, I. (1980). Utilization and disposal of fly ash and other coal residues in terrestrial ecosystems: A Review1. *Journal of Environmental Quality, 9,* 333.

15. Yao, W., Jiang, S., Fei, W., & Cai, T. (2017). Correlation between the compressive, tensile strength of old concrete under marine environment and prediction of long-term strength. *Advances in Materials Science and Engineering*.

16. Carino, N. J., & Lew, H. S. (1982). Re-examination of the relation between splitting tensile and compressive strength of normal weight concrete. *ACI Journal Proceedings, 79,* 214–219.

17. Akinpelu, M. A., Odeyemi, S. O., Olafusi, O. S., Muhammed, F. Z. (2018). Evaluation of splitting tensile and compressive strength relationship of self-compacting concrete. *Journal of King Saud University-Engineering Sciences*.

18. ACI Committee 318. (2014). *Building code requirements for structural concrete and commentary*. Farmington Hills, MI: American Concrete Institute.

19. Mokhtarzadeh, A., & French, C. (2000). Mechanical properties of high-strength concrete with consideration for precast applications. *ACI Materials Journal, 97*(2), 136–147.

20. ACI 363R-92 (Reapporved 1997): *Report on high strength concrete*. Farmington Hills, MI: American Concrete Institute.

21. Oluokun, F. A., Burdette, E. G., & Deatherage, J. H. (1991). Splitting tensile strength and compressive strength relationships at early ages. *ACI Materials Journal, 88*(2), 115–121.

22. Neville, A. M. (1995). *Properties of concrete* (4th ed.). Essex: Longman Group Ltd.

Empirical Expression for the Fundamental Natural Period of Buildings on Slopes

Ajay Kumar Sreerama, Sreenath Gundoji, Bharat Prakke and Venkata Dilip Kumar Pasupuleti

Abstract Seismic codes worldwide provide empirical formulas for estimating the fundamental natural period of vibrations (T_a), preferably suitable for regular buildings. As per IS 1893:2016, the fundamental natural period is an inherent building property which is a function of height and base dimensions of the building. However, the formula specified in the existing code is not suitable for a building that is irregular both in plan and elevation. One such case of irregular buildings is building structures on slopes, which are supported on foundations at different horizontal levels leading to non-uniform column heights, where the present period formula is not suitable for estimation of T_a. In the present study, an attempt is made to develop an empirical expression for estimating T_a for buildings on slopes, by performing a regression analysis of numerically obtained natural periods. A total of 180 RC moment-resisting frame structures with varying floor heights and slope angles have been modelled and analyzed using SAP 2000 for the study and an empirical expression has been presented.

Keywords Building structures on slopes · Fundamental natural period · Regression analysis

1 Introduction

In the context of seismic design and assessment, the fundamental natural period (T_a) is the essential and dynamic property for the design of buildings to determine its elastic demand. Typically, the design codes worldwide provide an empirical formula to calculate the design base shear and lateral design loads. As per IS 1893:2016 [1], the fundamental natural period is a function of height and base dimensions of the building. The period formula given by Goel and Chopra [2] which is adopted in most

A. K. Sreerama (✉) · S. Gundoji · B. Prakke · V. D. K. Pasupuleti
Mahindra École Centrale, College of Engineering, Hyderabad, Telangana, India
e-mail: ak.sreerama@meees.org

V. D. K. Pasupuleti
e-mail: venkata.pasupuleti@mechyd.ac.in

of the seismic codes suggests that it is not ideal for buildings that are irregular in plan and elevation. One such case is building structures resting on hill slopes.

In Indian subcontinent, nearly 60% of its landmass under seismic threat has seen a considerable rise in population density from a figure of 324/km^2 to that of 382/km^2, which is higher than the average population density of the world [3]. Especially, north and north-east India which falls under seismic zone IV and V with large scales of hilly terrain double the risk (Figs. 1, 2 and 3). Due to its economic growth and rapid urbanization, the construction of multi-storey RC building structures on slopes has a popular and pressing demand [4]. Structures on slopes are significantly different from those on flat surface, i.e. they are irregular and unsymmetrical in horizontal and vertical planes [5]. So, to understand the seismic safety of building structures on slopes, the finding of the fundamental natural period is a challenging task. But to estimate the dynamic property T_a, the present period formula is not suitable as these structures are supported on foundations at different horizontal levels leading to non-uniform column heights.

The actual fundamental period of a building depends on its mass and stiffness. But most of the codes calculate it by its height and plan dimensions, which is deliberately smaller so as to have a conservative estimate of base shear. Building codes like AS 1170.4-2007 [5], NBCC 2005 [6], EN 1998 1-2004 [7], Japan-2001 [8], and Taiwan-2005 [9] consider only the height of the structure, whereas IS 1893-2016 (Part I) and ASCE 7-10 [10] consider both height and the dimension of the building as an effective measure for the natural period. In general, the empirical formula [11] used worldwide is shown in Eq. (1).

$$T_a = a H^x D^y \tag{1}$$

where

a	is the constant obtained from regression analysis
H	is the height of the building
D_L or D_T	is the plan dimensions in longitudinal and transverse directions.

According to IS 1893-2016 (Part I), the approximate fundamental translational natural period T_a of oscillation shall be estimated by the following expressions:

(a) Bare moment-resisting frame (MRF) buildings (without any masonry infills)

$$T_a = 0.075 h^{0.75} \tag{2}$$

where h is the total height of the building (m)

(b) Buildings with reinforced concrete (RC) structural walls

$$T_a = \frac{0.075 h^{0.75}}{\sqrt{A_w}} \geq \frac{0.09 h}{\sqrt{d}} \tag{3}$$

where

h is the total height of the building (m)

A_w is a total effective cross-sectional area (m^2) of walls in each storey

d is the base dimension of building at the plinth level along the considered earthquake shaking (m)

    The present research work focuses on developing an empirical expression for estimating T_a for buildings on slopes, by performing a regression analysis of numerically obtained period data. A total of 180 RC moment-resisting frame structures with different bay dimensions, varying floor heights and slope angles have been modelled using SAP 2000 for the study (Fig. 4).
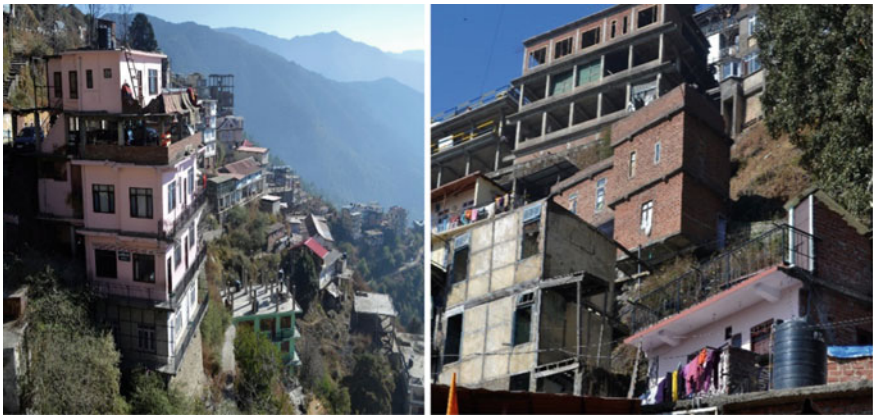
Fig. 1 RC building structures on slope with vertical and horizontal irregularities in Shimla, Himachal Pradesh

Fig. 2 Construction activity of RC buildings on slopes in Shimla, Himachal Pradesh

Fig. 3 Aerial view of buildings showing building density on hilly terrain in Shimla, Himachal Pradesh

2 Numerical Modelling

Three-dimensional RC moment-resisting frame structures as shown in Fig. 4, with different bay dimensions, varying height and slope angles have been designed according to the IS 456-2000 guidelines. A continuous element approach, viz. finite element
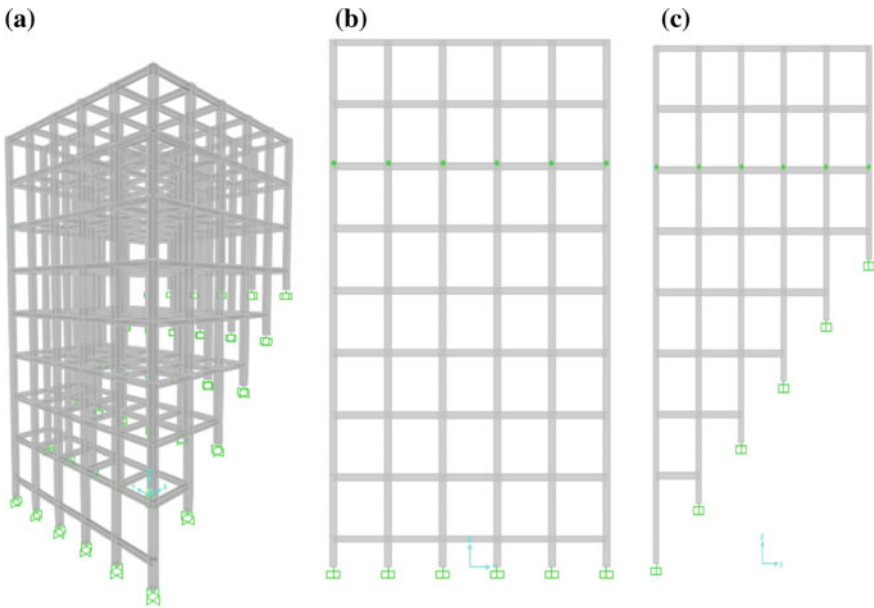
Fig. 4 Numerical model of (**a**) sample G+3 building model on 45° slope (**b**) elevation along valley direction (**c**) elevation along ridge direction

Table 1 Geometry of the structure

S. No.	Element type	Geometry (m)
1.	Beam dimension	0.23×0.30
2.	Column dimension	0.40×0.40
3.	Slab thickness	0.12
4.	Storey height	3.0
5.	Plinth height	1.5

Table 2 Loading on the structure

Elements	Dead load (kN/m^2)		Live load (kN/m^2)	
	Typical floor	Top floor	Typical floor	Top floor
Interior beams	21.5	14.62	13.5	9.0
Exterior beams	25.5	15.12	6.75	4.5

method (FEM) is used to model and analyze the selected buildings. The detailed geometry and considered structural configuration are summarized in Table 1.

For all the buildings, M25 grade of concrete and HYSD415 steel grade are used for all structural elements. Rigid floor diaphragms are assumed at each floor level. The loads acting on the structure are calculated based on IS 875(Part 1)-1987 and IS 456-2000 and are presented in Table 2. Two major assumptions and considerations are made to reduce the complexity in the calculation of the fundamental natural period of buildings on slopes, i.e. (a) buildings without infills [12] and plan symmetric, (b) calculation of natural period towards valley (i.e. along with the slope). For each model, i.e. with different bay dimensions 3×3, 3×4, 3×5, 4×3, 4×4, 4×5, 5×3, 5×4 and 5×5, varying floor heights from G+2 to G+6 and different slope angles 15°, 30°, 45° and 60°. SAP 2000 [13] is used to determine the elastic periods by performing linear modal analysis.

3 Comparison of Empirical Natural Periods (T_a) as Per IS 1893:2016 to Numerically Obtained Elastic Periods

As per IS 1893:2016, for bare MRF the time period value is a function of structural height, whereas the time period depends on the mass and stiffness of the structure. So, to understand explicitly a comparison has been made between natural time periods obtained from IS 1893:2016 to that of numerically obtained natural periods.

3.1 Case 1: Building Resting on 0° Slope (Regular Building)

From Table 3, it is observed that the time period values obtained from IS codes are nearly 50% lesser to that of numerical periods. It is also observed that as bay dimensions increase along with storey height, there is an increase in difference of 124.17% in T_a to that of code obtained value. As per equivalent static method, the calculation of base shear involves in estimating the acceleration coefficient (S_a/g), which is constant for a time period of less than 0.4 s. So, for G+2 and G+3 storey structures, the difference in the time period from code and numerical does not affect the conservative design approach of code, but whereas for G+4 to G+6 it fails. So, it is clearly seen the limitation of code specified empirical formula for regular buildings.

3.2 Case 2: Building Resting on 45° Slope

To understand the T_a of buildings structures on slopes, an attempt is made to observe the suitability of code specified equation to estimate the time period of buildings structures on slopes. The most interesting fact about buildings on slopes is, being supported on foundations at the different horizontal levels, has non-uniform column heights where the empirical formula does not fit. In the present case, the height of the shorter frame along the valley direction is considered in the calculation of empirical period. Comparatively, empirical periods are observed with an increase in difference from 103.66 to 152.31% as the height and bay dimensions changes to that of numerical periods (Table 4). To summarize the conservative design approach of IS 1893:2016 fails for slope buildings.

4 Development of Empirical Formula Using Regression Analysis

For determination of the natural frequencies of a system, there are two methods, viz. exact and approximate methods. In absence of exact method, an approximate method opts. One such method which is reliable in estimating natural periods is the Rayleigh method [14–16]. Most of the previous research and codebooks around the world calculated T_a using the Rayleigh method. On similar grounds as per the code IS 1893-2016, for the buildings without infill's the fundamental period is given in Eq. (2) is also developed using Rayleigh method.

Table 3 Different natural periods (T_a) obtained using numerical models and IS 1893:2016 of building on 0° slope

Storey	T_a (s)									
	IS 1893:2016	3×3	3×4	3×5	4×3	4×4	4×5	5×3	5×4	5×5
G+2	0.390	0.635	0.644	0.660	0.630	0.646	0.655	0.632	0.646	0.656
G+3	0.484	0.873	0.889	0.906	0.865	0.887	0.900	0.868	0.887	0.900
G+4	0.572	1.117	1.137	1.157	1.110	1.134	1.150	1.108	1.132	1.147
G+5	0.655	1.364	1.390	1.413	1.355	1.383	1.402	1.350	1.379	1.398
G+6	0.736	1.614	1.646	1.671	1.601	1.635	1.657	1.594	1.628	1.649

Table 4 Different natural periods (T_a) obtained using numerical models and IS 1893:2016 of building on 45° slope

Storey	T_a (s)										
	IS 1893:2016	3 × 3	3 × 4	3 × 5	4 × 3	4 × 4	4 × 5	5 × 3	5 × 4	5 × 5
G+2	0.390	0.794	0.811	0.822	0.806	0.823	0.835	0.817	0.835	0.846
G+3	0.484	1.038	1.060	1.075	1.048	1.070	1.085	1.058	1.080	1.095
G+4	0.572	1.287	1.314	1.332	1.294	1.321	1.338	1.301	1.329	1.346
G+5	0.655	1.540	1.572	1.593	1.542	1.574	1.595	1.548	1.579	1.600
G+6	0.736	1.795	1.832	1.856	1.793	1.830	1.854	1.796	1.832	1.856

By use of trial and error method, considering code formula and incorporating slope parameter, an empirical expression is derived as in Eq. (4). Following are the assumptions involved in developing the empirical equation: (a) the height is considered as the average height of all columns and (b) a coefficient/parameter with respect to the angle (i.e. trigonometric function) is added to the existing empirical formula.

The assumed general empirical form can be formulated as below

$$T = 0.075(H_{\text{average}})^{0.75}(1 + \sin \theta)^{\alpha} \tag{4}$$

where

$$H_{\text{average}} = \frac{h_1 + h_2 + h_3 + h_4 \ldots + h_n}{n} \tag{5}$$

θ slope angle of building
h_n height of corresponding column
n total number of columns
α slope coefficient.

A linear modal analysis is used to determine fundamental periods (Table 5) for each model, i.e. with different bay dimensions, varying floor heights and slope angles. To obtain the slope coefficient, Eq. (4) is recast as below

$$T_{\text{numerical}} = T_{\text{code}}(1 + \sin \theta)^{\alpha} \tag{6}$$

The numerical time periods and code time periods are used to calculate the α value for all cases and the value of α is computed as below

$$\alpha = \frac{\log(T_{\text{numerical}}/T_{\text{code}})}{\log(1 + \sin \theta)} \tag{7}$$

Regression analysis is carried out between coefficient 'α' and slope angle 'θ' for all the cases. The quadratic regression analysis is adopted which is in the form Eq. (8) to determine parameters C_1, C_2 and C_3.

$$\alpha = C_1\theta^2 + C_2\theta + C_3 \tag{8}$$

where 'θ' is in radians and C_1, C_2 and C_3 are regression coefficient

The coefficient of determination R^2 is the goodness of fit measure for linear regression models, which measures the strength of the relationship between the model and the dependent variable on a convenient scale of 0–1. In the present case, the R^2 values obtained are close to 0.9 that supports the strength of the assumed model. The best-fit curves are plotted by performing regression analysis in Fig. 5.

Table 5 Time period of buildings obtained from numerical analysis

Angle	Storey	T_a(s)								
		3 × 3	3 × 4	3 × 5	4 × 3	4 × 4	4 × 5	5 × 3	5 × 4	5 × 5
15°	G+2	0.782	0.799	0.819	0.791	0.808	0.820	0.800	0.817	0.829
	G+3	1.030	1.047	1.061	1.032	1.054	1.068	1.039	1.061	1.076
	G+4	1.272	1.298	1.316	1.276	1.303	1.320	1.281	1.308	1.325
	G+5	1.522	1.553	1.574	1.522	1.554	1.574	1.525	1.557	1.577
	G+6	1.774	1.811	1.841	1.770	1.806	1.830	1.771	1.807	1.831
30°	G+2	0.791	0.808	0.820	0.803	0.820	0.832	0.814	0.831	0.843
	G+3	1.035	1.057	1.071	1.044	1.066	1.081	1.053	1.076	1.090
	G+4	1.283	1.309	1.327	1.289	1.316	1.333	1.296	1.323	1.341
	G+5	1.533	1.565	1.586	1.536	1.568	1.588	1.541	1.573	1.594
	G+6	1.787	1.824	1.848	1.785	1.822	1.846	1.788	1.824	1.848
45°	G+2	0.794	0.811	0.822	0.806	0.823	0.835	0.817	0.835	0.846
	G+3	1.038	1.060	1.075	1.048	1.070	1.085	1.058	1.080	1.095
	G+4	1.287	1.314	1.332	1.294	1.321	1.338	1.301	1.329	1.346
	G+5	1.540	1.572	1.593	1.542	1.574	1.595	1.548	1.579	1.600
	G+6	1.795	1.832	1.856	1.793	1.830	1.854	1.796	1.832	1.856
60°	G+2	0.799	0.816	0.828	0.809	0.827	0.838	0.821	0.839	0.850
	G+3	1.045	1.068	1.082	1.058	1.075	1.089	1.063	1.085	1.100
	G+4	1.297	1.324	1.342	1.300	1.327	1.345	1.308	1.336	1.353
	G+5	1.551	1.584	1.605	1.551	1.583	1.604	1.556	1.588	1.609
	G+6	1.806	1.847	1.871	1.804	1.841	1.865	1.807	1.843	1.868
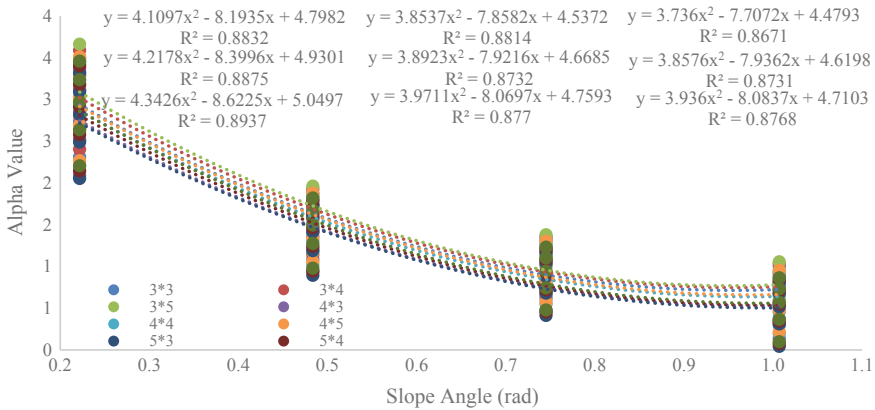
Fig. 5 Regression analysis between coefficient 'α' and slope angle 'θ' with best curve fitting equations

Table 6 Obtained α formula for different building cases

S. No.	No. of bays along		Value of α
	Valley	Ridge	
1	3	3	$\alpha = 4.109\theta^2 - 8.1935\theta + 4.7980$
2	3	4	$\alpha = 4.217\theta^2 - 8.3990\theta + 4.9300$
3	3	5	$\alpha = 4.342\theta^2 - 8.6225\theta + 5.0497$
4	4	3	$\alpha = 3.853\theta^2 - 7.8582\theta + 4.5372$
5	4	4	$\alpha = 3.892\theta^2 - 7.9216\theta + 4.6685$
6	4	5	$\alpha = 3.971\theta^2 - 8.0697\theta + 4.7593$
7	5	3	$\alpha = 3.736\theta^2 - 7.7072\theta + 4.4793$
8	5	4	$\alpha = 3.857\theta^2 - 7.9362\theta + 4.6198$
9	5	5	$\alpha = 3.936\theta^2 - 8.0837\theta + 4.7103$

5 Results and Discussion

Regression analysis implemented over data from Table 5 led to equations of α for nine different cases. The coefficient of determination 'R^2' value of 0.9 suggests that the assumed regression model is strong. By taking mean (μ) values of coefficients C_1, C_2 and C_3 of below nine equations in Table 6, a generalized formula for α considering slope is developed as in Eq. (9).

To quantify the variation amount and dispersion of data sets, one standard deviation ($\pm\mu$) is calculated for all cases. The regression coefficients obtained with one standard deviation of the mean are shown in Table 7.

$$\alpha = 3.99\theta^2 - 8.09\theta + 4.73 \qquad (9)$$

Table 7 Regression coefficients with one standard deviation of the mean

	C_1	C_2	C_3
μ	3.99	−8.09	4.73
$\mu + \sigma$	4.19	−7.80	4.91
$\mu - \sigma$	3.80	−8.37	4.55

where θ is in radians.

To validate the proposed empirical expression, buildings resting on different slopes with different floor heights are calculated and compared with the numerical time period as in Table 8. The results significantly show a negligible difference between time periods of the proposed formula to the numerical time periods. In general, taller buildings have higher time periods and low-rise have shorter time periods. Hence, to estimate T_a the coefficient values of $\mu - \sigma$ are considered for shear predominant, whereas coefficient values of $\mu + \sigma$ are taken for flexure predominant buildings.

6 Conclusion

Based on an analysis of 180 numerical modelled buildings of various floor heights on different slopes, a general-purpose time period formula for buildings on slopes is developed. From the proposed empirical equation, to estimate T_a, coefficient values of $\mu - \sigma$ are considered for shear predominant buildings, whereas coefficient values of $\mu + \sigma$ are taken for flexure predominant buildings. Hence, this study is clearly able to produce an empirical formula for calculating the fundamental time period of building resting on a slope which is equally valid to the regular building as per code. Experimental verification of the suggested formulae is required so as to recommend the same for adopting in the IS code.

Table 8 Comparison of T_a of the proposed empirical equation along with one standard deviation to numerical time periods

Slope	Storey	$H_{average}$	$T(s)$ (numerical)	α	$T(s)$ (proposed)	α	$T(s)$ $(\mu + \sigma)$	α	$T(s)$ $(\mu - \sigma)$
10	G+2	11.29	0.77	3.44	0.80	3.68	0.83	3.20	0.77
15	G+3	14.21	1.00	2.88	1.07	3.15	1.13	2.61	1.00
25	G+4	18.60	1.35	1.96	1.34	2.30	1.51	1.62	1.19
35	G+5	21.15	1.67	1.28	1.32	1.70	1.60	0.85	1.09
55	G+6	28.92	2.04	0.64	1.37	1.27	2.01	0.01	0.94

References

1. IS 1893-2016 (Part 1), Indian standard Criteria for earthquake resistant design of structures. Bureau of Indian Standards, New Delhi, India.
2. Goel, K. R., & Chopra, K. A. (1997). Period formulas for moment-resisting frame buildings. *Journal of Structural Engineering, ASCE, 123,* 1454–1461.
3. Pradeep Kumar, R., & Murthy, C. V. R. (2014). Point of view: Earthquake safety of houses in India: Understanding the bottlenecks in implementation. *The Indian Concrete Journal, 88*(9), 51.
4. Sreerama, A. K., & Pradeep Kumar R. (2013, October). Earthquake behaviour of reinforced concrete framed buildings on hill slopes. In *International Symposium on New Technologies for Urban Safety of Mega Cities in Asia (USMCA 2013)*, Hanoi, Vietnam.
5. As 1170.4-2007, Australian Standard, Structural design actions Part 4: Earthquake actions in Australia.
6. Canadian Commission on Building and Fire Code. (2005). *National Building Code of Canada*. Ottawa, ON: National Research Council of Canada.
7. EN 1998-1 (2004), Eurocode 8: Design of structures for earthquake resistance—Part 1: General rules, seismic actions and rules for buildings.
8. The building standard law of Japan, Ministry of Land, Infrastructure, Transport and Tourism, 2001.
9. Seismic Design Code of Buildings in Taiwan 2005, Construction and Planning Agency, Ministry of Interior, R.O.C.
10. ASCE standards, Minimum Design Loads of Buildings and other structures, ASCE/SEI 7-10, 2010, American Society of Civil Engineers.
11. Ditommaso, R., Vona, M., Gallipoli, M. R., & Mucciarelli, M. (2013). Evaluation and considerations about fundamental periods of damaged reinforced concrete buildings. *Natural Hazards and Earth Systems Sciences, 13,* 1903–1912.
12. Agarwal, P., & Shrikhande, M. (2006). *Earthquake resistant design of structures*. New Delhi: Prentice-Hall.
13. SAP 2000, Computers and Structures, Inc.
14. Housner, G. W., & Brady, A. G. (1963). Natural periods of vibration of buildings. *Journal of the Engineering Mechanics Division, 89*(4), 31–68.
15. Nassani D. E. (2014) A simple model for calculating the fundamental period of vibration in steel structures. *APCBEE Procedia, 9*, 339–346. ICCEN 2013: December 13–14, Stockholm, Sweden.
16. Asteris, P. G., Repapis, C. C., Cavaleri, L., Sarhosis, V., & Athanasopoulou, A. (2015). On the fundamental period of infilled RC frame buildings. *Structural Engineering and Mechanics, 54*(6), 1175–1200.

Prediction of Corrosion Levels in Reinforced TMT Bars in SCC Exposed to Marine Environment

V. Giridhar Kumar, B. Chandraiah, Y. Amarnath and P. Charan Kumar

Abstract Reinforced concrete structures have good potential to be durable and capable of withstanding adverse environmental conditions. Failures in RCC structures still occur as a result of premature reinforcement corrosion. Corrosion of steel has been recognised as one of the major durability problems in RCC structures. Damage due to corrosion of steel bars considerably reduces the strength, serviceability and life of structural components. Inspection and continuous monitoring techniques are necessary to be carried out to assess the steel corrosion in buildings and bridge components in order to ensure their safety and durability for longer time. These techniques are essentially required for easy maintenance and repairs of the structural components also. Few investigations were carried out to study the corrosion levels in reinforced steel bars exposed to marine environment. Very few investigations were carried out so far to predict the corrosion levels in self-compacting concrete (SCC) exposed to salts and chemical environments. The present paper outlines the investigations carried out to predict the corrosion levels in TMT bars in normal vibrated concrete (NVC) and SCC exposed to marine environment. It also shows the severity of concrete exposure condition on the progressive corrosion in TMT bars when immersed in salt solution.

Keywords Reinforcement corrosion · Self-compacting concrete (SCC) · De-ionised water · Reinforced thermo-mechanically treated (TMT) bars · Marine environment · Potential difference · Saturated calomel electrode (SCE) · Open-circuit potential (OCP) method

V. Giridhar Kumar · B. Chandraiah (✉) · Y. Amarnath · P. Charan Kumar
Srinivasa Ramanujan Institute of Technology, Anantapur, Andhra Pradesh, India
e-mail: chandraiahce23@gmail.com

V. Giridhar Kumar
e-mail: giridharkumar1967@gmail.com

Y. Amarnath
e-mail: y.amarnath@gmail.com

P. Charan Kumar
e-mail: charan.civ@srit.ac.in

1 Introduction

Reinforced concrete is widely used construction material for buildings, bridges, platforms and underground structures such as tunnels and pipelines. In general, reinforced concrete is a durable material that withstands severe exposure conditions like marine and industrial environments [1]. Majority of reinforced concrete structures show high durability and good long-term performance under adverse exposure conditions. Still, a large amount of structural concrete failures are identified as a result of reinforcement corrosion in steel bars. Corrosion is a process of chemical or electrochemical reaction between a metal and its surrounding environment that causes a deterioration of the parent metal and changes in its properties [2]. Carbonation of concrete and the ingress of chloride ions into concrete are the major causes of corrosion of steel in reinforced concrete structures. Depassivation leads to the rapid corrosion of steel and progressive deterioration of concrete in structures [3]. Formation of rust due to corrosion in steel sets up expansive stresses in concrete which further leads to the cracking and spalling of concrete cover. Loss due to the corrosion consumes a considerable portion of the budget of the country by the way of restoration and reconstruction measures of concrete. Proper monitoring for corrosion prevention in bars at an appropriate time will make enormous savings of the economy and thus leads to the best performance of the structure throughout its life. Quality control, good maintenance and proper planning along with non-destructive inspection methods and monitoring techniques help to detect corrosion levels in steel at early stages. Repairing, retrofitting and rehabilitation of corroded structures are complex and quite expensive methods. They require special treatments like cement grouting for the cracked concrete zone. Corrosion monitoring techniques will give quite complete information about timely changing conditions of embedded steel in RCC structures. It is necessary to study the problems associated with the corrosion in steel and its possibilities to occur in NVC and SCC structural components. These studies ensure for the safety and serviceability measures to be carried out in time. Present investigations concern about the experimental studies carried out to predict the corrosion levels in embedded TMT bars in SCC (Grades M20 and M25) when exposed to the marine environment. NVC and SCC specimens are immersed in de-ionised water with different concentrations of NaCl and $MgSO_4$ for immersion periods of 28, 60 and 90 days. Corrosion levels in TMT bars after the immersion period were then predicted by open-circuit potential method (OCP Method) with saturated calomel electrode (SCE).

2 Literature Review

Guneyisi et al. [4] conducted studies on concretes having two different water–cement ratios and two different cement contents by using a plain and four different blended Portland cements by testing specimens subjected to three different curing procedures

(uncontrolled, controlled and wet curing). The results showed that the wet curing was essential to achieve higher strength and durability characteristics for both plain and especially blended cement concretes. It also proved that cement type, w/c ratio, age and curing procedures had a significant effect on both strength and durability characteristics of concretes.

Soleymani and Ismail [2] conducted a laboratory study to estimate the corrosion activity of reinforcing steel embedded in two types of concrete, ordinary and high performance, using different corrosion measurement methods and to compare them. In their experiment, high-performance concrete specimens showed lower corrosion testing results.

Cabrera [3] has found a relationship between corrosion rate and crack pattern and intensity by using concrete beam s subjected to accelerated corrosion. The results show that there is an inverse relationship between reinforcement cover and degree of corrosion. He also found a relationship between corrosion rate and loss of structural serviceability from measurements of bond strength, cracking and deflection of concrete beams. It was found that fly ash concrete exhibited better resistance to corrosion damage than normal Portland cement.

3 Experimental Programme

The experimental programme consisted of procurement of materials, tests for physical properties of cement, coarse and fine aggregates and mix design procedure for normally vibrated conventional concrete and self-compacting concrete (SCC) in accordance with IS specifications (in accordance with SP:23-1982 and IS:10262-2009) and Nan Su method, respectively. It includes the preparation of test specimens and to make the test reports for the compressive strength of M20 and M25 grades conventional and SCCs. Preliminary investigations are carried out initially to find the compressive strength of plain conventional and SCC by accelerated curing method. Average corrosion activity levels raised in the specimen TMT bars when immersed in de-ionised water with and without NaCl and $MgSO_4$ salts are measured by open-circuit potential method. Specimens are immersed in two different concentrations of NaCl (0.20M and 0.25M) and $MgSO_4$ (0.02M and 0.025M) for 28, 45, 60 and 90 days. These test results and values are tabulated in Table 2 for reference purpose.

3.1 Materials

OPC of 53-Grade was used in both NVC and SCC throughout the experimental investigations. Locally available river sand with fineness modulus 3.07 and belonging to grading zone I of IS: 383 was used as fine aggregate for preparing normal conventional concrete and SCC. Similarly, a coarse aggregate of 25-mm maximum nominal size with fineness modulus 6.31 was used to prepare two types of concrete of Grades

M20 and Grade M25, respectively for NVC and SCC. Class-F Fly ash from Raichur Thermal Power Plant, Raichur, (Karnataka State) and GGBS from local steel industry nearby Kurnool, (Andhra Pradesh State) was used to prepare SCC. No plasticizer has been used to prepare normal conventional concrete whereas **CONPLAST SP430 @** the rate of 1.1% and viscosity modifying agent (VMA) at the rate of 5 ml per 50 kg (one bag) of cement were used to prepare SCC of two grades (M20 and M25).

3.2 Concrete Mix Proportions

Four concrete mixes designated as **A/20 NVC, B/25 NVC, C/20 SCC, D/25 SCC** were used in the experimental investigations. Mixes designated as A/20NVC (0.52:1:1.88:3.08), B/25 NVC (0.45:1:1.74:2.86) belong to normally vibrating concrete whereas C/20 SCC (0.42:1:1.997:1.18) and D/25 SCC (0.40:1:1.85:1.16) belong to SCC, respectively. These mixes were used to cast the test specimens to predict the corrosion levels when subjected to marine environment. One set consisting of 20 specimens of size **(100 mm × 100 mm × 450 mm)** with a conventional M20 grade design mix and another set consisting of 20 specimens of same size with M20 grade SCC design mix were casted. The same number of specimens was casted for the two varieties of concrete (NVC and SCC) for M25 grade design mix also. Each concrete specimen is reinforced with one TMT bar of 16-mm diameter and 350-mm length. The weight of TMT bars was noted initially before it is placed into concrete inside the moulds.

3.3 Preparation of Test Specimens

The exact proportions of cement, sand and crushed granite metal of 25-mm size were weighed and mixed thoroughly with pure water to produce the concrete mix. Concrete was filled in the moulds for a length of 450 mm. The position of the TMT steel bar at the time of concreting was so adjusted that it is placed horizontally near the central height of the mould and to obtain a projection of 50 mm to one side of the specimen. Workability characteristics of fresh conventional concrete were measured by slump and compaction factor methods. Filling, flowing and passing ability characteristics of SCC were maintained in accordance with **EFNARC guidelines**. These values corresponding to NVC and SCC are recorded and noted. Specimens are compacted on a vibrating table for proper compaction and kept for set for 24 h. The top surfaces of specimens were then levelled and made flush using a trowel. Specimens were demoulded a day after casting and cured in water till the date of testing. One set of concrete specimens of M20 and M25 grades of NVC and SCC was kept in de-ionised water without salts for 28, 45, 60 and 90 days immersion period. Similarly, another two sets of concrete specimens of same grade of NVC and SCC were immersed in de-ionised water with different concentrations of **NaCl (0.20M and 0.25M) and MgSO$_4$**

Slump flow test   **L-BoxTest**   **Beams**

Fig. 1 Preparation and casting of specimens

Table 1 Corrosion condition (ASTM C 876-1991)

Open-circuit potential (OCP) values, −mV		Corrosion condition
(mV vs. SCE)	(mV vs. CSE)	
< −426	< −500	Severe condition
< −276	< −350	High (< 90% risk of corrosion)
−126 to −275	−350 to −200	Intermediate (risk of corrosion)
> −125	> −200	Low (10% risk of corrosion)

(0.02M and 0.025M) for the same immersion period. Preparation and casting of concrete specimens are shown in Fig. 1.

The moulds were then stripped off after 24 h. One set of concrete specimens of M20 and M25 grades of NVC and SCC was kept in de-ionised water for 28, 45, 60 and 90 days immersion period. Similarly, another two sets of concrete specimens of NVC and SCC were immersed in de-ionised water with different concentrations of **NaCl (0.20M and 0.25M) and MgSO$_4$ (0.02M and 0.025M)** for the same immersion periods of 28, 45, 60 and 90 days in order to compare the corrosion levels with those of de-ionised water without salts. The details of immersed specimens and different concentrations of NaCl and MgSO$_4$ are summarised in Table 1. The prepared concrete specimens are shown in Fig. 2.

3.4 Test Procedure

The corrosion activity levels in the reinforced TMT bars of the concrete specimens subjected to marine environment were predicted by open-circuit potential (OCP) method. In this method, a SCE was used as a reference electrode. Concrete specimens were immersed in de-ionised water and salt solutions for periods of 28, 45,

Fig. 2 SCC specimens

Fig. 3 Test setup for OCP method
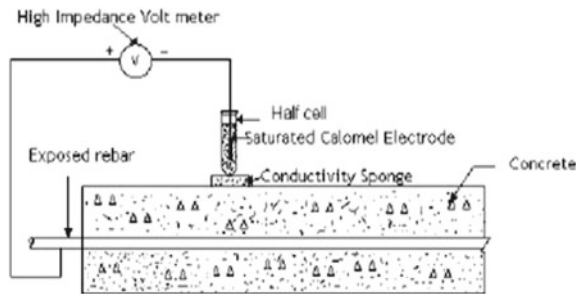
60 and 90 days, respectively. The positive terminal of the voltmeter is connected to the end of the TMT bar projecting out from the specimen and the negative terminal is connected to the reference electrode. The potential difference between the distinguished points over the concrete specimen is measured with SCE. Test setup for open-circuit potential method was shown in Fig. 3. The prediction of corrosion activity levels by open-circuit potential method is shown in Fig. 4.

4 Results and Discussion

Table 1 shows the corresponding standard corrosion activity levels in millivolts (mV) specified by ASTM C 876-91 for low, intermediate, high and severe risk conditions of exposure for normally vibrated concrete and SCC by open-circuit potential method.

Fig. 4 Prediction of corrosion levels by OCP method

Table 2 shows the experimental test results for M20 and M25 grade NVC and SCC for different exposure conditions of de-ionised water with and without salts. These values were compared with those values given by ASTM C 876-91 standards shown in Table 1. The probability of reinforcement corrosion in bars exposed to salt environment is predicted and shown in Table 2. The corrosion activity levels in TMT bars for different exposure conditions are shown in Graphs 1, 2, 3, 4, and 5. It is concluded that SCC is ideally good to reduce corrosion in TMT bars when compared to normal conventional concrete when exposed to same concentrations of NaCl and MgSO$_4$ salts.

Measured levels of corrosion in concrete specimens show that the risk of corrosion is high in NaCl solution of different molarities (0.2M and 0.25M) compared to MgSO$_4$ solution of different molarities (0.02M and 0.025M). High risk of corrosion occurs in 0.2M NaCl solution for M25 grade concrete. Results also show that SCC exhibits high resistance to MgSO$_4$ environment compared to NaCl environment. Similarly, as the grade of concrete is improved, the risk of corrosion is low (about 54%) for M20 and M25 grade concrete for MgSO$_4$ exposure conditions.

5   Conclusions

The following conclusions were drawn from the experimental investigations on SCC and NVC specimens:
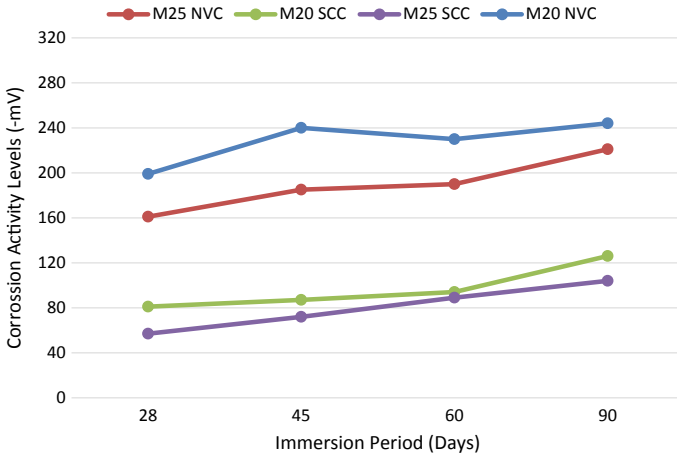
1. Corrosion activity levels in TMT bars for the specimens immersed in NaCl solution were observed to be higher than those for the specimens immersed in MgSO$_4$ solution for normal conventional concrete and SCC.

**Table 2** Prediction of corrosion levels for different exposure conditions

Sample set no.	Type of concrete	Grade of concrete	Exposure condition	Average open-circuit potential values (−mV)				Corrosion condition
				28-days	45-days	60-days	90-days	
1	NVC	M20	De-ionised water	93	108	110	142	Intermediate
		M25	De-ionised water	83	92	95	121	Low
2	SCC	M20	De-ionised water	15	23	37	57	Low
		M25	De-ionised water	14	18	18	27	Low
3	NVC	M20	NaCl-0.20M	199	240	230	244	Intermediate
		M25	NaCl-0.20M	161	185	190	221	Intermediate
4	SCC	M20	NaCl-0.20M	81	87	94	126	Intermediate
		M25	NaCl-0.20M	57	72	89	104	Low
5	NVC	M20	NaCl-0.25M	210	226	277	309	High
		M25	NaCl-0.25M	187	200	210	215	Intermediate
6	SCC	M20	NaCl-0.25M	109	112	121	123	Low
		M25	NaCl-0.25M	100	102	105	113	Low
7	NVC	M20	$MgSO_4$-0.02M	133	135	138	145	Intermediate
		M25	$MgSO_4$-0.02M	100	110	113	131	Intermediate
8	SCC	M20	$MgSO_4$-0.02M	42	57	56	64	Low
		M25	$MgSO_4$-0.02M	35	40	44	55	Low
9	NVC	M20	$MgSO_4$-0.025M	129	156	167	186	Intermediate
		M25	$MgSO_4$-0.025M	103	110	102	112	Low
10	SCC	M20	$MgSO_4$-0.025M	64	80	90	99	Low
		M25	$MgSO_4$-0.025M	51	60	59	72	Low
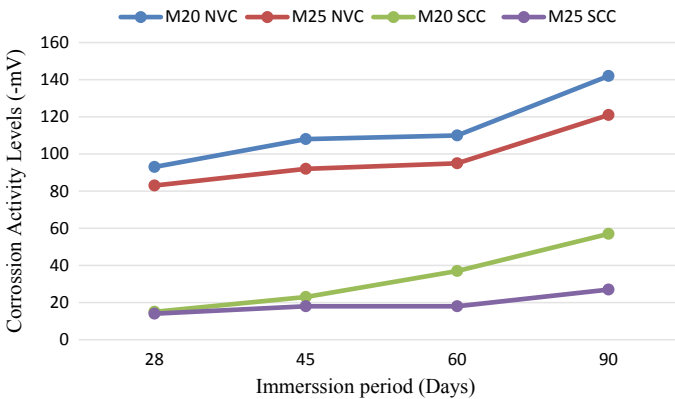
Graph 1 Corrosion levels in TMT bars for de-ionised water exposure condition

Graph 2 Corrosion levels in TMT bars for NaCl 0.2M exposure condition
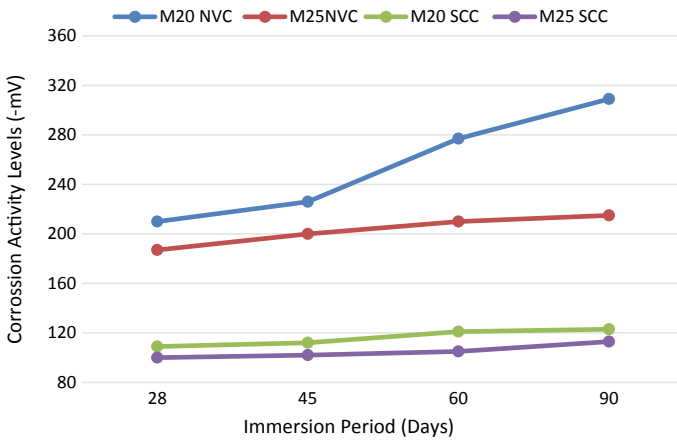
Graph 3 Corrosion levels in TMT bars for NaCl 0.25M exposure condition

2. Corrosion activity levels in TMT bars for SCC specimens were observed to be lower than those for normal vibrated concrete (NVC) specimens, when immersed in different concentrations of NaCl and $MgSO_4$ solutions for the same immersion period.

3. High corrosion levels in TMT bars when exposed to NaCl and $MgSO_4$ salt solutions cause significant changes in the mechanical properties of steel.

4. Corrosion reduces yield strength, ultimate tensile strength and may cause increase in the per cent elongation in TMT bars. This causes early fracture in bars and my affect the other similar properties of TMT bars when bars and concrete are exposed to severe and extreme exposure conditions.
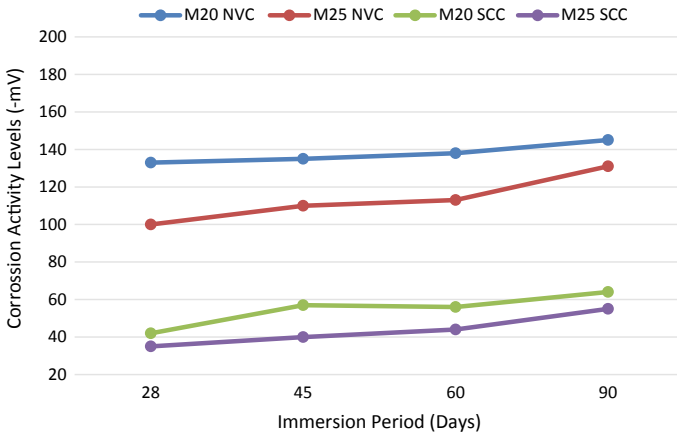
Graph 4 Corrosion levels in TMT bars for MgSO$_4$ 0.02M exposure condition
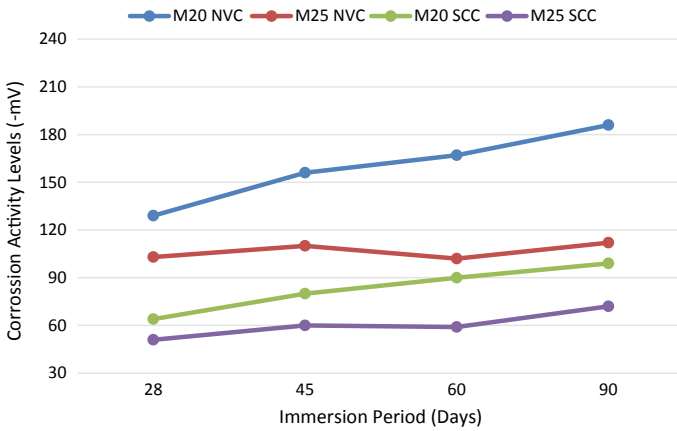
Graph 5 Corrosion levels in TMT bars for MgSO$_4$ 0.025M exposure Condition

5. SCC specimens perform better than normal concrete specimens, when structural elements are subjected to surrounding corrosion environment.
6. Further investigations are to be carried out to study the effects of long-term exposure conditions of salt environment on the strength and behaviour of TMT bars including NVC and SCC.

References

1. Girish, S., Ranganath, R. V., & Vengala, J. (2010). Influence of powder and paste on flow properties of SCC. *Construction and Building Materials, 24,* 2481–2488.
2. Soleymani, H., & Ismail, M. E. (2004). Comparing corrosion measurement methods to assess the corrosion activity of laboratory OPC and HPC concrete specimens. *Cement and Concrete Research, 34,* 2037.
3. Cabrera, J. G. (1996). Deterioration of concrete due to reinforcement steel corrosion. *Cement and Concrete Composites, 18,* 47–59.
4. Guneyisi, E., Ozturan, T., & Gesoglu, M. (2005). A study on reinforcement corrosion and related properties of plain and blended cement concretes under different curing conditions. *Cement and Concrete Composites, 27,* 449–461.
5. Nagataki, S., & Fujiwara, H. (1995). Self compacting property of highly-flowable concrete. *American Concrete Institute Special Publication, 154,* 301–314.
6. Naik, T. R., & Singh, S. (1997). Influence of fly ash on setting and hardening characteristics of concrete systems. *Materials Journal, 94*(5), 355–360.
7. Bouzoubaa, N., & Lachemi, M. (2001). Self compacting concrete incorporating high volumes of class F fly ash preliminary results. *Cement and Concrete Research, 31,* 413–420.
8. Su, N., Hsu, K. C., & Chai, H. W. (2001). A simple mix design method for self compacting concrete. *Cement and Concrete Research, 31,* 1799–1807.
9. Persson, B. (2001). A Comparison between mechanical properties of self compacting concrete and the corresponding properties of normal concrete. *Cement and Concrete Research, 31,* 193–198.
10. Subramanian, S., & Chattopadhyay, D. (2002). Experiments for mix proportioning of self compacting concrete. *Indian Concrete Journal, 76,* 13–20.
11. Okamura, H., & Ouchi, M. (2003). Self compacting concrete. *Journal of Advanced concrete Technology, 1,* 5–15.
12. Aggrawal, P., Aggrawal, Y., & Gupta, S. M. (2008). Self compacting concrete—Procedure for mix design. *Leonardo Electronic Journal of Practices and Technologies, 12,* 15–24.
13. Vanjare, M. B., & Mahure, S. H. (2012). Experimental Investigation on self compacting concrete using glass powder. *International Journal of Engineering Research and Applications (IJERA), 2*(3), 1488–1492. ISSN: 2248-9622. www.ijera.com.
14. Surabhi, C. S., Soman, M, Syam Prakash, V. (2009, November 6–7). Influence of lime stone powder on properties of self compacting concrete. In *10th National Conference on Technological Trends (NCTT09).*
15. Shah, S. N., Sutar, S. S., & Bhagwat, Y. (2008). Application of industrial waste in the manufacturing of self compacting concrete. Government College of Engineering, Karad.
16. ASTM C876-91 (Reapproved 1999) Standard test method for half cell potentials of uncoated reinforcing steel in concrete.
17. www.Corrossiondoctor.com.

Sustainability of Concrete Constructions: The Role of Materials and Practices

Saradhi Babu Daneti and Chat Tim Tam

Abstract With an ever-increasing population and the developments that are taking place around the world, sustainability of cement and concrete constructions is gaining importance. This revolves mainly around natural resource depletion issues associated with extensive mining for cement and concrete raw materials, and CO_2 emissions from the cement production process. It is important that these issues are addressed satisfactorily both for the well-being of our planet and for the continued growth of our society for generations to come. Concrete is one of the most widely used construction materials in the world after water. However, the production of ordinary Portland cement (OPC), an essential constituent of concrete, releases large amounts of CO_2 and is also energy-intensive. Aggregates occupy most of the volume in concrete and use of natural/virgin aggregates is not always viable due to depletion of natural resource and the environmental impact. Furthermore, it is not viable to reduce the use of cement and concrete; this impacts the employment opportunities associated with the cement, concrete and construction industry and also impacts the Nation's overall infrastructure development. Therefore, cement, concrete and construction industries must continue to evolve with the changing needs and expectations of the society while protecting the environment. One of the measures that are necessary to address this problem is by the use of alternative and/or recycled materials for production of cement and concrete, safely and economically. This paper presents the impact of cement and concrete production on environment and the Earth's natural resources and analyzes possible proposals for achieving sustainability in the concrete construction industry. In addition, the details of the R&D works on high replacements of ground granulated blast furnace slag (GGBS), recycled concrete aggregate (RCA), and manufactured sand (M-sand) and their effect on strength and/or durability of concrete are also presented.

S. B. Daneti (✉)
Alliance Concrete Singapore Pte Ltd., 72 Sungei Kadut Street 1, Singapore 729372, Singapore
e-mail: saradhibabu.daneti@allianceconcrete.com.sg

C. T. Tam
National University of Singapore, Singapore, Singapore

1 Introduction

As sustainability in construction is a burning issue all over the world, the 3R words "reduce, recycle and reuse" are the most important keywords today for achieving conservation of natural resources for future generations and reducing the impact on environment in terms of lowering CO_2 emissions and energy consumptions. Sustainable development is a broad and interdisciplinary field which was first expressed when the UN World Commission on Environment and Development (Brundtland Commission) published its "Our Common Future" report in 1987. In this report, Sustainable development was defined as "development which meets the needs of current generations without compromising the ability of future generations to meet their own needs" [1], in considerations of social, environmental and economic viewpoints/impacts.

According to a recent concrete CO_2 fact sheet [2], the CO_2 concentration in the atmosphere has increased by about ~100 ppm (by volume) after the industrial revolution in the late 1700s, and 50% of the CO_2 concentration (50 ppm) has increased in the recent past (1973–2006). This high CO_2 concentration not only affects the air quality but also increases average temperatures of the Earth's atmosphere (global warming). It is believed that the global warming will cause a rise in sea level, increase the intensity of extreme weather and cause effects like drop in agricultural yields, species extinctions and increased occurrence of diseases in the plant and animal world. These effects will severely impact the Earth's ability to support life.

The cement and concrete industry is amongst the important CO_2 emitters (though only contribute 5–7% of global emissions) while they use natural resources and energy. Hence, the sustainability of this industry is important for the well-being of our planet, continued growth of a society and human development. The environmental issues associated with CO_2 and greenhouse gas (GHG) emissions and natural resources issues in terms of depletion of limestone and clay for cement, concrete (sand and coarse) aggregates, water, etc., will play a leading role in the sustainable development of the cement and concrete constructions in this twenty-first century.

2 Impact of Cement and Concrete Production on Environment and Natural Recourses

2.1 Cement Production

The production of ordinary Portland cement (OPC), an essential constituent of concrete, impacts the most on release of CO_2 and GHGs (production of one ton of Portland cement produces about one ton of CO_2 and others gases such as NO_x), in

addition to the substantial consumption of natural recourses and energy. Sources of CO_2 and GHG emissions during the manufacturing of Portland cement (Malhotra 2004) [3] are as follows:

- From calcinations of limestone: 50–55%
- From fuel combustion: 40–50%
- From use of electric power: 0–10%.

Based on GlobalCarbonProject.org data published on 13 November 2017 for the year 2016 [4], the global CO_2 emissions from fossil fuel and industry were 36.2 ± 2 gigatonnes (Gt CO_2); this is 62% higher than 1990. The projection for 2017 was estimated to be 2.0% higher than 2016 (36.8 ± 2 Gt CO_2). The top four emitters in 2016 covered 59% of global emissions China (28%), USA (15%), EU28 (10%), India (7%). Based on 2016 data, the emissions of CO_2 with the use of coal, oil, gas, cement and gas flaring were accounted to be 40, 34, 19, 6 and 1%, respectively.

Portland cement requires huge amounts of natural resources in terms of limestone (~65%–calcareous rocks) and clay (~25%–argillaceous rocks) for its production. The world's cement production is constantly increasing; for the year 2016 as shown in Fig. 1, the cement production (4.2 billion tonnes) [5] was 65% higher than 2006 (2.54 billion tonnes) and most of this quantity is OPC. This increased rate of production impacts the environment the most in terms of depletion of (few billion tonnes) limestone, clay recourses, etc., in addition to the release of 4.2 billion tonnes CO_2 into atmosphere, which is responsible for >5% of CO_2 production in the world
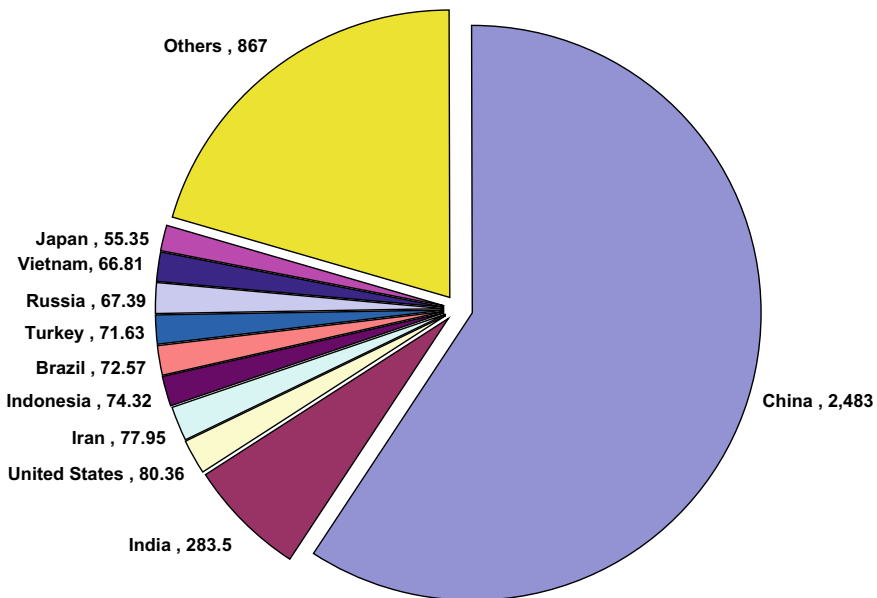

Fig. 1 2016 world cement production (4200 mil tonnes) [5]

based on past statistics. Furthermore, the clinker (composition: 95–100%) production (pyroprocessing) is the most energy-intensive stage (4.04 MJ/kg) of Portland cement production. The energy consumed in the production of Portland cement was reported to be about 4.88 MJ/kg of cement based on the US data [6].

2.2 Concrete Production

Concrete is the world's most important construction material and the second-largest consumed materials after water. Hence, it has an important role to play in our efforts to achieve sustainable development. Concrete industry is the largest user of natural resources in the world. The world's concrete demand/year was reported as 11.5 billion tonnes in 2012 [7] which are perhaps 12 billion tonnes by now. Assuming that ordinary concrete typically contains about 8% water and 75% aggregate by mass, apart from the cement used, demand would be about 1 billion tonnes of water and 9 billion tonnes of aggregates for global concrete production. Further, this demand for concrete is expected to grow to approximately 18 billion tonnes a year by 2050 [7].

Further to the substantial depletion of natural resources, the mining, processing and transport of huge quantities of concrete making raw materials consume considerable amount of energy and have adverse affect on the ecology of planet, though the concrete compares favourably to the other building materials such as steel, wood, etc. when analyzing energy consumption and CO_2 emissions [2]. A typical comparison of energy consumption for common building materials is given in Fig. 2.

In the same report, it is reported that energy required to produce one metric tonne of reinforced concrete was 2.5 GJ/tonnes compared to 30 GJ/tonnes for steel and 2.0 GJ/tonnes for wood. The CO_2 emissions per 1000 kg of building materials for
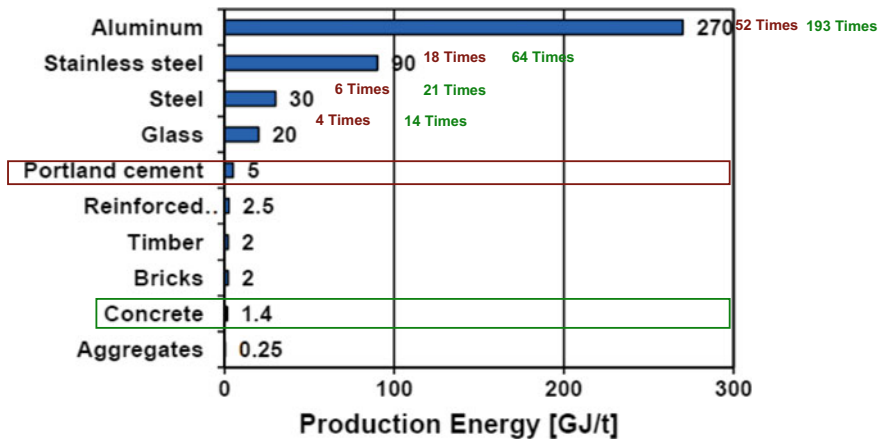

Fig. 2 Energy of production for common building materials [2]

residential construction accounted to be 147 kg for concrete, 3000 kg for metals and 127 kg for wood.

Although cement and concrete manufacturing contribute to CO_2 emissions, it is a small fraction of that generated by other human activity. Based on the US 2008 CO_2 emissions data [2], the four largest generators of CO_2 are

1. Heating and cooling of homes: 21%
2. Heating and cooling of commercial buildings: 19%
3. Transportation-driving cars and trucks: 33%
4. Industrial operations: 27%.

The process of mining sand and gravel, crushing stone, combining the materials in a ready mix concrete (RMC) plant and transporting concrete to the construction site requires very little energy and therefore only emits a relatively small amount of CO_2 into the atmosphere. The amounts of CO_2 embodied in concrete are primarily a function of the cement content in the mix designs.

3 Secondary Raw Materials for Cement and Concrete Productions

Concrete, being the most widely used material worldwide, is a natural target for conservation of natural resources. As Portland cement production is known to require large amounts of energy and is responsible for the release of GHG, any efforts to reduce the cement content in concrete and/or efforts on use of secondary raw materials have a good impact on sustainable development. Some measures include, use of by-products from other industries as cement substitutes (supplementary cementitious materials—SCM), and use of recycled concrete aggregates (RCA) and aggregate by-products like granite dust/manufactured sand (M-sand) to replace primary/natural aggregate. The use of secondary raw materials generally serves three purposes.

1. Waste by-products have an inherent negative value, as they require disposal, typically in landfills, subject to tipping/disposal fees that can be substantial. When used in concrete, the material's value increases considerably. As this replaces a certain fraction of the cement and/or aggregates, market value of these materials may approach that of cement and aggregate, respectively.
2. The tangible as well as intangible costs associated with landfilling the original waste materials are eliminated.
3. SCM with their latent hydraulic cementitious and/or pozzolanic properties not only help to achieve remarkable additional benefits like enhanced concrete performance in terms of mechanical strength, workability, or durability but also help to lessen the environmental impact in terms of cement production, in terms of energy use, depletion of natural resources, and air pollution, substantially.

3.1 Use of Supplementary Cementitious Materials/Blended Cements in Concrete

Considerable amount of work has been reported in the literature on the use of SCM, which have been covered in Table 1 of EN 197-1:2014 [8]. These include the 27 products in the family of common cements with different replacement ranges.

- Limestone powder (LS)
- Fly ash (Siliceous/Calcareous) (FA)
- Ground granulated blast furnace slag (GGBS)
- Silica fume (SF)
- Pozzolana (natural/natural calcined)
- Burnt shale powder.

Furthermore, Table 2 of EN 197-1:2014 [8] has covered another seven products in the family of sulphate resisting common cements, out of which two products are

Table 1 CO_2e of factory-made cements and cement combinations produced at the concrete works

Cement (factory-made cement)	Secondary main constituent (SMC)/(addition)	CO_2e, includes transport of constituents materials to the cement works but not transported to concrete plant
(Cement [CEM I and addition combined at concrete plant])	Low-high content (%)	SMC low-high (kg CO_2e/tonne)
CEM I (Pórtland cement)		**913**
CEM II/A-LL or L Pórtland limestone cement *(CEM II/A-LL or L)*	**6–20** **(Limestone)**	**859–745** *(863–745)*
CEM II/A–V Pórtland fly-ash cement *(CEM II/A–V)*	**6–20** **(Fly ash)**	**859–746** *(858–731)*
CEM II/B-V Pórtland fly-ash cement *(CEM II/B-V)*	**21–35** **(Fly ash)**	**728–615** *(722–595)*
CEM II/B-S Pórtland slag cement *(CEM II/B-S)*	**21–35** **(GGBS)**	**743–639** *(735–617)*
CEM III/A Blastfurnace cement *(CEM III/A)*	**36–65** **(GGBS)**	**622–398** *(608–363)*
CEM III/B Blastfurnace cement *(CEM III/B)*	**66–80** **(GGBS)**	**381–277** *(354–236)*
CEM IV/B-V Pozzolanic (Siliceous fly-ash cement) *(CEM IV/B-V)*	**36–65** **(Fly ash)**	**598–441** *(586–413)*

Table 2 Properties/quality of RCA and 20 mm aggregate

Source	Masonry content (%)	Water absorption (%)	Specific gravity OD SSD		Water-soluble chloride (%)	Total sulphate content (%)
A	3	5.04	2.26	2.41	0.00095	0.03
B	2.05	4.46	2.32	2.46	0.00265	0.13
C	2.42	4.34	2.31	2.44	0.0016	0.09
D	2.7	5.96	2.2	2.36	0.00105	0.18
Natural Agg	0	0.89	2.58	2.6	0.00088	0

with the use of high amounts of GGBS (66–80% and 80–95% by mass) and another two products are with the use of natural pozzolana or siliceous fly ash (21–35% and 36–55% by mass). These recommendations further reinforce the robustness/the role of SCM towards sustainability through enhanced concrete performance.

The use of cements made with SCM, called as blended cements, allows for reduction in the energy and reduces GHG emissions substantially based on the replacement levels. A recent UK report [9] confirms the substantial reduction in environmental impact in terms of CO_2 emissions, based on the cements produced in factory and at the concrete works with the use of LS, FA and GGBS. The details are given in Table 1.

There are various other SCM such as metakaolin, rice husk ash, volcanic ash, incineration ash, wood ash, etc. that are available worldwide, which may be proposed for use in concrete for structural and non-structural applications by establishing its quality and suitability for respective applications towards sustainability.

Based on recent study, the strength and durability performance of concretes produced at 50, 70 and 85% replacements of GGBS by mass and using 100% M-sand as fine aggregate is shown in Fig. 3. The concretes consist of 400 kg/m^3 of total cementitious content with designed water to binder ratio of 0.44 and polycarboxylate (PC)-based admixture of varied dosage to achieve the comparable initial workability/slump of 200 mm. For the quality of materials used, when compared to 100% OPC concrete, increase of GGBS content in concrete from 50 to 85% replacements resulted in reduced compressive strength of up to three days. The GGBS concretes with 50 and 70% replacements exhibited an increase in strength at seven days and beyond, and at 28 days and beyond, respectively, than compared to 100% OPC concrete. Concrete with 50% GGBS replacement was found to be optimal and resulted in relatively higher strength beyond seven days. The compressive strengths of GGBS concrete with up to 70% replacements show comparable and higher compressive strengths than 100% OPC concrete at 28 days and 56 days, respectively, when designed at equal w/c ratio basis, and produced to almost equal consistency. However, GGBS concrete at 85% replacement (CEM III/C) exhibited a consistently lower strength up to the 56 days of testing. Therefore, the need of additional cementitious contents may be essential when CEM III/C is specified in project specifications with a requirement
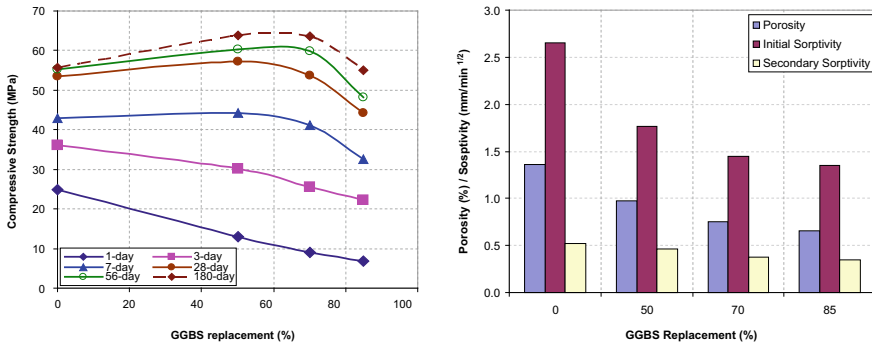
Fig. 3 Effect of GGBS content on compressive strength, porosity and sorptivity

of 28 days strength compliances. The effect of GGBS content in 100% M-sand concretes exhibited a decrease in sorptivity and porosity with increase of GGBS contents similar to that of the behaviour, which is generally observed in natural sand concrete. This enhanced strength and durability performance is due to the pore refinement associated with intrinsic secondary reactions of GGBS in concrete and increase in the calcium silicate hydrate (CSH) and other hydration products at the expense of calcium hydroxide ($CaOH_2$) [10].

Numerous studies on use of SCM/blended cements in concrete for their workability, strength and durability performances were readily available in the national and the international level literature in the area of concrete reach works.

3.2 Use of Secondary Aggregates in Concrete

Performance-based standards, like BS EN 206:2013 for concrete [11] and EN 12620:2002+A1:2008 aggregates for concrete [12], now allow the use of natural, manufactured or recycled materials and mixtures of these aggregates in concrete, which paves the way for greater adoption of the secondary aggregate materials that can be used for a wide range of applications. Literature on the use of recycled concrete aggregate (RCA: recycled aggregate comprising principally of crushed concrete) [13–15], and processed filler aggregates like granite fines/dust [16, 17] and M-sand [18–20] for use in concrete also suggests that there is scope for further improvements by considering secondary aggregate materials for sustainability in concrete constructions.

EN 206:2013 Annex E recent recommendations on use of good quality coarse RCA allow up to 30% by mass in concrete and its use is limited to up to a maximum strength class of C40/50 (M50). Recycled aggregates (RA: aggregate resulting from the processing of inorganic material previously used in construction) and recycled fine aggregates are not allowed to use in concrete for the casting of structural elements,

but these can be used for road base/non-structural instead of using natural/virgin materials towards sustainability.

3.2.1 Use of Recycled Concrete Aggregates (RCA) in Concrete

Recently, the effect of RCA quality and its replacements on mechanical properties were evaluated. RCA was collected from four major local recycling plants and labelled as sources A, B, C and D, to maintain confidentiality of the recycling plants pertaining to the quality of the RCA produced. The properties/quality of RCA and 20 mm aggregate used are given in Table 2. The average testing results for compressive strength (f_{cu}), flexural strength (f_r) and modulus of elasticity (E) at 28 days for the strength classes C32/40 (M40), C50/60 (M60) and C65/80 (M80) produced with RCA replacements at 0% (control), 20, 50 and 100% using different sources of RCA are given in Table 3. Full details of this research work including the mix proportions are reported elsewhere [21].

Based on the analysis of the results, the average maximum reductions in compressive strengths (C32/40, C50/60 and C65/80) were 9.3, 19.6 and 27.7% at 20, 50 and 100% RCA replacements, respectively. Modulus of elasticity was found to be the least affected correspondingly of 5.7, 7.7 and 11.8%. The reduction in mechanical properties was found to be higher with increase of strength class and with increase of replacement levels. However, unlike the case of C32/40 concrete, higher grade concretes with RCA were generally not able to achieve the design strength. In particular, the C65/80 concrete for all the replacement percentages had compressive strength lower than 80 N/mm^2. This shows that it becomes increasingly difficult to achieve higher strength class concrete with RCA. It is also noteworthy that for RCA replacement percentage of 100%, strength class C50/60 and C65/80 concretes achieved only 53.5 MPa and 61.3 MPa, respectively.

The RCA from source D consistently produced concrete of the lowest strength in all the grades considered due to the lowest particle density/specific gravity and highest water absorption associated with higher quantity of mortar adhering to this aggregate amongst the four sources. Based on this, it can be concluded that the quantity of adhering mortar, and hence, the quality of the RCA, strongly dictates the strength of the concrete. Furthermore, aggregate-cement matrix interface (interfacial transition zone—ITZ) is the weakest link in concrete failures, in general, and high strength concretes in particular. It is apparent that the presence of adhering mortar to the RCA in concrete has a tendency of formation of two layers of ITZ for concrete designed with RCA. The implication, therefore, is that to design moderate and high strength concrete with RCA, the direct replacement of virgin aggregate with RCA is surely not sufficient to achieve design strengths, and some adjustments/enrichment of design mixes are to be considered in terms of use of higher cementitious contents (lower water to binder ratios). Based on this study, it can concur that use of 20% RCA replacement for up to C50/60 concrete had negligible effect on the compressive strength with all the sources of local RCA. In practice, designing concrete for a higher

Table 3 Effect of RCA quality and its replacements on mechanical properties

N. Agg		f_{cu} (MPa)	f_r (MPa)	E (GPa)	f_{cu} (MPa)	f_r (MPa)	E (GPa)	f_{cu} (MPa)	f_r (MPa)	E (GPa)
		C32/40 (M40)			C50/60 (M60)			C65/80 (M80)		
A	Control	45.41	4.65	30.44	65.04	5.96	33.04	82.57	7.97	35.18
A	RCA @ 20%	44.67	4.51	30.25	61.36	5.67	32.74	73.36	6.27	34.97
B		41.19	4.46	28.23	63.20	5.56	32.94	79.42	6.76	35.07
C		44.66	4.58	28.68	63.99	5.82	31.80	76.40	6.33	33.92
D		44.29	4.51	29.82	60.13	5.35	31.59	62.61	7.68	33.24
Max. reduction (%)		9.29	4.09	7.26	7.55	10.23	4.39	11.15	21.33	5.51
A	RCA @ 50%	41.12	4.53	29.30	57.86	5.59	31.57	65.85	5.73	33.34
B		40.25	4.36	27.75	61.27	5.30	32.81	74.00	6.36	34.90
C		44.57	4.20	28.90	61.44	5.25	30.78	68.69	6.30	32.61
D		39.09	4.36	28.54	53.02	5.07	31.18	60.87	7.07	32.54
Max. reduction (%)		13.92	9.68	8.84	18.48	14.93	6.84	26.28	28.11	7.50
A	RCA @ 100%	38.52	4.47	28.94	50.21	4.76	30.95	57.94	5.71	33.00
B		40.21	3.53	27.82	54.07	5.04	32.46	68.81	5.86	32.58
C		43.64	3.67	27.61	56.93	4.82	28.68	65.36	5.83	31.99
D		34.32	3.52	27.55	52.80	4.54	28.43	52.99	5.54	31.02
Max. reduction (%)		24.42	24.30	9.49	22.80	23.83	13.95	35.82	30.49	11.82

strength class is needed and its cost-effectiveness depends on cost of component materials which may vary as scarcity of resources becomes more critical.

3.2.2 Use of Manufactured Sand (M-Sand) in Concrete

M-sand that is re-processed to improve its shape (e.g. vertical shaft impact-VSI produced) or by washing or sieving out to reduce particles finer than 0.063 mm and the granite/quarry dust that is not further treated. BS EN 12620 [12] has recommended categories of fines content up to 22% by mass and any value above this has to be declared. The M-sand in this study is under the category of f_3, the lowest category with less than 3% by mass passing the 0.063 mm sieve. The strength and durability performance of concretes produced at 25, 50, 75 and 100% replacements of M-sand by mass and using CEM IIIA (50% GGBS by mass) as binder is shown Fig. 4. The concretes consist of 400 kg/m^3 of total cementitious content with designed water to binder ratio of 0.44 and polycarboxylate (PC)-based admixture of varied dosage to achieve the comparable initial workability/slump of 200 mm. For the quality of materials used in this study, the strength development of all the concretes was found to be consistent at different M-sand content for a given type of cement (50% GGBS content—CEM III/A).

When compared to NS-100% concrete, the increase of M-sand content in concrete from 0 to 100% replacements resulted in no decrease in compressive strength up to 50% and even beyond that of up to 100%, the decrease in compressive strength is found to be very negligible (~ 5–8%) at 28 days and beyond, when concretes designed at equal w/b ratio and produced to almost equal consistency. Based on the results, use of M-sand in concrete a comparable or marginally better strength performance is due to possible improved particle packing density combined with improved interlocking effects than when 100% natural sand is used as fine aggregate. Almost a comparable initial and secondary sorptivity values to that of (100%) natural sand concrete was observed. A marginal higher sorptivity by about 7% at 100% M-sand replacement
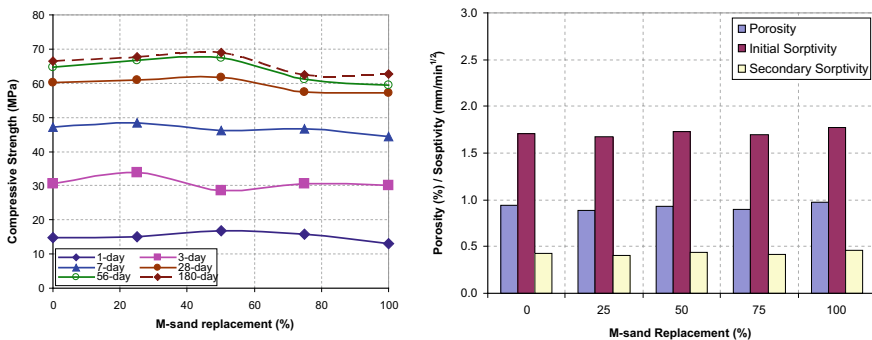

Fig. 4 Effect of M-sand content on compressive strength, porosity and sorptivity

than 100% natural sand concrete coincides well with the marginal increase of porosity for the former concrete. Compared to the durability performance of 100% M-sand concretes consists of 100% OPC and 50% GGBS as binders (Figs. 3 and 4), a marginal higher (7%) sorptivity in 50% GGBS content (CEM III/A) concrete is still lower than the sorptivity of 100% OPC concrete by about 11%. Therefore, the high GGBS replacement levels at ($\geq$50% by mass) combined with secondary aggregates like M-sand/RCA shall further benefit the concrete performance.

4 Sustainable Concrete Practices

Sustainable concrete practices are very imperative worldwide and many countries have started implementing the same. Recycling of construction and demolition wastes (CDW) is significantly beneficial to a country like Singapore which has scarcity of land, no natural resources and building and infrastructure constructions are growing at a rapid rate in order to house its population (increased by >30% from 2004 to 2014) and businesses. Moreover, due to the changing needs and tastes of today's population and limited land, many of the building structures are being demolished much earlier than the intended designed life (for example, the tallest building Housing and Development Board (HDB) used to construct a 1–2 decade ago was only 22 storey. Now, 40 storey buildings are already in occupation and several 50–71 storey public and private buildings for housings are under construction). However, this problem is not only just unique to Singapore. Dhir et al. [13] pointed out that the construction industry worldwide is using natural resources and disposing of CDW in landfills in very large quantities. Both these practices are damaging to the environment and are no longer considered sustainable at their current levels. Many governments throughout the world are therefore actively promoting policies aiming at reducing the use of primary resources and increasing reuse and recycling.

The concrete wastes such as fresh concrete waste generated at ready mix concrete (RMC) and precast plants arise from (1) Trial mixes, (2) Over-ordered fresh concrete, (3) Unwanted or rejected concrete caused by the poor consistency at the time of placing, (4) Washing out truck mixer drums and batching plant. The fresh concrete wastes become hardened concrete wastes, if not minimized effectively. Furthermore, hardened concrete wastes such as CDW other sources demolition of concrete mock-up blocks and 150 mm standard cube sample testing for strength and other parameters. Hardened concrete waste disposal involves additional costs and land space. Some of the sustainable practices to minimize concrete wastes are as follows:

- Recycling of fresh concrete waste is one of the best options towards sustainable practices to minimize the fresh concrete wastes at batching plants by reclaiming both the coarse and fine aggregate from the waste using a "reclaimer" (Fig. 5).

A "reclaimer" includes a concrete processor having a rotating inclined screen and a pipe discharging water. Fresh concrete being disposed is poured at open end of inlet by mixing with additional water which passes through the reclaimer screens,

Fig. 5 Typical view of recycling of fresh concrete waste (reclaimer)

whereby the coarse aggregate, fine aggregate and sludge (cement paste + water) are separated and discharged to the pre-constructed designated compartments. The reclaimed aggregate can be used for concrete production.

- Adoption of environmentally friendly practices in line with BS 8500-2 recommendation [22] towards sustainability by using 100 mm cubes instead of 150 mm cubes for strength assessments. This was supported with large populations of over 100 batches of test data for three strength class levels, reported elsewhere [23]. This has been adopted by the Housing Development Board, Singapore for over a decade.
- The acceptance of EN 206 product conformity certificates for the certified products/respective strength class of concrete to avoid trial mixes at RMC and precast plants.
- Consideration of trial mix for one batch of concrete instead of three batches of concrete for those design mixes yet to have the product conformity certificates as per EN 206.
- Collection of reasonable and required amounts of fresh concrete at construction sites for slump/slump flow tests and/or standard test sample preparation, termed "identity tests" in EN 206.
- The required number of mock-up blocks for assessing suitability of design mixes shall be minimized with proper planning and review of the design mixes, and/or considerations of well-documented test reports from the other projects for the same design mixes and/or finding other means of testing.

Furthermore, initiations and recommendations on use of green materials such as supplementary cementitious materials (GGBS, fly ash, etc.) and secondary aggregates (RCA, M-sand, etc.) in concrete productions at national (NTPC [24] and BCA [25], etc.) and international levels through government bodies and/or standards are also very important towards sustainability practices.

5   Conclusions

- Use of secondary raw materials for cement and concrete production together with minimization of fresh and hardened concrete wastes are viable options towards sustainability in concrete construction. A sustainable concrete structure has minimal total societal impact during its entire life cycle. Designing with sustainability in view includes consideration of short-term and long-term consequences of the structure in service (durability). To decrease the long-term impact of structures, the creation of durable (concrete) structures is paramount with the use of secondary raw materials like SCMs.
- Studies on high volumes of GGBS, RCA and M-sand, the use GGBS up to 70% replacement levels (of OPC), RCA at 20% replacement levels (of virgin 20 mm) and M-sand up to 100% replacement levels (of natural sand) have exhibited good strength and/or durability performance based on the quality of materials used and which show the secondary raw materials (SCM and aggregates) have significant potential towards sustainability and the need of its implementations/practices is vital.
- For the urbanized and critical land-scarce countries like Singapore, the consideration of local initiatives/proposals towards sustainability together with the adoption of current performance-based EN standards to minimize the concrete wastes is important. Further, with the assurance on quality of raw materials and concrete, the development of sustainable concrete structures would minimize the environmental impact in the future.

References

1. UNFCCC COP9 Report. (2004). *Delivering the Kyoto baby*. Refocus, International Renewable Energy Magazine, pp. 52–53.
2. NRMCA Publication Number 2PCO2. (2012). *Concrete CO$_2$ Fact Sheet*, USA, pp. 1–11.
3. Malhotra, V. M. (2004). Role of supplementary cementing materials and superplasticizers in reducing greenhouse gas emissions. In *Proceeding of ICFRC International Conference on Fiber Composites, High-Performance Concrete, and Smart Materials, Indian Institute of Technology*, Chennai, India, pp. 489–499. http://www.globalwarmingart.com.
4. http://www.globalcarbonproject.org/.
5. http://en.wikipedia.org/wiki/List_of_countries_by_cement_production.
6. Leslie, S., & Jonathan G. (2004). How sustainable is concrete? In *International Workshop on Sustainable Development and Concrete Technology*, USA, pp. 201–211.
7. www.ce.berkeley.edu/…/Concrete%20and%20the%20Environment.pdf.
8. BS EN 197-1:2011, Cement. Part 1: Composition, specifications and conformity criteria for common cements, BSI.
9. http://cement.mineralproducts.org/documents/Factsheet_18.pdf.
10. Malhotra, V. M., & Mehta, P. K. (1996). *Pozzolanic and cementitious materials: Advances in concrete technology*. London: Gordon and Breach.
11. BS EN 206-1:2013, *Concrete—Specifications, performance, production and conformity*. London, UK: British Standards Institute.

12. BS EN 12620:2002+A1:2008, *Aggregates for concrete*. London, UK: British Standards Institute.
13. Dhir, R. K., Henderson, N. A., & Limbachiya, M. C. (1998, November 11–12). Sustainable construction: Use of recycled concrete aggregate. In *Proceedings of the International Symposium Organised by the Concrete Technology Unit* (p. iii). University of Dundee and Thomas Telford: London, UK.
14. WRAP. (2007, February). *Performance related approach to use of recycled aggregates*. Banbury: Waste & Resources Action Programme.
15. Tamilselvan, T., & Ong, G. K. C. (2015, January 16). Use of recycled aggregate in concrete—A performance based approach. In *Workshop on Sustainable Concrete*, Singapore.
16. Gonçalves, J. P., Tavares, L. M., Filho, R. D. T., Fairbairn, E. M. R., & Cunha, E. R. (2007). Comparison of natural and manufactured fine aggregates in cement mortars. *Cement and Concrete Research, 37,* 924–932.
17. Li, B., Ke, G., & Zhou, M. (2011). Influence of manufactured sand characteristics on strength and abrasion resistance of pavement cement concrete. *Construction and Building Materials, 25,* 3849–3853.
18. Daneti, S. B., & Tam, C. T. (2018). Effect of GGBS and M-sand contents on strength and durability performance of concretes. *Green Materials Journal, ICE Publishing*. Under review.
19. CCAA Guide. (2008). *Guide to the specification and use of manufactured sand in concrete*. Cement Concrete & Aggregates Australia.
20. Martins, P., Diane, G., & Robert, L. (2016). An investigation into the use of manufactured sand as a 100% replacement for fine aggregate in concrete. *Materials, 9*(440), 1–19.
21. Daneti, S. B., Tamilselvan, T., & Ong K. C. G. (2015). Sustainability of concrete constructions for the 21st century. In *The Seminar on Sustainable Construction, RMCAS and BCA Singapore*, pp. 115–128.
22. BS 8500-2:2015, *Concrete—Complementary British standard to BS EN 206 Part 2: Specification for constituent materials and concrete*. London, UK: British Standards Institute.
23. Daneti, S. B., Li, W., & Tam, C. T. (2016). EN 206 conformity testing for concrete strength in compression. *Journal—The Institution of Engineers Malaysia, 77*(2), 1–11.
24. NTPC Ltd. Fly Ash Bricks A Useful & Environment Friendly Building Product, Ash Utilization Division, Noida, UP, India.
25. Building and Construction Authority (BCA). (2008). *Sustainable construction—A guide on the use of recycled materials*. BCA Sustainable Construction Series 4.